Structural and functional analysis of the *Drosophila* antennal lobe

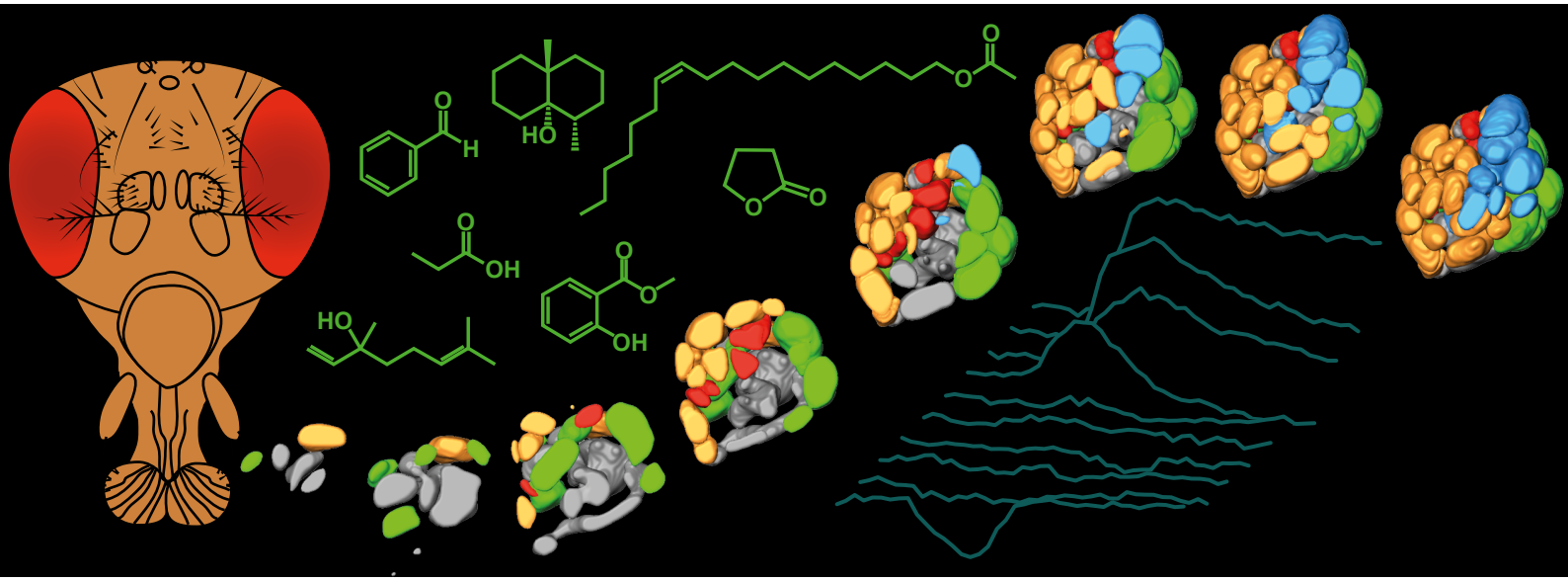

A PhD Thesis by Veit Grabe

Friedrich-Schiller-Universität Jena
seit 1558

MAX-PLANCK-GESELLSCHAFT

Structural and functional analysis of the *Drosophila* antennal lobe

Dissertation

To Fulfill the
Requirements for the Degree of
„doctor rerum naturalium“(Dr. rer. nat.)

Submitted to the Council of the Faculty
of Biology and Pharmacy
of the Friedrich Schiller University Jena

by Veit Grabe
born on 20.03.1985 in Bad Frankenhausen, Germany

Reviewers

1. Prof. Dr. Bill S. Hansson

Max-Planck-Institute for Chemical Ecology Jena

2. Prof. Dr. André Fiala

Georg-August-University Göttingen

3. Prof. Dr. Rolf Beutel

Friedrich-Schiller-University Jena

Date of public defense

30.04.2015

Dedicated to

Fritz

and

Harald

Table of contents

Introduction

Orientation and navigation in complex habitats demand a proper evaluation of available landmarks and the integration of various modalities to decide and execute appropriate behavior. The possibilities to perceive this surrounding are numerous in the sense of optical, thermosensory, hygrosensory, mechanosensory and chemosensory stimuli. Chemosensation, in contrast to the other modalities, is not oriented along a rather simple scale with discrete steps such as wavelength, temperature or humidity. Instead, chemical senses have to deal with a nearly infinite number of possible combinations of molecules expanding the variability of every other sense. This environmental challenge led to the evolution of a sensory system of similar complexity – the olfactory system.

As a favored model organism, the vinegar fly *Drosophila melanogaster* and its unprecedented genetic modifications allow a comprehensive examination of the olfactory system. The fact that vertebrate and invertebrate chemosensation share various structural attributes (Eisthen, 2002) emphasizes the beneficial use of insect neuroscience, generating a solid foundation for the understanding of the chemical sense. Investigating ways to fight crop pests (Lee et al., 2011) and disease vectors (Kain et al., 2013; McMeniman et al., 2014) is another crucial origin of invertebrate neuroscience. Each of these two approaches is either focused on a mechanistic understanding, such as the search for effective insect deterrents (Kain et al., 2013), or on an extensive physiological analysis leading to an improved understanding of the detailed olfactory circuitry (Wilson, 2013). The latter one is often combined with anatomical observations to support a new hypothesis (Caron et al., 2013; Mosca and Luo, 2014) or to challenge an outdated one (Zhu et al., 2013). Except for the pheromone pathways (Boeckh and Tolbert, 1993; Galizia et al., 1999; Hansson et al., 1992; Schneiderman et al., 1986), an actual relation of form and function is usually neglected.

The olfactory system of *Drosophila melanogaster*

To investigate a putative correlation of function and structure, the antennal lobe (AL) of *Drosophila melanogaster* and its connected neuropils (Fig 1) represent a perfect research object (Liang and Luo, 2010; Vosshall and Stocker, 2007). On one hand, the availability of extensive functional data for various units of the system (Hansson et al., 2010), and on the other hand the steady increasing methodological possibilities

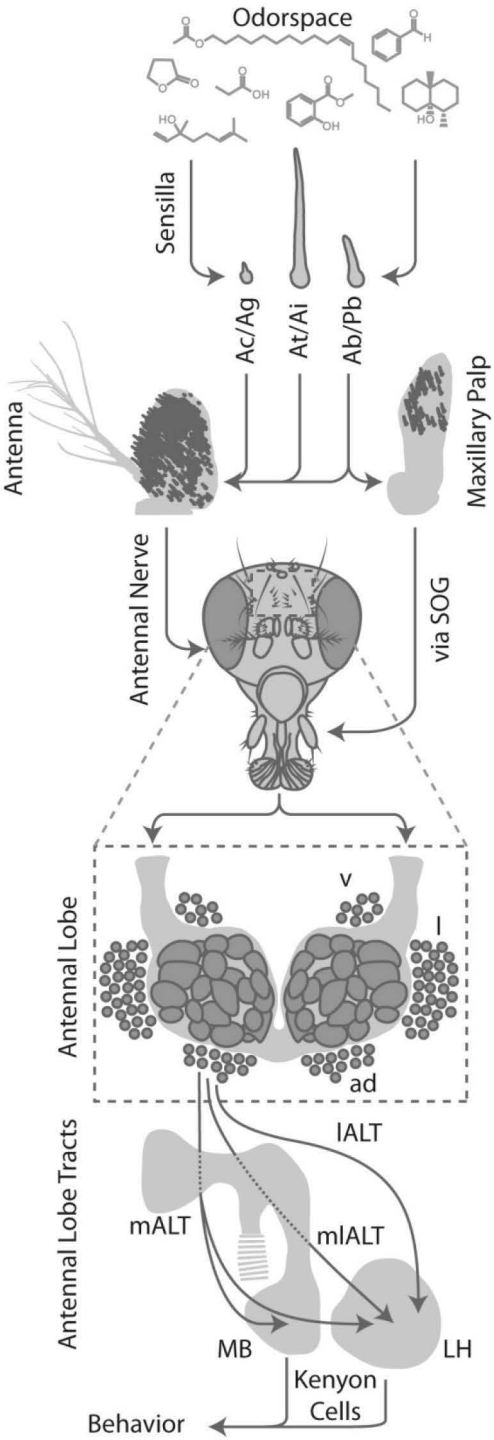

to approach open questions (Adam et al., 2014; Stachniak et al., 2014), permit a thorough examination of the interdependence of form and function.

Volatile cues are initially perceived by a set of three different classes of chemosensory receptors (CRs, (Benton et al., 2009; Clyne, 2000; Vosshall et al., 1999)) in combination with specific co-receptors (Larsson et al., 2004) expressed in olfactory sensory neurons (OSNs) on the third segment of the flies' antenna – the funiculus – or the maxillary palp (MP). A defined combination of one to four OSNs is housed in a single sensillum (Shanbhag et al., 1999) with their somata directly at the base and their dendrites, exposing the CRs, branching in the sensillum. After entering the sensillum through a pore and solving in the sensillum lymph, the odors are bound to gustatory (GRs), olfactory (ORs) or ionotropic glutamate receptors (IRs) depending on the sensillum type, putatively supported by odorant binding proteins (OBPs, (Fan et al., 2011)). If the threshold for activation of an OSN is reached, the resulting action potential is propagated via the antennal nerve (AN) to the protocerebrum. The AN is a dense

Figure 1| Olfactory system of *Drosophila melanogaster*

Schematic of the wiring of the different peripheral and central parts of the chemosensory system. Ab – antennal basiconic sensilla, Ac – antennal coeloconics sensilla, ad – anterodorsal somata cluster, Ag – antennal grooved sensilla, Ai – antennal intermediate sensilla, At – antennal trichoid sensilla, Pb – palp basiconic sensilla, l – lateral somata cluster, mALT – medial AL tract, MB – mushroom body, mlALT – mediolateral AL tract, lALT – lateral AL tract, LH – lateral horn, SOG – suboesophageal ganglion, v – ventral somata cluster.

neuron bundle consisting of a chemosensory part coming from the funiculus, which innervates the AL, and a mechanosensory part originating from the arista and the Johnston's organ innervating the antennal mechanosensory and motor center (Lai et al., 2012). OSNs present on the MP are descending through the suboesophageal ganglion to the AL (Singh and Nayak, 1985). Once the OSNs reach the AL they are distributing to innervate the neuropil subunits, called olfactory glomeruli. Each of these glomeruli receives input of a particular type of OSNs expressing a certain CR (Fishilevich and Vosshall, 2005). Because of the common expectation that every glomerulus is innervated by the same number of input neurons (Ramaekers et al., 2005; Vosshall and Stocker, 2007), understanding of overall uniformity across these structures arose. I depicted together with my collaborators the precise mapping of OSNs and sensilla in Manuscript II and for the first time provided a thorough mapping of the different sensilla types beyond the long known spatial distribution of the different classes (De Bruyne et al., 1999; Shanbhag et al., 1999). We originally displayed a precise atlas of nearly all known antennal basiconic, coeloconic, intermediate, trichoid and palp basiconic sensilla with the additional advantage of being able to quantify their exact numbers separated by gender. In addition, we generated the first *in vivo* atlas of the AL itself (Fig 3D, Manuscript I) which allowed the most inartificial estimation of the ALs' and especially the glomeruli' dimensions. This, in turn, resulted in the foundation of a reliable analysis of the correlations between different structural properties and, the combination of those with respective functions. To widen the scope of this approach we focused on further glomerulus-specific morphological characteristics.

Neuronal composition of the glomerulus

Since all OSNs expressing a certain receptor, converge onto the same glomerulus (Gao et al., 2000), mostly ipsi- as well as contralateral via a commissure (Stocker and Lawrence, 1981), their information is gathered by a less specific population of second order projection neurons (PNs). These two neuron types form cholinergic synapses (Stocker, 1994; Vosshall and Stocker, 2007) in the glomerulus periphery as OSNs are mainly innervating the outer perimeter of each glomerulus (Fig 2, (Hummel and Zipursky, 2004)). Uni- and multiglomerular PNs are shaping the core of each glomerulus and propagate the information via three separated tracts (Chiang et al., 2011; Stocker et al., 1990) to higher brain centers in the protocerebrum (Fig1, 2)

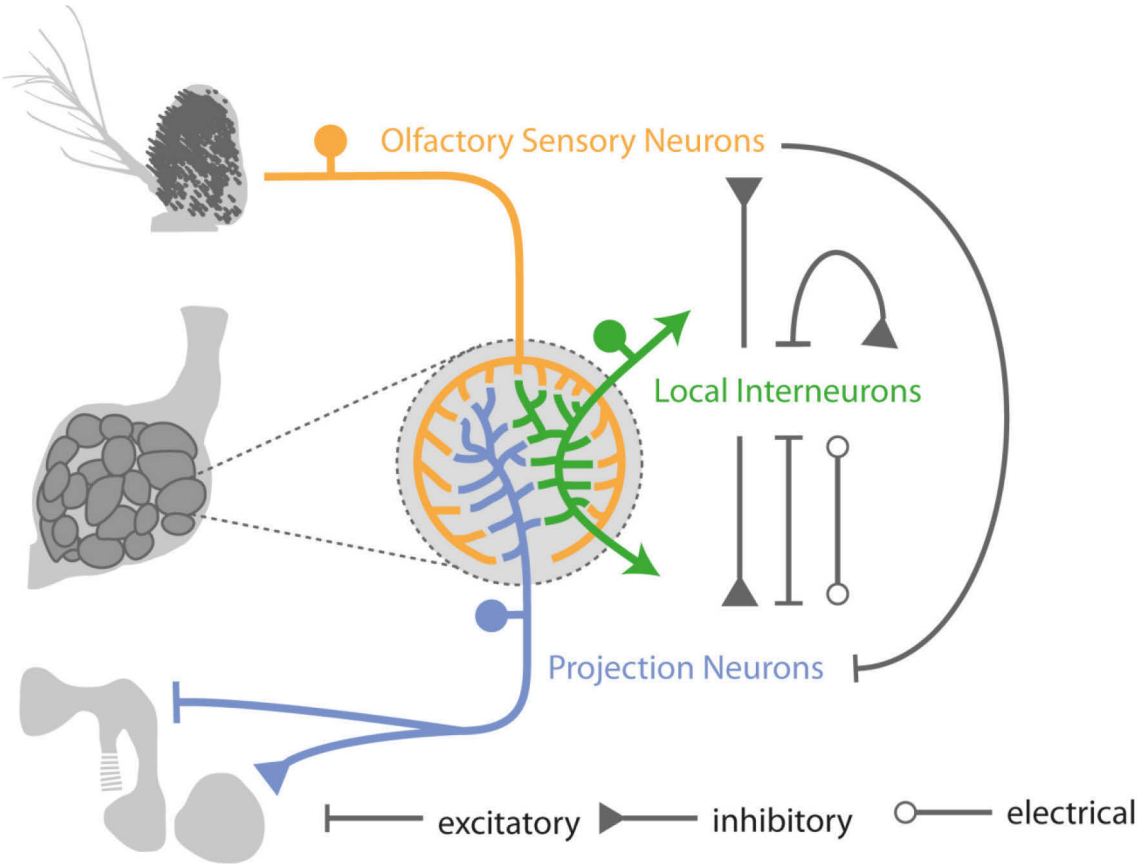

Figure 2 | Intraglomerular circuitry of the three major neuron types

Schematic internal composition of the glomeruli in the AL of *Drosophila melanogaster* and of their synaptic connectivity. Orange – olfactory sensory neurons, green – local interneurons, blue – projection neurons. The icons for the different synaptic types are indicated in the figure.

such as the mushroom body calyx and the lateral horn. Moreover, the glomerulus core houses a third neuron population, the local interneurons (LNs) which form electrical (Yaksi and Wilson, 2010) as well as GABAergic and cholinergic chemical synapses with OSNs (Olsen et al., 2007; Root et al., 2008), PNs (Ng et al., 2002; Shang et al., 2007) but also with other LNs. As this neuron type is quite versatile regarding its innervation pattern (Chou et al., 2010), neurotransmitter repertoire (Liu and Wilson, 2013; Seki et al., 2010), physiology (Seki et al., 2010) and putatively input-dependent output modalities (Zhu et al., 2013) it is fair to assume the function of the LNs to be variable but at least highly complex. One known function is mediated by their inhibitory synapses with OSNs leading to a presynaptic gain control which dampens overly strong odor responses guaranteeing an approximately average odor

representation for optimal evaluation (Root et al., 2008). Although we are familiar with the superficial anatomical situation of the three participating neuron classes ((Stocker et al., 1990; Stocker, 1994), Fig 2) as well as with a number of intraneuronal properties (Chou et al., 2010; Liu and Wilson, 2013; Mosca and Luo, 2014; Root et al., 2014; Yaksi and Wilson, 2010), these factors are rarely related to known functions. Only the sexual dimorphism as well as large dimensions of macroglomerular complexes, responsible for pheromone perception, is often used to underline the behavioral significance of the transmitted information (Boeckh and Tolbert, 1993; Galizia et al., 1999; Hansson et al., 1992; Schneiderman et al., 1986). This drawback partly originates in the scarcity of comprehensive screens for glomerulus-specific morphology which could potentially bridge the gap between form and function.

In Manuscript II I carried out a comprehensive screen of excitatory uniglomerular PNs by the use of photoactivatable GFP (PA-GFP, (Patterson and Lippincott-Schwartz, 2002)) in GH146, as a GAL4-line which labels the majority of uniglomerular PNs in the AL (Stocker et al., 1997). The GAL4:UAS-system, a binary expression system from the yeast *Saccharomyces cerevisiae,* was transferred into the vinegar fly by Brand and Perrimon (Brand and Perrimon, 1993) and used to express a gene of choice under the control of a tissue specific promoter. This allows selective labeling and observing structures in the living fly and, in our case, to use PA-GFP to quantify small clusters of output neurons in glomeruli. The according screen in Manuscript II gathered the actual numbers of uniglomerular excitatory PNs for a large set of glomeruli allowing to investigate the relation of these and the former mentioned volume and OSN quantity (Manuscript II) per glomerulus with known functional importance. Next to the excitatory uniglomerular PNs we also investigated the structure and function of inhibitory multiglomerular neurons labelled by MZ699 (Ito et al., 1997) in Manuscript III. We show that the distinct innervation pattern of this PN population deals with the integration of odor quality and intensity in the lateral horn, a neuropil in the protocerebrum of *Drosophila melanogaster* described to code for innate behavior (Wang et al., 2003b) in contrast to the learning tasks of the mushroom body calyx (Heisenberg, 2003). The glomerulus-specific but random PN output in the calyx (Caron et al., 2013; Murthy et al., 2008) also opposes the determined PN targeting in the lateral horn which even allows a subdivision of the neuropil (Manuscript III) similar to the discrete spherical glomeruli of the AL.

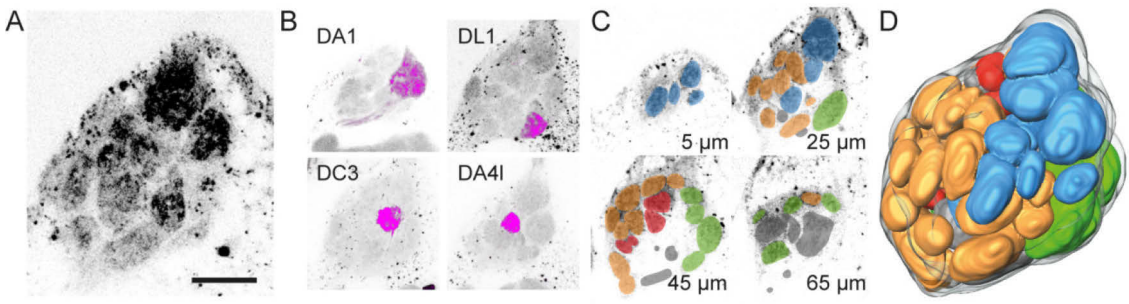

Figure 3 | Schematic of the 3-dimensional reconstruction procedure of the AL

Simplified workflow for the generation of the *in vivo* atlas of the *Drosophila* AL. After *in vivo* confocal scanning of the template stack of the END1-2 fly line (A) it is crossed with a selected set of landmark receptor lines each marking a single glomerulus (B), which eases the later identification. Every level of the template stack was manually reconstructed (C). From this labelling the final 3D model has been calculated (D). Blue – antennal trichoid sensilla, green – antennal coeloconic sensilla, orange – antennal basiconic sensilla, red – maxillary palp basiconic sensilla. Scale bar = 20 µm.

Studies on the functional relevance of certain glomeruli provide a diverse spectrum of purposes ranging from hard wired aversion to CO_2 coded by the V glomerulus (Gr21a, (Suh et al., 2004)), to acids by DC4 (Ir64a, (Ai et al., 2010)) or geosmin by DA2 (Or56a, (Stensmyr et al., 2012)) to oviposition site evaluation via farnesol in the DC3 (Or83c, (Dweck et al., 2013; Ronderos et al., 2014)) and sex specific attraction or aversion to the pheromone cis-vaccenylacetate (cVA) in DA1 (Or67d, (Kurtovic et al., 2007)). Some glomeruli are also described to have rather unspecific functions like the DM2 (Or22a, (Pelz et al., 2006)) or modulatory effects on others like the VA2 on the CO_2 avoidance ((Turner and Ray, 2009)). However, some glomeruli are until now nearly uncharacterized (Or65a, (van der Goes van Naters and Carlson, 2007), Manuscript IV). The specificity of a CR or the respective glomerulus is hard to evaluate due to the non-discrete nature of ligands. A commonly used approach to quantify the odor tuning properties of a receptor is to calculate its lifetime sparseness ((Bhandawat et al., 2007; Perez-Orive et al., 2002; Vinje, 2000), Manuscript II) which is based on the recorded responses for a possibly large set of variable odors and predicts the likeliness of a receptor to respond to any other given odor – its selectivity.

Necessity of and *in vivo* atlas of the antennal lobe

Investigating the above described physiological and functional properties in such a minute but complex tissue as the *Drosophila* AL demands a comprehensive knowledge of its composition and substructures. In Manuscript I **we** dealt with the complicated application of *in vitro* morphology during *in vivo* experiments. The presence of fixation artifacts in *in vitro* experiments, like immunostaining, is well known but hard to investigate or to evade and therefore an inevitable drawback. Same applies for the olfactory system of *Drosophila melanogaster*, especially for the AL as a rather flexible neuropil. Available *in vitro* atlases of the structure are numerous and improved significantly over the past decades (Couto et al., 2005; Endo et al., 2007; Laissue et al., 1999; Silbering et al., 2011; Stocker et al., 1990; Stocker et al., 1983; Tanaka et al., 2012) reaching a reliable status of glomerulus identification and nomenclature. However, the increasing number of *in vivo* applications, which rely on precise and detailed orientation within complex tissues, demands an appropriate anatomy which is free from unpredictable distortions and shrinkage (Manuscript I). To solve this issue we developed a novel transgenic fly line – END1-2 (Fig 3A) – expressing synaptobrevin, a presynaptic peptide, in direct fusion with DsRed (*Discosoma sp.* Red fluorescent protein). This leads to a presynaptic labeling of the living brain which simulates the favored *in vitro* labeling with antibody nc82 (Laissue et al., 1999; Rein et al., 2002). This *in vivo* labelling allows confocal scanning of the complete AL neuropil in the living fly for 3D reconstruction (Fig 3C and D) and the proper assignment of structures, assisted by specific CR-GAL4 lines labeling single glomeruli (Fig 3B). Beneficial qualities of the 3D reconstruction are the maintained orientation and dimension of the AL and the glomeruli and the inartificial measurable volume for each of the structures. Since actual volume measurements of glomeruli are rare (Acebes and Ferrús, 2001; Devaud et al., 2001; Kondoh et al., 2003) and obtained under varying artificial conditions, we generated the first precise estimates of their *in vivo* dimensions (Manuscript I and II). Moreover, by comparing the *in vivo* situation with *in vitro* volumes and glomerular positioning we depicted a precise map of the actual effects, fixation has on the AL and its subunits (Manuscript I). Eventually, we provided a more reliable foundation for AL orientation of the increasing multitude of *in vivo* applications.

Optical imaging of odor responses in the olfactory system

One of the most common methods for acquiring *in vivo* data from the olfactory system is the optical imaging technique via genetically encoded Ca^{2+}/Cl^{-} indicators (GECIs, (Hires et al., 2008)) besides electrophysiological techniques like single sensillum recordings (SSR, (Clyne et al., 1997)). Therefore a transgenic fly line expressing a specific Ca^{2+}-sensitive protein – e.g. GCaMP3 (Tian et al., 2009) –its

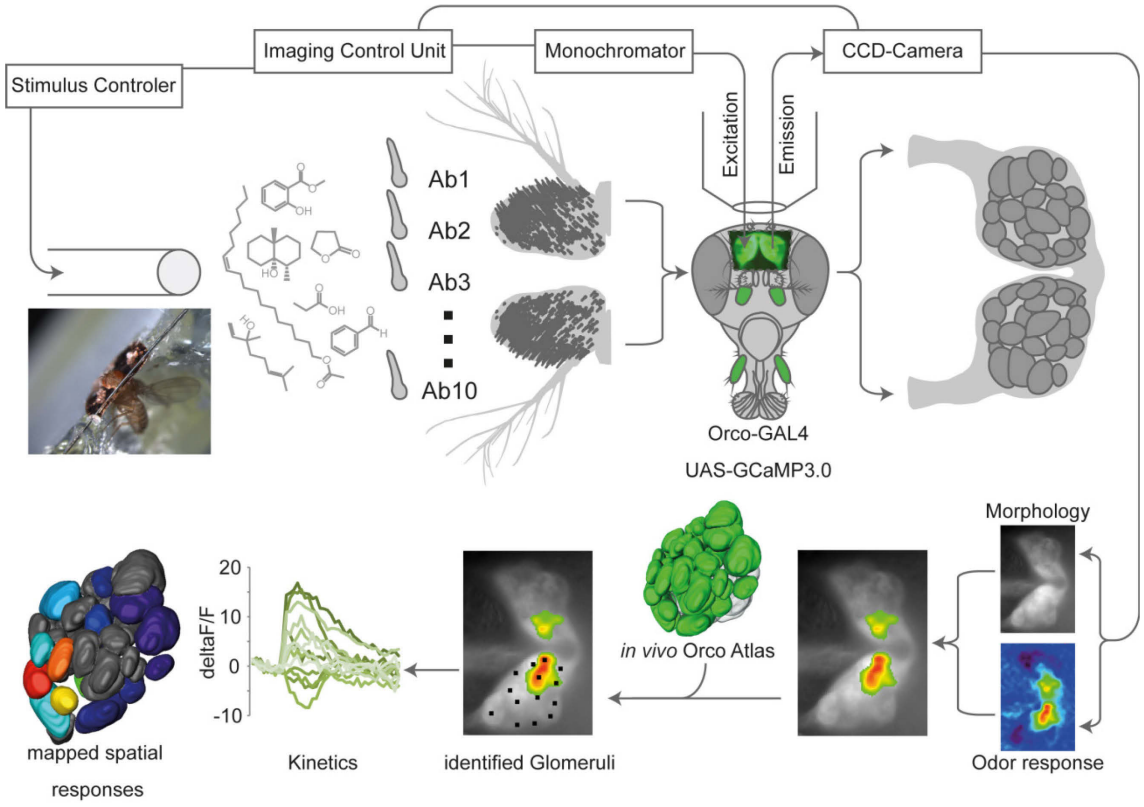

Figure 4 | Optical Imaging

Schematic workflow of the acquisition procedure (upper panel) and evaluation of data (lower panel) in an optical imaging experiment. The puffed presentation of volatile odors to the antenna leads to activation of a subset of OSNs and is paralleled with the acquisition of emission coming from GCaMP3 via a CCD camera on top of a fluorescence microscope. AL morphology (basic fluorescence of GCaMP3) and the spatiotemporal response pattern (emission change) are merged and for visualizing purpose, the response is cropped at a predefined threshold. The glomeruli are identified supported by the *in vivo* atlas (Manuscript I) and known ligand receptor combinations (Galizia et al., 2010). Certain properties of the temporal kinetics, like maximum response, are extracted and can be used for a 16-range color coded mapping of the response onto the reconstructed AL. Ab – antennal basiconic sensillum.

OSNs, achieved via the GAL4-UAS system (Brand and Perrimon, 1993) using the promoter for the olfactory receptor co-receptor (Orco, (Larsson et al., 2004)), is mounted and her head capsule is opened (Fig 4, (Strutz et al., 2012)). This allows simultaneous excitation of the protein in the OSNs and recording of their emission. Once a certain odor is puffed onto the fly's' antenna, interacts as a ligand with the respective CR, the OSN gets eventually excited. The Ca^{2+} influx leads to binding of Ca^{2+} to the respective calmodulin sites of the GCaMP3 and hence to a conformational change resulting in stronger emission by the GFP-fluorophore (Akerboom et al., 2009) visible at the antenna and in the AL. The Ca^{2+} binding results in an odor-specific spatiotemporal activity pattern of the antenna, AL glomeruli or lateral horn regions (Fig4**,** Manuscript III and IV, (Wang et al., 2003a)). By screening large sets of various odors for specific CRs both via SSR and optical imaging (Galizia et al., 2010; Hallem and Carlson, 2006; Kreher et al., 2008), the best ligands were identified and a specific response profile for most receptors could be acquired. These initial physiological characterizations were then correlated with behavioral assays to identify the link between physiology and behavior ((Dweck et al., 2013; Knaden et al., 2012; Ronderos et al., 2014; Stensmyr et al., 2012) Manuscript III). Alternatively the primary examination of a certain behavior can provoke an inquiry about the physiological representation which than is pinned down in with the help of physiological experiments (Manuscript IV). An example is the olfactory pathway of Or65a and its respective glomerulus DL3. The receptor is well characterized in the sense of not responding to any of the numerous tested odors (Hallem and Carlson, 2006) which implies a very selective response profile and suggests a similar specific behavioral output. Our morphological data emphasized the prediction of DL3 having a specific putatively sex-specific importance (Manuscript II) and finally it turned out to play a crucial role in female postmating receptivity (Manuscript IV). Unfortunately the precise ligand being responsible for this effect is still missing. This example demonstrated the potential benefits of combined structural and functional studies underlining the often underestimated relation of form and function.

In this cumulative thesis I present two manuscripts dealing with the structural basis of the AL, the first center of olfactory computation in the brain of the vinegar fly *Drosophila melanogaster*, and two further manuscripts depicting the functional specificity which arises from the previously described anatomical foundation. Initially, I and my colleagues provide the first ever *in vivo* atlas of the AL supporting a more

compelling application of morphology in the increasing number of physiological *in vivo* applications. The additional description of largely variable fixation artifacts determines the urgent necessity for *in vivo* morphology as the basis for *in vivo* physiology. Second, I used this novel morphological foundation suggesting a link between the anatomy of the AL subunits, the glomeruli, and their partially extreme functional specificity of odor ligands. By comprehensively screening several structural attributes of the glomeruli and comparing them with the respective physiological features provides a crucial step in understanding the correlation between glomerular composition and relevance. Third, the variable possibilities of glomerular function in accordance with their structural uniqueness are exemplified in the Or65a/DL3 olfactory pathway, an scarcely represented unit of the AL. Its lack of physiological characterization is challenged by the notion of it taking part in a behavioral switch in pheromone attraction of female flies after mating. Finally, the glomerulus-specific odor representations in the AL are shown to evoke a robust coding of quality and intensity in the downstream centers of olfaction. Therefore, the depicted principle of structural and functional correlation is also recurring in the glomerular inhibitory output regions, the higher brain centers in the protocerebrum such as the lateral horn.

Overview of Manuscripts

Manuscript I

Digital *in vivo* 3D atlas of the antennal lobe of *Drosophila melanogaster*

Veit Grabe, Antonia Strutz, Amelie Baschwitz, Bill S. Hansson, Silke Sachse

Published in Journal of Comparative Neurology, 15 February 2015

In this study we provided a thorough atlas of the antennal lobe in the *in vivo* situation. Further we depicted for the first time the actual impact of fixation artifacts on a flexible neuropil as the antennal lobe. Therefore we emphasized the importance of comprehensive morphological groundwork with least artificial techniques to allow reliable assignment of physiological studies.

Author contributions:

Conceived and designed experiments: V. Grabe, A. Strutz, A. Baschwitz, B. S. Hansson and S. Sachse

Performed experiments: V. Grabe, A. Strutz and A. Baschwitz

Analyzed the Data: V. Grabe, A. Baschwitz and S. Sachse

Wrote the manuscript: V. Grabe, A. Strutz, A. Baschwitz, B. S. Hansson and S. Sachse

Manuscript II

The Specific Glomerulus, or: How unique can a Glomerulus be?

Veit Grabe, Amelie Baschwitz, Hany Dweck, Bill S. Hansson and Silke Sachse

In preparation as a resource article for Neuron

This manuscript deals with glomerulus-specific morphology of the *Drosophila* antennal lobe and provides detailed screens for the most critical elements of neuropil anatomy as sensory neuron quantity, mapping, receptor specificity, *in vivo* volume and projection neuron amounts. These parameters allow a thorough analysis of the

glomerular versatility, to propose potentially important glomeruli which are underrepresented and underline their uniqueness.

Author contributions:

Conceived and designed experiments: V. Grabe, A. Baschwitz, B. S. Hansson and S. Sachse

Performed experiments: V. Grabe, A. Baschwitz and H. Dweck

Analyzed the Data: V. Grabe, A. Baschwitz, H. Dweck and S. Sachse

Wrote the manuscript: V. Grabe, A. Baschwitz, B. S. Hansson and S. Sachse

Manuscript III

Decoding Odor Attraction and Intensity in the *Drosophila* brain

Antonia Strutz, Jan Soelter, Amelie Baschwitz, Abu Farhan, Veit Grabe, Jürgen Rybak, Markus Knaden, Michael Schmucker, Bill S. Hansson, Silke Sachse

Published in eLIFE, 16 December 2014

In this study we depicted the diversity of a certain group of inhibitory projection neurons leaving the antennal lobe which are coding for valence across odor identity and concentration. The coding is maintained due to the glomerulus-specific innervation pattern in the antennal lobe and the regionalized arborizations in the lateral horn, a higher brain center in the protocerebrum. This linking of certain behavior to downstream mapping of specific odor responses points out the particular importance of glomerulus-specific output via projection neurons.

Author contributions:

Conceived and designed experiments: A. Strutz and S. Sachse

Performed experiments: A. Strutz, A. Farhan, M. Knaden, A. Baschwitz, J. Rybak and V. Grabe

Analyzed the Data: A. Strutz, J. Soelter and S. Sachse

Wrote the manuscript: A. Strutz, S. Sachse and B. S. Hansson

Manuscript IV

Pheromone exposure decreases postmating attraction and sexual receptivity in Drosophila females via Or65a olfactory neurons

Sébastien Lebreton, Veit Grabe, Aman B. Omondi, Rickard Ignell, Paul G. Becher, Bill S. Hansson, Silke Sachse and Peter Witzgall

Published online in Scientific Reports, 19 November 2014

In this study we showed that Or65a and its respective glomerulus DL3 are responsible for a behavioral switch in female Drosophila by turning off the attraction to the pheromone cis-Vaccenyl acetate. This post mating effect underlines the specific capabilities of single glomeruli to alter usually hard wired behavior and therefore points out their significance.

Author contributions:

Conceived and designed experiments: S. Lebreton, V. Grabe, A. B. Omondi, P. G. Becher, S. Sachse and P. Witzgall

Performed experiments: S. Lebreton, V. Grabe and A. B. Omondi

Analyzed the Data: S. Lebreton, V. Grabe and A. B. Omondi

Wrote the manuscript: S. Lebreton, V. Grabe, A. B. Omondi, R. Ignell, P. G. Becher, B. S. Hansson, S. Sachse and P. Witzgall

Manuscript I

Digital *In Vivo* 3D Atlas of the Antennal Lobe of *Drosophila* melanogaster

Veit Grabe, Antonia Strutz, Amelie Baschwitz, Bill S. Hansson and Silke Sachse

Published in Journal of Comparative Neurology, 15 February 2015

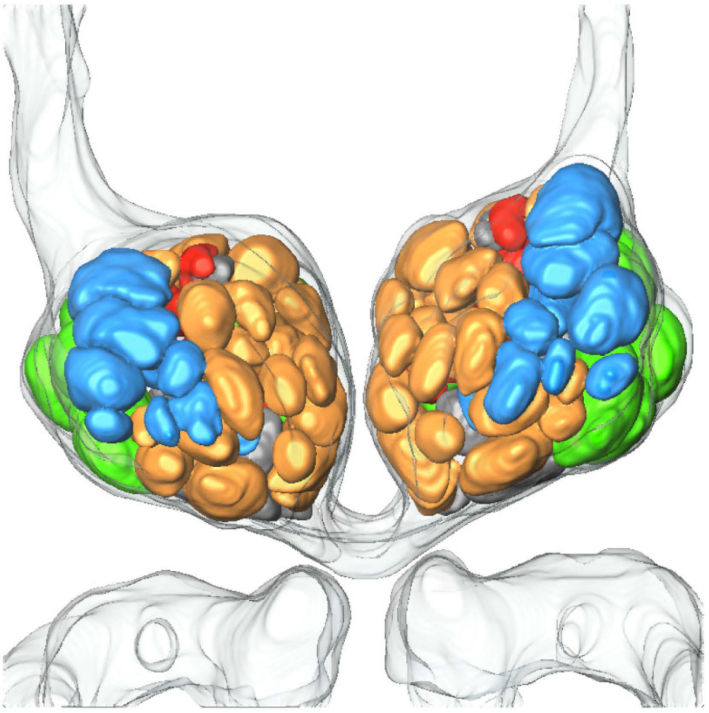

RESEARCH ARTICLE

Digital *In Vivo* 3D Atlas of the Antennal Lobe of *Drosophila melanogaster*

Veit Grabe, Antonia Strutz, Amelie Baschwitz, Bill S. Hansson, and Silke Sachse*

Department of Evolutionary Neuroethology, Max Planck Institute for Chemical Ecology, 07745 Jena, Germany

ABSTRACT

As a model for primary olfactory perception, the antennal lobe (AL) of *Drosophila melanogaster* is among the most thoroughly investigated and well-understood neuronal structures. Most studies investigating the functional properties and neuronal wiring of the AL are conducted *in vivo*, although so far the AL morphology has been mainly analyzed *in vitro*. Identifying the morphological subunits of the AL—the olfactory glomeruli—is usually done using *in vitro* AL atlases. However, the dissection and fixation procedure causes not only strong volumetric but also geometrical modifications; the result is unpredictable dislocation and a distortion of the AL glomeruli between the *in vitro* and *in vivo* brains. Hence, to characterize these artifacts, which are caused by *in vitro* processing, and to reliably identify glomeruli for *in vivo* applications, we generated a transgenic fly that expresses the red fluorescent protein DsRed directly fused to the presynaptic protein *n*-synaptobrevin, under the control of the pan-neuronal promotor elav to label the neuropil in the live animal. Using this fly line, we generated a digital 3D atlas of the live *Drosophila* AL; this atlas, the first of its kind, provides an excellent geometric match for *in vivo* studies. We verified the identity of 63% of AL glomeruli by mapping the projections of 34 GAL4-lines of individual chemosensory receptor genes. Moreover, we characterized the innervation patterns of the two most frequently used GAL4-lines in olfactory research: Orco- and GH146-GAL4. The new *in vivo* AL atlas will be accessible online to the neuroscience community. J. Comp. Neurol. 000:000–000, 2014.

INDEXING TERMS: *Drosophila melanogaster*; olfactory system; glomeruli; *in vivo* neuropil marker; *in vitro* artifacts

The chemical environment consists of a vast and quickly changing array of volatile cues, each of which has different ecological relevance. To orient itself within this complex environment, the vinegar fly *Drosophila melanogaster* possesses an elaborate olfactory system consisting on the periphery of a set of four classes of sensilla present in stereotypical patterns on the third antennal segment and the maxillary palp (Vosshall and Stocker, 2007). Each type of sensillum—antennal basiconic, trichoid, coeloconic, or palp basiconic—houses from one to four olfactory sensory neurons (OSNs). Each OSN expresses a repertoire of one or two chemosensory receptors (CRs); each CR has a unique molecular receptive range (Shanbhag et al., 1999; de Bruyne et al., 2001; Hallem and Carlson, 2006; Silbering et al., 2011). The information gathered on volatile odorants intercepted by the antenna is forwarded to the primary center of the olfactory pathway, the antennal lobe (AL). The *Drosophila* AL represents one of the most comprehensively investigated neuronal structures in nature (Stocker et al., 1990; Masse et al., 2009; Galizia and Sachse, 2010; Hansson et al., 2010; Wilson, 2013). It consists of discrete neuropil subunits, called olfactory glomeruli, which are conserved among individuals and can be identified by their specific position and size (Laissue et al., 1999). Each glomerulus collects OSN axons of only one type due to the strict convergence of OSNs expressing the same CR type (Gao et al., 2000; Vosshall et al., 2000).

In order to study the odor-coding mechanisms of the AL, a broad spectrum of *in vivo* or *ex vivo* techniques, such as the photolesioning of specified tracts (Liang et al., 2013), the photoactivation of single neurons

The first two authors contributed equally to this work.

Grant sponsor: Federal Ministry of Research and Education (BMBF); Grant sponsor: Max Planck Society (MPG).

*CORRESPONDENCE TO: Silke Sachse, Department of Evolutionary Neuroethology, Max Planck Institute for Chemical Ecology, Hans-Knöll-Str. 8, 07745 Jena, Germany. E-mail: ssachse@ice.mpg.de

Received September 4, 2014; Revised October 6, 2014; Accepted October 14, 2014.
DOI 10.1002/cne.23697
Published online Month 00, 2014 in Wiley Online Library (wileyonlinelibrary.com)

(Datta et al., 2008; Ruta et al., 2010; Caron et al., 2013), patch clamp recordings (Wilson et al., 2004; Chou et al., 2010; Seki et al., 2010), as well as functional imaging (Fiala et al., 2002; Ng et al., 2002; Wang et al., 2003; Silbering et al., 2008; Stökl et al., 2010; Schubert et al., 2014) has been established over the last years. All these techniques demand an adequate atlas for the identification of the anatomical substructures–the glomeruli–so that they can be applied *in vivo*. However, all previous 3D atlases of the *Drosophila* AL have derived from *in vitro* data (Stocker et al., 1983; Laissue et al., 1999; Couto et al., 2005; Endo et al., 2007; Silbering et al., 2011; Tanaka et al., 2012). Since the dissection and fixation procedure causes not only strong volumetric but also geometric modifications (Ma et al., 2008), the result is the unpredictable dislocation and distortion of the AL glomeruli between the *in vitro* and *in vivo* brains. In order to reliably identify glomeruli in the live fly brain, an atlas of the *in vivo* AL is essential.

In this study we present the first digital 3D atlas of the live *Drosophila* AL. To identify glomeruli *in vivo*, we generated a transgenic fly that expresses the red fluorescent protein DsRed directly fused to the presynaptic protein *n*-synaptobrevin, under the control of the panneuronal promotor elav (Yao et al., 1993) to selectively label the neuropil in the live animal. In addition, we expressed a green fluorescent protein under the control of 34 individual chemosensory receptor genes (Couto et al., 2005; Fishilevich and Vosshall, 2005; Silbering et al., 2011) to confirm the correct identification of most glomeruli by its type of OSN innervation. Once quantified and compared to *in vitro* data, the new *in vivo* data were used to demonstrate nontrivial and unexpected structural deformations and distortions of the majority of glomeruli caused by *in vitro* processing. These results support the need for a digital *in vivo* 3D atlas of the fly AL to find geometric matches for *in vivo* studies. Furthermore, we characterized the glomerular innervation patterns of the two most frequently used GAL4-lines in olfactory research: Orco-GAL4 as well as GH146-GAL4. The new *in vivo* 3D AL atlas will be publicly accessible to the neuroscience community through our website (www.ice.mpg.de/ext/invivoALatlas.html).

MATERIALS AND METHODS

Fly lines

P[END1-2] (elav *n*-synaptobrevin-DsRed 1-2) was generated using a modified pCaST-elav-GAL4AD vector (plasmid 15307, Addgene, Cambridge, MA). The GAD domain present in the original vector was excised using NotI and FspAI enzymes; the FspAI recognition site was located within the DsRed coding sequence. A DNA oligonucleotide containing a modified *n*-synaptobrevin-coding ORF (*n*-syb) (DiAntonio et al., 1993), upstream of a sequence identical to the excised DsRed fragment, and a *Drosophila* Kozak site (caaaATG) and recognition sites for NotI and FspAI were synthesized and inserted into the vector. The *n*-syb contains one silent mutation (C168T) to eliminate an FspAI-recognition site within the fragment. Excision, synthesis, and ligation were performed by MWG Eurofins (Ebersberg, Germany). The resulting plasmid was amplified in *E. coli* (One Shot Top10 *E. coli*, Invitrogen, Eugene, OR) and purified using a Qiagen midi-prep kit (Qiagen, Hilden, Germany). Embryo transformation to generate transgenic lines was performed by Aktogen (Cambridge, UK).

All fly stocks were maintained on conventional cornmeal-agar-molasses medium under a 12-hour light: dark cycle at 25°C. Transgenic lines used were as follows: Gr21a-GAL4 (Scott et al., 2001), Ir40a-GAL4 (RRID:BDSC_41727), Ir41a-GAL4 (RRID:BDSC_41749), Ir75a-GAL4 (RRID:BDSC_41748 (Silbering et al., 2011)), Ir76a-GAL4 (RRID:BDSC_41735 (Benton et al., 2009)), Ir92a-GAL4 (RRID:BDSC_41733 (Abuin et al., 2011)), Or10a-GAL4 (RRID:BDSC_9944), Or13a-GAL4 (RRID:BDSC_23886), Or22a-GAL4 (RRID:BDSC_9951), Or33c-GAL4 (RRID:BDSC_9966), Or35a-GAL4 (RRID:BDSC_9968), Or42a-GAL4 (RRID:BDSC_9969), Or42b-GAL4 (RRID:BDSC_9972), Or43a-GAL4 (RRID:BDSC_9973), Or43b-GAL4 (RRID:BDSC_23895), Or46aA-GAL4 (RRID:BDSC_9979), Or47a-GAL4 (RRID:BDSC_9982), Or47b-GAL4 (RRID:BDSC_9984), Or49a-GAL4 (RRID:BDSC_9985), Or56a-GAL4 (RRID:BDSC_23896), Or59b-GAL4 (RRID:BDSC_23897), Or59c-GAL4 (RRID:BDSC_23899), Or67a-GAL4 (RRID:BDSC_23904), Or67c-GAL4 (RRID:BDSC_24856), Or69a-GAL4 (RRID:BDSC_10000), Or71a-GAL4 (RRID:BDSC_23121), Or83c-GAL4 (RRID:BDSC_23132), Or85a-GAL4 (RRID:BDSC_24461), Or85b-GAL4 (RRID:BDSC_23912), Or85d-GAL4 (RRID:BDSC_24148), Or88a-GAL4 (RRID:BDSC_23137), Or92a-GAL4 (RRID:BDSC_23139), Or98a-GAL4 (RRID:BDSC_23141 (Vosshall et al., 2000; Fishilevich and Vosshall, 2005)), Or67d-GAL4 (RRID:BDSC_23906 (Kurtovic et al., 2007)), UAS-GCaMP3.0 (RRID:BDSC_32116 (Tian et al., 2009)), GH146-GAL4 (RRID:BDSC_30026 (Stocker et al., 1997)), Orco-GAL4 (RRID:BDSC_26818 (Larsson et al., 2004)).

In vivo antenna and brain preparation

Between 3 to 6 days after hatching, female flies were anesthetized with CO_2. In order to scan labeled OSN somata on the third segment of the antenna (Fig. 1D), the whole antenna was gently severed using forceps and transferred to a drop of saline with Triton-X on an object holder. The antennae were then gathered

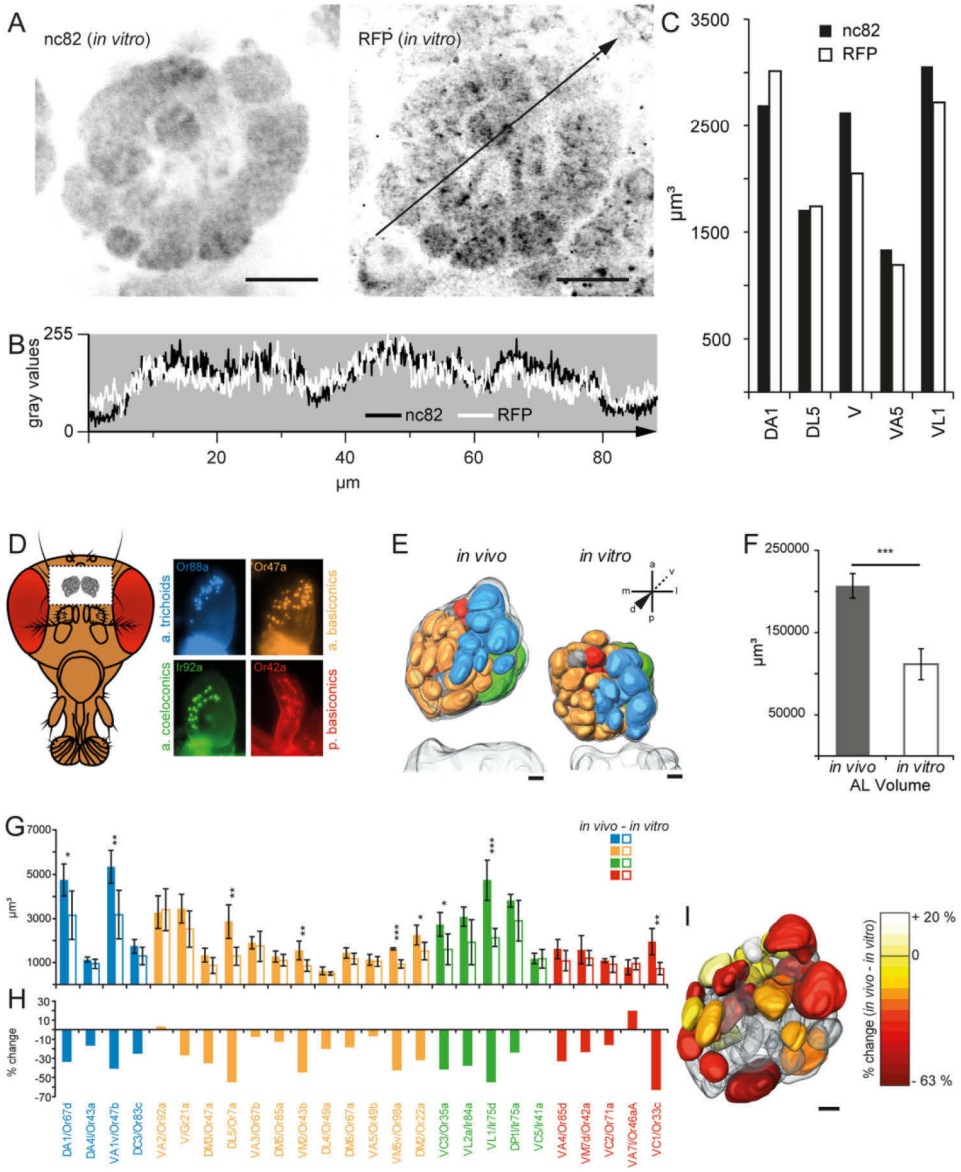

Figure 1. Characterization of volumetric differences between *in vivo* and *in vitro* antennal lobes. **A:** Immuno double staining of an *in vitro* *Drosophila* antennal lobe (AL) with nc82 (left) and anti-RFP (right) in inverted gray values. Both stainings visualize the glomerular borders in a comparable manner. **B:** Profile of gray values along a transverse line across the AL as shown in (A) of the nc82 (black line) and anti-RFP (white line) double-stained AL. **C:** Volume comparison of a subset of five glomeruli between the nc82 (black) and anti-RFP (white) staining in one animal. **D:** Left, schematic of the head of *D. melanogaster* with a superimposed window depicting the *in vivo* dissection area and position of the ALs. Right, images of the olfactory organs showing the distribution of four sensillum types representative for the different classes of sensilla acquired with specific GAL4 receptor lines (blue: antennal trichoids (Or88a-GAL4 / type: At4), yellow: antennal basiconics (Or47a-GAL4 / type: Ab5), green: antennal coeloconics (Ir92a-GAL4 / type: Ac1), red: palp basiconics (Or42a-GAL4 / type: Pb1)). **E:** Dorsal view on two 3D-reconstructed ALs with individual glomeruli. The left AL derives from an *in vivo* scan of the END1-2 neuropil labeling; the one on the right represents an AL after *in vitro* processing and nc82 antibody staining. The color code denotes the glomerular innervation by the four sensilla classes as shown in (D). **F:** Comparison of the averaged whole AL volume *in vivo* ($n = 4$) and *in vitro* ($n = 7$) based on 3D-reconstructions as shown in (E). Error bars represent SD; $***P < 0.001$, unpaired *t*-test. **G:** Comparison of the glomerulus-specific volume of *in vivo* (filled columns, $n = 4$) and *in vitro* processed ALs (empty columns, $n = 7$) based on 3D-reconstructions as shown in (E). Error bars represent SD; $*P < 0.5$, $**P < 0.1$, $***P < 0.001$, unpaired *t*-test. The color code indicates the classes of sensilla as shown in (D). **H:** Percentage of the glomerulus-specific volume change between the *in vivo* and *in vitro* datasets indicating an unequal fixation effect. **I:** Glomerulus-specific volume changes are heat-mapped onto the reconstructed *in vivo* AL. White represents an increase, yellow no change, and red a decrease in volume. For glomerular identities please see Fig. 5E. Scale bars = 20 µm.

and embedded in VectaShield (Vector Laboratories, Burlingame, CA) between a 22 × 22 mm and a 24 × 60 mm object slide. Scans were carried out with an Axio Imager.Z1 (Carl Zeiss, Jena, Germany) using a 20× water immersion objective (W Plan-Apochromat 20×/0.8, Carl Zeiss) from both sides of each antenna. The *in vivo* fly brain dissection was carried out as previously described (Strutz et al., 2012) in saline (130 mM NaCl, 5 mM KCl, 2 mM $MgCl_2$, 2 mM $CaCl_2$, 36 mM saccharose, and 5 mM Hepes) at pH 7.3 adjusted with 1 M NaOH.

In vitro immunohistochemistry

Female flies aged between 3 to 6 days after hatching were used. Fly brains were dissected and stained as described by Wu and Luo (2006) and scanned with a Zeiss LSM 710 NLO confocal microscope (Carl Zeiss, Jena, Germany) set on a Smart Table UT2 (Newport, Irvine, CA) using a 40× water immersions objective (W Plan-Apochromat 40×/1.0 DIC M27; Carl Zeiss). Primary antibodies were rabbit α-RFP (1:100, Invitrogen, Eugene, OR; Molecular Probes Cat. no. R10367 RRID:AB_2315269) against DsRed and mouse α-nc82 (1:30; Developmental Studies Hybridoma Bank [DSHB], Iowa City, IA; Cat. no. nc82 RRID:AB_528108). All primary antibodies are characterized below. Secondary antibodies were Alexa Fluor 633, goat anti-rabbit IgG (Invitrogen, Eugene, OR, Life Technologies; Cat. no. A21070 RRID:AB_10562894) and Alexa Fluor 488, goat anti-mouse IgG (both 1:250, Invitrogen, Life Technologies Cat. no. A11001 RRID:AB_10566289) (Fig. 1A-C). For the generation of the *in vitro* AL atlas (Fig. 1E), primary antibody was mouse α-nc82 (1:30; DSHB), secondary antibody was Alexa Fluor 488, goat anti-mouse IgG (1:200, Invitrogen). Z-stacks were scanned at 1-µm intervals at 512 × 512 or 1024 × 1024 pixel resolution.

We used monoclonal nc82 raised in a hybridoma screen against fly head homogenate. It was characterized by Daniels et al. (2008) with respect to labeling neuropil compartments in larval and adult *Drosophila*. Polyclonal RFP antibody was raised against full-length recombinant denatured and nondenatured TagRFP and characterized by Marcucci et al. (2011). No immunolabeling was observed with wildtype fly brains (data not shown).

3D reconstruction and identification of glomeruli

Confocal scans were obtained with a ZEISS LSM 710 NLO using a 40× water immersions objective (W Plan-Apochromat 40×/1.0 DIC M27; Carl Zeiss). Individual glomeruli were reconstructed using the segmentation software AMIRA 5.5.0 (FEI Visualization Sciences Group, Burlington, MA; Advanced 3D Visualization and Volume Modeling, RRID:nif-0000-00262). The identification of glomeruli was verified by *in vivo* scans using 34 specific receptor GAL4-lines crossed to UAS-GCaMP3.0 and combined with the END1-2 neuropil labeling. We analyzed scans of at least three specimens for each GAL4 receptor line. Using information on the voxel size from the LSM scans as well as the number of voxels labeled for each neuropil, we calculated the volume of the glomeruli and the whole AL.

We reconstructed *in vivo* ALs including all glomeruli of four female flies and selected one representative AL on the basis of the best signal-to-noise ratio, i.e., the clearest END1-2 staining, as the template for the *in vivo* AL atlas. The other specimens were used as references. All 54 glomeruli that are included in the *in vivo* atlas could be identified unambiguously in all reference specimens. Although our *in vivo* AL atlas derives from a female AL, it can be used as a template for male flies as well, since it has been shown that the glomerular identity is not clearly sexually dimorphic (Laissue et al., 1999). The sexual dimorphism that has been observed so far affects the volume of the three glomeruli DA1, VA1v, and VL2a (Kondoh et al., 2003; Stockinger et al., 2005). These glomeruli are innervated by OSNs that express the male-specific fruitless gene and are larger in males than in females. However, since these studies derive from *in vitro* brain dissections, it still remains to be elucidated whether the described dimorphism holds true for the *in vivo* condition or whether more striking effects will be observed.

Generation of a 3D PDF of the *in vivo* AL atlas followed the described procedure (Ruthensteiner and Heβ, 2008; Rybak et al., 2010). Reconstructed surfaces from AMIRA were imported to FIJI (ImageJ 1.48r, National Institutes of Health, Bethesda, MD; Fiji, RRID:SciRes_000137) and transformed into wavefront format (.obj). Sorting and grouping of the glomerular materials was done in Deep Exploration (5.0.5, Right Hemisphere, San Ramon, CA) saved in u3d-format. Final adjustments of visualization parameters were done in Adobe Acrobat X Pro (Adobe Systems, San Jose, CA).

Statistical analyses

Central coordinates (xyz) for each glomerulus were extracted from the reconstructed specimens' 3D labels via the "MaterialStatistics" tool in AMIRA. Reconstructed ALs were aligned beforehand by inverting corresponding axes, turning all ALs into right ones facing the same direction. Furthermore, distribution along the x-, y-, and z-axes was aligned, i.e., all *in vivo* and *in vitro* ALs were registered in a Cartesian coordinate

system of the same dimensions. The single axes are oriented in mediolateral (x), anteroposterior (y), and dorsoventral (z) directions through the AL. We calculated the minimal and maximal glomerular central coordinates along each axis for each individual AL as well as the average of these minimal and maximal coordinates across all *in vivo* and *in vitro* ALs separately. The difference between the individual and average minimal and maximal values was averaged per specimen, displaying the necessary shift along all three axes for every glomerulus per specimen to align the entire AL. This was done by subtracting the average per axis per specimen from each of its central glomerular coordinates. The same procedure was carried out for the averaged *in vivo* and *in vitro* ALs. Distances between central glomeruli coordinates were calculated as Euclidean distances in the Cartesian coordinate system for the *in vivo* and *in vitro* averaged ALs:

$$ED=\sqrt{(x_2-x_1)^2+(y_2-y_1)^2+(z_2-z_1)^2}$$

To eliminate the impact of the overall shrinkage of the ALs on the relative change, distances were normalized to the maximum distance in the average *in vivo* and *in vitro* AL datasets, respectively. To calculate the position change between a pair of glomeruli from *in vivo* to *in vitro* we placed one of the two glomeruli in the center of the coordinate system ($glom_0$) by subtracting its xyz coordinates from all other glomeruli in all specimens of the *in vivo* and *in vitro* dataset. Then we calculated the cosine of the angle of the position vector between $glom_0$ and another glomerulus *in vivo* ($coor_1$) and *in vitro* ($coor_2$). Based on the cosine we calculated the radian measure of the angle using the arc cosine and multiplied the radian with $180/\pi$, converting it to degree. All analyses were done in Excel.

$$\cos\varphi=\frac{coor_1 * coor_2}{|coor_1| * |coor_2|}$$

$$\cos\varphi=\frac{(x_1 * x_2+y_1 * y_2+z_1 * z_2)}{\sqrt{x_1^2+y_1^2+z_1^2} * \sqrt{x_2^2+y_2^2+z_2^2}}$$

RESULTS

In vivo neuropil labeling

We generated a transgenic fly line that expresses the presynaptic protein *n*-synaptobrevin directly fused to the red fluorescent protein DsRed under the control of the pan-neuronal promotor elav (Yao et al., 1993), subsequently called END1-2. Our *in vivo* END1-2 labeling features a comparable neuropil staining as the most commonly used neuropil-specific monoclonal antibody nc82 *in vitro* (Hofbauer, 1991; Laissue et al., 1999; Rein et al., 2002). In order to show that the END1-2 neuropil labeling correlates with the nc82 antibody staining, we carried out a double *in vitro* immunostaining with anti-RFP against DsRed and nc82 (Fig. 1A). Both antibodies show a distinct but comparable staining of glomeruli. To quantify the distribution of tagged antibodies, we analyzed gray values across the AL. Although the stains are not completely overlapping, in their gray value profiles similar glomerular borders can be seen (Fig. 1B). In addition, staining nc82 and anti-RFP results in similar glomerular volumes as analyzed for a subset of five glomeruli (Fig. 1C).

We next verified that the protein DsRed itself is not influencing the glomerular volume *in vivo*, since it has been shown to oligomerize (Baird et al., 2000). In order to visualize individual glomeruli in flies that are END1-2 negative, we selectively expressed UAS-GCaMP3.0 in Or22a-OSNs. Subsequently, we compared the volume of the respective glomerulus DM2 with and without the expression of END1-2. The results do not reveal any significant difference in volume ($n = 3$, data not shown).

Volumetric fixation effects on the antennal lobe

In order to analyze the effects caused by *in vitro* processing, we first quantified volumetric differences between the *in vivo* and *in vitro* AL morphology. To reduce the preparatory artifacts onto the brain to a minimum, we executed an *in vivo* preparation usually used for functional imaging (Silbering et al., 2012; Strutz et al., 2012). By immobilizing the fly in a Plexiglas stage and opening the head capsule under saline, we were able to remove the tracheal sacks and fat tissue to gain free access to the ALs; during this time, the brain was retained in the head capsule and the antennal nerves remained intact (Fig. 1D). Using the *n*-synaptobrevin::DsRed labeling as a neuropil marker in the live fly, we scanned the brain with the confocal microscope and reconstructed the whole AL, including all glomeruli, *in vivo* (Fig. 1E, left). In parallel, we carried out antibody staining according to Wu and Luo (2006) with the neuropil marker nc82 *in vitro* as well as scanned and reconstructed these *in vitro* ALs using the same procedures as for the *in vivo* data (Fig. 1E, right). In addition, to facilitate the comparison between the *in vivo* and *in vitro* generated datasets, we reconstructed the mushroom body β/β'- and γ lobes as anatomical landmarks. As a quantitative measure, we used the number of voxels in the reconstructed ALs and calculated the total AL volume based on their dimensions (Fig. 1F). A comparison of the *in vivo* and *in vitro* datasets shows that the AL volume decreased by about 43% due to the dissection and fixation procedure. The shrinkage of the whole AL neuropil *in vitro*

would not impair the identification of glomeruli for *in vivo* experiments, if the glomeruli were evenly affected. We therefore quantified and compared the volume of individual glomeruli for the *in vivo* and *in vitro* dataset.

Glomerulus-specific analysis of volumetric differences between *in vivo* and *in vitro* brains

In order to ensure correct glomerulus identification, the END1-2 flies were recombined with UAS-GCaMP3.0 and crossed with 34 receptor GAL4-lines each, i.e., two-thirds of glomeruli were thus labeled according to their corresponding OSN innervation (Couto et al., 2005; Fishilevich and Vosshall, 2005; Silbering et al., 2011). For the detailed quantification of the fixation artifacts, we selected a group of 26 representative glomeruli spanning throughout the AL neuropil and covering different classes of sensilla. Notably, we observed a clear unequal reduction of these glomerular volumes due to fixation (Fig. 1G). Whereas some glomeruli revealed a volume reduction of up to 60% (e.g., VC1) due to *in vitro* processing, other glomeruli shrank by 30% (e.g., DA1) or retained their volume (e.g., VA2) (Fig. 1H). By mapping these glomerulus-specific volumetric effects onto the reconstructed *in vivo* AL, it is obvious that the shrinkage correlates neither with the specific position nor with the total volume of the individual glomeruli (Fig. 1I). Since every glomerulus is shrinking to a different degree, in the next step we analyzed whether the *in vitro* processing caused any geometrical modifications of the glomerular arrangement.

Effect of fixation on the AL geometry

To evaluate possible dislocations of glomeruli following *in vitro* processing (Fig. 2A), we determined Euclidean distances by giving each glomerulus an x, y, and z-coordinate representing its center in the Cartesian system (see Materials and Methods). For each glomerulus, center-to-center distances were calculated in relation to every other glomerulus and subsequently averaged per glomerulus over the *in vivo* and *in vitro* datasets. We then normalized the Euclidean distances to the maximum glomerular distance per dataset and subtracted the normalized *in vivo* distance from the *in vitro* distance. Hence, a negative Δ *Distance* represents the approach of two glomeruli, while a positive Δ *Distance* reveals the increased interglomerular distance due to *in vitro* processing (Fig. 2B). Averaging the positive and negative distance changes per glomerulus over all *in vivo* and *in vitro* specimens, respectively (Fig. 2C, $n = 4$-7), shows various kinds of strong glomerular dislocations; for example, glomeruli VA2 and VM2 increase their distance to most other glomeruli in the *in vitro* dataset, while DL5 and DP1l show the opposite effect. Glomerulus VA1v is affected in both directions, as it ranks highest for an increased as well as decreased interglomerular distance change. Mapping these data onto the reconstructed *in vivo* AL illustrates the spatial distribution of the various effects of glomerular dislocation for the whole AL (Fig. 2D,E). One major reason for the strong geometrical modifications between the *in vivo* and *in vitro* AL is most likely the transection of the antennal nerve, a process in which the brain is extracted from the head capsule. Since the nerve provides tension to the AL, severing it deforms the whole AL neuropil (Fig. 1E).

Even though some glomeruli do not reveal pronounced interglomerular dislocation effects (e.g., DA4l, DM5, and VM7d), we cannot exclude that their position is affected without substantially changing their interglomerular distance. To estimate glomerular distortions independent of their distance, we determined the angle between the two position vectors of each possible glomerular combination for the *in vivo* and *in vitro* datasets (Fig. 2F,G). In order to obtain a glomerulus-specific estimation of the overall angle between *in vivo* and *in vitro* vectors, we calculated the average angle per glomerulus (Fig. 2H). Most glomeruli exhibit an angle above 30°, meaning that the positional arrangement of most glomeruli is considerably affected by the *in vitro* processing. Again, mapping these glomerular distortions on the reconstructed AL (Fig. 2I) reveals that the posterior area is affected strongest. In summary, due to the strong and so far unpredictable fixation artifacts in AL volume and geometry, a digital *in vivo* 3D atlas of the fly AL is essential in order to identify individual glomeruli in *in vivo* studies.

In vivo atlas of the antennal lobe

Previous *in vitro* studies established several AL atlases for *Drosophila* with varying nomenclature and numbers of glomeruli (Stocker et al., 1983; Laissue et al., 1999; Couto et al., 2005; Endo et al., 2007; Silbering et al., 2011). We are referring to the most recent nomenclature from Tanaka et al. (2012), who describe glomerulus VM7 as VM7d and the former unnamed glomerulus "1" (Couto et al., 2005) as its ventral counterpart VM7v. The split of glomerulus VC3 into VC3l and VC3m could not be confirmed at a morphological level, since both parts are innervated by OSNs expressing Or35a (Silbering et al., 2011). We therefore refer to this glomerulus as VC3. Even though no OR is yet known for glomerulus VA7m, we kept the anatomical division in the lateral and medial parts, since the two parts represent different subunits defined by the

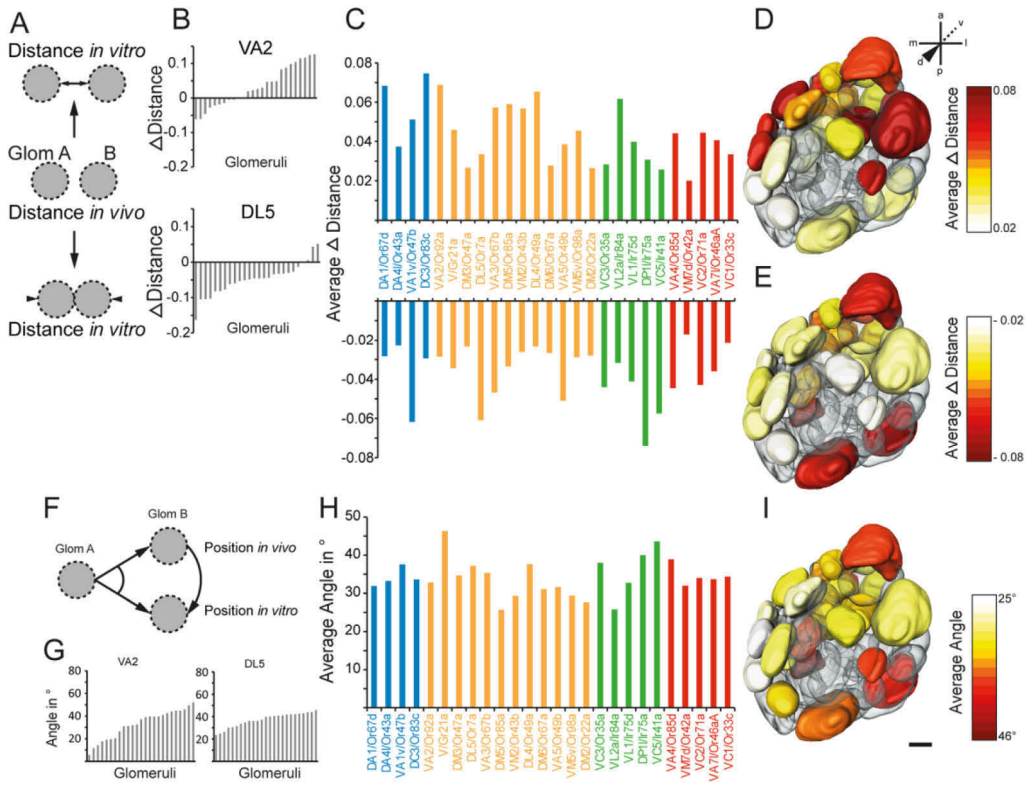

Figure 2. *In vitro* dissection and fixation leads to geometrical modifications of various glomeruli. **A:** Schematic of the investigated Euclidean distance changes between glomeruli as shown in B–E (for details, see Materials and Methods). **B:** Example of normalized center-to-center distance changes (Δ *Distance*) of two representative glomeruli in relation to all other glomeruli between the *in vivo* and *in vitro* dataset. **C:** Averaged positive (top) and negative (bottom) normalized distance changes per glomerulus in relation to all other glomeruli between all *in vivo* ($n = 4$) and *in vitro* specimens ($n = 7$). Positive values indicate an increased interglomerular distance; negative values represent a decrease. Various glomeruli display strong positive and/or negative distance changes underlining nonuniform dislocations of the glomerular arrangement. The color code indicates the classes of sensilla as shown in Figure 1. **D,E:** Positive (top) and negative (bottom) distance changes are heat-mapped onto the reconstructed *in vivo* AL. **F:** Schematic of the investigated angle between two position vectors of each glomerular pair as shown in (G–I). **G:** Example of calculated angles of two representative glomeruli between their positional vectors in relation to all other glomeruli of the *in vivo* and *in vitro* datasets. **H:** Averaged angles between the *in vivo* ($n = 4$) and *in vitro* ($n = 7$) positional vectors for each glomerulus. The positional arrangement of most glomeruli is considerably affected by dissection and *in vitro* processing. **I:** Averaged angles between *in vivo* and *in vitro* positional vectors are heat-mapped onto the reconstructed AL. For glomerular identities please see Fig. 5E. Scale bar = 20 μm.

convergence of OSNs expressing Or46aA to the VA7l part (Couto et al., 2005). Moreover, we fused glomerulus VP1 with glomerulus VM6, since they are morphologically not distinguishable and both are said to share most of their projection neurons (Yu et al., 2010), indicating their uniform nature. In addition, our *in vivo* AL atlas comprises the often neglected glomeruli VP1 and VP4 (Silbering et al., 2011; Kain et al., 2013), although their exact morphology is cryptic without the simultaneous expression of Ir40a-GAL4 that we employed for reliable identification. We also included the thermosensory glomeruli VP2 and VP3 in our AL atlas; these appear as part of the AL rather than as part of the proximal antennal protocerebrum as described previously (Gallio et al., 2011), since their input neurons are ascending along with the OSNs of other glomeruli.

By selectively expressing 34 receptor GAL4-lines combined with GCaMP3.0 into the END1-2 background (see Materials and Methods), we generated a new digital 3D atlas of the *in vivo Drosophila* AL (Fig. 3). First, we selected the most suitable confocal stack out of 13 scans of the END1-2 neuropil labeling (Fig. 3A) as a

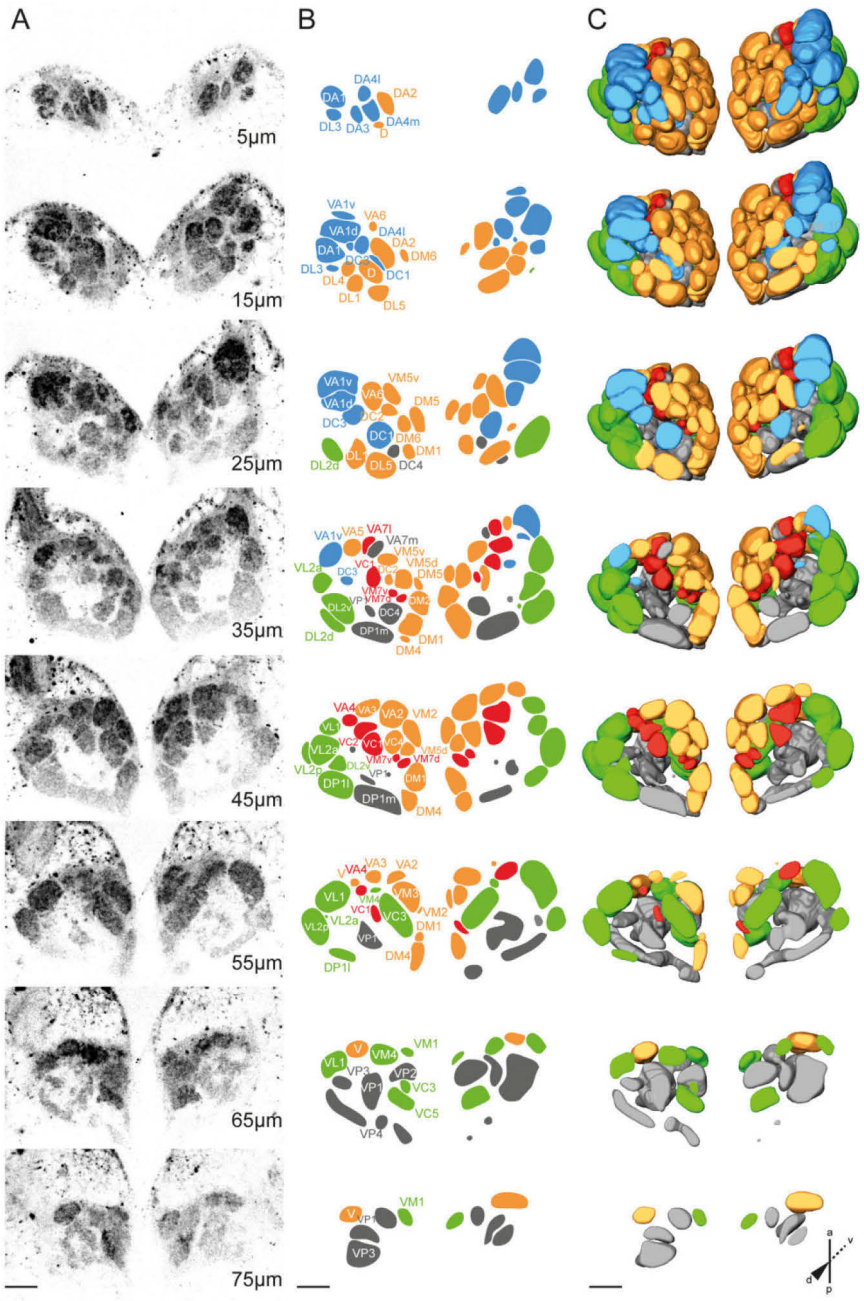

Figure 3. *In vivo* 3D atlas of the *Drosophila* antennal lobe. **A:** Representative confocal stack of an *in vivo* AL expressing the END1–2 neuropil labeling. Eight planes from dorsal to ventral (top to bottom) through a female AL are shown at 10-µm intervals displayed in an inverted gray scale. **B:** Identified and reconstructed glomeruli of the confocal stack shown in (A). **C:** Dorsal view on the 3D-reconstruction of the labels shown in (B). The glomeruli are successively removed as the scan moves from dorsal to ventral through the AL. The color code indicates the classes of sensilla as shown in Figure 1, extended by glomeruli that receive input from the grooved coeloconic sensilla of the sacculus and the aristal shaft (shown in gray). Scale bars = 20 µm.

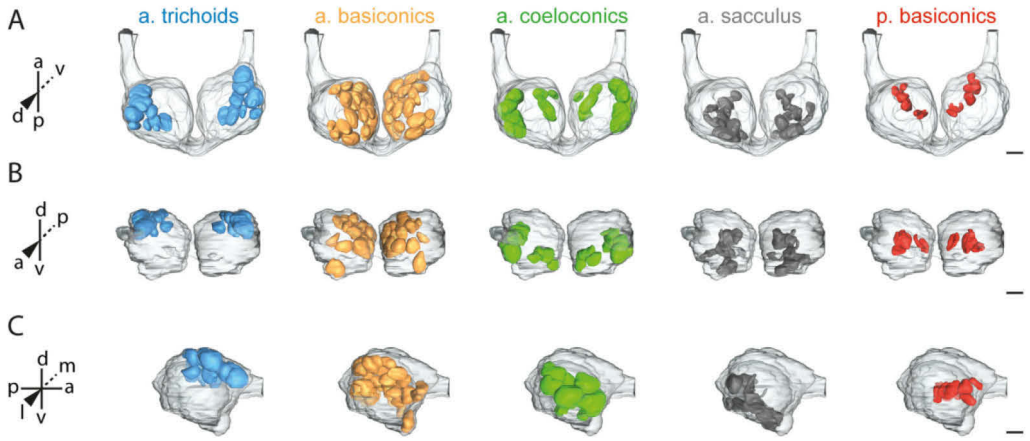

Figure 4. Segregation of the classes of sensilla in the AL. **A–C:** Innervation of glomeruli separately represented for each class of sensillum of the corresponding OSN class in a dorsal (A), frontal (B), and lateral (C) view. The color code refers to Fig. 3. For glomerular identities please see Figure 5E–G. Scale bars = 20 μm.

template for 3D reconstructions, based on the best signal-to-noise ratio throughout the entire scanned distance of ~100 μm. To securely identify the reconstructed glomeruli in the selected stack, in the initial scans we employed specific receptor GAL4-lines for 63% of the AL glomeruli and used the stereotypical OSN innervation patterns and their positions to verify glomerular identity. Based on the precise identification via the receptor GAL4-lines, we morphologically identified the remaining neuropils comprising a total of 54 glomeruli (Fig. 3B). The template scan was then properly reconstructed, improved through the OSN mapping and morphological assignment, and color-coded according to the class of sensilla projecting onto each glomerulus (Fig. 3C). In addition, we performed complete 3D glomerular reconstructions of three further specimens and used them as references. All 54 glomeruli that are included in the *in vivo* AL atlas could be identified unambiguously in all of these reference specimens.

Application of the *in vivo* AL atlas

Our *in vivo* AL atlas represents an accurate match for *in vivo* applications and provides a novel basis for reconsidering neuroanatomical features as exemplified by the glomerular clustering according to the class of sensilla of the OSN input (Couto et al., 2005). The discovery of ionotropic glutamate receptors in insects (IRs) (Benton et al., 2009) underlined this functional and morphological subdivision of the AL and revealed a clear segregation of glomeruli innervated by olfactory receptors (ORs) and IRs (Silbering et al., 2011). Revisiting this feature for the *in vivo* condition, the above-described segregation is present also in the live AL (Fig. 4). In addition, the glomerulus cluster that receives input from coeloconic sensilla can be further divided into two subtypes: Glomeruli that are innervated by OSNs from the sacculus expressing Ir40a and Ir64a (Ai et al., 2010; Silbering et al., 2011) are located separately from glomeruli receiving input from the remaining coeloconic sensilla. This segregation is most obvious in the lateral view of the AL (Fig. 4C), where glomeruli originating in the sacculus and situated most ventroposteriorly are followed in dorsoanterior direction by three layers of glomeruli receiving input from coeloconic, basiconic (antenna and palp), and trichoid sensilla.

As another example, we demonstrate the application of two of the most frequently used GAL4-lines in olfactory research: Orco-GAL4 and GH146-GAL4. The Orco-GAL4 line labels all OSNs that express the coreceptor Orco, formerly known as Or83b (Larsson et al., 2004); the enhancer trap line GH146-GAL4 labels the majority of uniglomerular projection neurons (PNs) in the AL (Stocker et al., 1997). Confocal *in vivo* scans of the Orco-GAL4 line combined with END1-2 and GCaMP3.0 reveal the clear innervation of the majority of glomeruli (39 glomeruli out of 54); the IR-positive glomeruli and the thermosensory center consisting of VP2 and VP3 are not labeled (Fig. 5A,B). The Orco-negative glomeruli group at the ventroposterior region of the AL, as they are congruent with the glomeruli innervated by coeloconic sensilla. Similarly, the innervation of the GH146-GAL4 line labels a total of 39 glomeruli; however, only

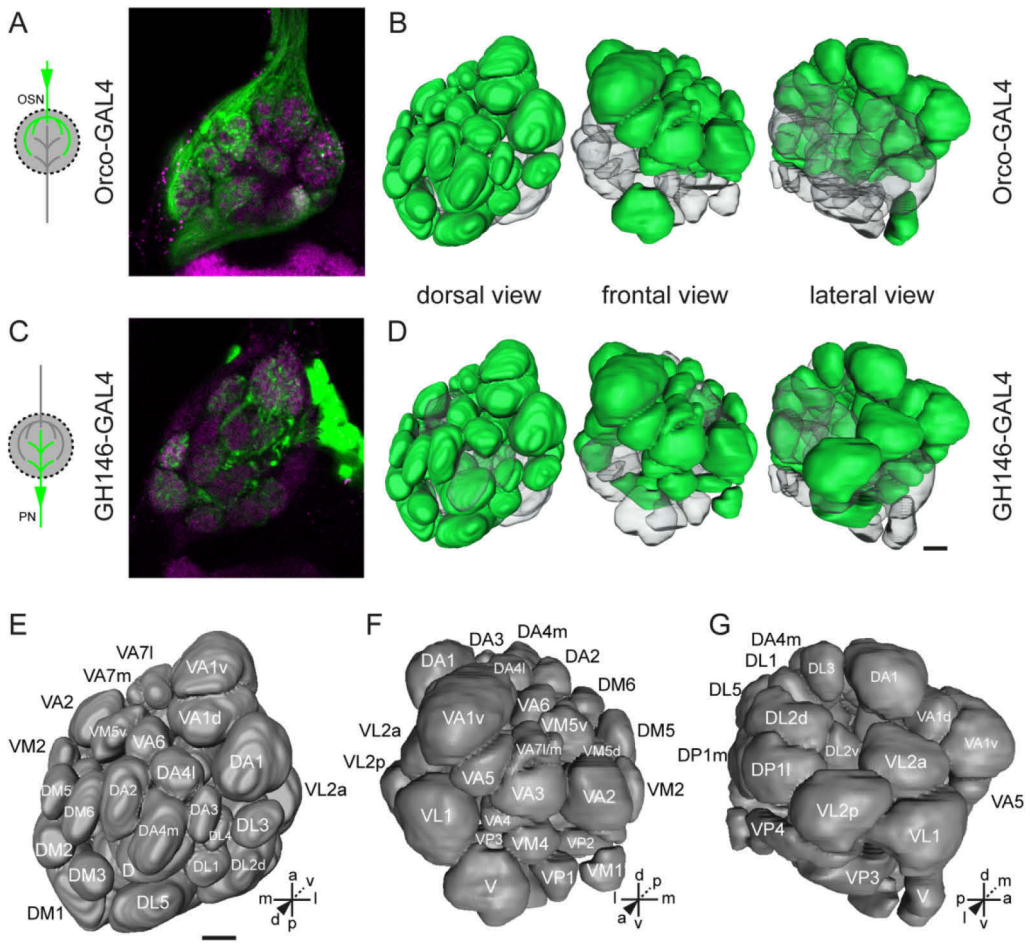

Figure 5. Characterization of the glomerular innervation patterns of two widely used GAL4-lines. **A:** Representative *in vivo* confocal scan of an AL expressing GCaMP3.0 under the control of the Orco promotor (green) combined with the END1-2 neuropil labeling (magenta) at 20 µm depth. The Orco-GAL4 line labels the majority of olfactory sensory neurons as depicted in the schematic on the left side. **B:** Glomerular innervations of the Orco-GAL4 line represented via the *in vivo* 3D AL atlas (green: innervated; transparent: not innervated). Depicted are the dorsal, frontal, and lateral views onto the AL. **C:** Representative *in vivo* confocal scan of an AL expressing GCaMP3.0 under the control of the GH146-GAL4 driver line (green) combined with the END1-2 neuropil labeling (magenta) at 30 µm depth. The GH146-GAL4 line labels the majority of projection neurons as depicted in the schematic on the left side. **D:** Glomerular innervations of the GH146-GAL4 line represented via the *in vivo* 3D AL atlas (green: innervated; transparent: not innervated). Depicted are the dorsal, frontal, and lateral views onto the AL. **E-G:** Complete glomerular assignment of the *in vivo* AL atlas from dorsal (E), frontal (F), and lateral views (G) corresponding to the perspectives in (B) and (D). Scale bars = 20 µm.

32 of which overlap the innervation of Orco-GAL4 (Fig. 5C,D; for glomerular identities, see Fig. 5E-G). Hence, if these two lines are employed simultaneously, functional studies that compare the input and output properties of specific glomeruli should be analyzed with caution. Although GH146-GAL4 is said to label one ventral PN innervating the whole AL (Marin et al., 2002), we were not able to observe any multiglomerular innervation. Due to the sparse glomerular innervation of multiglomerular PNs (Lai et al., 2008), the GCaMP3.0 expression level in this PN, which is below the detection level, can also be ignored for imaging experiments of the whole AL. For a detailed overview, all innervated glomeruli are listed for each GAL4-line in Table 1.

In summary, our *in vivo* AL atlas can be used to reliably identify glomeruli throughout the entire neuropil in

TABLE 1.
Glomeruli Innervated by the Orco-GAL4 and GH146-GAL4 Line

Glomerulus	Receptor type	Sensillum type	Orco-GAL4	GH146-GAL4
D	Or69a	Ab9	■	■
DA1	Or67d	At1	■	■
DA2	Or56a	Ab4	■	■
DA3	Or23a	At2	■	■
DA4l	Or43a	At3	■	■
DA4m	Or2a	At3	■	■
DC1	Or19a	At3	■	■
DC2	Or13a	Ab6	■	■
DC3	Or83c	At2	■	■
DC4	Ir64a	Sac III	■	■
DL1	Or10a	Ab1	■	■
DL2d	Ir75a/b/c	Ac3		
DL2v	Ir75a/b/c	Ac3		
DL3	Or65a	At4	■	■
DL4	Or49a(Or85f)	Ab10	■	■
DL5	Or7a	Ab4	■	■
DM1	Or42b	Ab1	■	■
DM2	Or22a	Ab3	■	■
DM3	Or47a	Ab5	■	■
DM4	Or59b	Ab2	■	■
DM5	Or85a(Or33b)	Ab2	■	■
DM6	Or67a	Ab10	■	■
DP1l	Ir75a	Ac2		
DP1m	Ir64a	Sac III		■
V	Gr21a	Ab1	■	
VA1d	Or88a	At4	■	■
VA1v	Or47b	At4	■	■
VA2	Or92a	Ab1	■	■
VA3	Or67b	Ab9	■	■
VA4	Or85d	Pb3	■	■
VA5	Or49b	Ab6	■	■
VA6	Or82a	Ab5	■	■
VA7l	Or46aA	Pb2	■	■
VA7m	?	?	■	■
VC1	Or33c	Pb2	■	■
VC2	Or71a	Pb1	■	■
VC3	Or35a	Ac3	■	■
VC4	Or67c	Ab7	■	■
VC5	Ir41a	Ac2	■	■
VL1	Ir75d	Ac1/2/4	■	■
VL2a	Ir84a	Ac4		■
VL2p	Ir31a	Ac1		■
VM1	Ir92a	Ac1		■
VM2	Or43b	Ab8	■	■
VM3	Or9a	Ab8	■	■
VM4	Ir76a	Ac4	■	■
VM5d	Or85b	Ab3	■	■
VM5v	Or98a	Ab7	■	■
VM7d	Or42a	Pb1	■	■
VM7v	Or59c	Pb3	■	■
VP1	Ir40a	Sac I	■	■
VP2	hot	Arista		■
VP3	cold	Arista		■
VP4	Ir40a	Sac I		■

These two lines refer to the olfactory sensory neurons and projection neurons, respectively. Black filled cells indicate innervation by the indicated line; white represents no innervation. Ab, antennal basiconic; Ac, antennal coeloconic; At, antennal trichoid; Pb, palp basiconic; Sac, sacculus; Or, olfactory receptor; Ir, ionotropic receptor; Gr, gustatory receptor.

the live fly brain; the atlas preserves the spatial arrangement of individual glomeruli as well as interglomerular differences regarding shape and size.

DISCUSSION

In vivo atlas for enhanced applicability

In this study we used a newly generated transgenic fly line, referred to as the END1-2 line, to provide *in vivo* neuropil labeling of the AL; this label is comparable to the nc82 immunostaining of *in vitro* whole mount brains (Fig. 1A-C) (Hofbauer, 1991; Laissue et al., 1999; Rein et al., 2002). The END1-2 line enables synaptically dense glomerular areas to be separated from synaptically sparse interglomerular areas (Boeckh et al., 1970; Tolbert and Hildebrand, 1981) by the expression of the presynaptic fusion protein *n*-synaptobrevin::DsRed in all neurons. By obtaining confocal stacks of this line and reconstructing individual glomeruli, we generated a 3D map of the AL of *Drosophila melanogaster* that accurately matches the AL in the living fly (Fig. 3). By taking advantage of the near-complete maps of receptor gene expression and OSN targeting (Couto et al., 2005; Fishilevich and Vosshall, 2005; Silbering et al., 2011), we verified the identity of 63% of AL glomeruli using specific receptor-GAL4 lines. This assisted identification allowed us to develop an *in vivo* AL atlas and a way to label neuropils that enables the orientation within and attribution of individual brain regions without *in vitro* processing. In addition, we demonstrate two applications of the new *in vivo* AL atlas by revisiting the segregation of glomeruli innervated by different types of sensilla (Fig. 4) (Couto et al., 2005), as well as by characterizing the glomerular innervation patterns of two of the most crucial GAL4-lines for targeting OSNs and PNs in the fly AL (Fig. 5).

In light of the number of glomeruli published over the last few years, which ranges from 35 (Stocker et al., 1990) to over 43 (Laissue et al., 1999) and up to 56 in current nomenclature (Tanaka et al., 2012), clearly the identification of glomeruli is not trivial. The subdividing of glomeruli, such as DL2, DP1, VA1, VA7, VC3, VL2 (Laissue et al., 1999), DA4, VM5, and VM7 (Couto et al., 2005) and the merging of others, such as VA1l and VA1m, VC3l and VC3m (Couto et al., 2005) as well as the addition of newly defined ones (e.g., VC5; Silbering et al., 2011) outline the challenge of distinguishing reliably between glomeruli. Consider glomerulus VM6, which cannot be distinguished from glomerulus VP1 by plain morphology. We merged the two glomeruli as VP1 since Yu et al. (2010) only observed PNs innervating both structures together via a twin-spot MARCM study. In addition, we were not able to assign glomerulus DL6,

which has been mentioned in two studies (Marin et al., 2005; Yu et al., 2010). However, its limited description to date leads us to assume that this glomerulus has been mislabeled and represents in fact glomerulus DC3. Hence, the new *in vivo* AL atlas of the vinegar fly consists of 54 glomeruli, of which 52 are innervated by chemosensory and two by thermosensory neurons (Gallio et al., 2011).

In vivo compared to *in vitro*

Our idea to create an *in vivo* AL atlas derived from the need to identify glomeruli in functional imaging experiments. Glomerular identification has proven challenging for *in vivo* data with the available *in vitro* atlases. Moreover, since there are not many investigations into the fixation artifacts of flexible neuropils such as the AL, we quantified the volumetric and geometrical modifications, such as shrinkage, dislocation, and distortion following *in vitro* processing. These three substantial effects of fixation on the AL were distributed dissimilarly across the AL neuropil (Figs. 1, 2). First, the heterogeneous shrinkage of glomeruli is most likely due to the different density of intraglomerular arborizations of OSNs, PNs, or LNs (Ignell et al., 2005), which leads to a small volumetric decrease in densely packed glomeruli, while sparsely innervated glomeruli are strongly affected.

Second, the dislocation of glomeruli during fixation affects mainly those glomeruli located anteriorly (VA1v, DA1, VA2) and posteriorly (DL5, DP1l), which reflects a longitudinal distortion of the entire AL neuropil. This global deformation is most likely based on the transection of the antennal nerve, which is required for *in vitro* dissection. In addition, the transection causes general changes in glomerular visibility: Under *in vivo* conditions the anterior glomeruli of the VA cluster are invisible when viewed from a dorsal perspective; they become visible in the surface layer following *in vitro* processing. The opposite effect happens for the posteriorly located glomeruli of the DL and DP clusters, as they are hidden beneath the DA glomeruli in the *in vitro* dissection.

Third, in addition to analyzing the dislocation of several glomeruli, we also investigated distortions regarding the relative positions of glomerular pairs. Again, we observed distortions mainly in glomerular pairs that are located anteriorly and posteriorly, which parallels the dislocation effect seen in individuals; however, the posterior glomeruli are more affected. These deformations highlight the rearrangement of most glomeruli around the ventroposterior basis, where the AL is attached to the protocerebrum. These diverse fixation artifacts emphasize the need for a thorough *in vivo* 3D AL atlas which has an enhanced application for characterizing GAL4 lines combined with the *in vivo* neuropil labeling in single- and multiphoton imaging experiments throughout the whole AL.

In vivo GAL4-line evaluations

As most of the ubiquitous GAL4-lines used for functional imaging studies are characterized by *in vitro* whole-mount brain immunochemistry, their maps suffer from the same issues as the initial identification of glomeruli described above. One can now screen any GAL4 line with the END1-2 neuropil label combined with mCD8-GFP (Lee and Luo, 1999) by maintaining the same conditions as in the actual *in vivo* experiment. END1-2, in contrast to ENG3 (Estes et al., 2000), can also be combined with various green fluorophores (Patterson and Lippincott-Schwartz, 2002; Tian et al., 2009) to visualize the neuropil while live measurements are running. For the characterization of new GAL4-lines labeling the olfactory pathway, we recommend identifying a reliable set of landmark glomeruli (such as DA1, DL5, DM2, VA2, VL1, and VM2) that is evenly spread over the whole AL neuropil.

Advantages and limitations of the new *in vivo* atlas

Our new approach for *in vivo* morphology based on END1-2 neuropil labeling has both advantages and limitations. The new method allowed us to depict the actual volume, distance, and angle artifacts influencing the *in vitro* atlases. The *in vivo* AL atlas does not suffer from those artifacts and its application in *in vivo* experiments is thus easier, especially as it has been generated from a perspective identical to the *in vivo* dissection for functional imaging experiments (Silbering et al., 2012; Strutz et al., 2012). On the other hand, this approach is limited by the age of flies used in the END1-2 staining: By using flies of 3-6 days after hatching, we obtained a clearly stained neuropil. However, stains made with older flies revealed an increasingly indistinct distribution of the DsRed labeling, which interferes with the identification of glomeruli (data not shown). Although we are not completely sure why older flies would have this effect, we assume that it represents a disassembly of the endocytotic recycling process of SNARE complexes (Südhof, 2004; Burgalossi et al., 2010). Disassembling the whole complex could lead to enriched levels of DsRed in the synaptic cleft. Alternatively, the fusion of DsRed to *n*-synaptobrevin might constrain vesicle recycling. Hence, to achieve the most distinct *in vivo* neuropil labeling, the age dependency should be kept in mind.

In summary, the new *in vivo* 3D digital atlas of the *Drosophila* AL represented here provides an invaluable

research tool for fly brain morphology and functional imaging studies. Publicly available and downloadable as a 3D PDF file, the atlas allows the AL or subgroups of glomeruli to be visualized from any angle. In addition, the *in vivo* neuropil labeling can be used to characterize the morphology of novel driver and enhancer trap lines in the commonly used GAL4 (Brand and Perrimon, 1993), LexA (Lai and Lee, 2006), and Q systems (Potter et al., 2010) for broad applications in *Drosophila* neuroscience.

ACKNOWLEDGMENTS

We thank Silke Trautheim and Regina Stieber for excellent technical assistance, Jürgen Rybak for help with the AMIRA software and advice on the article, Christine Miβbach for support regarding the antennal preparations, Michael Thoma for statistical advice, Enrico Garbe and Julia van Beesel for help with the *in vitro* 3D reconstructions, and Emily Wheeler for editorial assistance. Stocks obtained from the Bloomington Drosophila Stock Center (NIH P40OD018537) were used in this study.

CONFLICT OF INTEREST

The authors have no known or potential conflict of interest including any financial, personal, or other relationships with other people or organizations within the years of beginning the submitted work that could inappropriately influence or be perceived to influence the work.

ROLE OF AUTHORS

All authors had full access to all the data in the study and take responsibility for the integrity of the data and the accuracy of the data analysis. Study concept and design: Silke Sachse, Veit Grabe, Antonia Strutz, Bill S. Hansson. Acquisition of data: Veit Grabe, Amelie Baschwitz. Analysis and interpretation of data: Veit Grabe, Silke Sachse. Drafting of the article: Veit Grabe, Silke Sachse. Obtained funding: Silke Sachse, Bill S. Hansson. Material support (generation of GAL4-lines): Antonia Strutz. Critical revision of the article for important intellectual content: all authors. Study supervision: Silke Sachse.

LITERATURE CITED

Abuin L, Bargeton B, Ulbrich MH, Isacoff EY, Kellenberger S, Benton R. 2011. Functional architecture of olfactory ionotropic glutamate receptors. Neuron 69:44-60.

Ai M, Min S, Grosjean Y, Leblanc C, Bell R, Benton R, Suh GSB. 2010. Acid sensing by the Drosophila olfactory system. Nature 468:691-695.

Baird GS, Zacharias DA, Tsien RY. 2000. Biochemistry, mutagenesis, and oligomerization of DsRed, a red fluorescent protein from coral. Proc Natl Acad Sci U S A 97:11984-11989.

Benton R, Vannice KS, Gomez-Diaz C, Vosshall LB. 2009. Variant ionotropic glutamate receptors as chemosensory receptors in Drosophila. Cell 136:149-162.

Boeckh J, Sandri C, Akert K. 1970. Sensory inputs and synaptic connections in the insect CNS. Experimental degeneration in the antennal afferent pathway in the supraesophageal ganglia of flies and cockroaches. Z Zellforsch Mikrosk Anat 103:429-446.

Brand AH, Perrimon N. 1993. Targeted gene expression as a means of altering cell fates and generating dominant phenotypes. Development 118:401-415.

Burgalossi A, Jung S, Meyer G, Jockusch WJ, Jahn O, Taschenberger H, O'Connor VM, Nishiki T-I, Takahashi M, Brose N, Rhee J-S. 2010. SNARE protein recycling by αSNAP and βSNAP supports synaptic vesicle priming. Neuron 68:473-487.

Caron SJC, Ruta V, Abbott LF, Axel R. 2013. Random convergence of olfactory inputs in the Drosophila mushroom body. Nature 497:113-117.

Chou Y-H, Spletter ML, Yaksi E, Leong JCS, Wilson RI, Luo L. 2010. Diversity and wiring variability of olfactory local interneurons in the Drosophila antennal lobe. Nat Neurosci 13:439-449.

Couto A, Alenius M, Dickson BJ. 2005. Molecular, anatomical, and functional organization of the *Drosophila* olfactory system. Curr Biol 15:1535-1547.

Daniels RW, Gelfand MV, Collins CA, DiAntonio A. 2008. Visualizing glutamatergic cell bodies and synapses in Drosophila larval and adult CNS. J Comp Neurol 508:131-152.

Datta SR, Vasconcelos ML, Ruta V, Luo S, Wong A, Demir E, Flores J, Balonze K, Dickson BJ, Axel R. 2008. The Drosophila pheromone cVA activates a sexually dimorphic neural circuit. Nature 452:473-477.

de Bruyne M, Foster K, Carlson JR. 2001. Odor coding in the *Drosophila* antenna. Neuron 30:537-552.

DiAntonio A, Burgess RW, Chin AC, Deitcher DL, Scheller RH, Schwarz TL. 1993. Identification and characterization of Drosophila genes for synaptic vesicle proteins. J Neurosci 13:4924-4935.

Endo K, Aoki T, Yoda Y, Kimura K-i, Hama C. 2007. Notch signal organizes the Drosophila olfactory circuitry by diversifying the sensory neuronal lineages. Nat Neurosci 10:153-160.

Fiala A, Spall T, Diegelmann S, Eisermann B, Sachse S, Devaud JM, Buchner E, Galizia CG. 2002. Genetically expressed cameleon in *Drosophila melanogaster* is used to visualize olfactory information in projection neurons. Curr Biol 12:1877-1884.

Fishilevich E, Vosshall LB. 2005. Genetic and functional subdivision of the *Drosophila* antennal lobe. Curr Biol 15:1548-1553.

Galizia CG, Sachse S. 2010. Odor coding in insects. In: Menini A, editor. The neurobiology of olfaction. Boca Raton, FL: CRC Press. p 35-70.

Gallio M, Ofstad TA, Macpherson LJ, Wang JW, Zuker CS. 2011. The coding of temperature in the Drosophila brain. Cell 144:614-624.

Gao Q, Yuan B, Chess A. 2000. Convergent projections of *Drosophila* olfactory neurons to specific glomeruli in the antennal lobe. Nat Neurosci 3:780-785.

Hallem EA, Carlson JR. 2006. Coding of odors by a receptor repertoire. Cell 125:143-160.

Hansson BS, Knaden M, Sachse S, Stensmyr MC, Wicher D. 2010. Towards plant-odor-related olfactory neuroethology in *Drosophila*. Chemoecology 20:51-61.

Hofbauer A. 1991. Eine Bibliothek monoklonaler Antikörrper gegen das Gehirn von *Drosophila melanogaster* [Habilitation thesis]. Würzburg, Germany: University of Würzburg.

Ignell R, Dekker T, Ghaninia M, Hansson BS. 2005. Neuronal architecture of the mosquito deutocerebrum. J Comp Neurol 493:207-240.

Kain P, Boyle SM, Tharadra SK, Guda T, Pham C, Dahanukar A, Ray A. 2013. Odour receptors and neurons for DEET and new insect repellents. Nature 502:507-512.

Kondoh Y, Kaneshiro KY, Kimura K, Yamamoto D. 2003. Evolution of sexual dimorphism in the olfactory brain of Hawaiian *Drosophila*. Proc R Soc Lond B 270:1005-1013.

Kurtovic A, Widmer A, Dickson BJ. 2007. A single class of olfactory neurons mediates behavioural responses to a Drosophila sex pheromone. Nature 446:542-546.

Lai S-L, Lee T. 2006. Genetic mosaic with dual binary transcriptional systems in Drosophila. Nat Neurosci 9:703-709.

Lai S-L, Awasaki T, Ito K, Lee T. 2008. Clonal analysis of Drosophila antennal lobe neurons: diverse neuronal architectures in the lateral neuroblast lineage. Development 135: 2883-2893.

Laissue PP, Reiter C, Hiesinger PR, Halter S, Fischbach KF, Stocker RF. 1999. Three-dimensional reconstruction of the antennal lobe in *Drosophila melanogaster*. J Comp Neurol 405:543-552.

Larsson MC, Domingos AI, Jones WD, Chiappe ME, Amrein H, Vosshall LB. 2004. *Or83b* encodes a broadly expressed odorant receptor essential for *Drosophila* olfaction. Neuron 43:703-714.

Lee T, Luo L. 1999. Mosaic analysis with a repressible cell marker for studies of gene function in neuronal morphogenesis. Neuron 22:451-461.

Liang L, Li Y, Potter CJ, Yizhar O, Deisseroth K, Tsien Richard W, Luo L. 2013. GABAergic projection neurons route selective olfactory inputs to specific higher-order neurons. Neuron 79:917-931.

Ma Y, Smith D, Hof PR, Foerster B, Hamilton S, Blackband SJ, Yu M, Benveniste H. 2008. In vivo 3D digital atlas database of the adult C57BL/6J mouse brain by magnetic resonance microscopy. Front Neuroanat 2:1.

Marcucci F, Maier-Balough E, Zou D-J, Firestein S. 2011. Exuberant growth and synapse formation of olfactory sensory neuron axonal arborizations. J Comp Neurol 519: 3713-3726.

Marin EC, Jefferis GSXE, Komiyama T, Zhu H, Luo L. 2002. Representation of the glomerular olfactory map in the Drosophila brain. Cell 109:243-255.

Marin EC, Watts RJ, Tanaka NK, Ito K, Luo L. 2005. Developmentally programmed remodeling of the Drosophila olfactory circuit. Development 132:725-737.

Masse NY, Turner GC, Jefferis GSXE. 2009. Olfactory information processing in Drosophila. Curr Biol 19:R700-R713.

Ng M, Roorda RD, Lima SQ, Zemelman BV, Morcillo P, Miesenbock G. 2002. Transmission of olfactory information between three populations of neurons in the antennal lobe of the fly. Neuron 36:463-474.

Patterson GH, Lippincott-Schwartz J. 2002. A photoactivatable GFP for selective photolabeling of proteins and cells. Science 297:1873-1877.

Potter CJ, Tasic B, Russler EV, Liang L, Luo L. 2010. The Q system: a repressible binary system for transgene expression, lineage tracing, and mosaic analysis. Cell 141:536-548.

Rein K, Zöckler M, Mader MT, Grübel C, Heisenberg M. 2002. The drosophila standard brain. Curr Biol 12:227-231.

Ruta V, Datta SR, Vasconcelos ML, Freeland J, Looger LL, Axel R. 2010. A dimorphic pheromone circuit in Drosophila from sensory input to descending output. Nature 468: 686-690.

Ruthensteiner B, Heβ M. 2008. Embedding 3D models of biological specimens in PDF publications. Microsc Res Tech 71:778-786.

Rybak J, Kuss A, Hans L, Zachow S, Hege H-C, Lienhard M, Singer J, Neubert K, Menzel R. 2010. The digital bee brain: integrating and managing neurons in a common 3D reference system. Front Syst Neurosci 4.

Schubert M, Hansson BS, Sachse S. 2014. The banana code—natural blend processing in the olfactory circuitry of Drosophila melanogaster. Front Physiol 5:59.

Scott K, Brady R Jr, Cravchik A, Morozov P, Rzhetsky A, Zuker C, Axel R. 2001. A chemosensory gene family encoding candidate gustatory and olfactory receptors in *Drosophila*. Cell 104:661-673.

Seki Y, Rybak J, Wicher D, Sachse S, Hansson BS. 2010. Physiological and morphological characterization of local interneurons in the Drosophila antennal lobe. J Neurophysiol 104:1007-1019.

Shanbhag SR, Muller B, Steinbrecht RA. 1999. Atlas of olfactory organs of *Drosophila melanogaster*. 1. Types, external organization, innervation and distribution of olfactory sensilla. Int J Insect Morphol Embryol 28:377-397.

Silbering AF, Okada R, Ito K, Galizia CG. 2008. Olfactory information processing in the Drosophila antennal lobe: anything goes? J Neurosci 28:13075-13087.

Silbering AF, Rytz R, Grosjean Y, Abuin L, Ramdya P, Jefferis GSXE, Benton R. 2011. Complementary function and integrated wiring of the evolutionarily distinct Drosophila olfactory subsystems. J Neurosci 31:13357-13375.

Silbering AF, Bell R, Galizia CG, Benton R. 2012. Calcium imaging of odor-evoked responses in the Drosophila antennal lobe. JoVE:e2976.

Stocker RF, Singh RN, Schorderet M, Siddiqi O. 1983. Projection patterns of different types of antennal sensilla in the antennal glomeruli of *Drosophila melanogaster*. Cell Tissue Res 232:237-248.

Stocker RF, Lienhard MC, Borst A, Fischbach KF. 1990. Neuronal architecture of the antennal lobe in *Drosophila melanogaster*. Cell Tissue Res 262:9-34.

Stocker RF, Heimbeck G, Gendre N, de Belle JS. 1997. Neuroblast ablation in *Drosophila* P[GAL4] lines reveals origins of olfactory interneurons. J Neurobiol 32:443-456.

Stockinger P, Kvitsiani D, Rotkopf S, Tirian L, Dickson BJ. 2005. Neural circuitry that governs *Drosophila* male courtship behavior. Cell 121:795-807.

Stökl J, Strutz A, Dafni A, Svatos A, Doubsky J, Knaden M, Sachse S, Hansson BS, Stensmyr MC. 2010. A deceptive pollination system targeting drosophilids through olfactory mimicry of yeast. Curr Biol 20:1846-1852.

Strutz A, Voeller T, Riemensperger T, Fiala A, Sachse S. 2012. Calcium imaging of neural activity in the olfactory system of *Drosophila*. In: Martin J-R, editor. Genetically encoded functional indicators. New York: Springer Science+Business Media. p 43-70.

Südhof TC. 2004. The synaptic vesicle cycle. Annu Rev Neurosci 27:509-547.

Tanaka NK, Endo K, Ito K. 2012. Organization of antennal lobe-associated neurons in adult Drosophila melanogaster brain. J Comp Neurol 520:4067-4130.

Tian L, Hires SA, Mao T, Huber D, Chiappe ME, Chalasani SH, Petreanu L, Akerboom J, McKinney SA, Schreiter ER, Bargmann CI, Jayaraman V, Svoboda K, Looger LL. 2009. Imaging neural activity in worms, flies and mice with

improved GCaMP calcium indicators. Nat Meth 6:875-881.
Tolbert LP, Hildebrand JG. 1981. Organization and synaptic ultrastructure of glomeruli in the antennal lobes of the moth Manduca sexta: a study using thin sections and freeze-fracture. Proc R Soc Lond Ser B Biol Sci 213:279-301.
Vosshall LB, Stocker RF. 2007. Molecular architecture of smell and taste in Drosophila. Annu Rev Neurosci 30: 505-533.
Vosshall LB, Wong AM, Axel R. 2000. An olfactory sensory map in the fly brain. Cell 102:147-159.
Wang JW, Wong AM, Flores J, Vosshall LB, Axel R. 2003. Two-photon calcium imaging reveals an odor-evoked map of activity in the fly brain. Cell 112:271-282.
Wilson RI. 2013. Early olfactory processing in Drosophila: mechanisms and principles. Annu Rev Neurosci 36:217-241.
Wilson RI, Turner GC, Laurent G. 2004. Transformation of olfactory representations in the *Drosophila* antennal lobe. Science 303:366-370.
Wu JS, Luo L. 2006. A protocol for dissecting Drosophila melanogaster brains for live imaging or immunostaining. Nat Protocols 1:2110-2115.
Yao K-M, Samson M-L, Reeves R, White K. 1993. Gene elav of Drosophila melanogaster: a prototype for neuronal-specific RNA binding protein gene family that is conserved in flies and humans. J Neurobiol 24:723-739.
Yu H-H, Kao C-F, He Y, Ding P, Kao J-C, Lee T. 2010. A complete developmental sequence of a *Drosophila* neuronal lineage as revealed by twin-spot MARCM. PLoS Biol 8:e1000461.

Manuscript II

The Specific Glomerulus, or: How unique can a Glomerulus be?

Veit Grabe, Amelie Baschwitz, Hany Dweck, Bill S. Hansson and Silke Sachse

In preparation as a NeuroResources article for Neuron

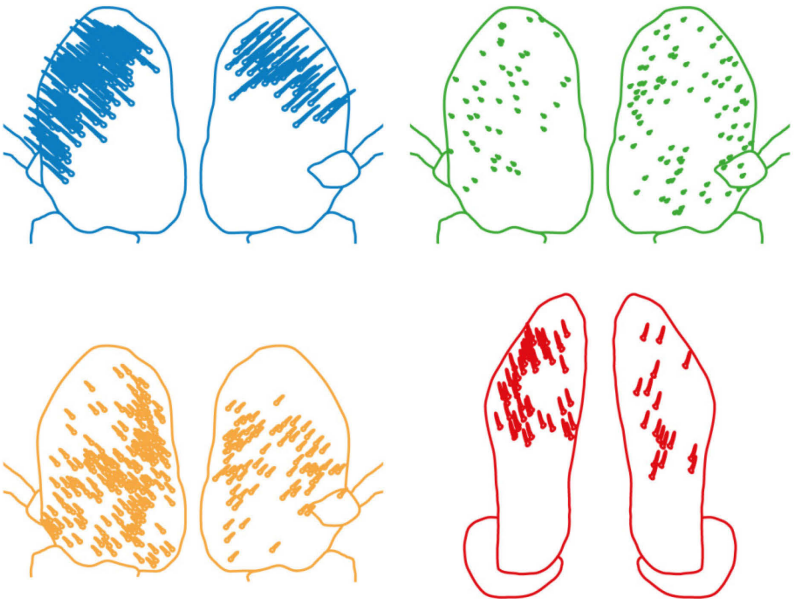

The Specific Glomerulus, or:
How unique can a Glomerulus be?

Veit Grabe[§], Amelie Baschwitz[§], Hany Dweck, Bill S. Hansson and Silke Sachse*

Department of Evolutionary Neuroethology, Max Planck Institute for Chemical Ecology, Hans-Knöll-Str. 8, 07745 Jena, Germany

[§]These authors contributed equally to this work.

*Correspondence to Dr. Silke Sachse, Department of Evolutionary Neuroethology, Max Planck Institute for Chemical Ecology, Hans-Knöll-Str. 8, 07745 Jena, Germany.
Tel: +49-3641-571416, Fax: +49-3641-571402
Email: ssachse@ice.mpg.de

Abstract

Subunits of the insect antennal lobe, the glomeruli, are morphologically conserved spherical compartments of the olfactory system, solely distinguishable by their chemosensory repertoire, anatomical position and volume. Most glomeruli, except the putative pheromone-receptive structures, are often thought to be part of a morphologically and physiologically homogeneous cluster. Previous as well as more recent studies describe an increasing proportion of single glomeruli with very specific functionalities. In this study, we provide a screen of glomerulus-specific morphological properties and search for a link between these and respective glomerular functions. We disprove the assumption of glomerular uniformity and propose an overall uniqueness not only at the level of sensory input and superficial morphology but also at a more detailed level of intraglomerular connectivity. We depict a basic relation of neuronal quantity and glomerular volume and make predictions regarding the importance of scarcely investigated glomeruli supported by their morphological parameters.

Key Words:

Drosophila melanogaster, olfactory glomeruli, convergence, sensory neuron mapping, input-output connectivity, lifetime sparseness

Introduction

The complex and fast changing chemical environment of *Drosophila melanogaster* led to the development of a large set of unique receptors in the olfactory system. They are expressed in olfactory sensory neurons (OSNs) which are housed in four different classes of sensilla - basiconic, trichoid (Shanbhag et al., 1999), intermediate (Dweck et al., 2013; Ronderos et al., 2014) and coeloconic sensilla (Silbering et al., 2011) - present on the 3rd antennal segment - the funiculus – as well as the maxillary palp (De Bruyne et al., 1999).

OSNs expressing the same chemosensory receptor (CR) converge into one out of 54 discrete spherical structures (Gao et al., 2000; Grabe et al., 2014), the olfactory glomeruli, which represent the structural and functional subunits of the antennal lobe (AL). Within the glomeruli OSNs synapse via defined synapse numbers (Mosca and Luo, 2014) with most of the multiglomerular local interneurons (LNs (Chou et al.,

2010)) and about three projection neurons each (PNs (Wong et al., 2002)). The exact numbers of and connectivity between the different neuronal types within the glomeruli remain however unclear (Kazama and Wilson, 2009), which leads to a common assumption of glomerular uniformity. Past the peripheral level of CRs per neuron, the different subunits of the primary olfactory center are seen in an indifferent light. The glomerular composition of the AL allows a spatiotemporal segregated representation of complex stimuli (Wang et al., 2003) perceived by the rather diffusely distributed peripheral sensilla types (Shanbhag et al., 1999; Stocker, 1994). Several studies revealed that each CR does not only possess an exclusive molecular receptive range (Galizia et al., 2010; Hallem and Carlson, 2006; Kreher et al., 2008; Pelz et al., 2006), but it also exhibits a unique function regarding the coding of specific behavioral-relevant odors, such as cis-vaccenylacetate (cVA), which is coded by Or67d and targets glomerulus DA1 (Ha and Smith, 2006; Kurtovic et al., 2007), CO_2 coded by Gr21a targeting the V glomerulus (Suh et al., 2004), geosmin coded by Or56a targeting glomerulus DA2 (Stensmyr et al., 2012) as well as farnesol activating Or83c targeting glomerulus DC3 (Dweck et al., 2013; Ronderos et al., 2014). Such selective response patterns can be quantified using the lifetime sparseness (Bhandawat et al., 2007; Perez-Orive et al., 2002; Vinje, 2000), a measure of a receptors‘ probability to respond to any given odor.

Specific behavioral functions are largely investigated in higher brain centers, such as the mushroom body calyx and the lateral horn. Here, each glomerulus targets restricted areas and hence induces specific output patterns via PNs (Jefferis et al., 2007; Luo, 2007), which mediate associative (Caron et al., 2013; Heisenberg, 2003) or innate behavior (Heimbeck et al., 2001; Parnas et al., 2013; Strutz et al., 2014). Therefore the AL is assumed to function as an olfactory center which solely represents sensory odor maps and propagates these via PNs from the periphery to the protocerebrum (Jefferis et al., 2001), where they integrate with other sensory modalities leading to complex behavior (Busto et al., 2010). Interestingly, several studies report the AL glomeruli reveal some degree of plasticity resulting in an enlarged volume due to an increased OSN number (Acebes and Ferrús, 2001; Dekker et al., 2006; Linz et al., 2013) as well as their sexual dimorphism (Kondoh et al., 2003) permitted by the fruitless protein. Furthermore LNs of the AL, which maintain a gain control function (Root et al., 2008) to reduce strong and to increase weak responses via a complex network of inhibition and disinhibition through

chemical and electrical synapses (Yaksi and Wilson, 2010), are described to almost homogenously innervate all glomeruli (Okada et al., 2009; Seki et al., 2010). Additional work depicted a rather specific innervation frequency of certain types of LNs (Chou et al., 2010). Beyond the described morphological uniformity, each glomerulus has a unique shape and size pointing out intrinsic differences between glomeruli (Grabe et al., 2014). Recent studies on the diversified neurotransmitter repertoire in the olfactory system in general (Chiang et al., 2011) and specifically the AL (Busch et al., 2009; Carlsson et al., 2010; Liu and Wilson, 2013) support this potential uniqueness.

Common anatomical and physiological descriptors for glomeruli represent the sensilla input (De Bruyne et al., 1999; Shanbhag et al., 1999), the CR expressed in each ONS (Couto et al., 2005; Silbering et al., 2011), the receptor's molecular receptive range (Hallem and Carlson, 2006; Pelz et al., 2006), the glomerular size (Devaud et al., 2001), developmental alterations (Endo et al., 2007), sex specificity (Ito et al., 2012; Stockinger et al., 2005) as well as their target areas in higher brain centers (Caron et al., 2013; Jefferis et al., 2007; Marin et al., 2002; Strutz et al., 2014; Tanaka et al., 2012; Wong et al., 2002). Most of these criteria are only available for a restricted set of glomeruli and therefore prevent a thorough investigation of glomerular uniqueness.

In this study, we report a nearly complete quantitative mapping of *Drosophila* sensilla types basing on sex specific receptor distributions and a comprehensive screen of the corresponding sex specific glomerular volumes (complementary to (Grabe et al., 2014)). The data disproves the so far assumed universal 30:1 convergence of OSNs per glomerulus and demonstrates the impact of the OSN number on glomerular dimensions. We also pronounce sex specific differences in fruitless negative glomeruli. In combination with the quantified number of uniglomerular PNs, ranging from one to ten, the data reveal a glomerulus-specific connectivity from input to output underlining a glomerular uniqueness. Based on these morphological descriptors in combination with published LN innervation frequency data (Chou et al., 2010) and the calculation of receptor lifetime sparseness from odor tuning datasets (Bhandawat et al., 2007; Galizia et al., 2010) we propose a potential importance for so far weakly described glomeruli and suggest a systematic investigation of the neurotransmitter repertoire of AL output neurons. Further we postulate that every

glomerulus is unique regarding its morphology and therefore putatively unique in its functionality beyond the receptor mediated affinity to certain volatile cues.

Experimental Procedures

Drosophila Genetics

Flies were reared for 3-6 d at 25°C and 70% humidity on a 12h-12h day-night cycle. We used the following fly lines ordered from the Bloomington *Drosophila* stock center (http://flystocks.bio.indiana.edu/): *GH146-GAL4 (Stocker et al., 1997), UAS-GCaMP3.0 (Tian et al., 2009), ChA-GAL4 (Salvaterra and Kitamoto, 2001), Or10a-GAL4, Or13a-GAL4, Or22a-GAL4, Or33c-GAL4, Or35a-GAL4, Or42a-GAL4, Or42b-GAL4, Or43a-GAL4, Or43b-GAL4, Or46aA-GAL4, Or47a-GAL4, Or49a-GAL4, Or56a-GAL4, Or59c-GAL4, Or67c-GAL4, Or69a-GAL4, Or83c-GAL4, Or85a-GAL4, Or88a-GAL4, Or92a-GAL4* and *Or98a-GAL4* (all (Fishilevich and Vosshall, 2005; Vosshall et al., 2000). Additional lines were kindly provided by Richard Benton (*Ir40a-GAL4, Ir41a-GAL4 (Silbering et al., 2011), IR76a-GAL4* (Benton et al., 2009) and *Ir92a-GAL4 (Abuin et al., 2011)*), Barry Dickson (*Or67d-GAL4,* (Kurtovic et al., 2007)) and Bob Datta (*UAS-C3PA,* (Ruta et al., 2010)).

Scanning electron microscopy

Flies were anesthetized on CO_2, placed in 5 ml 25% EtOH and incubated for 12-24 h at room temperature. In an EtOH-row the flies were further dehydrated in 50%, 75% and two times 100% EtOH for 12-24 h each at room temperature. Samples were then critical point dried i. e., EtOH was replaced with liquid CO_2 under high pressure then warmed till the CO_2 turned gaseous and finally evaporated out of the dry sample. After mounting the samples with T. V. tube coat (Ted Pella Inc., Redding, CA, USA) onto the SEM stubs we sputter coated them with a 25 nm thick platinum coat. Images of the sensilla types on the 3rd antennal segment and the maxillary palp were acquired using a LEO 1450 VP scanning electron microscope (Carl Zeiss, Jena, Germany).

OSN quantification and mapping

To quantify the number of OSNs innervating each glomerulus, 3-6 d old flies were anesthetized with CO_2 and their antennae or palps were removed. After covering the antennae or palps with a solution of saline and Triton-X, they were mounted in

VectaShield (Vector Laboratories Inc., Burlingame, CA, USA) and sealed with nail polish between a 22x22 mm and a 24x60 mm object slide – both 1mm thick – to allow for double-sided scanning. No spacer was needed since the layer of nail polish provided enough space to fix the antennae or palp but not crush it. Scans of both sides of each antenna were carried out with an Axio Imager.Z1 (Carl Zeiss, Jena, Germany) using a 20x water immersion objective (W Plan-Apochromat 20x/0.8, Carl Zeiss, Jena, Germany) in combination with a GFP filter cube (HE 38, EX BP 470/40, BS FT 495, EM BP 525/50, Carl Zeiss, Jena, Germany). To allow a reliable mapping of the sensilla, an additional transmitted light scan of each antenna was acquired. This scan was utilized to register all antennae by hand, based on the position of the arista and the sacculus. The quantification of OSN cell bodies was done in FIJI (ImageJ 1.48r, National Institute of Health, USA) software.

Confocal Microscopy and 3D-Reconstruction

The dissection of fly brains was carried out as previously described (Silbering et al., 2011; Strutz et al., 2012). Confocal scans were obtained at a MPCLSM (Zeiss LSM 710 NLO confocal microscope, Carl Zeiss, Jena, Germany) using a 40x water immersions objective (W Plan-Apochromat 40x/1.0 DIC M27; Carl Zeiss, Jena, Germany) in combination with the internal Argon 488 (LASOS, Jena, Germany) and Helium-Neon 543 (Carl Zeiss, Jena, Germany) laser lines. Reconstruction of whole ALs and individual glomeruli was done using the segmentation software AMIRA 5.5.0 (FEI Visualization Sciences Group, Burlington, MA, USA). Identification of glomeruli was verified by the *in vivo* scans of the specific OR-lines crossed into the END1-2 background fir *in vivo* neuropil labeling (Grabe et al., 2014). We analyzed at least scans of three specimens for each GAL4 receptor line. Using information on the voxel size from the LSM scans as well as the number of voxels labeled for each neuropil, we calculated the volume of the glomeruli and the whole AL.

Photoactivation of PNs

In vivo-labeling of single glomeruli of 4-6 d old male and female flies of the genotype +;*GH146-GAL4*/(CyO);*UAS-C3PA*/(TM6B) at a MPCLSM (Zeiss LSM 710 NLO confocal microscope, Carl Zeiss, Jena, Germany) equipped with an infrared Chameleon Ultra ™ diode-pumped laser (Coherent, Santa Clara, CA). Flies were prepared as previously described (Silbering et al., 2011; Strutz et al., 2012). ROIs were continuously activated for 5-15 min at a wavelength of 760 nm with a 40x water

immersions objective (W Plan-Apochromat 40x/1.0 DIC M27; Carl Zeiss, Jena, Germany) with laser power of approximately 1.5 mW. Z-stacks of the pre- and post-activation states were scanned at 925 nm with 1024 x 1024 pixel resolution. The identification of glomeruli was based on the previously published screen of GH146-GAL4/UAS-GCaMP3.0 under the same conditions (Grabe et al., 2014).

Single Sensillum Recording (SSR)

Adult flies were immobilized in pipette tips and the 3rd antennal segment or the palps were placed in a stable position onto a glass coverslip. Sensilla were localized under a binocular at 100x magnification and the extracellular signals originating from the OSNs were measured by inserting a tungsten wire electrode in the base of a sensillum. The reference electrode was inserted into the eye. Signals were amplified (10x; Syntech Universal AC/DC Probe, Syntech), sampled (10,667.0. samples/s) and filtered (100–3000 Hz with 50/60 Hz suppression) via USB-IDAC connection to a computer (Syntech). Action potentials were extracted using Syntech Auto Spike 32 software. Neuron activities were recorded for 10 s, starting 2 s before a stimulation period of 0.5 s. Responses from individual neurons were calculated as the increase (or decrease) in the action potential frequency (spikes/s) relative to the pre-stimulus frequency.

Lifetime Sparseness (LS)

Acquired responses were used to calculate a receptors response profile by calculating its lifetime sparseness (Bhandawat et al., 2007; Perez-Orive et al., 2002; Vinje, 2000). This is a non-parametric statistic providing a measure of the likeliness of an OSN to respond. The value ranges from $0 \leq S \leq 1$ where 0 means, the OSN responds to every odor in the same way, and 1, the receptor exclusively responds to one odor in the set. Calculation was carried out with following formula:

$$S = \left(\frac{1}{1-\frac{1}{N}}\right) * \left(1 - \frac{\left(\sum_{j=1}^{N} \frac{r_j}{N}\right)^2}{\sum_{j=1}^{N} \frac{r_j{}^2}{N}}\right)$$

Where S = lifetime sparseness, N = number of tested odors per receptor and r_j = response to a given odor j. Any values of r_j <0 were set to zero before computing lifetime sparseness. Used datasets are taken from (Hallem and Carlson, 2006) and

the database of olfactory receptors (Galizia et al., 2010) and combined with original response profiles acquired via SSR.

Results

OSNs convergence in the AL is glomerulus-specific

Although it was shown that OSNs expressing a certain CR occur in various number ranging from 10 up to 40 (Gao et al., 2000), a uniform convergence of 30:1 per glomerulus is usually assumed (Ramaekers et al., 2005; Stocker, 2001; Vosshall and Stocker, 2007). Here we present a receptor specific analysis of the exact convergence per glomerulus building the foundation for a diversified connectivity already at the sensory level. To understand the logic of this connectivity we quantified the number of OSNs that express a certain CR using specific CRX-GAL4 driver lines and combined them with UAS-GCaMP3.0 responder lines. We selected at least one receptor type which is described to be specific for each sensillum type (Couto et al., 2005; Silbering et al., 2011)enabling the precise mapping of sensilla clusters after dissecting the antennae and scanning the 3rd antennal segment (Fig 1A, B). We observed the patterned distribution of the different sensilla classes described earlier (Benton et al., 2009; De Bruyne et al., 2001; Shanbhag et al., 1999; Silbering et al., 2011). The basiconic sensilla are located almost all over the funiculus but in a higher density in the anterior proximal region and they are not present at the distal tip. The trichoid sensilla are located more distal, incorporating the two intermediate types (Ai2/At2 and Ai3/At3, (Dweck et al., 2013; Shanbhag et al., 1999). To simplify things we refer to them unified as trichoids from now on in the text. Coeloconic sensilla are evenly distributed, similar to the basiconic ones but with a higher density on the posterior side. The basiconic sensilla found on the maxillary palp (MP) are evenly spread at the distal region of the appendage as described by (De Bruyne et al., 1999). Using the specific receptor driver lines we were able to assign these broad descriptions of whole clusters (De Bruyne et al., 2001; Shanbhag et al., 1999; Vosshall et al., 2000) to detailed maps for each functional sensillum type (Fig 1C). The antennal trichoids are found in broad anterior and posterior patches along the lateral edge reaching to the distal tip. Male flies house significantly more At2 and At4 than female flies. Large basiconics are situated proximal along the anteromedial and/or posteromedial edge. In contrast, we found the thin and small basiconics in a

broad medial diagonal band which reaches from the proximolateral to the mediodistal edge on both sides of the third segment. Sensilla Ab1 and Ab8 are only found anterior and Ab3 only posterior. Notably, several basiconic sensilla types are significantly more abundant in females than in males (Ab1, Ab2, Ab6, and Ab10). Or22a-positive neurons were previously described with 18 and 29 OSNs in males and females, respectively, (Dobritsa et al., 2003) but we never gained an equal count (Fig 1D, Table 1). The coeloconic sensilla 1 and 2 are found only at the posterior side of the 3rd antennal segment; Ac3 is almost evenly distributed over the whole antenna and Ac4 is found alongside the lateral edge of the funiculus confirming previous studies (Benton et al., 2009; Silbering et al., 2011). Only Ac4 displays a sexual dimorphism where females have significantly more sensilla of this type. Since our dissection method did not allow for any reliable quantification of chemosensory sensilla or neurons in the different sacculus chambers (Shanbhag et al., 1995), we obtained the numbers from recent studies for this structure. Ir64a-positive neurons are described as 16 OSNs per antenna lying around the third chamber of the sacculus (Ai et al., 2010) next to the described ~4 Ir40a-positive neurons per antenna, surrounding the first chamber (Kain et al., 2013). According to (Shanbhag et al., 1995), the remaining sensilla are poreless hygro- or thermosensors similar to the 6 hot or cold sensors situated in the arista basis (Gallio et al., 2011). Adding up to the antenna derived afferents to the AL we also quantified the OSN pattern for the MP. Most sensilla were found on the lateral side of the MP including half of the Pb1, most Pb2 and all Pb3. The remaining Pb1 and Pb2 were found in the dorsal and dorsomedial regions. Confirming previous studies (De Bruyne et al., 1999; Stocker, 1994), we did not observe any significant sexual dimorphism regarding the number of OSNs on the palps. Along with the spatial mapping of the sensilla types, we quantified the number of neurons per CR type by counting at least one type per sensillum (Fig 1D). The number of OSNs in trichoid sensilla per CR type ranges around 20 OSNs (At2, At3, At4) with the exception of At1 (~60 OSNs), whereas OSNs in the antennal basiconic sensilla are covering a broad scale from 10 up to 40. Similar quantities are found for the coeloconic sensilla ranging from 10 to 46 OSNs. The palp basiconic sensilla are housing 14 (Pb1), 13 (Pb2) and 30 (Pb3) OSNs. Having counted one specific OSN type per sensillum and knowing the amount of housed OSNs within the particular sensillum type (Couto et al., 2005; Silbering et al., 2011), we estimated the total number of sensilla per class on the antenna as well as

on the palp (Fig 1B) and further calculated the total number of OSNs in both organs per sensilla class (Fig 1A). Males had slightly more At sensilla than females housing 240 OSNs and 232 OSNs, respectively. Basiconic sensilla are more abundant in females than in males with 500 OSNs and 397 OSNs, respectively. This was also the case for the coeloconics, where females had 274 OSNs compared to males with 240. The palp basiconics were more abundant in males than in females. These quantities form a total median amount of palp basiconics of 56 OSNs, which is similar to the data shown by (De Bruyne et al., 1999). We have now provided a detailed view on the general numbers of sensilla and somata on the antenna in total with 414. Our quantifications are in line with classic morphological studies (Shanbhag et al., 1999; Stocker, 1994). However, but we would like to emphasize the immense variability that the olfactory system displays already at the peripheral level, which is far from a uniform 30:1 convergence (Ramaekers et al., 2005; Stocker, 2001; Vosshall and Stocker, 2007) of OSNs on their way to the AL. Furthermore, we show a sexual dimorphism at the level of single sensilla types which was so far only described for the whole sensilla classes (Shanbhag et al., 1999) or for individual receptors (Dobritsa et al., 2003). Hereby, we state that only some types display the sexual dimorphism described for the sensilla classes. Thus, the drastic female superiority in basiconics was only represented by Ab1, 2, 6 and 10, whereas males had more At2 and At4, leading to a significantly higher number of trichoids in general in males. The coeloconic sensilla display a significant difference in general numbers but only Ac4 was significantly more numerous in females.

OSN numbers determine the glomerular volume

Having the exact data per CR, we next correlated these with the glomerulus--specific volume, analyzing the potential connection between the two glomerular attributes as it was shown a causal relation (Acebes and Ferrús, 2001). Lacking comprehensive *in vivo* glomerulus volume data, we used the *in vivo* neuropil labeling via END1-2 (Grabe et al., 2014) for *in vivo* reconstructions of the AL. Available *in vivo* data is mostly restricted to assorted single glomeruli (Devaud et al., 2001; Devaud et al., 2003) although most studies were done *in vitro* (Kondoh et al., 2003) which turned out to be problematic comparing them with *in vivo* datasets (Grabe et al., 2014). Building on our previously published volumetric dataset for *in vivo* female glomeruli we used the exact same approach gathering data for all lacking female glomeruli as

well as for all of them in males. Our possibilities in gaining glomerulus-specific *in vivo* volume data in combination with our established comprehensive atlas and the obtained OSN quantities enabled us to question a correlation between the number of glomerulus-specific OSNs and glomerular volume. The input data show that the sexual dimorphism in the OSN quantity described for the sensilla classes (Shanbhag et al., 1999; Stocker, 1994) is not an attribute of the whole class but of single specific CR types (Fig 1). Hence, we wondered whether these sex-specific numbers of OSN afferents converging onto glomeruli are reflected in the glomerular volume. We determined the volume for all glomeruli from *in vivo* confocal scans of END1-2 flies, except the VP cluster, where only VP1 and VP4 receive chemosensory input (Kain et al., 2013) in contrast to the thermosensory VP2 and VP3 (Gallio et al., 2011). In order to adjust for sex-specific inter-individual variability (Fig 2A), we compared the glomerular volume relative to the size of the summed glomerular volume per animal. We observed that the glomeruli, which receive input from trichoid sensilla (DA1, DA3, DA4l, DA4m, DC1, DC3, DL3, VA1d and VA1v), cover about 22% of the complete AL volume (Fig 2B). This volumetric proportion corresponds to their proportion of corresponding OSNs (22.7%). DA1, VA1d and VA1v represent the largest glomeruli (4-7% of the AL, Fig 2D), while DC1 and DC3 have an intermediate volume (around 2%). The glomeruli receiving basiconic input are more uniform in their volumetric distribution. They sum up to 39% of the glomerular AL volume (41.8% of total OSNs). Glomeruli with coeloconic input scale from 1% to 5% and sum up to 30% of the glomerular AL volume (24.8% of total OSNs). The glomeruli getting input from the palps (VA4, VA7l, VC1, VC2, VM7d and VM7v) have an equally small size which adds up to 8% in total of the complete AL volume (10.7% of OSNs). Summed glomerular volumes per sensilla input class are strongly correlated with the summed OSN quantity (Fig 2C) underlining the major role of OSNs in glomerular volume definition (Acebes and Ferrús, 2001). Regarding the sexual dimorphism, it has already been shown that glomeruli DA1 and VA1v are significantly larger in females than in males (Kondoh et al., 2003). However, we observed only gender related differences in glomeruli DA4m, VA2 and VA6, which are larger in males than in females, as well as in glomeruli DM1, DL5, DP1l and VM5d, which are larger in females than in males. These glomeruli are responsive to a broad range of volatile cues (De Bruyne et al., 2001; Dobritsa et al., 2003; Galizia et al., 2010; Hallem and Carlson, 2004, 2006; Silbering et al., 2011) making it difficult to assign a general

origin for the sexual dimorphism. For DM1 and VA2 we also observed a dimorphic OSN quantity leading to a potential sex-specificity regarding their ligands (Acebes and Ferrús, 2001). These two glomeruli receive higher OSN input in females than in males (Fig 1D), which correlates very well to a significant bigger volume of glomerulus DM1 in females. However, such a correlation is not true for glomerulus VA2 indicating that the OSN number is not the only determinant for the glomerular volume. Notably, none of the seven glomeruli that we found to be sexually dimorphic are fruitless-positive (Ito et al., 1996; Ito et al., 2012; Lee et al., 2000; Neville et al., 2014; Stockinger et al., 2005) suggesting that there might be another underlying factor that affects sexual dimorphism. We could not observe the described difference for the VL2a, being larger in males than in females (Stockinger et al., 2005), possibly due to the fact that it is described as only slightly but significantly bigger. However, future studies are needed to analyze whether these CRs/glomeruli are indeed involved in gender-specific behavior. In summary the total number of OSNs significantly correlates to the glomerular volume (Fig 2E). Analyzing the comparison of glomerulus-specific OSNs and the respective volume separately for each sensillum class, the correlation holds true for the antennal basiconics (Fig 2G) but not for the trichoids, coeloconics and palp basiconics (Fig 2F, 2H and 2I) and their respective glomeruli. Therefore the fact that some glomeruli which receive quantitatively identical input from the same sensillum type display in the periphery an enormous difference regarding their volume (e.g. DL3 and VA1d/v or DM4 and DM5) indicates that also other neurons than OSNs might affect the volume. This variability could be explained either by a difference in the innervation density of the OSN axon terminals or by diverse numbers or density of innervating LNs and PNs, or by a combination of both. The glomeruli DL4 and DM6, both receiving input from the same number of OSNs ascending from sensillum Ab10, display significantly different numbers of synapses per OSN in each glomerulus (Mosca and Luo, 2014). These variable factors could lead to two glomeruli that seem to be morphologically identical but bear entirely different intraglomerular neuronal circuitry and by this serve a totally different function. Glomeruli that receive quantitatively non-uniform input from the antenna should display differences regarding their volume (Chou et al., 2010; Dekker et al., 2006; Linz et al., 2013) as well as differences in their sensitivity (Acebes and Ferrús, 2001), especially if every OSN synapses with every PN within a single glomerulus (Kazama and Wilson, 2009). In this study we did not consider the fact that in

dipterans a large proportion of OSNs is actually bilateral and not solely ipsilateral (Stocker et al., 1990; Strausfeld, 1976).

Number of output neurons is diverse and glomerulus-specific

We found an overall correlation of the number of OSNs per glomerulus and the respective glomerular volume (Fig 2E to I). We wondered next, whether each glomerulus is innervated by a uniform number of output neurons or if this number is also glomerulus-specific analogue to the number of OSNs. To quantify the number of output neurons for each glomerulus, we expressed photoactivatable GFP (Patterson and Lippincott-Schwartz, 2002) under the control of the enhancer trap line GH146-GAL4 (Stocker et al., 1997). This line is described to label about 66% of uniglomerular excitatory PNs (ePNs (Jefferis et al., 2001; Lai et al., 2008)) which project almost exclusively via the medial AL tract to the MB calyx and further to the LH. A small proportion is projecting via the mediolateral AL tract to the LH and further to the MB calyx. Nomenclature of the neuronal tracts follows the nomenclature of (Ito et al., 2014). After obtaining a pre-photoactivation scan of the AL, we identified the target glomerulus and photoactivated it in a single central plane. The diffused C3PA then highlighted the corresponding somata of all innervating PNs in one of the three cell clusters around the AL (Fig 3A) as well as the axonal projections to the MB calyx and LH. Notable, our results reveal that the so far assumed number of 1-3 innervating uniglomerular PNs per glomerulus (Wong et al., 2002) applies for most cases (Fig 3B). However, we also observed that some glomeruli, as D, DA1, DA2, DC3, DL3 and VA1v are innervated by a considerable higher number of PNs. These glomeruli were innervated by on average 6 (± 2) PNs. Notable, all of them belong to crucial information pathways. The three glomeruli receiving trichoid input (DA1, DL3 and VA1v) are known to, or at least putatively expected to, play a role in courtship and mating (Kurtovic et al., 2007; Lebreton et al., 2014; Liu et al., 2011; Stockinger et al., 2005), DA2 is encoding strong aversion behavior to Geosmin (Stensmyr et al., 2012), DC3 codes for odors which induce egg laying on citrus fruits (Dweck et al., 2013; Ronderos et al., 2014) but D is unknown.

We frequently observed a multiglomerular vPN for some glomeruli but not all, although it is described that GH146 includes one vPN which is innervating the entire AL (Marin et al., 2002). Possibly we do not label this neuron due to its described sparse innervation in single glomeruli since we are only activating single focal planes

of each glomerulus. Plotting the glomerulus-specific PN quantities with the glomerular volume, a weak, but not significant correlation is visible. This is also the case if we analyze the sensilla classes separately (Fig 3D through 3G) except for the antennal basiconics (Fig 3E), which are surprisingly negatively correlated. Since PNs are numerically underrepresented in relation to the glomerulus-specific OSNs, their weaker impact on the glomerular volume is not surprising. (Chou et al., 2010) described specific LNs of several classes with diverse glomerular innervation frequencies that possibly are having more impact on the glomerulus volume.

Quantification of all excitatory PNs

Adding the GH146 positive uniglomerular PNs to the specific OSNs did not improve the correlation between the number of glomerulus-specific neurons and the respective volume (data not shown). Since GH146 is not labelling all excitatory PNs leaving the AL we extended the experimental scope and expressed photoactivatable GFP under the control of ChA-GAL4 (Fig S1A) to analyze whether we underestimated the number of excitatory uniglomerular output neurons per glomerulus. We selected mainly sparsely innervated glomeruli which are targeted by only one or two uniglomerular PNs (DC1, DM1, DM3, DM2 and VL2a) and some densely innervated glomeruli (DA1, VA1v, DA2). Additionally we aimed for two glomeruli (V and VM5v) which are known to be GH146 negative (Grabe et al., 2014). Our analysis of all cholinergic PNs shows that in general our quantification of ePNs per glomerulus is appropriate. DC1 and DM2 for example (Fig S1B) possess one additional uniglomerular cholinergic neuron each. We observed furthermore that glomeruli DM2 and VL2a were innervated by one to three additional cholinergic ventral PNs (vPNs, Fig S1B). Notably, PNs belonging to the ventral cell cluster have so far been described as mostly GABAergic (Okada et al., 2009; Wilson and Laurent, 2005). On the contrary, we labeled less anterodorsal and lateral PNs in glomeruli DA1, DA2 and VA1v using ChA-GAL4 than using GH146-GAL4. These findings imply the possibility of uniglomerular PNs in the lateral and anterodorsal cluster labelled by GH146 which are neither cholinergic nor GABAergic (Wilson and Laurent, 2005).

LN innervation frequency is negatively correlated with PN quantity

Completing the glomerulus neuronal components and searching for more evidences regarding functional classifications we integrated one additional dataset from (Chou et al., 2010) where they thoroughly investigated the glomerulus-specific frequency of

LNs. By incorporating this screen we could compensate for the lack of this neuron class in our approach. First, we analyzed the frequency of LN innervation related to each sensilla class (Fig 4A). Basiconics are evenly represented at all levels, trichoids display an overall reduced LN frequency, while coeloconics show either a very high (DP1l, VC3) or very low frequency (VL1, VM4) and palp basiconics receive generally frequent LN innervation. This initial trend for clustering with the sensilla class indicates a potential impact of LN frequency on a functional classification based on glomerular anatomy. Furthermore we observed that the specific LN frequency significantly correlates with the glomerular volume (Fig 4B); in contrast to our PN count (Fig 3C). Notably, we do not see any correlation of LN frequency with the OSN number (Fig 4C), while we observe a negative correlation with the number of PNs (Fig 4D). This finding indicates that putative narrowly tuned glomeruli with a high number of PNs (Fig 3B) are less innervated by LNs and therefore possess less lateral input as well as exhibit fainter lateral excitatory as well as inhibitory output. The LN based correlations with other morphological parameters do not allow any functional classification supported by crucial glomerular descriptors (Fig 4E, 4F and 4G) such as attractive (cyan) or aversive hedonic valence (magenta, both from (Knaden et al., 2012; Semmelhack and Wang, 2009)) and being fruitless positive (green, (Stockinger et al., 2005)).

Lifetime sparseness allows to link morphology and physiology

Having generated this large variety of morphological attributes we wondered whether the glomerulus-specific innervation ratios correlate with the odor response profile. In order to quantify the odor tuning of a certain glomerulus, we calculated the lifetime sparseness (Bhandawat et al., 2007; Perez-Orive et al., 2002; Vinje, 2000) to evaluate a glomerulus‘ likeliness to respond to any given odor on the basis of the knowledge of its characterized odor responses (Galizia et al., 2010; Hallem and Carlson, 2006). Associating this glomerulus-specific factor with the corresponding morphological features we observed that the number of OSNs shows no correlation at all (Fig 5A) even though the lifetime sparseness data are based on OSN response properties. Hence the selectivity of the chemosensory receptors seems not to be represented in the plain number of OSNs where it is expressed. One step further, at the PN level (Fig 5B), we observe a significant correlation between the number of PNs and the tuning properties, meaning that a high PN number is related to a sparse

response profile underlining the putative selectivity of glomeruli having a numerous output (Fig 3B). By comparing the lifetime sparseness with LN innervation frequency (Chou et al., 2010), we gathered even more evidence for this assumption (Fig 5C) seeing that more selective glomeruli are less frequently innervated by LNs thus performing less LN processing.

Discussion

Neuroanatomical studies often point out an obvious link of form and function when macroglomerular complexes are depicted as putative sites of pheromone perception (Boeckh and Tolbert, 1993; Galizia et al., 1999; Hansson et al., 1992; Schneiderman et al., 1986) based on the size of a glomerulus underlining its importance. Furthermore this relation is frequently brought up if sexual dimorphism has to be pointed out due to volumetric differences in glomerular size or input quantity. Past this point, a meaning of glomerular appearance according to its role in the olfactory system of *Drosophila melanogaster* is usually neglected. The understanding of glomerular uniformity most likely originates in the general assumption that the neuronal composition of glomeruli is mostly identical (Ramaekers et al., 2005; Vosshall and Stocker, 2007). Several studies have shown that even slight differences in glomerular volume can result in a different amount of neuronal components (Acebes and Ferrús, 2001) and that the glomerular composition of the AL and the regarding peripheral units are quite plastic between various drosophilid species (Dekker et al., 2006; Linz et al., 2013). Although different glomeruli are also described gathering different amounts of input within one species (De Bruyne et al., 2001; Shanbhag et al., 1999) the dogma of glomerular uniformity is widely accepted. On the other hand ultrastructural studies are uncovering more and more glomerulus-specific properties such as a fixed number of synapses per OSN which is different for the OSNs of every glomerulus (Mosca and Luo, 2014) or specific intraglomerular innervation patterns for every neuronal type (Chou et al., 2010). These anatomical specificities are in line with the increasing number of studies showing extremely specific functionalities for single glomeruli (Kurtovic et al., 2007; Ronderos et al., 2014; Stensmyr et al., 2012; Suh et al., 2004). Solely the lack of thorough morphological screens at a glomerulus-specific level prohibits the link of form and

function besides the pheromone circuitry (Boeckh and Tolbert, 1993; Galizia et al., 1999; Hansson et al., 1992; Schneiderman et al., 1986).

Our study bridges the gap between the superficial and detailed levels of anatomy by providing a comprehensive screen of glomerulus-specific morphological attributes, divided by the two sexes, such as the exact mapping and quantification of the input neurons, *in vivo* volume of each glomerulus and the precise count for uniglomerular excitatory output neurons (PNs). In combination with the functional characterization of the odor tuning of so far underrepresented CRs in addition to previous studies (Hallem and Carlson, 2006; Kreher et al., 2008) our study allows the first correlation of functional specifications with anatomical attributes, such as neuronal numbers and glomerular volumes.

Various OSN types and glomeruli are sexually dimorphic

Our knowledge regarding the distribution of the different OSN classes on the funiculus, the third antennal segment, where most of the chemosensory sensilla are located, and the maxillary palp has made large progress over the last decades, beginning with morphological characterizations of sensilla types (Shanbhag et al., 1999; Stocker et al., 1990) over mapped OSN recordings (De Bruyne et al., 1999), *in situ* studies (Couto et al., 2005; Dobritsa et al., 2003) to the employment of specific receptor GAL4-lines in combination with LacZ- (Fishilevich and Vosshall, 2005) or nls:GFP-staining (Silbering et al., 2011). In our study, we were able to precisely map for the first time 95% of sensilla types by using 21 specific chemosensory receptor GAL4-lines (Fishilevich and Vosshall, 2005; Kurtovic et al., 2007; Silbering et al., 2011). The obtained map provides the detailed expression patterns for sensilla classes (Fig 1B) and types (Fig 1C). By comparing our results with previous publications (De Bruyne et al., 1999; Shanbhag et al., 1999; Silbering et al., 2011; Stocker, 1994), we can confirm the depicted distributions of the five sensilla classes (Fig 1B) and their housing OSN types (Fig 1A). Trichoid and intermediate sensilla are mainly found on the distal tip of the funiculus, while coeloconics and antennal basiconics occur over the whole antennal structure. Palp basiconics show a similar pattern and are evenly distributed with a majority being presented on the lateral side of the palp. The overall number of sensilla per class corresponds with previously published counts (Shanbhag et al., 1999; Stocker, 2001) and displays the described sexual dimorphism for trichoids and antennal basiconics but not for the palp

basiconics. We additionally depict a putatively high variance of these numbers based on the described deviation for each sensilla type quantity (Fig 1D and Table 1). Whether this deviation is necessary for plasticity or represents plain interspecies variability remains to be analyzed.

The so far assumed 30:1 convergence of OSNs per glomerulus (Ramaekers et al., 2005; Vosshall and Stocker, 2007) served as the basis for glomerular uniformity. However, by quantifying the exact number of OSNs that converge onto each glomerulus, we can show that this number is glomerulus-specific and largely variable across the AL ranging from 8 up to 60 OSNs (Fig 1D and Table 1). This finding breaks the initial dogma of glomerular uniformity in the first place. Moreover, we observed a group of glomeruli showing various levels of sexual dimorphism at the periphery which have not been described so far in addition to the well-characterized fruitless circuit (Ito et al., 2012; Stockinger et al., 2005) such as glomeruli VA1d, DL3, VA2, V, DM1, DL1, DM4, DM5, DM6, DL4, VA5, DC2, VL1 and VM4. Some of these glomeruli are putative pheromone-coding glomeruli, like VA1d (Dweck, 2014), or are described to play crucial roles in mating (glomerulus DL3; (Lebreton et al., 2014)), or CO_2 avoidance (glomerulus V (Suh et al., 2004)). The relevance of the observed sexual dimorphism of these various glomeruli remains to be analyzed further. Interestingly, we see no sexual specificity for the glomerulus DA1 (Fig 1D and Table 1), being the most thoroughly investigated fruitless-positive pheromone glomerulus (Stockinger et al., 2005). Pointing out that OSN quantity alone is not sufficient to describe the sexual dimorphism of glomeruli.

OSN and LN quantity determines the glomerular volume

Being able to measure the *in vivo* volume of glomeruli in a less artificial way (Grabe et al., 2014) we quantified the whole AL (Fig 2 and Table 1) providing a comprehensive dataset for both sexes only missing the most ventroposterior glomeruli which are difficult to assess with our approach. Reliability of our data is verified as we can confirm the previously described presence (DA1 and VA1v) and absence (DL3 and VA1d) of sexual dimorphism for a few glomeruli ((Kondoh et al., 2003), Fig 2D). Linkage between the number of OSNs and the glomerular volume was indirectly shown using the *gigas*-mutation (Acebes and Ferrús, 2001) in *Drosophila melanogaster* and from an evolutionary perspective in *Drosophila sechellia* (Dekker et al., 2006) and *Drosophila erecta* (Linz et al., 2013). Our

correlation analysis reveals that the OSN number is in fact determining the volume of a glomerulus (Fig 2C). If we break this correlation down to the single receptor/glomerulus level, we observe a strikingly significant correlation of input quantity and volumetric properties of the regarding glomerulus (Fig 2E). Notably, when we correlate the number of LNs with glomerular volume, we also observe a significant, but weaker correlation compared to the OSNs (Fig 4B). A similar morphological coherence has been described for LNs in *Anopheles gambiae* (Ignell et al., 2005). Interestingly there is hardly any correlation of PN quantity with the respective volume measure (Fig 3C) although the number of PNs is glomerulus-specific (Fig 3B). Instead we observe a negative correlation between the projection neuron density and the local interneuron abundance (Fig 4D) showing that glomeruli with higher output neuron count (DA1, DA2, DL3, VA1v) are less likely to be innervated by local interneurons, underlining the proposed feed forward nature of narrowly tuned glomeruli (Stensmyr et al., 2012; Suh et al., 2004) being potentially less affected by lateral input via local interneurons. As narrow neurons are putatively seldom activated they don't need large filtering in contrast to broad tuned OSNs which are almost constantly on and therefore need a huge amount of filtering by local interneurons.

Our thorough mapping of PNs complements the previously published single cell clones of GH146-positive PNs (Jefferis et al., 2007; Marin et al., 2002; Marin et al., 2005; Wong et al., 2002) and proves the estimated count of one to three projection neurons per glomerulus (Wong et al., 2002) is true for most glomeruli (Fig 3B).

Glomerular response profile correlates with LN / PN number

Notably, we observed a negative correlation between the glomerulus-specific PN numbers and the LN innervation frequency (Fig 4D) showing that glomeruli with a higher number of PNs (such as DA1, DA2, DL3, VA1v) are less innervated by LNs. This highlights a feed forward characteristic of narrowly tuned glomeruli being potentially less affected by lateral input via LNs. Interestingly glomeruli that have a higher number of PNs are described to be part of crucial pathways involved in reproduction and survival, such as the perception of pheromone (VA1d, VA1v, DL3, DA1, (Dweck, 2014; Kondoh et al., 2003; Lebreton et al., 2014; Stockinger et al., 2005)) or strongly aversive cues (DA2, V, (Stensmyr et al., 2012; Suh et al., 2004)) Since, sparsely tuned glomeruli become hardly activated, it is therefore highly

important that their signals are transferred to the higher brain centers. Hence, a higher number of PNs can ensure a reliable output. In addition the variable PNs might have multiple functions and might encode various features of the stimulus, such as e.g. different intensities as shown for the CO_2 circuitry (Lin et al., 2013). Moreover does the minor LN innervation indicate a decreased integration of glomeruli in the lateral network of the AL (Chou et al., 2010; Root et al., 2008).

Diverse neurotransmitter repertoire

In order to cover the majority of PNs for each glomerulus, we employed photoactivation using the GH146-GAL4 line (Stocker et al., 1997). Since this line is not covering all glomeruli (Grabe et al., 2014), except for one multiglomerular vPN (Marin et al., 2002) and possibly not all PNs we also utilized ChA-GAL4 (Salvaterra and Kitamoto, 2001) since PNs are described to be cholinergic (Jefferis et al., 2001; Lai et al., 2008) while multiglomerular PNs are characterized as GABAergic (Jefferis et al., 2001; Lai et al., 2008; Liang et al., 2013; Okada et al., 2009; Strutz et al., 2014). Further neurotransmitters such as glutamate are known for LNs of the AL in particular (Liu and Wilson, 2013) but also dopamine, octopamine and serotonin occur in the fly's olfactory system in general (Chiang et al., 2011). The fact, that we observed less PN somata in the lateral cluster after photoactivation in ChA-GAL4 than in GH146 for glomerulus DA2 (Fig S1B), suggests the potential occurrence of additional neurotransmitters. Since only 6 ventral PNs are described as GABAergic (Wilson and Laurent, 2005) and the remaining ventral, lateral and anterodorsal ones are cholinergic (Wilson et al., 2004), our findings strengthen the question for additional neurotransmitters in the system and show that one glomerulus can be innervated by PNs originating from more than one cluster (Lai et al., 2008). Just recently bilingual neurons were discovered in rodents expressing two different neurotransmitters (Root et al., 2014) adding another eventuality to the understanding, although this circumstance seems not necessary for neurons to be bimodal. Single LNs in zebra fish were depicted being excitatory and inhibitory through a shift from electrical (excitation) to chemical (inhibition) coupling depending on an activity dependent threshold (Zhu et al., 2013).

Missing link of form and function

Based on the detailed mapping and quantification of input-output neurons, the glomerular volume, and the novel physiological characterization of CRs (Fig S2) in

combination with the glomerular innervation frequency of LNs (Chou et al., 2010), we can now correlate the morphological properties of individual glomeruli with their functionalities. This allows classifying glomeruli as subunits of the AL in a joint context of anatomy and physiology and hence, to predict the role of so far not characterized glomeruli. As an initial example we picked the two glomeruli DA2 and DL5 (Fig 5D), both receiving input from 22 OSNs housed in the same sensillum Ab4 on the funiculus. The known response profile of Or7a which targets glomerulus DL5 (Galizia et al., 2010), being very broad, and Or56a targeting glomerulus DA2 (Fig S2), being narrowly tuned, exhibit quite diverse response profiles depicting an odd glomerular couple. Therefore glomerulus DL5 is not affiliated with a succinct behavioral task and seems not to play a crucial role in olfactory perception. On the other side, glomerulus DA2 has been characterized as the indicator for an extremely important information pathway on the presence of harmful bacteria leading to robust aversion (Stensmyr et al., 2012). The significance of DA2 as an aversion-coding glomerulus is supported by its high number of excitatory PNs having potentially larger random input on mushroom body Kenyon cells (Caron et al., 2013; Gruntman and Turner, 2013). Moreover the high ePN number supports plasticity (Heimbeck et al., 2001; Heisenberg, 2003)and exhibits potentially more synapse to third order neurons of the lateral horn (Jefferis et al., 2007; Liang et al., 2013; Marin et al., 2002; Parnas et al., 2013; Strutz et al., 2014; Tanaka et al., 2004; Wong et al., 2002) than the single PN leaving the DL5 (Fig 3B). The difference in output quantity is connected to an inverse proportionate LN innervation frequency (Fig 4D) underlining the more independent nature of DA2 as it is putatively innervated by less LNs (Chou et al., 2010) and therefore has fewer lateral interactions (Olsen et al., 2007; Shang et al., 2007) with other glomeruli such as presynaptic gain control (Root et al., 2008). DL5, in contrast, represents an example for stronger implementation in the AL-LN circuitry with a putatively larger amount of lateral output and input as well as feedback. Interestingly is the DL5 way larger than the DA2 which contradicts the common assumption of a link between plain size and importance like in the pheromone systems and macroglomerular complexes (Boeckh and Tolbert, 1993; Galizia et al., 1999; Hansson et al., 1992; Schneiderman et al., 1986). The dissimilarity in size may originate mainly in the higher amount of LNs (Fig 4B) unaffected by the inverse PN relations, of six ePNs in DA2 and only one in DL5, as their influence on the volume is minute (Fig 3C) in contrast to previous findings showing a rough correlation (Yu et al.,

2010). Alternatively the altering intraneuronal density of synapses per OSN (Mosca and Luo, 2014) may interact with the volume although the overall OSN density per glomeruli is described to be stable. In fact there has to be at least one more reason for glomerular volumetric composition as we cannot trace the observed sexual dimorphism in DL5 (Fig 2D) in any of the other morphological properties.

Based on our novel morphological knowledge of olfactory pathways which are physiologically and behaviorally well characterized, such as Or67d/DA1, Or47b/VA1v – involved in courtship – and Or56a/DA2 – involved in avoidance – we can propose putatively similar crucial functions for an example group of underrepresented pathways like Or69a/D, Or83c/DC3 and Or65a/DL3. As a rather small glomerulus (Fig 2D), Or69a/D receives input of only ~20 OSNs (Fig 1D) and has a medium LN innervation frequency (Fig 4A). The characterization of Or69a (Fig S2) shows a quite broad tuning curve which contradicts an extremely specialized function but the medium high number of four PNs (Fig 3B) in combination with the mentioned low LN frequency resembles the overall appearance of the Or56a/DA2 pathway. Not knowing any particular behavioral necessity of the D glomerulus we would propose a rather high importance based on its morphological representation.

Similar predictions can be made for the Or83c/DC3 pathway. Its described selectivity for farnesol (Ronderos et al., 2014) in combination with a high LN frequency and intermediate and sex specific PN quantity, shaping a medium sized glomerulus with the same input quantity as Or69a/D, predict a putatively gender selective role as it is described for its impact in inducing egg laying behavior in female flies (Dweck et al., 2013; Ronderos et al., 2014).

A third prediction can be done for the Or65a/DL3 pathway. Again, having low input counts (~20 OSNs), small volume in combination with a high PN count (6 ePNs) and low LN frequency, predicts a potential behavioral importance. As it is already described to have a modulatory impact on mating behavior in female *Drosophila* (Lebreton et al., 2014) the lack of a known ligand is the last step to a thorough examination of this pathway.

Glomerulus uniqueness

These three above mentioned examples represent a set of about 15 glomeruli in total, which are so far underrepresented in recent studies, for which we generated a comprehensive morphological database supporting future physiological studies and

re-evaluation of previous ones further adding up with the characterization of 14 well examined glomeruli.

Morphologically screening of the glomerulus-specific variables such as sensory input quantity (Fig 1), *in vivo* volume (Fig 2), PN quantity (Fig 3) and improving the characterization of receptor selectivity (Fig S2) expands the level of complexity of the glomerular venue. Moreover we described new relations of morphological properties such as the negative correlation of LN innervation frequency and PN quantity (Fig 4) or their opposed correlation with the lifetime sparseness (Fig 5). Furthermore we could emphasize known relations, like the crucial impact of the OSN count on glomerular volume ((Acebes and Ferrús, 2001), Fig 2), as well as specify the diverse impact of PNs (Fig 3) and LNs (Fig 4) on the glomerular volume. And finally we depicted so far unknown sexual dimorphisms at the glomerular level.

One limitation of our study is that we cannot draw conclusions regarding any intraglomerular circuits and intraneuronal properties which are to date generally rare in flies (Chou et al., 2010; Mosca and Luo, 2014). Therefore we cannot take them into account omitting neuronal specialties which would putatively add complexity to the model like specific gap junction distributions (Yaksi and Wilson, 2010), explicit neuropeptide repertoires of the neuronal classes (Busch et al., 2009; Carlsson et al., 2010; Chiang et al., 2011; Liu and Wilson, 2013), glomerulus shaping effects of glial cells (Kazama and Wilson, 2009) or LN classification (Chou et al., 2010; Seki et al., 2010; Wilson and Laurent, 2005) potentially indicating glomerulus ultrastructural subdivision as observed in crustaceans (Polanska et al., 2012).

However, we postulate that each glomerulus represents a unique morphological and functional structure as there are no two glomeruli sharing the exact same properties. The recent advances in superresolution microscopy (Willig and Barrantes, 2014) may contribute to solving these barriers.

Table 1 | Glomerulus-specific dataset

[a] Data from (Ai et al., 2010). [b] Data obtained by photoactivation with ChA-GAL4. [c] Alternative count with ChA is 4 PNs (± 0.6). [d] Data from (Kain et al., 2013). [e] Data from (Gallio et al., 2011).

Sensillum	Receptor	Glomerulus	OSNs (±SD)		*In vivo* Volume (µm³ ±SD)		PNs (±SD)		Lifetime Sparseness (Source)
			female	male	female	male	female	male	
Ab9	Or69a	D	24 (6.1)	17.5 (4.3)	1170 (473)	1579 (552)	4 (0.7)	4 (1)	0.46 (original)
At1	Or67d	DA1	62.5 (10.8)	62.25 (11)	4738 (732)	6182 (1037)	8 (1.9)	10 (1)	0.98 (original)
Ab4	Or56a	DA2	24 (1.9)	21 (3.6)	1630 (677)	1050 (361)	6.5 (1)	5 (1.3)	0.99 (original)
At2	Or23a	DA3	15	18	629 (99)	692 (24)	GH146 negative		-
At3	Or43a	DA4l	27 (3)	22 (6.6)	1135 (119)	1041 (193)	1 (0)	1 (1.2)	0.79 (DoOR)
At3	Or2a	DA4m	27	22	935 (269)	1435 (275)	GH146 negative		-
At3	Or19a	DC1	27	22	2820 (593)	2532 (919)	1 (0.5)	1 (0)	0.70 (DoOR)
Ab6	Or13a	DC2	15 (2.5)	11 (1)	1415 (378)	1803 (239)	2 (0.9)	2 (0)	0.75 (DoOR)
At2	Or83c	DC3	15 (2.9)	18 (2.2)	1743 (311)	2017 (255)	4 (0.45)	2 (0.6)	0.74 (original)
Sac III	Ir64a	DC4	15[a]		1975 (312)	1875 (300)	GH146 negative		
Ab1	Or10a	DL1	37.5 (6.5)	26 (4)	2267 (603)	2037 (277)	3 (0.6)	2 (0.6)	0.84 (DoOR)
Ac3?	Ir75a/b/c	DL2d	-	-	2591 (1045)	2077 (432)	GH146 negative		-
Ac3?	Ir75a/b/c	DL2v	-	-	2362 (655)	2025 (716)	GH146 negative		-
At4	Or65a	DL3	19.5	25.5	615 (177)	791 (329)	5 (1.1)	6 (1.3)	-
Ab10	Or49a/Or85f	DL4	18 (3.2)	10.5 (2)	622 (177)	946 (305)	1 (0.4)	1 (0)	0.96 (original)
Ab4	Or7a	DL5	24	21	2865 (759)	1456 (334)	1 (0.6)	1 (0)	0.72 (DoOR)
Ab1	Or42b	DM1	38.5 (4.6)	32 (5.9)	4211 (493)	2821 (470)	1 (0)	1 (0)	0.57 (DoOR)
Ab3	Or22a/b	DM2	8 (3.9)	8 (2.9)	2241 (453)	2085 (267)	2 (0)	2 (0)	0.60 (DoOR)
Ab5	Or47a	DM3	34 (8)	31 (5.4)	1336 (305)	1420 (296)	1 (0)	2 (0.8)	0.67 (DoOR)
Ab2	Or59b	DM4	23	15.5	2597 (693)	2806 (503)	1 (0)	-	0.78 (DoOR)
Ab2	Or85a/Or33b	DM5	23 (6)	15.5 (3.6)	1269 (253)	912 (313)	2 (0.5)	1 (0.6)	0.85 (DoOR)
Ab10	Or67a	DM6	18	10.5	1439 (236)	1631 (191)	3 (0.4)	-	0.60 (DoOR)
Ac2	Ir75a	DP1l	15	12	3805 (297)	2659 (244)	GH146 negative		-

Sac III	Ir64a	DP1m	15[a]		5288 (812)	4244 (331)	1 (0)	1 (0)	-
Ab1	Gr21a	V	39.8	30	3438 (644)	3392 (1106)	5.5 (0.57)[b]		0.96 (DoOR)
At4	Or88a	VA1d	19.5 (3.7)	25.5 (4)	4433 (1200)	4502 (179)	3 (1)	3 (0)	0.94 (original)
At4	Or47b	VA1v	19.5	25.5	5347 (748)	6175 (409)	6 (0.9)	5 (1)	0.99 (original)
Ab1	Or92a	VA2	43.5	32 (7.3)	3278 (738)	4051 (455)	1 (0.4)	1 (0.5)	0.73 (DoOR)
Ab9	Or67b	VA3	24	17.5	1886 (274)	1470 (250)	2 (0.5)	2 (0.5)	0.69 (DoOR)
Pb3	Or85d	VA4	29	30.5	1619 (437)	1307 (334)	2 (0)	1 (0)	0.93 (original)
Ab6	Or49b	VA5	15	11	1126 (247)	1293 (484)	2 (0.5)	3 (0.75)	0.91 (DoOR)
Ab5	Or82a	VA6	34	31	2520 (218)	2667 (309)	1 (0.4)	2.5 (1.3)	0.75 (DoOR)
Pb2	Or46aA	VA7l	14.5 (2.7)	11.5 (0.9)	784 (330)	972 (295)	1 (0.5)	1 (0)	0.91 (original)
-	-	VA7m	-	-	1187 (489)	927 (229)	3 (0)	3 (0.6)	-
Pb2	Or33c	VC1	12 (1)	14 (2.2)	1953 (593)	1497 (126)	1 (0.5)	2 (0.5)	0.81 (original)
Pb1	Or71a	VC2	11.5	15	1090 (95)	1018 (152)	1 (0.5)	3 (1.5)	0.88 (original)
Ac3	Or35a	VC3	47.5 (6.9)	42 (10.3)	2728 (539)	2332 (568)	GH146 negative		0.59 (DoOR)
Ab7	Or67c	VC4	14 (4)	12 (1.3)	1588 (332)	1263 (306)	GH146 negative		0.73 (Hallem)
Ac2	Ir41a	VC5	15 (2.7)	12 (2.4	1182 (240)	1173 (466)	GH146 negative		-
Ac1	Ir75d	VL1	15	16	4729 (914)	3657 (318)	GH146 negative		-
Ac4	Ir84a	VL2a	29.5	24	3081 (446)	2693 (512)	1 (0)[c]	2 (1)[c]	-
Ac1	Ir31a	VL2p	15	16	3989 (709)	3378 (684)	3 (0)	-	-
Ac1	Ir92a	VM1	15 (1.7)	16 (2.5)	1509 (391)	1543 (415)	2 (0.4)	1.5 (1)	-
Ab8	Or43b	VM2	18 (6.5)	15 (2.4)	1551 (423)	1296 (528)	3 (0.8)	2 (0)	0.65 (DoOR)
Ab8	Or9a	VM3	18	15	1898 (170)	1309 (328)	2 (0.5)	2 (0.6)	0.56 (DoOR)
Ac4	Ir76a	VM4	29.5 (2.8)	24 (2.9)	2382 (391)	1703 (302)	1 (0.5)	1 (0.6)	-
Ab3	Or85b	VM5d	8	8	2097 (289)	1304 (370)	GH146 negative		0.61 (Hallem)
Ab7	Or98a	VM5v	8.5 (2.9)	9 (3.2)	1628 (46)	1385 (198)	5 (0.5)[b]		0.71 (Hallem)
Pb1	Or42a	VM7d	11.5 (6.5)	15 (4.5)	1578 (638)	1660 (531)	2 (0.8)	3 (0.4)	0.74 (original)
Pb3	Or59c	VM7v	29 (10.4)	30.5 (3.2)	1296 (632)	1085 (562)	3 (0.8)	2.5 (1)	0.81 (original)
Sac I	Ir40a	VP1+VM6	11 (2.8)[d]	9 (1.8)[d]	-	-	GH146 negative		-
Arista	hot	VP2	3[e]	3[e]	-	-	-	-	-
Arista	cold	VP3	3[e]	3[e]	-	-	-	-	-
Sac I	Ir40a	VP4	=VP1[d]	=VP1[d]	-	-	GH146 negative		-
			1047.8	**934.25**	**111593**	**103168**	**80.5**	**83**	**-**

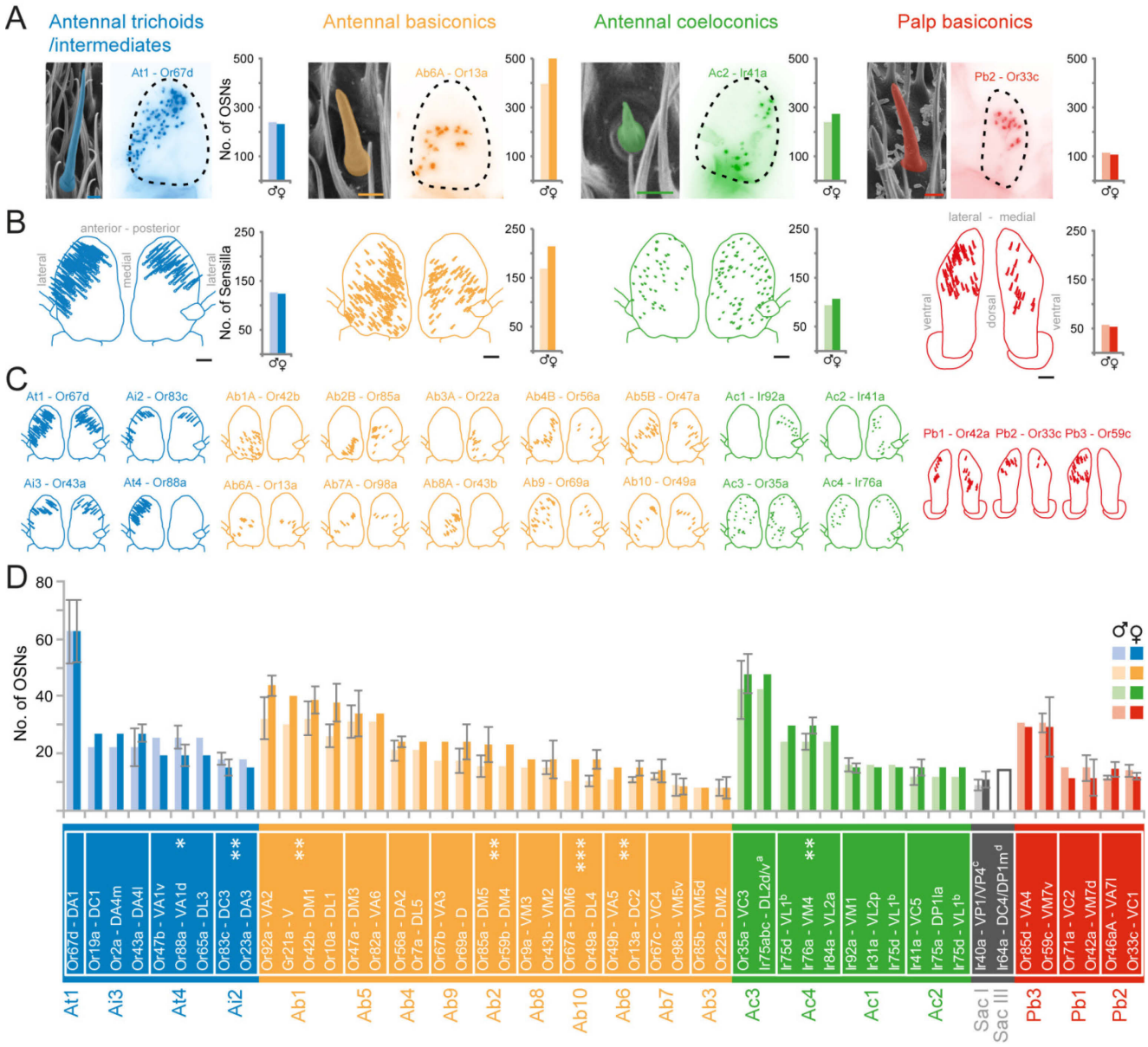

Figure 1 | Quantification and mapping of sensilla classes and OSNs

(A) Electron microscopic scans of each sensilla class (left), exemplified OR/IR mappings of the four sensilla classes (center) and sex specific differences in olfactory sensory neurons (OSN) quantity (right). (B) Mapping of all sensilla of a certain class (left) and sex specific differences in sensilla classes quantity (right). (C) Mapping of the single sensilla types in females. (D) Receptor specific quantities of OSNs. Columns with error bars have been counted, while columns without error bars have been interpolated. For Gr21a the mean of all Ab1 neurons was used (Or92a, Or42b and Or10a). Data represent median ± SD. Statistical differences between sexes were determined by Student's t test, *p < 0.5, **p < 0.1, *** p < 0.001. n = 5-

30. Colors indicate the sensilla classes antennal trichoids (blue), antennal basiconics (orange), antennal coeloconics (green), palp basiconics (red), sensilla housed in the sacculus (grey). Males are indicated by light colors and females by dark colors. The scale bar equals 2 µm in the electron microscopic images and 20 µm in the schematics. [a] After (Silbering et al., 2011) both parts of DL2 receive putative input from Ir75abc in Ac3; [b] After (Silbering et al., 2011) receiving input from Ac1, Ac2 and Ac3; [c] Data from (Kain et al., 2013); [d] Data from (Ai et al., 2010).

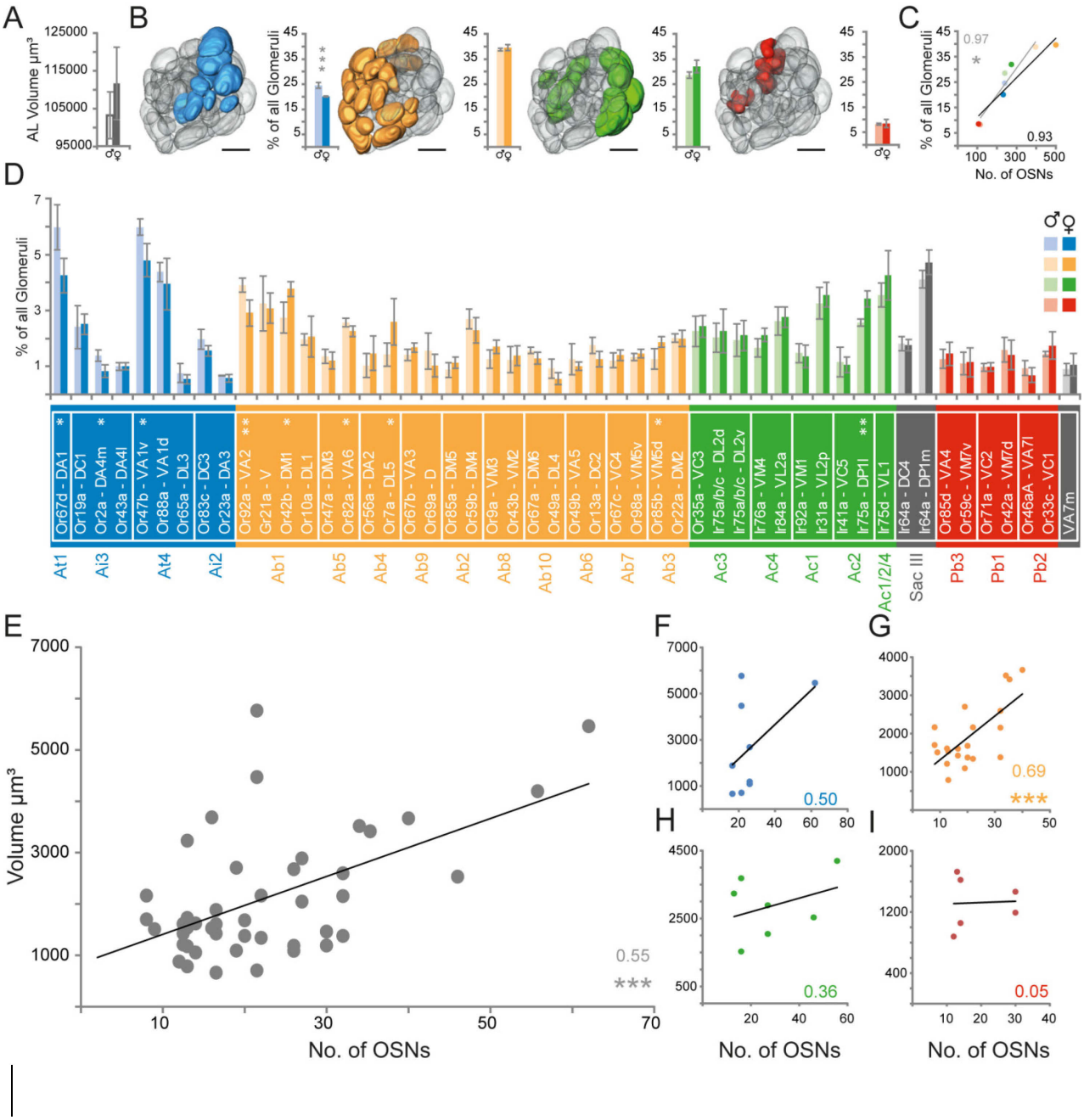

Figure 2 | Glomerulus-specific relative volume

(A) Entire AL volume of males (empty column) and females (filled column). Data represent median ± SD. (B) 3D reconstructed AL with selective coloring of the sensilla affiliated glomeruli clusters (left) and the sexually dimorphic AL proportion of the clusters (right). The scale bar equals 20 µm. Glomerulus-specific volume relative to the sum of all labelled glomeruli per animal. The color code refers to Fig 1 with the expansion of thermosensory glomeruli and unassigned ones (grey). (C) Correlation of the summed number of OSNs per sensilla class and the respective summed glomerular volume for males and females (color code as in B). The two trend lines

are for males (grey) and females (black). R-values are inset. Two tailed probability of the Pearson correlation coefficient is *p < 0.5. (D) Glomerulus-specific volumes shown as percentage of all labeled glomeruli per specimen. Data in A, B and D are median ± SD. Statistical differences between sexes were determined by Student's t test, *p < 0.5, **p < 0.1, ***p < 0.01. n = 4 for males and females each. (E) Correlation of glomerular volume and number of glomerulus-specific OSNs and (F-I) segregated for each sensilla class. The r-value is inset and two tailed probability of the Pearson correlation coefficient is ***p < 0.01. The color code refers to Fig 1.

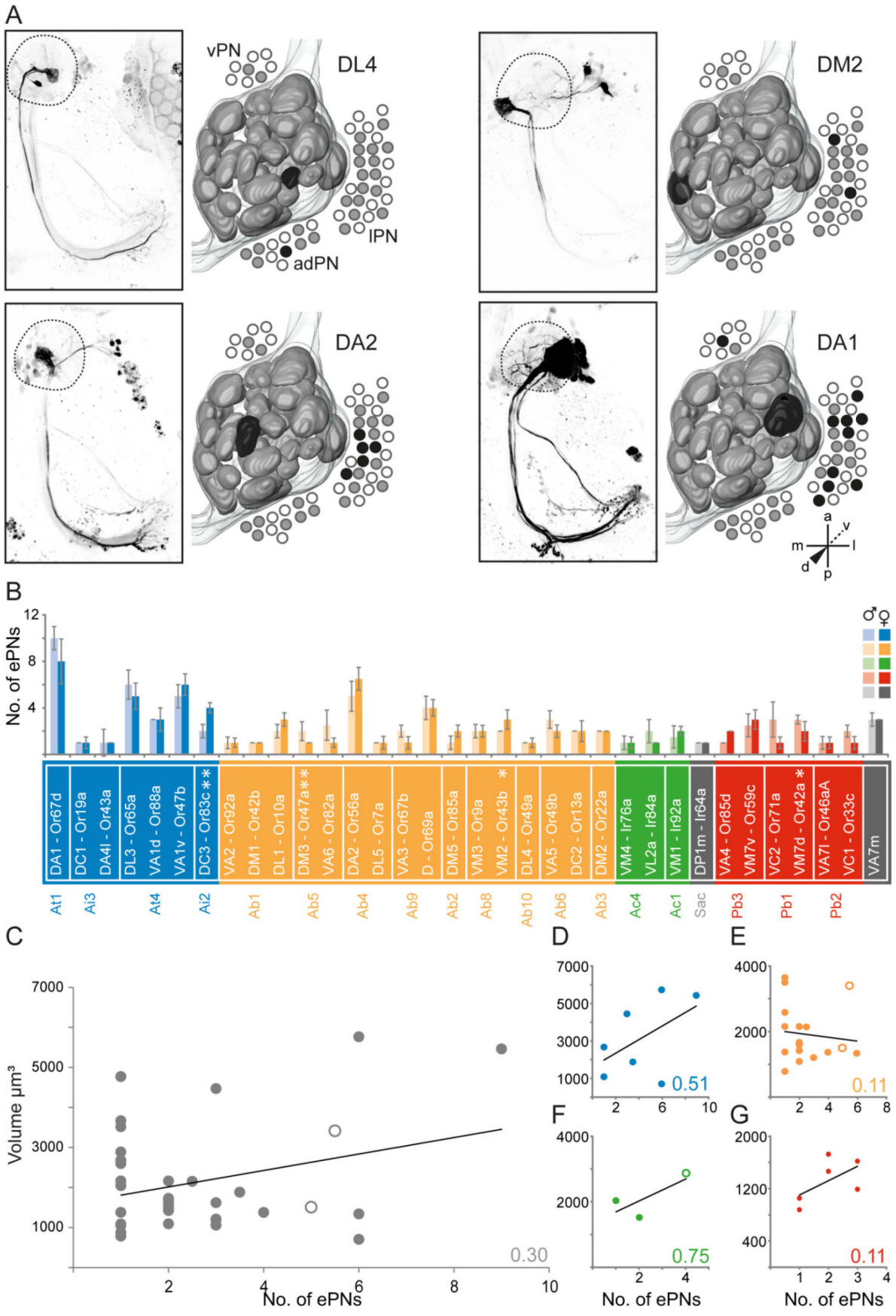

Figure 3 | Quantification of uniglomerular excitatory PNs via photoactivation

(A) Z-projection of four different GH146 scans of the AL, MB calyx and LH after photoactivation of a specific glomerulus (DL4, DM2, DA2 and DA1). (B) Glomerulus-specific number of excitatory PNs labelled with GH146-GAL4;UAS-C3PA. Data are median ± SD. Statistical differences between sexes were determined by Student's t test, *p < 0.5, **p < 0.1. n = 3-10. (C) Correlation of glomerular volume and number of glomerulus-specific PNs and (D-G) segregated for the sensilla class. Empty circles in C, E, and F are ChA-GAL4;UAS-C3PA based data (Fig S1). The r-value is inset and the two tailed probability of the Pearson correlation coefficient is **p < 0.1 and ***p<0.01. adPN = anterodorsal PN soma cluster, lPN = lateral PN soma cluster, vPN = ventral PN soma cluster. The color code refers to Fig 1.

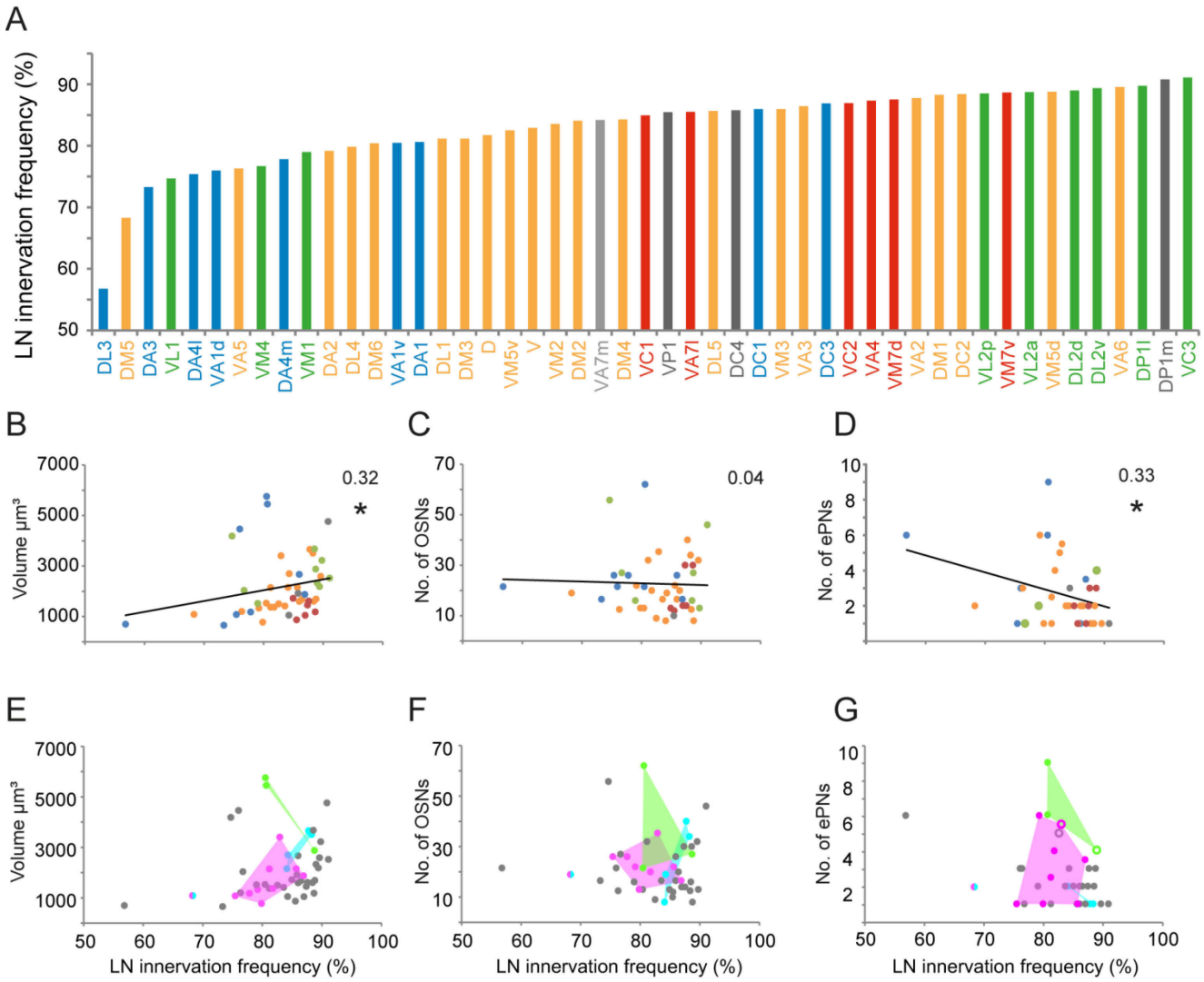

Figure 4 | LNs negatively correlate with PN quantity

(A) Data set of the glomerulus-specific LN innervation frequency acquired via MARCM of several LN GAL4-Lines (data from (Chou et al., 2010)). (B, C, D) Scatterplots showing the correlation of the LN frequency with glomerulus-specific volume (B), OSN count (C) or PN count (D). The r-value is inset and the two tailed probability of the Pearson correlation coefficient is *p < 0.5. (E, F, G) Same plots as in (B-D) with emphasis on potential clustering of attractive (cyan), aversive (magenta) and fruitless (green) glomeruli. Except for E, F and G the color code refers to Fig 1.

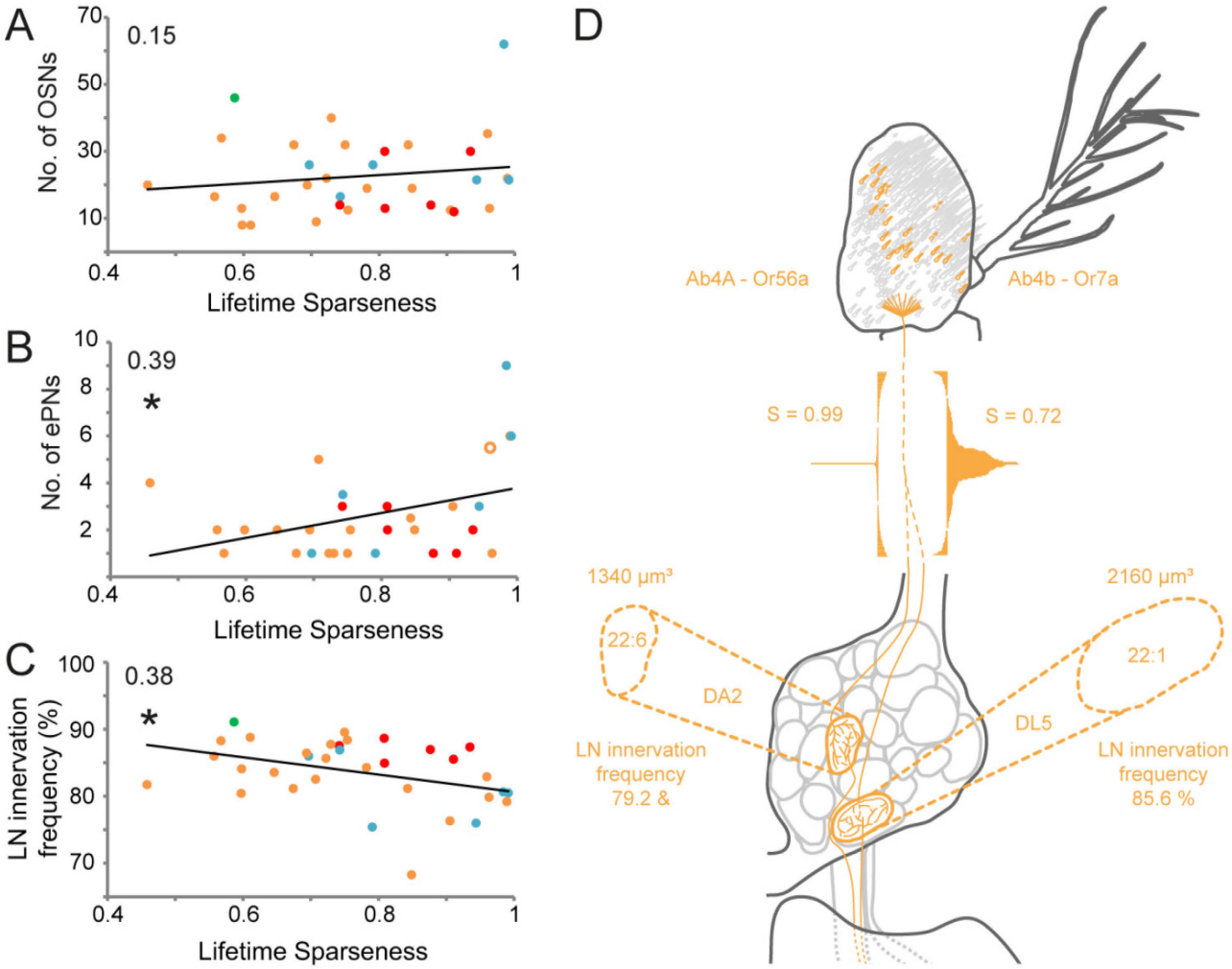

Figure 5 | OR lifetime sparseness and modeling glomerular uniqueness

(A, B, C) Scatter plots depicting the correlation of the calculated lifetime sparseness with OSNs number in the periphery (A), the number of PNs in the respective glomerulus (B) and the corresponding LN frequency per glomerulus (C). The r-value is inset and the two tailed probability of the Pearson correlation coefficient is *p < 0.5. (D) Schematic model displaying the morphological properties of two selected CR pathways – Or56a/DA2 and Or7a/DL5, both descending from the Ab4 sensillum – from the peripheral distribution of their sensilla over the odor response profile and lifetime sparseness (*S*) to their glomerular volume, convergence ratio and LN innervation frequency (Chou et al., 2010). The values for the OR-specific lifetime sparseness derive from original odor response profiles shown in Fig S2, (Galizia et al., 2010; Hallem and Carlson, 2006)). The color code refers to Fig 1.

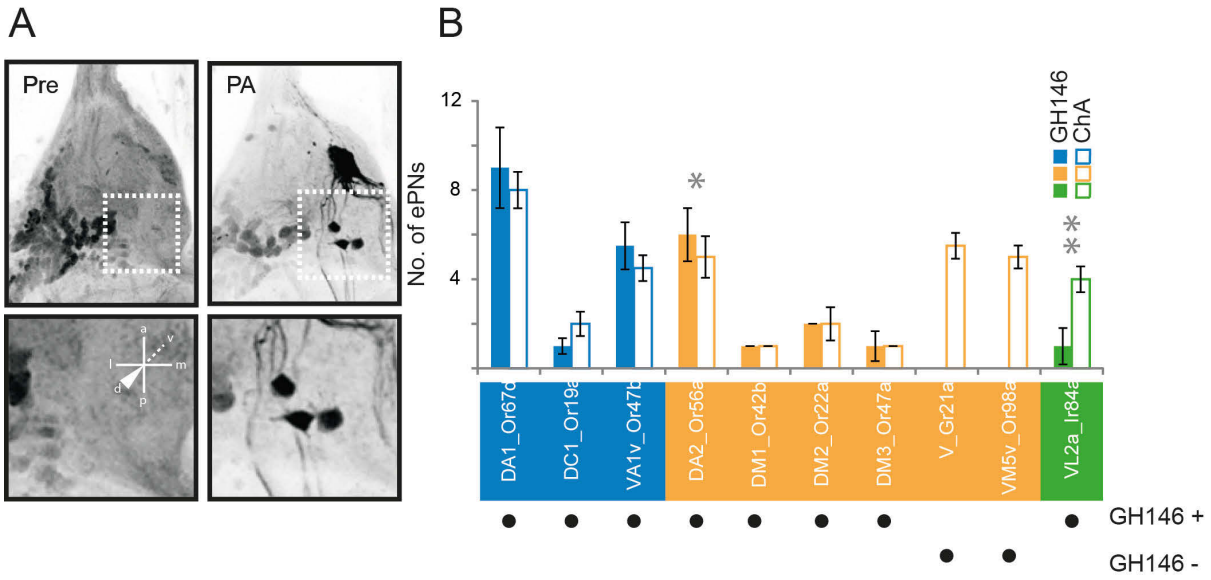

Figure S1 | Comparison of labelled ChA and GH146 positive uniglomerular PNs

(A, left) Z-Projection of a ChA-GAL4 scan of a left AL prior to the photoactivation. (A, right) Z-projection of a ChA-GAL4 scan of the same AL after photoactivation of glomerulus DM2. (B) Comparison of a subset of photoactivated glomeruli in GH146-GAL4 (filled) and female ChA-GAL4 (empty). Data represent median ± SD. Statistical differences between sexes were determined by Student's t test, *p < 0.5, **p < 0.1. n = 3-6. The color code refers to Fig 1.

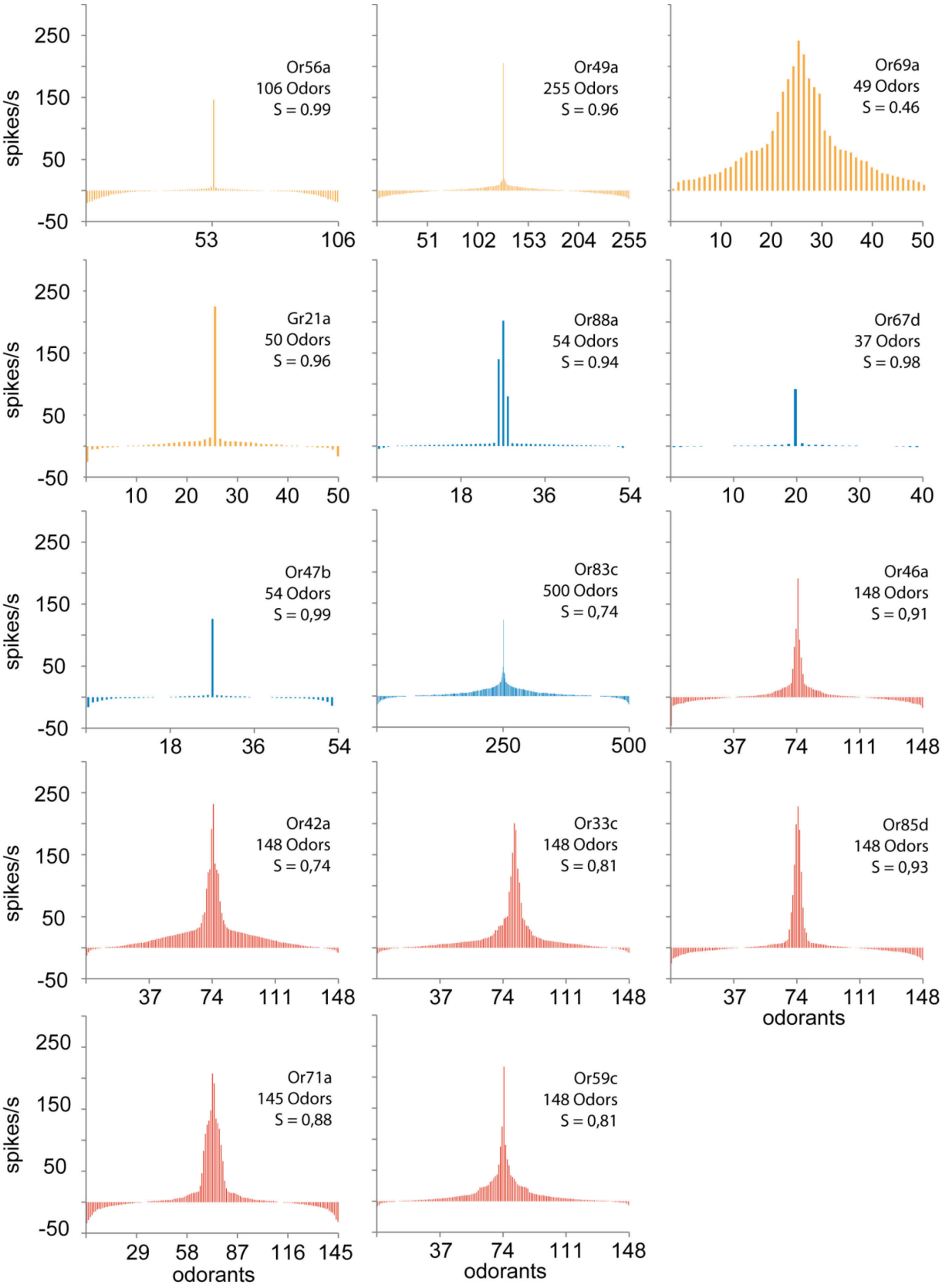

Figure S2 | Novel odor response profiles

Odor response profiles for 14 olfactory receptors – underrepresented in (Galizia et al., 2010) – generated from SSR recordings of the respective sensillum. Inset is the name of the receptor, the number of used odors for characterization and the lifetime sparseness (*S*). Color code refers to Fig 1

References

Abuin, L., Bargeton, B., Ulbrich, M.H., Isacoff, E.Y., Kellenberger, S., and Benton, R. (2011). Functional architecture of olfactory ionotropic glutamate receptors. Neuron 69, 44-60.

Acebes, A., and Ferrús, A. (2001). Increasing the Number of Synapses Modifies Olfactory Perception in Drosophila. The Journal of neuroscience : the official journal of the Society for Neuroscience 21, 6264-6273.

Ai, M., Min, S., Grosjean, Y., Leblanc, C., Bell, R., Benton, R., and Suh, G.S. (2010). Acid sensing by the Drosophila olfactory system. Nature 468, 691-695.

Benton, R., Vannice, K.S., Gomez-Diaz, C., and Vosshall, L.B. (2009). Variant ionotropic glutamate receptors as chemosensory receptors in Drosophila. Cell 136, 149-162.

Bhandawat, V., Olsen, S.R., Gouwens, N.W., Schlief, M.L., and Wilson, R.I. (2007). Sensory processing in the Drosophila antennal lobe increases reliability and separability of ensemble odor representations. Nature neuroscience 10, 1474-1482.

Boeckh, J., and Tolbert, L.P. (1993). Synaptic Organization and Development of the Antennal Lobe in Insects. Microsc Res Tech 24, 260-280.

Busch, S., Selcho, M., Ito, K., and Tanimoto, H. (2009). A map of octopaminergic neurons in the Drosophila brain. The Journal of comparative neurology 513, 643-667.

Busto, G.U., Cervantes-Sandoval, I., and Davis, R.L. (2010). Olfactory learning in Drosophila. Physiology 25, 338-346.

Carlsson, M.A., Diesner, M., Schachtner, J., and Nassel, D.R. (2010). Multiple neuropeptides in the Drosophila antennal lobe suggest complex modulatory circuits. The Journal of comparative neurology 518, 3359-3380.

Caron, S.J., Ruta, V., Abbott, L.F., and Axel, R. (2013). Random convergence of olfactory inputs in the Drosophila mushroom body. Nature 497, 113-117.

Chiang, A.S., Lin, C.Y., Chuang, C.C., Chang, H.M., Hsieh, C.H., Yeh, C.W., Shih, C.T., Wu, J.J., Wang, G.T., Chen, Y.C., *et al.* (2011). Three-dimensional reconstruction of brain-wide wiring networks in Drosophila at single-cell resolution. Current biology : CB 21, 1-11.

Chou, Y.H., Spletter, M.L., Yaksi, E., Leong, J.C., Wilson, R.I., and Luo, L. (2010). Diversity and wiring variability of olfactory local interneurons in the Drosophila antennal lobe. Nature neuroscience 13, 439-449.

Couto, A., Alenius, M., and Dickson, B.J. (2005). Molecular, anatomical, and functional organization of the Drosophila olfactory system. Current biology : CB 15, 1535-1547.

De Bruyne, M., Clyne, P.J., and Carlson, J.R. (1999). Odor Coding in a Model Olfactory Organ: The Drosophila Maxillary Palp. The Journal of neuroscience : the official journal of the Society for Neuroscience 19, 4520-4532.

De Bruyne, M., Foster, K., and Carlson, J.R. (2001). Odor Coding in the Drosophila Antenna. Neuron 30, 537-552.

Dekker, T., Ibba, I., Siju, K.P., Stensmyr, M.C., and Hansson, B.S. (2006). Olfactory shifts parallel superspecialism for toxic fruit in Drosophila melanogaster sibling, D. sechellia. Current biology : CB 16, 101-109.

Devaud, J.-M., Acebes, A., and Ferrús, A. (2001). Odor Exposure Cuases Central Adaptation and Morphological Changes in Selected Olfactory Glomeruli in Drosophila. The Journal of neuroscience : the official journal of the Society for Neuroscience 21, 6274-6282.

Devaud, J.-M., Acebes, A., Ramaswami, M., and Ferrús, A. (2003). Structural and Functional Changes in the Olfactory Pathway of Adult Drosophila Take Place at a Critical Age. J Neurobiol, 13-23.

Dobritsa, A., Van der Goes van Naters, W., Warr, C.G., Steinbrecht, R.A., and Carlson, J.R. (2003). Integrating the molecular and Cellular Basis of Odor Coding in the Drosophila Antenna. Neuron 37, 827-841.

Dweck, H.K. (2014). Novel pheromones mediate copulation and aggregation in Drosophila.

Dweck, H.K., Ebrahim, S.A., Kromann, S., Bown, D., Hillbur, Y., Sachse, S., Hansson, B.S., and Stensmyr, M.C. (2013). Olfactory preference for egg laying on citrus substrates in Drosophila. Current biology : CB 23, 2472-2480.

Endo, K., Aoki, T., Yoda, Y., Kimura, K., and Hama, C. (2007). Notch signal organizes the Drosophila olfactory circuitry by diversifying the sensory neuronal lineages. Nature neuroscience 10, 153-160.

Fishilevich, E., and Vosshall, L.B. (2005). Genetic and functional subdivision of the Drosophila antennal lobe. Current biology : CB 15, 1548-1553.

Galizia, C.G., Munch, D., Strauch, M., Nissler, A., and Ma, S. (2010). Integrating heterogeneous odor response data into a common response model: A DoOR to the complete olfactome. Chemical senses 35, 551-563.

Galizia, C.G., Sachse, S., Rappert, A., and Menzel, R. (1999). The glomerular code for odor representation is species specific in the honeybee Apis mellifera. Nature neuroscience 2, 473-478.

Gallio, M., Ofstad, T.A., Macpherson, L.J., Wang, J.W., and Zuker, C.S. (2011). The coding of temperature in the Drosophila brain. Cell 144, 614-624.

Gao, Q., Yuan, B., and Chess, A. (2000). Convergent projections of Drosophila olfactory neurons to specific glomeruli in the antennal lobe. Nature neuroscience 3, 780-785.

Grabe, V., Strutz, A., Baschwitz, A., Hansson, B.S., and Sachse, S. (2014). Digital in vivo 3D atlas of the antennal lobe of Drosophila melanogaster. The Journal of comparative neurology.

Gruntman, E., and Turner, G.C. (2013). Integration of the olfactory code across dendritic claws of single mushroom body neurons. Nature neuroscience 16, 1821-1829.

Ha, T.S., and Smith, D.P. (2006). A pheromone receptor mediates 11-cis-vaccenyl acetate-induced responses in Drosophila. The Journal of neuroscience : the official journal of the Society for Neuroscience 26, 8727-8733.

Hallem, E.A., and Carlson, J.R. (2004). The odor coding system of Drosophila. Trends in genetics : TIG 20, 453-459.

Hallem, E.A., and Carlson, J.R. (2006). Coding of odors by a receptor repertoire. Cell 125, 143-160.

Hansson, B.S., Ljungberg, H., Hallberg, E., and Löfstedt, C. (1992). Functional Specialization of Olfactory Glomeruli in a Moth. Science 256, 1313-1315.

Heimbeck, G., Bugnon, V., Gendre, N., Keller, A., and Stocker, R.F. (2001). A central neural circuit for experience-independent olfactory and courtship behavior in Drosophila melanogaster. Proc Natl Acad Sci U S A 98, 15336-15341.

Heisenberg, M. (2003). Mushroom body memoir: from maps to models. Nature reviews Neuroscience 4, 266-275.

Ignell, R., Dekker, T., Ghaninia, M., and Hansson, B.S. (2005). Neuronal architecture of the mosquito deutocerebrum. The Journal of comparative neurology 493, 207-240.

Ito, H., Fujitani, K., Usui, K., Shimizu-Nishikawa, K., Tanaka, S., and Yamamoto, D. (1996). Sexual orientation in Drosophila ia altered by the satori mutation in the sex-determination gene fruitless that encodes a zinc finger protein with aBTB domain. Proc Natl Acad Sci U S A 93, 9687-9692.

Ito, H., Sato, K., Koganezawa, M., Ote, M., Matsumoto, K., Hama, C., and Yamamoto, D. (2012). Fruitless recruits two antagonistic chromatin factors to establish single-neuron sexual dimorphism. Cell 149, 1327-1338.

Ito, K., Shinomiya, K., Ito, M., Armstrong, J.D., Boyan, G., Hartenstein, V., Harzsch, S., Heisenberg, M., Homberg, U., Jenett, A.*, et al.* (2014). A systematic nomenclature for the insect brain. Neuron 81, 755-765.

Jefferis, G.S., Marin, E.C., Stocker, R., and Luo, L. (2001). Target neuron prespecification in the olfactory map of Drosophila. Nature 414, 204-208.

Jefferis, G.S., Potter, C.J., Chan, A.M., Marin, E.C., Rohlfing, T., Maurer, C.R., Jr., and Luo, L. (2007). Comprehensive maps of Drosophila higher olfactory centers: spatially segregated fruit and pheromone representation. Cell 128, 1187-1203.

Kain, P., Boyle, S.M., Tharadra, S.K., Guda, T., Pham, C., Dahanukar, A., and Ray, A. (2013). Odour receptors and neurons for DEET and new insect repellents. Nature 502, 507-512.

Kazama, H., and Wilson, R.I. (2009). Origins of correlated activity in an olfactory circuit. Nature neuroscience 12, 1136-1144.

Knaden, M., Strutz, A., Ahsan, J., Sachse, S., and Hansson, B.S. (2012). Spatial representation of odorant valence in an insect brain. Cell reports 1, 392-399.

Kondoh, Y., Kaneshiro, K.Y., Kimura, K., and Yamamoto, D. (2003). Evolution of sexual dimorphism in the olfactory brain of Hawaiian Drosophila. Proceedings Biological sciences / The Royal Society 270, 1005-1013.

Kreher, S.A., Mathew, D., Kim, J., and Carlson, J.R. (2008). Translation of sensory input into behavioral output via an olfactory system. Neuron 59, 110-124.

Kurtovic, A., Widmer, A., and Dickson, B.J. (2007). A single class of olfactory neurons mediates behavioural responses to a Drosophila sex pheromone. Nature 446, 542-546.

Lai, S.L., Awasaki, T., Ito, K., and Lee, T. (2008). Clonal analysis of Drosophila antennal lobe neurons: diverse neuronal architectures in the lateral neuroblast lineage. Development 135, 2883-2893.

Lebreton, S., Grabe, V., Omondi, A.B., Ignell, R., Becher, P.G., Hansson, B.S., Sachse, S., and Witzgall, P. (2014). Love makes smell blind: mating suppresses pheromone attraction in Drosophila females via Or65a olfactory neurons. Scientific reports 4, 7119.

Lee, G., Foss, M., Goodwin, S.F., Carlo, T., Taylor, B.J., and Hall, J.C. (2000). Spatial, Temporal and Sexually Dimorphic Expression Patterns of the fruitless Gene in the Drosophila Central Nervous System. J Neurobiol, 404-426.

Liang, L., Li, Y., Potter, C.J., Yizhar, O., Deisseroth, K., Tsien, R.W., and Luo, L. (2013). GABAergic projection neurons route selective olfactory inputs to specific higher-order neurons. Neuron 79, 917-931.

Lin, H.H., Chu, L.A., Fu, T.F., Dickson, B.J., and Chiang, A.S. (2013). Parallel neural pathways mediate CO2 avoidance responses in Drosophila. Science 340, 1338-1341.

Linz, J., Baschwitz, A., Strutz, A., Dweck, H.K., Sachse, S., Hansson, B.S., and Stensmyr, M.C. (2013). Host plant-driven sensory specialization in Drosophila erecta. Proceedings Biological sciences / The Royal Society 280, 20130626.

Liu, W., Liang, X., Gong, J., Yang, Z., Zhang, Y.H., Zhang, J.X., and Rao, Y. (2011). Social regulation of aggression by pheromonal activation of Or65a olfactory neurons in Drosophila. Nature neuroscience 14, 896-902.

Liu, W., and Wilson, R.I. (2013). Glutamate is an inhibitory neurotransmitter in the Drosophila olfactory system. Proc Natl Acad Sci U S A 110, 10294-10299.

Luo, L. (2007). Fly MARCM and mouse MADM: genetic methods of labeling and manipulating single neurons. Brain research reviews 55, 220-227.

Marin, E.C., Jefferis, G.S., Komiyama, T., Zhu, H., and Luo, L. (2002). Representation of the Glomerular Olfactory Map in the Drosophila Brain. Cell 109, 243-255.

Marin, E.C., Watts, R.J., Tanaka, N.K., Ito, K., and Luo, L. (2005). Developmentally programmed remodeling of the Drosophila olfactory circuit. Development 132, 725-737.

Mosca, T.J., and Luo, L. (2014). Synaptic organization of the Drosophila antennal lobe and its regulation by the Teneurins. eLife.

Neville, M.C., Nojima, T., Ashley, E., Parker, D.J., Walker, J., Southall, T., Van de Sande, B., Marques, A.C., Fischer, B., Brand, A.H.*, et al.* (2014). Male-specific fruitless isoforms target neurodevelopmental genes to specify a sexually dimorphic nervous system. Current biology : CB 24, 229-241.

Okada, R., Awasaki, T., and Ito, K. (2009). Gamma-aminobutyric acid (GABA)-mediated neural connections in the Drosophila antennal lobe. The Journal of comparative neurology 514, 74-91.

Olsen, S.R., Bhandawat, V., and Wilson, R.I. (2007). Excitaory Interactions Between Olfactory Processing Channels in the Drosophila Antennal Lobe. Neuron 54, 89-103.

Parnas, M., Lin, A.C., Huetteroth, W., and Miesenbock, G. (2013). Odor discrimination in Drosophila: from neural population codes to behavior. Neuron 79, 932-944.

Patterson, G.H., and Lippincott-Schwartz, J. (2002). A photoactivatable GFP for selective photolabeling of proteins and cells. Science 297, 1873-1877.

Pelz, D., Roeske, T., Syed, Z., de Bruyne, M., and Galizia, C.G. (2006). The molecular receptive range of an olfactory receptor in vivo (Drosophila melanogaster Or22a). J Neurobiol 66, 1544-1563.

Perez-Orive, J., Mazor, O., Turner, G.C., Cassenaer, S., Wilson, R.I., and Laurent, G. (2002). Oscillations and sparsening of odor representations in the mushroom body. Science 297, 359-365.

Polanska, M.A., Tuchina, O., Agricola, H., Hansson, B.S., and Harzsch, S. (2012). Neuropeptide complexity in the crustacean central olfactory pathway: immunolocalization of A-type allatostatins and RFamide-like peptides in the brain of a terrestrial hermit crab. Molecular brain 5, 29.

Ramaekers, A., Magnenat, E., Marin, E.C., Gendre, N., Jefferis, G.S., Luo, L., and Stocker, R.F. (2005). Glomerular maps without cellular redundancy at successive levels of the Drosophila larval olfactory circuit. Current biology : CB 15, 982-992.

Ronderos, D.S., Lin, C.C., Potter, C.J., and Smith, D.P. (2014). Farnesol-detecting olfactory neurons in Drosophila. The Journal of neuroscience : the official journal of the Society for Neuroscience 34, 3959-3968.

Root, C.M., Masuyama, K., Green, D.S., Enell, L.E., Nassel, D.R., Lee, C.H., and Wang, J.W. (2008). A presynaptic gain control mechanism fine-tunes olfactory behavior. Neuron 59, 311-321.

Root, D.H., Mejias-Aponte, C.A., Zhang, S., Wang, H.L., Hoffman, A.F., Lupica, C.R., and Morales, M. (2014). Single rodent mesohabenular axons release glutamate and GABA. Nature neuroscience 17, 1543-1551.

Ruta, V., Datta, S.R., Vasconcelos, M.L., Freeland, J., Looger, L.L., and Axel, R. (2010). A dimorphic pheromone circuit in Drosophila from sensory input to descending output. Nature 468, 686-690.

Salvaterra, P.M., and Kitamoto, T. (2001). Drosophila cholinergic neurons and processes visualized with Gal4/UAS-GFP. Gene Expr Patterns 1, 73-82.

Schneiderman, A.M., Hildebrand, J.G., Brennan, M.M., and Tumlinson, J.H. (1986). Trans-sexually grafted antennae alter pheromone-directed behaviour in a moth. Nature 323, 801-803.

Seki, Y., Rybak, J., Wicher, D., Sachse, S., and Hansson, B.S. (2010). Physiological and morphological characterization of local interneurons in the Drosophila antennal lobe. Journal of neurophysiology 104, 1007-1019.

Semmelhack, J.L., and Wang, J.W. (2009). Select Drosophila glomeruli mediate innate olfactory attraction and aversion. Nature 459, 218-223.

Shanbhag, S.R., Müller, B., and Steinbrecht, R.A. (1999). Atlas of olfactory organs of Drosophila melanogaster 1. Types, external organization, innervation and distribution of olfactory sensilla. Int J Insect Morphol & Embryol 28, 377-397.

Shanbhag, S.R., Singh, K., and Singh, R.N. (1995). Fine structure and primary sensory projection of sensilla located in the sacculus of the antenna of Drosophila melanogaster. Cell and tissue research 282, 237-249.

Shang, Y., Claridge-Chang, A., Sjulson, L., Pypaert, M., and Miesenbock, G. (2007). Excitatory local circuits and their implications for olfactory processing in the fly antennal lobe. Cell 128, 601-612.

Silbering, A.F., Rytz, R., Grosjean, Y., Abuin, L., Ramdya, P., Jefferis, G.S., and Benton, R. (2011). Complementary function and integrated wiring of the evolutionarily distinct Drosophila olfactory subsystems. The Journal of neuroscience : the official journal of the Society for Neuroscience 31, 13357-13375.

Stensmyr, M.C., Dweck, H.K., Farhan, A., Ibba, I., Strutz, A., Mukunda, L., Linz, J., Grabe, V., Steck, K., Lavista-Llanos, S.*, et al.* (2012). A conserved dedicated olfactory circuit for detecting harmful microbes in Drosophila. Cell 151, 1345-1357.

Stocker, R., Lienhard, M.C., Borst, A., and Fischbach, K.-F. (1990). Neuronal architecture of the antennal lobe in Drosophila melanogaster. Cell and tissue research 262, 9-34.

Stocker, R.F. (1994). The organization of the chemosensory system in Drosophila melanogaster: a review. Cell and tissue research 275, 3-26.

Stocker, R.F. (2001). Drosophila as a focus in olfactory research: mapping of olfactory sensilla by fine structure, odor specificity, odorant receptor expression, and central connectivity. Microsc Res Tech 55, 284-296.

Stocker, R.F., Heimbeck, G., Gendre, N., and de Belle, J.S. (1997). Neuroblast Ablation in Drosophila P [GAL4] Lines Reveals Origins of Olfactory Interneurons. J Neurobiol 32, 443-457.

Stockinger, P., Kvitsiani, D., Rotkopf, S., Tirian, L., and Dickson, B.J. (2005). Neural circuitry that governs Drosophila male courtship behavior. Cell 121, 795-807.

Strausfeld, N. (1976). Atlas of an Insect Brain (Springer Verlag).

Strutz, A., Soelter, J., Baschwitz, A., Farhan, A., Grabe, V., Rybak, J., Knaden, M., Schmuker, M., Hansson, B.S., and Sachse, S. (2014). Decoding Odor Quality and Intensity in the Drosophila brain. eLIFE.

Strutz, A., Völler, T., Riemensperger, T., Fiala, A., and Sachse, S. (2012). Calcium Imaging of Neural Activity in the Olfactory System of Drosophila. In Genetically Encoded Functional Indicators, J.-R. Martin, ed. (Springer Science+Business Media), pp. 43-70.

Suh, G.S., Wong, A.M., Hergarden, A.C., Wang, J.W., Simon, A.F., Benzer, S., Axel, R., and Anderson, D.J. (2004). A single population of olfactory sensory neurons mediates an innate avoidance behaviour in Drosophila. Nature 431, 854-859.

Tanaka, N.K., Awasaki, T., Shimada, T., and Ito, K. (2004). Integration of chemosensory pathways in the Drosophila second-order olfactory centers. Current biology : CB 14, 449-457.

Tanaka, N.K., Endo, K., and Ito, K. (2012). Organization of antennal lobe-associated neurons in adult Drosophila melanogaster brain. The Journal of comparative neurology 520, 4067-4130.

Tian, L., Hires, S.A., Mao, T., Huber, D., Chiappe, M.E., Chalasani, S.H., Petreanu, L., Akerboom, J., McKinney, S.A., Schreiter, E.R.*, et al.* (2009). Imaging neural activity in worms, flies and mice with improved GCaMP calcium indicators. Nature methods 6, 875-881.

Vinje, W.E. (2000). Sparse Coding and Decorrelation in Primary Visual Cortex During Natural Vision. Science 287, 1273-1276.

Vosshall, L.B., and Stocker, R.F. (2007). Molecular architecture of smell and taste in Drosophila. Annu Rev Neurosci 30, 505-533.

Vosshall, L.B., Wong, A.M., and Axel, R. (2000). An Olfactory Sensory Map in the Fly Brain. Cell 102, 147-159.

Wang, J.W., Wong, A.M., Flores, J., Vosshall, L.B., and Axel, R. (2003). Two-Photon Calcium Imaging Reveals an Odor-Evoked Map of Activity in the Fly Brain. Cell 112, 271-282.

Willig, K.I., and Barrantes, F.J. (2014). Recent applications of superresolution microscopy in neurobiology. Current opinion in chemical biology 20, 16-21.

Wilson, R.I., and Laurent, G. (2005). Role of GABAergic inhibition in shaping odor-evoked spatiotemporal patterns in the Drosophila antennal lobe. The Journal of neuroscience : the official journal of the Society for Neuroscience 25, 9069-9079.

Wilson, R.I., Turner, G.C., and Laurent, G. (2004). Transformation of olfactory representations in the Drosophila antennal lobe. Science 303, 366-370.

Wong, A.M., Wang, J.W., and Axel, R. (2002). Spatial Representation of the Glomerular Map in the Drosophila Protocerebrum. Cell 109, 229-241.

Yaksi, E., and Wilson, R.I. (2010). Electrical coupling between olfactory glomeruli. Neuron 67, 1034-1047.

Yu, H.H., Kao, C.F., He, Y., Ding, P., Kao, J.C., and Lee, T. (2010). A complete developmental sequence of a Drosophila neuronal lineage as revealed by twin-spot MARCM. PLoS biology 8.

Zhu, P., Frank, T., and Friedrich, R.W. (2013). Equalization of odor representations by a network of electrically coupled inhibitory interneurons. Nature neuroscience 16, 1678-1686.

Manuscript III

Decoding Odor Quality and Intensity in the *Drosophila* brain

Antonia Strutz, Jan Soelter, Amelie Baschwitz, Abu Farhan, Veit Grabe, Jürgen Rybak, Markus Knaden, Michael Schmucker, Bill S. Hansson and Silke Sachse

Published in eLIFE, 16 December 2014

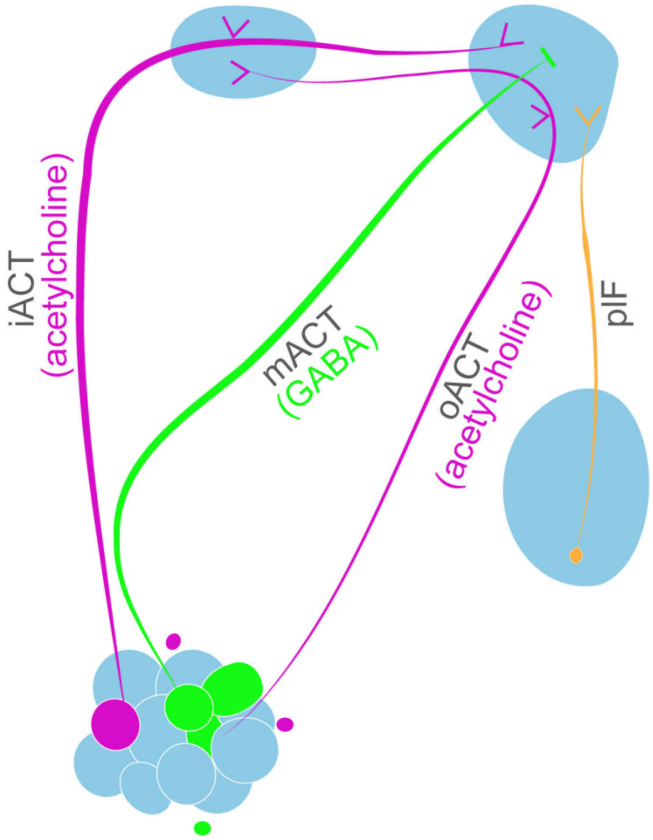

eLIFE elifesciences.org

RESEARCH ARTICLE

Decoding odor quality and intensity in the *Drosophila* brain

Antonia Strutz[1], Jan Soelter[2], Amelie Baschwitz[1], Abu Farhan[1], Veit Grabe[1], Jürgen Rybak[1], Markus Knaden[1], Michael Schmuker[2], Bill S Hansson[1], Silke Sachse[1]*

[1]Department of Evolutionary Neuroethology, Max Planck Institute for Chemical Ecology, Jena, Germany; [2]Department for Biology, Pharmacy and Chemistry, Free University Berlin, Neuroinformatics and Theoretical Neuroscience, Berlin, Germany

Abstract To internally reflect the sensory environment, animals create neural maps encoding the external stimulus space. From that primary neural code relevant information has to be extracted for accurate navigation. We analyzed how different odor features such as hedonic valence and intensity are functionally integrated in the lateral horn (LH) of the vinegar fly, *Drosophila melanogaster*. We characterized an olfactory-processing pathway, comprised of inhibitory projection neurons (iPNs) that target the LH exclusively, at morphological, functional and behavioral levels. We demonstrate that iPNs are subdivided into two morphological groups encoding positive hedonic valence or intensity information and conveying these features into separate domains in the LH. Silencing iPNs severely diminished flies' attraction behavior. Moreover, functional imaging disclosed a LH region tuned to repulsive odors comprised exclusively of third-order neurons. We provide evidence for a feature-based map in the LH, and elucidate its role as the center for integrating behaviorally relevant olfactory information.
DOI: 10.7554/eLife.04147.001

***For correspondence:** ssachse@ice.mpg.de

Competing interests: See page 19

Funding: See page 19

Received: 24 July 2014
Accepted: 09 November 2014
Published: xxx

Reviewing editor: Mani Ramaswami, Trinity College Dublin, Ireland

Introduction

To navigate the environment in a way that optimizes their survival and reproduction, animals have evolved sensory systems. These have three essential tasks: First, the external world has to be translated into an internal representation in the form of an accurate neural map. Second, the neural map has to be readable and interpretable, that is, the generated neural code must allow common attributes to be extracted across stimuli to enable the animal to make the best decisions. Third, the animal has to be able to adapt to environmental changes and to form a sensory memory of new stimuli. Many studies have been dedicated to unraveling the primary transformation from a stimulus into an initial neural representation within various sensory systems (***Manni and Petrosini, 2004***; ***Vosshall and Stocker, 2007***; ***Sanes and Zipursky, 2010***) and to elucidating neuronal plasticity and sensory memory formation in higher-level processing centers (***Heisenberg, 2003***; ***Pasternak and Greenlee, 2005***). The ability to extract features and integrate stimulus modalities have so far mainly been studied in the visual system (***Livingstone and Hubel, 1988***; ***Bausenwein et al., 1992***; ***Nassi and Callaway, 2009***). We addressed the question of how stimulus features such as odor valence and intensity are coded and integrated within the olfactory system using the model organism *Drosophila melanogaster*.

The olfactory system of the vinegar fly provides an excellent model system for deciphering olfactory processing mechanisms, since it displays remarkable similarities to the mammalian system but is less complex and highly genetically tractable. Like other sensory systems, the olfactory system employs a spatio-temporal map to translate the variables in chemosensory space into neuronal activity patterns in the brain. This map emerges when the olfactory sensory neurons (OSNs) with the same chemosensory receptors converge into one exclusive glomerulus in the antennal lobe (AL) which represents the

eLife digest Organisms need to sense and adapt to their environment in order to survive. Senses such as vision and smell allow an organism to absorb information about the external environment and translate it into a meaningful internal image. This internal image helps the organism to remember incidents and act accordingly when they encounter similar situations again. A typical example is when organisms are repeatedly attracted to odors that are essential for survival, such as food and pheromones, and are repulsed by odors that threaten survival.

Strutz et al. addressed how attractiveness or repulsiveness of a smell, and also the strength of a smell, are processed by a part of the olfactory system called the lateral horn in fruit flies. This involved mapping the neuronal patterns that were generated in the lateral horn when a fly was exposed to particular odors.

Strutz et al. found that a subset of neurons called inhibitory projection neurons processes information about whether the odor is attractive or repulsive, and that a second subset of these neurons process information about the intensity of the odor. Other insects, such as honey bees and hawk moths, have olfactory systems with a similar architecture and might also employ a similar spatial approach to encoding information the intensity and identity of odors. Locusts, on the other hand, employ a temporal approach to encoding information about odors.

The work of Strutz et al. shows that certain qualities of odors are contained in a spatial map in a specific brain region of the fly. This opens up the question of how the information in this spatial map influences decisions made by the fly.

DOI: 10.7554/eLife.04147.002

equivalent to the mammalian olfactory bulb (***Hildebrand and Shepherd, 1997***; ***Vosshall et al., 2000***; ***Vosshall and Stocker, 2007***). Glomeruli, the functional and morphological units of the AL, are microcircuits comprising OSNs, multiglomerular local interneurons (LNs) and uniglomerular output neurons, so-called excitatory projection neurons (ePNs) (***Wilson and Mainen, 2006***; ***Vosshall and Stocker, 2007***) that convey the olfactory information to higher brain centers, as the mushroom body calyx (MBc) and the lateral horn (LH) (***Stocker et al., 1997***). The stringent spatial arrangement of OSNs and ePNs in the AL generates a spatial map containing characteristic combinatorial glomerular activity patterns for all odorants (***Fiala et al., 2002***; ***Wang et al., 2003a***; ***Couto et al., 2005***; ***Fishilevich and Vosshall, 2005***). The MBc is involved in olfactory memory formation (***Heisenberg, 2003***) and enables a contextualization of the odor space (***Caron et al., 2013***). By exclusion, the LH is believed to be involved in innate olfactory behavior (***de Belle and Heisenberg, 1994***; ***Jefferis et al., 2007***). Excitatory PNs retain the sensory information encoded in the AL and form glomerulus-dependent, stereotypic axonal terminal fields in the LH (***Marin et al., 2002***; ***Wong et al., 2002***; ***Tanaka et al., 2004***). Compartmentalization in the LH has been observed in form of a spatial segregation of ePNs innervating specific glomerular subgroups (***Tanaka et al., 2004***), fruit and pheromone odor information processing ePNs (***Jefferis et al., 2007***) as well as ammonia and amine vs carbon dioxide coding ePNs (***Min et al., 2013***).

Like many other sensory networks, the olfactory circuit of the fly contains spatially distinct pathways to the higher brain, namely the inner, middle and outer antennocerebral tract (iACT, mACT and oACT) (***Stocker et al., 1990***). Notably, the mACT projects from the AL to the LH exclusively and consists of inhibitory PNs (iPNs), which exhibit also uniglomerular but mainly multiglomerular AL innervations (***Ito et al., 1997***; ***Jefferis et al., 2007***; ***Lai et al., 2008***; ***Okada et al., 2009***; ***Liang et al., 2013***). Both PN populations have been attributed different coding properties: Although both PN populations exhibit odor responses to overlapping odor ligands, iPNs seems to be broader tuned than ePNs (***Wang et al., 2014***). Furthermore, while ePNs encode rather odor identity (***Wang et al., 2003a***; ***Wilson et al., 2004***; ***Silbering et al., 2008***), iPNs have been shown to enhance innate discrimination of closely related odors (***Parnas et al., 2013***). Together, these PN populations process information on dual olfactory pathways (***Liang et al., 2013***; ***Wang et al., 2014***), as do processing mechanisms in other sensory modalities (***Nassi and Callaway, 2009***), and most likely accomplish different olfactory behaviors. The mainly multiglomerular AL pattern of iPNs suggests that these neurons extract characteristic stimulus features from the AL code and re-integrate this information into the LH to mediate innate odorant-guided behavior. This assumption is further supported by two recent studies showing that the

inhibitory input from the AL to the LH is module-specific, that is, selective for food odors and pheromones (**Liang et al., 2013**; **Fisek and Wilson, 2014**), while the connectivity in the MBc is rather probabilistic (**Murthy et al., 2008**; **Caron et al., 2013**).

However, it still remains open if and how different odor features as hedonic valence or intensity are functionally coded and integrated in the LH. In this study, we characterized and dissected the iPN olfactory processing pathway regarding the coding of odor quality and intensity at morphological, functional and behavioral levels. By linking odor-evoked activity patterns in the LH to odor-guided behavior, we provide evidence that iPNs mediate odor attraction. Furthermore, our data demonstrate a feature-based, spatially segregated activity map in the LH comprised of iPNs and third-order neurons and thus expand its role as a center for integrating behaviorally relevant olfactory information.

Results

Dendrites of iPNs innervate two-thirds of olfactory glomeruli

Cell bodies of iPNs are exclusively located in the ventral cell cluster which consists of ~50 iPNs (**Lai et al., 2008**) that project via the mACT to the LH, thereby bypassing the MBc (**Ito et al., 1997**) (**Figure 1A,B**). In contrast, ePN somata are located anterodorsally and laterally of the AL, and their axons project through the iACT or oACT to the MBc and the LH (**Stocker et al., 1997**; **Marin et al., 2002**; **Wong et al., 2002**; **Lai et al., 2008**). To analyze the innervation patterns of iPNs and ePNs, we labeled both PN populations simultaneously in vivo using the enhancer trap lines *GH146-GAL4* and *MZ699-GAL4* that label the majority of ePNs (60%) and iPNs (86%), respectively (**Lai et al., 2008**). Double-labeling shows that both PN types innervate overlapping regions in the AL and the LH, while a small posterior-lateral LH area is targeted only by ePNs (**Figure 1A**, **Figure 1—figure supplement 1**). In GH146-positive (GH146+) PNs, immunolabeling reveals GABA production in all ~6 PNs of the ventral cell cluster (**Wilson and Laurent, 2005**), whereas ePNs of this line are exclusively cholinergic (**Shang et al., 2007**). For the ~45 MZ699-positive (MZ699+) iPNs (**Lai et al., 2008**), GAD1 (glutamic acid decarboxylase) in situ hybridizations imply GABA synthesis (**Okada et al., 2009**), which was recently verified via immunostaining (**Liang et al., 2013**; **Parnas et al., 2013**). The polarity of both PN populations has been studied in detail, showing that both possess dendritic regions in the AL, indicating the AL as their cholinergic input site, while the LH represents their major output site (**Jefferis et al., 2001**; **Okada et al., 2009**; **Liang et al., 2013**; **Parnas et al., 2013**).

To further characterize PNs labeled by *MZ699-GAL4* and *GH146-GAL4*, we analyzed their precise glomerular innervation to unravel how selectively they acquire information in the AL. To allow glomerulus identification in vivo, we employed a transgenic fly carrying elav-n-synaptobrevin:DsRed (END1-2) to express the presynaptically targeted fusion protein under the control of the neuron-specific elav promotor (**Figure 1—figure supplement 2A**) (Grabe et al., in press). The reconstruction and identification of all AL glomeruli provided 53 glomeruli, of which 75% were innervated by MZ699+ iPNs (40) while 70% (37) were covered by GH146+ ePNs (**Figure 1C**, **Figure 1—figure supplement 2B**). 55% of all glomeruli were innervated by both lines. Notably, dendritic *MZ699-GAL4* innervation density was not homogeneous. Certain glomeruli were densely innervated (e.g., DM2, DM4 and DM5), while others did not reveal any postsynaptic sites (e.g., DL1, DL4 and DL5). Hence MZ699+ iPNs target specific glomerular subsets selectively, which suggests that these neurons have a particular function within the olfactory network.

Calcium signals in the lateral horn spatially segregate into distinct response domains

Probabilistic synaptic density maps of GH146+ PNs predicted a regionalized neuronal activity in the LH (**Jefferis et al., 2007**). Do iPNs functionally segregate in a comparable way? To address this question, we expressed the Ca^{2+}-sensitive reporter G-CaMP3.0 (**Nakai et al., 2001**; **Tian et al., 2009**) in iPNs using MZ699-GAL4 and performed functional imaging in the LH (**Figure 2A–C**). We initially tested three odors with potential relevance for *Drosophila* at different concentrations: acetoin acetate, an attractive byproduct of the yeast fermentation process, balsamic vinegar, an attractive natural odor mixture, and benzaldehyde, a well-known fly repellant (**Magee and Kosaric, 1987**; **Keene et al., 2004**; **Semmelhack and Wang, 2009**). We observed that odor evoked Ca^{2+} responses separate in certain regions of the LH in an odor-specific and concentration-dependent manner (**Figure 2C**). Acetoin acetate and balsamic vinegar evoked Ca^{2+} activity in spatially similar regions. At higher concentrations, an

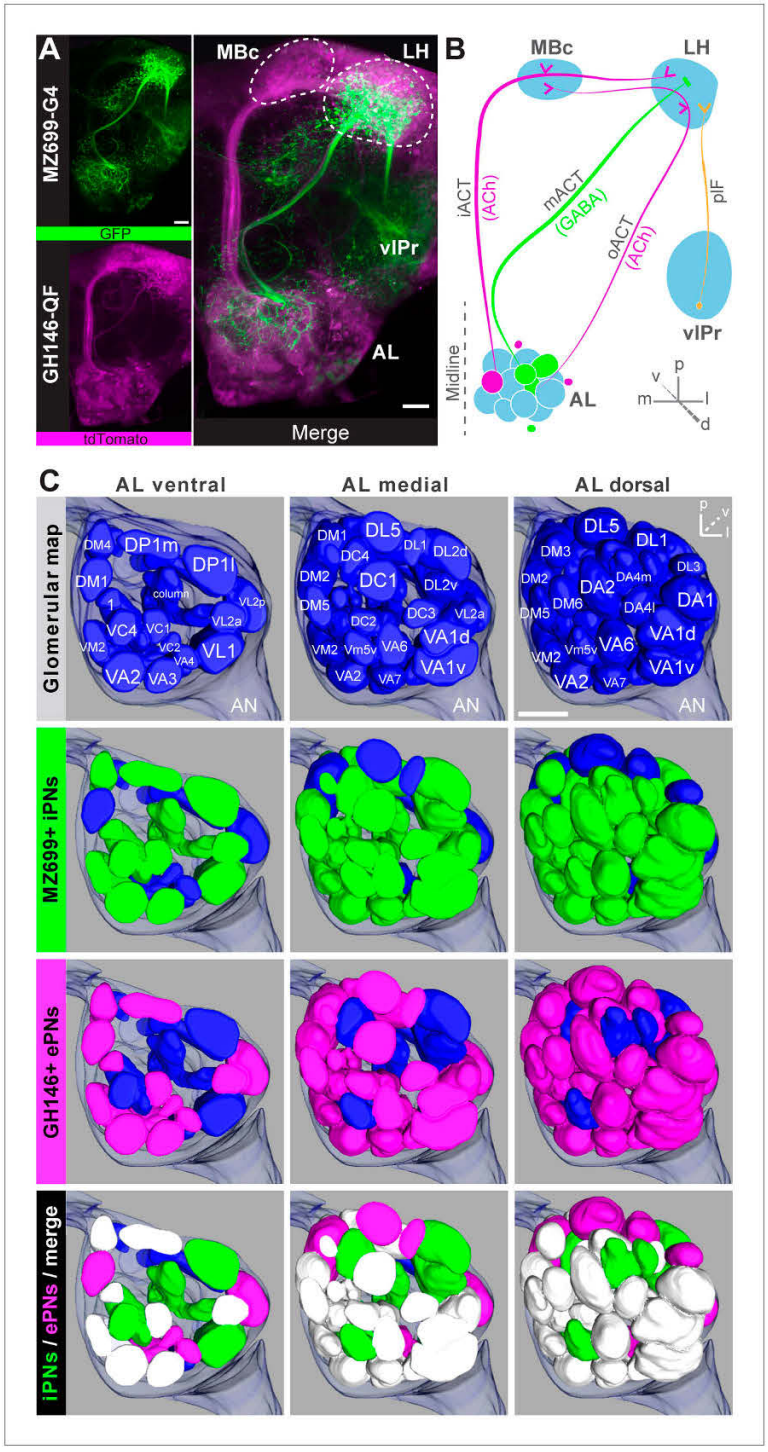

Figure 1. Detailed glomerular innervations of excitatory and inhibitory projection neurons in the AL. (**A**) Simultaneous labeling of inhibitory projections neurons (iPNs, labeled by MZ699-GAL4;G-CaMP) and excitatory projection neurons (ePNs, labeled by GH146-QF;tdTomato) in vivo reveals distinct projections to the lateral horn (LH). All iPNs

Figure 1. Continued on next page

Figure 1. Continued

bypass the mushroom body calyx (MBc) and innervate the LH exclusively. The MZ699 line labels a few ventrolateral protocerebral neurons (vlPr neurons) projecting via the posterior lateral fascicle (plF) from the ventrolateral protocerebrum (vlPr) to the LH. (**B**) Schematic of the PN connectivity relay from the antennal lobe (AL) to higher brain centers (ePNs in magenta, iPNs in green, and vlPr neurons in orange). (**C**) Above, complete glomerular assignment of the AL neuropil (right AL), labeled with elav-n-synaptobrevin:DsRed (END1-2). Below, glomerular innervations of both PN populations related to in vivo images in ***Figure 1—figure supplement 2***. Depicted are the ventral level (~−40 µm), the medial level (~−20 µm) and the dorsal view onto the AL. Color annotation: blue glomeruli are not innervated by any of the used GAL4-lines; green glomeruli are innervated by MZ699+ iPNs and magenta by GH146+ ePNs; white glomeruli are innervated by both enhancer trap lines. Scale bar, 20 µm.

DOI: 10.7554/eLife.04147.003

The following figure supplements are available for figure 1:

Figure supplement 1. Characterization of excitatory and inhibitory projection neurons.

DOI: 10.7554/eLife.04147.004

Figure supplement 2. Glomerular innervations of ePNs an iPNs.

DOI: 10.7554/eLife.04147.005

additional region was recruited. Benzaldehyde elicited no response at very low concentrations, but induced clear activity at median and high concentrations in a third region, which was completely separate from the regions activated by the other two odors. Observed patterns were highly reproducible within one animal and stereotypic among different individuals, as shown for the stimulation with 1-octen-3-ol (***Figure 2D***) as well as other odors (***Figure 2—figure supplement 1***).

Due to the lack of morphological landmarks in the LH, functional data were analyzed using the pattern recognition algorithm Non-Negative Matrix Factorization (NNMF) (***Lee and Seung, 1999***), which automatically extracts spatial areas possessing a common distinct time-course, further termed LH odor response domains (ORDs). The NNMF analysis extracted three clearly reproducible and spatially robust ORDs (***Figure 2E***, see NNMF part in the 'Materials and methods' section). Notably, ORDs occupying common temporal kinetics exhibited highly stereotypic spatial patterns. We termed the ORDs LH-PM (LH-posterior-medial), LH-AM (LH-anterior-medial) and LH-AL (LH-anterior-lateral) according to their anatomical positions. To validate our observations, we extended our stimulus array to 11 additional odorants and applied each at three concentrations. Odorants were chosen according to chemical classes, hedonic valence and biological value. Hence, the odor set included acids, lactones, terpenes, aromatics, alcohols, esters, ketones and the natural blend, balsamic vinegar. Remarkably, analysis of the additional odorants revealed neuronal activity exclusively within the three described ORDs (***Figure 2F***, ***Figure 2—figure supplements 2,3***). Furthermore, median NNMF-extracted Ca^{2+} response traces with indicated statistical quartiles illustrate very low variability and highly reproducible LH signals. The LH-PM area chiefly revealed robust odor-evoked responses across concentrations, while the LH-AM and LH-AL were mainly activated at very high odor concentrations by distinct odorants. The global responsiveness within separate ORDs in the LH substantiates our finding of a relatively broad AL input to MZ699+ iPNs which converges into three spatially regionalized and stereotypic LH activity domains.

iPNs can be divided into two morphological classes

We next investigated if the spatially regionalized odor-evoked response patterns are reflected in the axonal terminal fields of MZ699+ iPNs in the LH. To analyze these neurons at the single neuron level, we performed neural tracing by employing a genetically encoded photoactivatable GFP (PA-GFP) (***Patterson and Lippincott-Schwartz, 2002***; ***Datta et al., 2008***; ***Ruta et al., 2010***). The photoconversion of all MZ699+ neurons leaving the AL confirmed the homogeneous distribution of iPN neurites in the LH and the sparse innervation of the posterior-lateral region as mentioned above (***Figure 3A***). Next we illuminated PA-GFP in single somata to selectively label individual MZ699+ iPNs from the soma up to the farthest axonal terminals in the LH. Individual iPNs were reconstructed and transformed into a reference brain using the END1-2 background (Grabe et al., in press) to align neurons of different individuals. Based on their innervation pattern in the LH, MZ699+ iPNs could be assigned to two major morphological classes (***Figure 3B,C***). As expected from the extracted ORDs, one iPN group diverged to the LH-PM region (8/25 of iPNs), while a second group extended their axonal terminations within the LH-AM area (10/25 of iPNs). In order to statistically substantiate our observation, we

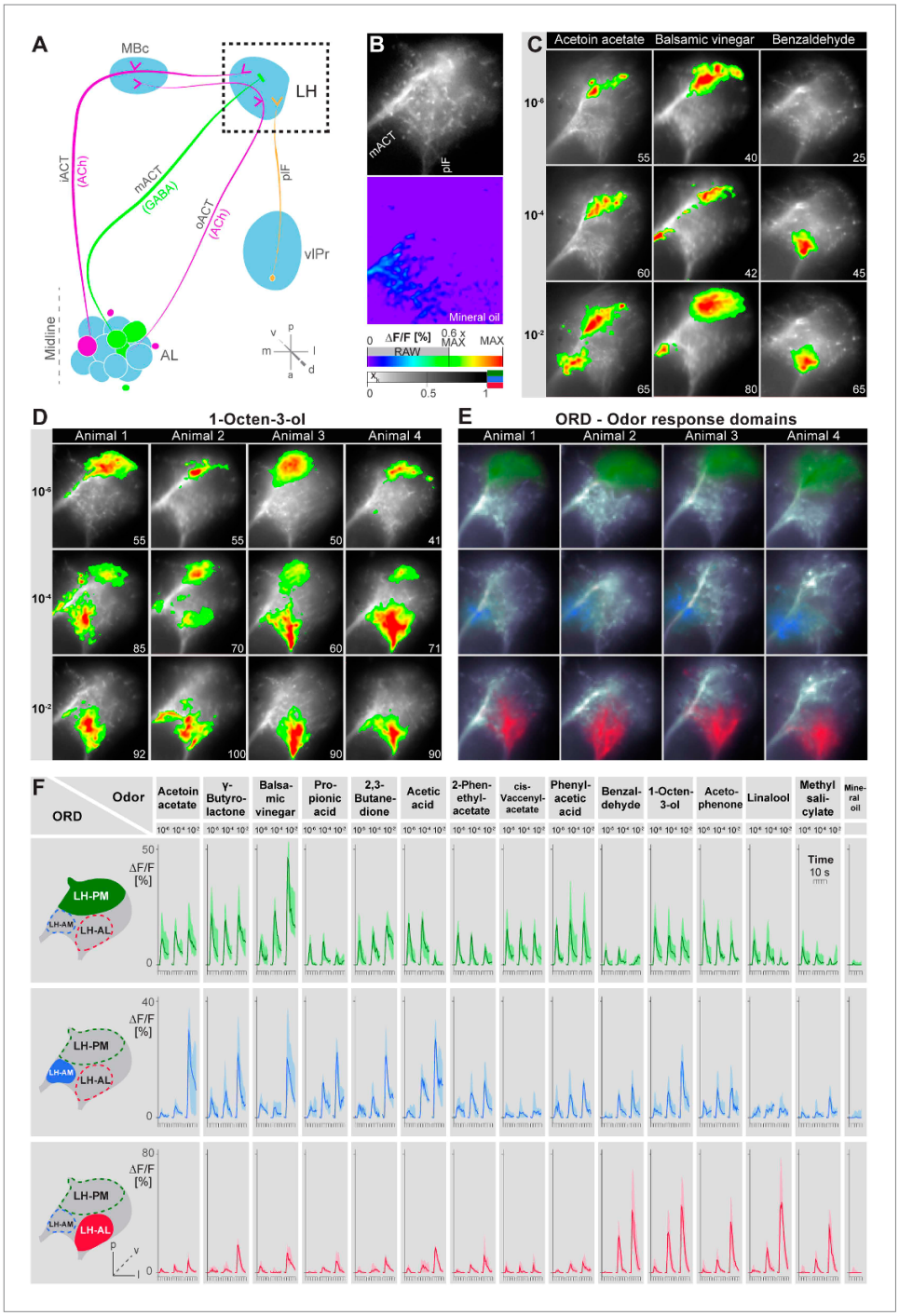

Figure 2. Odors evoke specific and stereotypic calcium responses in the LH subdivided into three distinct odor response domains. (**A**) Schematic of the olfactory circuit with the investigated area highlighted. (**B**) RAW image of the LH (top picture) depicting the recorded area of figures (**C**–**E**) and the false color image (bottom picture) during the solvent application. The ΔF/F scale bar applies for all false color-coded pictures; the alpha-bar for the pixel

Figure 2. Continued on next page

Figure 2. Continued

participation x_k of the indicated colors applies for (**E**–**F**). (**C**) Representative LH Ca^{2+} responses (ΔF/F%) of acetoin acetate, balsamic vinegar and benzaldehyde at three concentrations. Numbers in the lower right corner indicate individual maxima. (**D**) Odor-evoked Ca^{2+} responses (ΔF/F%) are exemplarily depicted for 1-octen-3ol- at three concentrations in four animals. (**E**) NNMF-extracted LH odor response domains (ORD) of four representative animals: three LH ORDs were fully reproducible after being extracted from all measured animals. Domains classified as identical are similarly color-coded: the green ORD is located in the posterior-medial region of the LH (LH-PM); blue, in the anterior-medial (LH-AM), and red in the anterior-lateral LH area (LH-AL). The alpha-bar for green, blue and red shades is placed in (**B**). (**F**) Left, schematic outlines of the LH with indicated ORDs. Right, median activity traces of all odors at three concentrations are depicted for each colored ORD. Shadows represent lower and upper quartiles (n = 6–7).

DOI: 10.7554/eLife.04147.006

The following figure supplements are available for figure 2:

Figure supplement 1. Odor-evoked activity patterns in the LH are reproducible and stereotypic.

DOI: 10.7554/eLife.04147.007

Figure supplement 2. Odor-evoked activity patterns in the LH can be reconstructed with five components.

DOI: 10.7554/eLife.04147.008

Figure supplement 3. Odor-evoked activity patterns in the LH cluster into three components.

DOI: 10.7554/eLife.04147.009

performed a cluster analysis based on a similarity score (***Kohl et al., 2013***) of the target areas of all terminals of each iPN in the LH (for details see 'Materials and methods'). The dendrogram of morphological similarity between each individual iPN shows that all, except one iPN, could be clustered according to their target region in either the LH-AM or LH-PM area (***Figure 3D***) which confirms the classification into two major categories. Additionally, we performed a principal component analysis based on the distances of the similarity scores showing that both neuronal classes possess significantly different target areas in the LH (***Figure 3—figure supplement 1A***; $p < 0.001$, one-way ANOSIM).

We did not observe any clear panglomerular innervations of individual MZ699+ iPNs that spanned the entire AL, consistent with ***Liang et al. (2013)***. Instead, MZ699+ iPNs develop mainly oligoglomerular patterns innervating on average 5.4 ± 3.9 glomeruli (mean ± SD), which are not necessarily in close proximity. It is important to note here, that the glomerular innervations of iPNs are rather sparse in comparison to the innervation of ePNs which complicates the identification of truly innervated glomeruli. After classifying all registered neurons according to their LH zones along with their glomerular innervations, we noted a spatial subdivision of MZ699+ iPN dendritic fields in the AL (***Figure 3—figure supplement 2***). Whereas LH-PM iPNs extended dendrites mainly into glomeruli from the ventro- or dorsomedial area of the AL (e.g., DM4, DM2, VM7, VM5d), iPNs targeting the LH-AM zone innervated glomeruli ranging from the ventro- and dorsoanterior to the dorsocentral region (e.g., DC3, VC1, VA6, VL1). We observed that a glomerulus is typically innervated by only LH-PM iPNs or LH-AM iPNs. However, we also found a few cases where a glomerulus can be innervated by both iPN types (e.g., glomeruli D and DC2). In order to analyze whether the two categories of iPNs can also be statistically separated according to their glomerular innervations in the AL, we performed a cluster analysis based on the glomeruli innervated by each individual iPN (***Figure 3E***). Notably, the two iPN classes could be clearly clustered into two groups due to their specific AL innervations. This finding is further supported by a principal component analysis showing that iPNs targeting the LH-PM region innervate a significant different glomerular subset than iPNs that send their axonal terminals to the LH-AM area (***Figure 3—figure supplement 1B***; $p < 0.001$, one-way ANOSIM). In accordance with our finding of two major iPN categories is the study by ***Lai et al. (2008)*** who observed several different stereotyped projection patterns of multiglomerular MZ699+ single-cell clones that could be broadly categorized into two groups based on the dendritic and axonal projection patterns. While we observed corresponding innervated areas in the AL, the described target areas in the LH seem to differ. However, due to the lack of 3D reconstruction of the single-cell clone data, the innervation patterns cannot be compared in detail.

In addition to the oligoglomerular iPNs, we observed a few uniglomerular MZ699+ iPNs innervating either glomerulus DA1 or VL1 (4/25 of iPNs), consistent with ***Lai et al. (2008)***, which target the LH-AM region (***Figure 3—figure supplement 2***). Moreover, we identified three other MZ699+ neurons that did not innervate the AL and sent their axons through the mACT to the LH and/or the MBc.

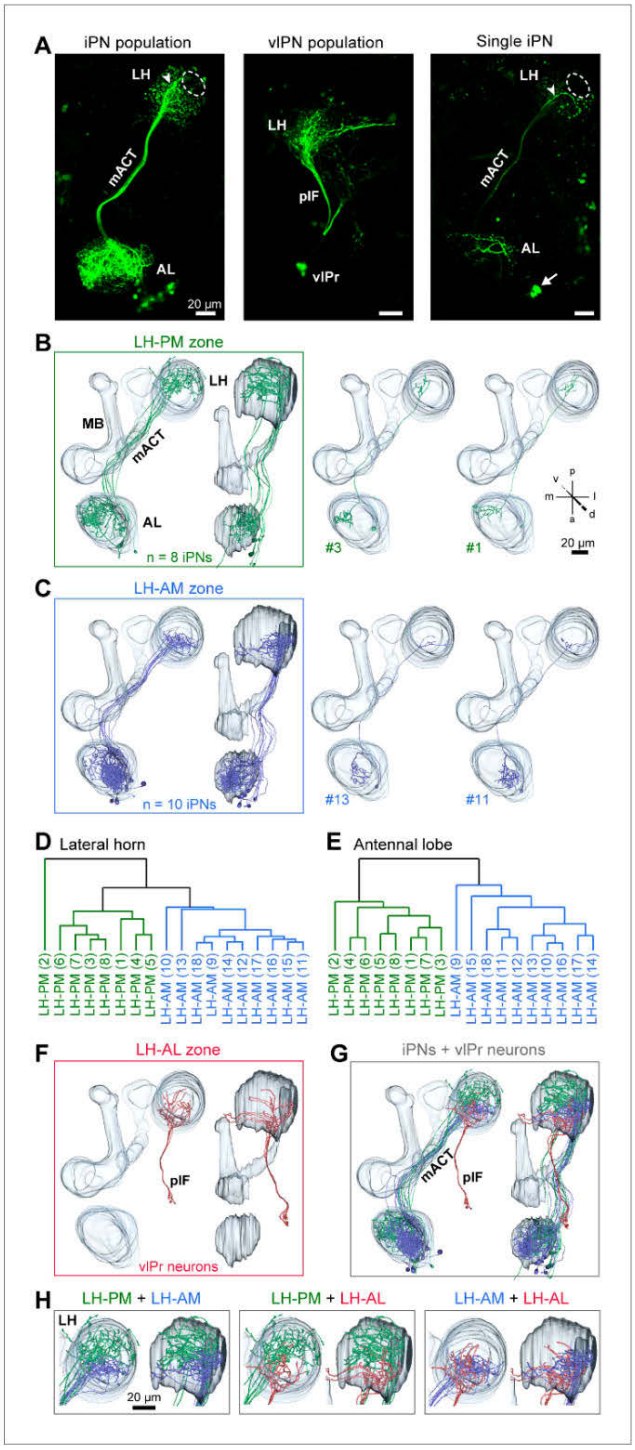

Figure 3. iPNs can be classified according to their projection pattern in three distinct LH zones. (**A**) Complete population of MZ699+ iPNs labeled using PA-GFP (left image), the posterior-lateral LH region is encircled, arrowhead indicates the final common projection point of iPN axons. Middle image: photoactivation of all vlPr

Figure 3. Continued on next page

Figure 3. Continued

neurons of the MZ699-GAL4 line that project from the LH to the vlPr via the plF. Right image: exemplary single iPN, labeled by photoconverting PA-GFP in a single soma (arrow). Scale bar, 20 µm. (**B**) Framed images: neuronal reconstructions of all iPNs projecting to the LH-PM zone (n = 8) with outlined olfactory neuropils. View from dorsal (left) and lateral (right). Right part represents two exemplary registered individual iPNs. (**C**) Neuronal reconstructions of all iPNs projecting into the LH-AM zone (n = 10), images are arranged as in (**B**). (**D** and **E**) Cluster analyses based on the target areas of all terminals of each iPN in the LH (**D**) or based on the innervated glomeruli in the AL (**E**). The dendrograms are split into colored subclusters. Below each dendrogram, each individual iPN is specified according to the labels in ***Figure 3—figure supplement 2***. Note, that iPNs can be morphologically clustered according to their target or input regions. (**F**) Neuronal reconstruction of vlPr neurons projecting through the plF to the LH-AL zone. (**G**) Combination of all registered neurons. (**H**) Dual combinations of all registered neurons with their projections in the LH.

DOI: 10.7554/eLife.04147.010

The following figure supplements are available for figure 3:

Figure supplement 1. iPNs can be morphologically segregated according to their target and input region.

DOI: 10.7554/eLife.04147.011

Figure supplement 2. Glomerular innervations of individual iPNs.

DOI: 10.7554/eLife.04147.012

Since the MZ699-GAL4 line labels also neurons connecting the LH and the ventrolateral protocerebrum (vlPr) (***Ito et al., 1997***; ***Liang et al., 2013***; ***Parnas et al., 2013***), we illuminated a small fraction of the posterior lateral fascicle (plF) to target these putative third-order neurons (***Figure 3A***). The plF comprised axons of ventrolateral protocerebral neurons (vlPr neurons), which bifurcated within the LH-AL (***Figure 3F***). Combinations of all registered neuron types within the assigned zones revealed that iPNs of the LH-AM area and vlPr neurons of the LH-AL region intermingle (***Figure 3G,H***).

Odor response domains contain the activity of distinct neuronal populations

To illustrate higher-order connectivity, we labeled the three major neuron types, that is, MZ699+ iPNs, GH146+ ePNs and vlPr neurons, targeting the LH within the olfactory circuitry using PA-GFP (***Figure 4A***). Since our observed Ca^{2+} responses in the LH-AL region might reflect activity from vlPr neurons rather than iPNs, we dissected the neuronal contributions within each extracted ORD by conducting transection experiments using two-photon laser-mediated microdissection (***Figure 4B***). By transecting the mACT, we aimed at abolishing LH-responses deriving from MZ699+ iPNs, while cutting the plF connection should eliminate potential odor-evoked vlPr neuron activity. To achieve unambiguous and comparable results, functional imaging was performed in both brain hemispheres simultaneously. Immediately after the intact brain areas were imaged, the tracts were selectively transected on one brain side each (***Figure 4C***) and the imaging procedure was repeated. We applied a reduced odor set that elicited activity in all ORDs and performed NNMF for pre- and post-lesion recordings. Transecting the mACT significantly reduced responses in the LH-PM and LH-AM region, whereas LH-AL responses were significantly abolished by plF-ablation (***Figure 4D***). Notably, we observed that LH-AL responses to some odors were significantly increased after mACT transection as a consequence of the suppression of iPN inhibition of vlPr neurons confirming the study by ***Liang et al. (2013)***. Hence, activity in the LH-PM and LH-AM domain can be assigned to MZ699+ iPNs, while LH-AL activity is mainly evoked by vlPr neurons (***Figure 4E***).

iPN activity in the lateral horn mediates flies' attraction to odors

We next addressed the behavioral relevance of MZ699+ iPN activity in the LH for innate odor-guided behavior. To precisely target iPN function, we expressed an RNAi construct against glutamic acid decarboxylase 1 (GADi) to selectively knock-down the GABA synthesis in MZ699+ iPNs (***Figure 5A***). We confirmed the reduction in GABA production via immunostaining (***Figure 5B***). Since vlPr neurons are not GABAergic, they were not affected by the RNAi expression (***Liang et al., 2013***; ***Parnas et al., 2013***). Using wild-type flies and parental controls, we conducted T-maze assays (***Tully and Quinn, 1985***; ***Chakraborty et al., 2009***) with nine of the odorants applied in functional imaging experiments at medium and high concentrations. Notably, flies with silenced MZ699+ iPN GABA production revealed a neutral or aversive behavioral response to attractive odors, while repellent odors

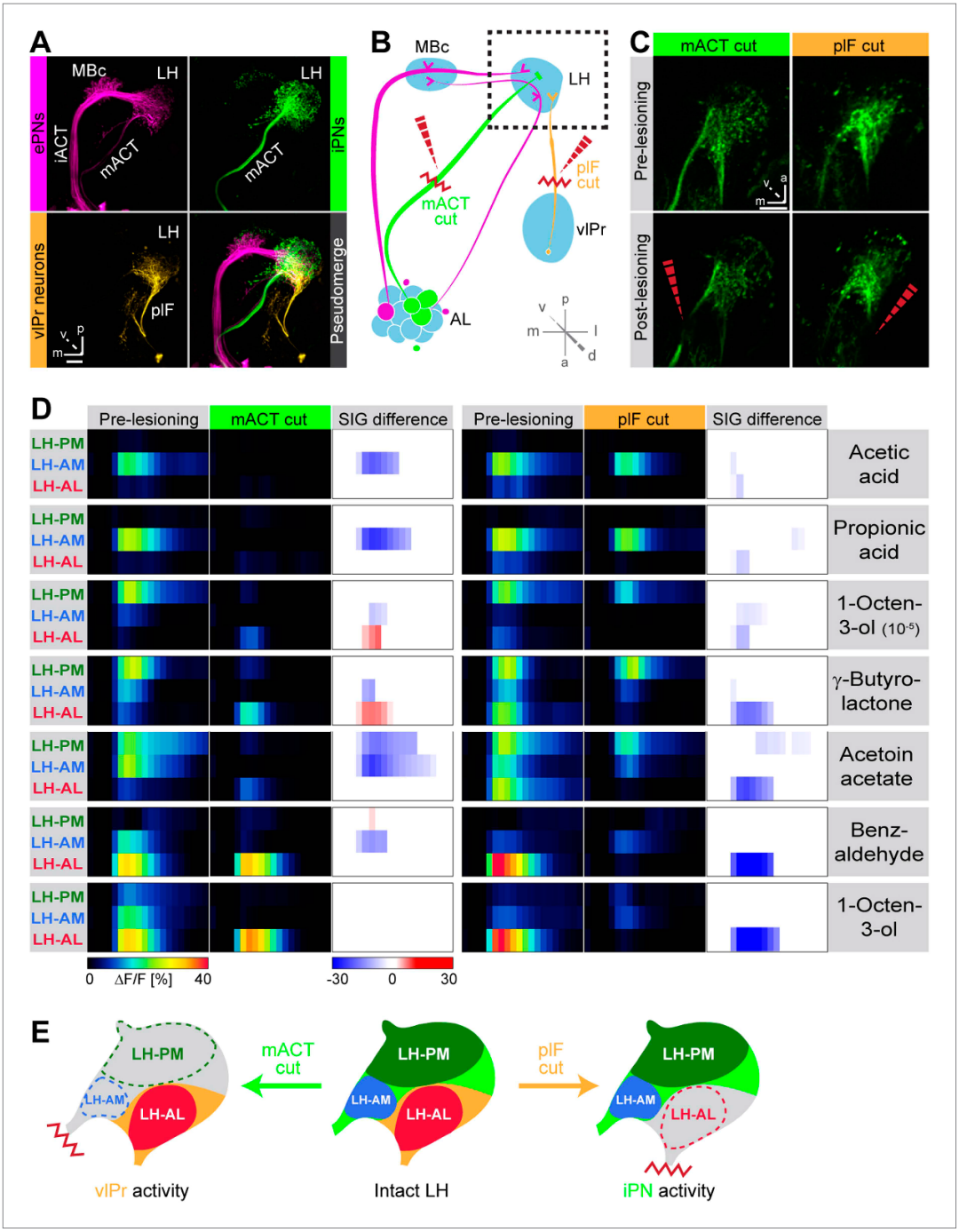

Figure 4. Distinct odor response domains in the LH constitute neuronal activity of iPNs and vlPr neurons. (**A**) Representation of all ePNs (magenta) and iPNs (green) labeled by GH146-GAL4 and MZ699-GAL4 using PA-GFP, respectively. Photoactivation of vlPr neurons (orange, MZ699-GAL4) connecting the LH and the vlPr via the pIF. The overlay image depicts a pseudo-merge image of the different GAL4 driver lines. (**B**) Schematic of the olfactory circuit with integrated layout of the transection experiment. After simultaneous Ca^{2+} imaging of bilateral LHs, the ipsilateral pIF and contralateral mACT was transected (red zigzag line) with an infrared laser (dashed red arrow). (**C**) Projection images of a 7 µm stack of the LH area prior and post transection. Left

Figure 4. Continued on next page

Figure 4. Continued

images, mACT transected; right image, plF transected. The ablated region is indicated by the dashed red arrow. Scale bar, 20 μm. (**D**) Median time traces displaying percental change of ΔF/F values for indicated ORDs prior to post transection of the mACT (green, left) and the plF (orange, right) for different odorants. Significant changes of odor-evoked Ca^{2+} signals due to transection are shown in the column SIG difference. Differences were tested with a two-tailed paired Student's *t* test ($p < 0.05$). Color codes are indicated by the corresponding scale bar below, n = 4–5. Transecting the mACT eliminates Ca^{2+} signals in the LH-PM and LH-AM domain, while lesioning the plF significantly abolishes LH-AL responses. Notably, the LH-AL domain is significantly stronger activated after mACT transection following application of 1-octen-3-ol and γ-butyrolactone. (**E**) Summarized cartoon of the neuron populations contributing to ORD activity prior and post transection of axons of iPNs or vlPr neurons.

DOI: 10.7554/eLife.04147.013

evoked an even stronger aversion (***Figure 5C***). To compare the T-maze data more accurately, we calculated the average change of behavioral response indices (RIs) between GADi flies and parental controls (***Figure 5D***). Indeed, all responses changed in a negative direction, indicating MZ699+ iPNs play a crucial role in mediating attraction behavior. The sole exception involved high concentrations of the most repulsive odor, acetophenone, since this odor had already induced maximum aversion. Overall, these experiments reveal a crucial function of MZ699+ iPNs in mediating attraction behavior by releasing GABA in the LH.

The lateral horn integrates hedonic valence and odor intensity into separate domains

The behavioral effect of the iPN knock-down suggests that MZ699+ iPNs encode positive hedonic valences. To correlate the complete ORD pattern array with innate behavioral preferences, we assigned behavioral RIs for all odors at median and high odor concentrations using the T-maze assay as in our previous experiment (***Figure 6A***). Since extremely low concentrations rarely evoked any behavioral response, we excluded the 10^{-6} concentration in this analysis. It is important to note here, that different behavioral assays for testing olfactory preferences in flies might lead to contradictory results. However, the majority of odors used here was also tested in two other behavioral paradigms, the trap assay (***Stökl et al., 2010***; ***Knaden et al., 2012***) and the FlyWalk (***Steck et al., 2012***) (pers. comm. M Knaden) and yielded similar results (see ***Figure 6—figure supplement 1***). When we plotted median odor-evoked activity in a three-dimensional space defined by the three ORDs, we saw a clear clustering of responses evoked by aversive and attractive odorants (***Figure 6B***). The LH-AL domain, constituted mainly by vlPr neurons, is coding aversive odors, while attractive odors activated only the LH-PM and LH-AM domains that derive from MZ699+ iPNs. This result is in accordance with our finding that iPNs mediate odor attraction.

We next correlated ORD activity to odor valence separately for all ORDs. This evaluation enabled us to analyze iPN and vlPr neuron coding properties apart from each other (***Figure 6C***). As expected, the analysis revealed a significant correlation between positive valence and the LH-PM domain, whereas Ca^{2+} responses in the LH-AL were strongly negatively correlated to hedonic valence. The LH-AM domain exhibited a positive but not significant correlation for odor valence. Remarkably, activity within the LH-PM was totally independent of concentration, whereas activity in both anterior domains was significantly correlated to odor intensity (***Figure 6D***). Hence, MZ699+ iPNs integrate odor attraction information into the LH-PM domain independent of odor intensity, confirming behavioral experiments. Intensity coding is in turn conducted separately by distinct iPNs within the LH-AM domain. In contrast, putative third-order vlPr neurons projecting into the LH-AL area code both negative valence and odor intensity.

Finally, we wondered if this valence-specific LH representation is already reflected at the primary level of olfactory processing. The odor-evoked responses in iPNs are generally similar to those in OSNs (***Wang et al., 2014***), indicating a straight forward transduction of cholinergic OSN responses. We therefore performed functional imaging of odor-evoked Ca^{2+} dynamics at the AL input level by expressing G-CaMP in OSNs using Orco-GAL4 (***Larsson et al., 2004***) (***Figure 6—figure supplement 2***). In order to compare the activity patterns at both processing levels, we calculated correlation distances for all pair-wise combinations of odor-evoked response patterns and plotted these with respect to maximal ORD pattern similarity in the LH (***Figure 6E***). As expected, odor representations in the LH clearly clustered within three separated parts of the matrix, reflecting our observed ORDs. However, this coding similarity could not predict AL activity patterns, even if the correlation matrix was sorted with respect to pattern similarity in the AL (***Figure 6—figure supplement 3***).

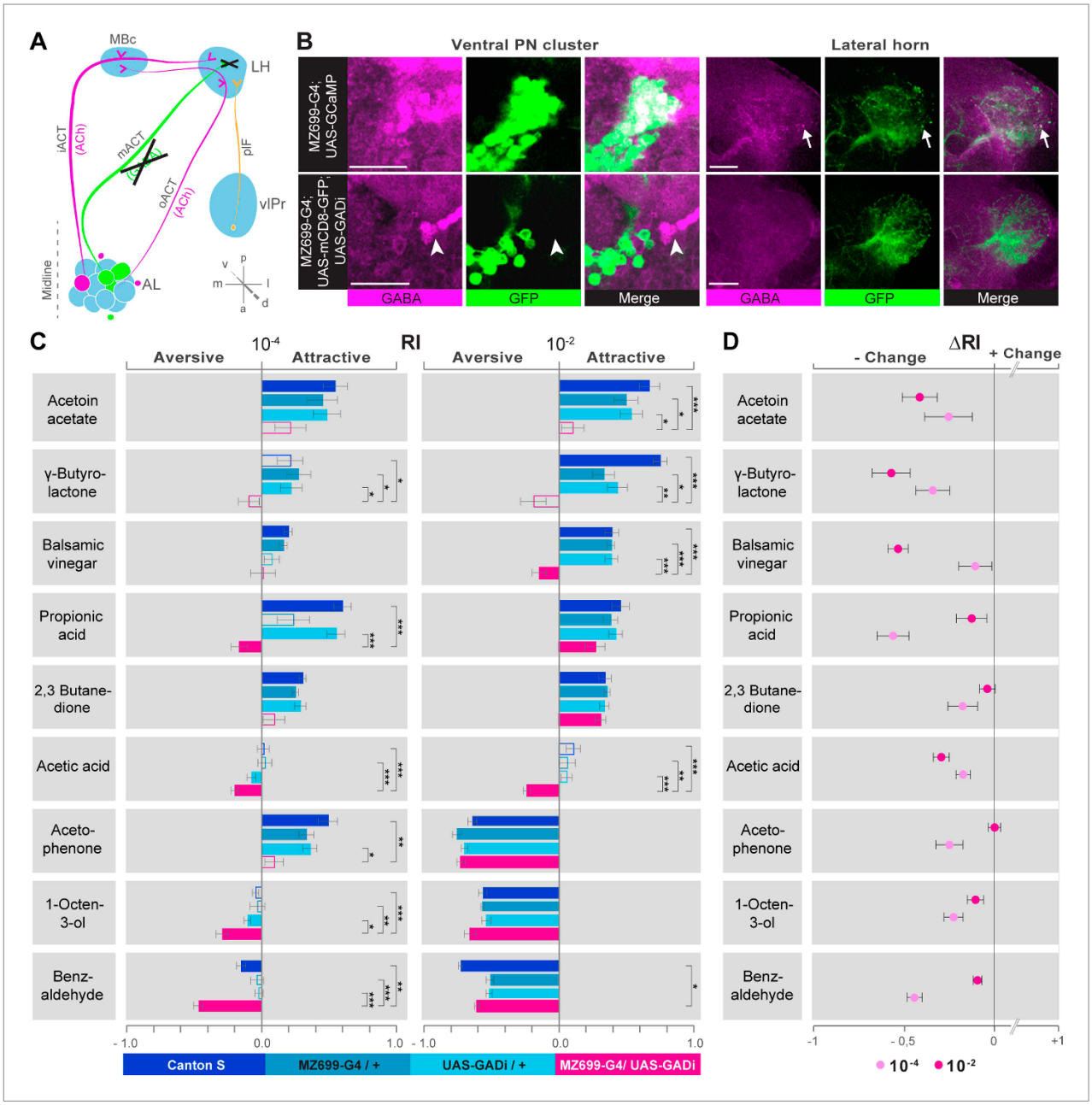

Figure 5. iPN GABA release in the LH mediates odor attraction behavior. (**A**) Experimental layout: iPN GABA production was selectively silenced via GADi expression in MZ699+ iPNs; ePN and vlPr neuron activity remained unaffected. (**B**) Immunostaining against GABA and GFP within AL somata (left) and LH neurites (right) of iPNs with intact (top) and silenced GABA production (bottom). GADi flies show GABA signals in somata of iPNs labeled by GH146 only (arrowhead). The arrow head points to an exemplary GABA-positive bouton in the LH. Scale bar, 20 μm. (**C**) Averaged behavioral response indices (RIs) determined with a T-maze assay for wild-type flies (dark blue), parental controls (light blue) and experimental animals (magenta) for nine odorants at two concentrations. Empty boxes display no response (Wilcoxon signed-rank test). Dunn's Multiple Comparison Test was used for global differences in the dataset followed by a posthoc test for selected pairs (p* < 0.05; **p < 0.01; ***p < 0.001). Error bars represent SEM. (**D**) RI differences between GADi flies and averaged parental controls. RI differences are negative for all but one odor indicating that GADi expression shifts odor-guided behavior towards aversion. Error bars indicate SEM.

DOI: 10.7554/eLife.04147.014

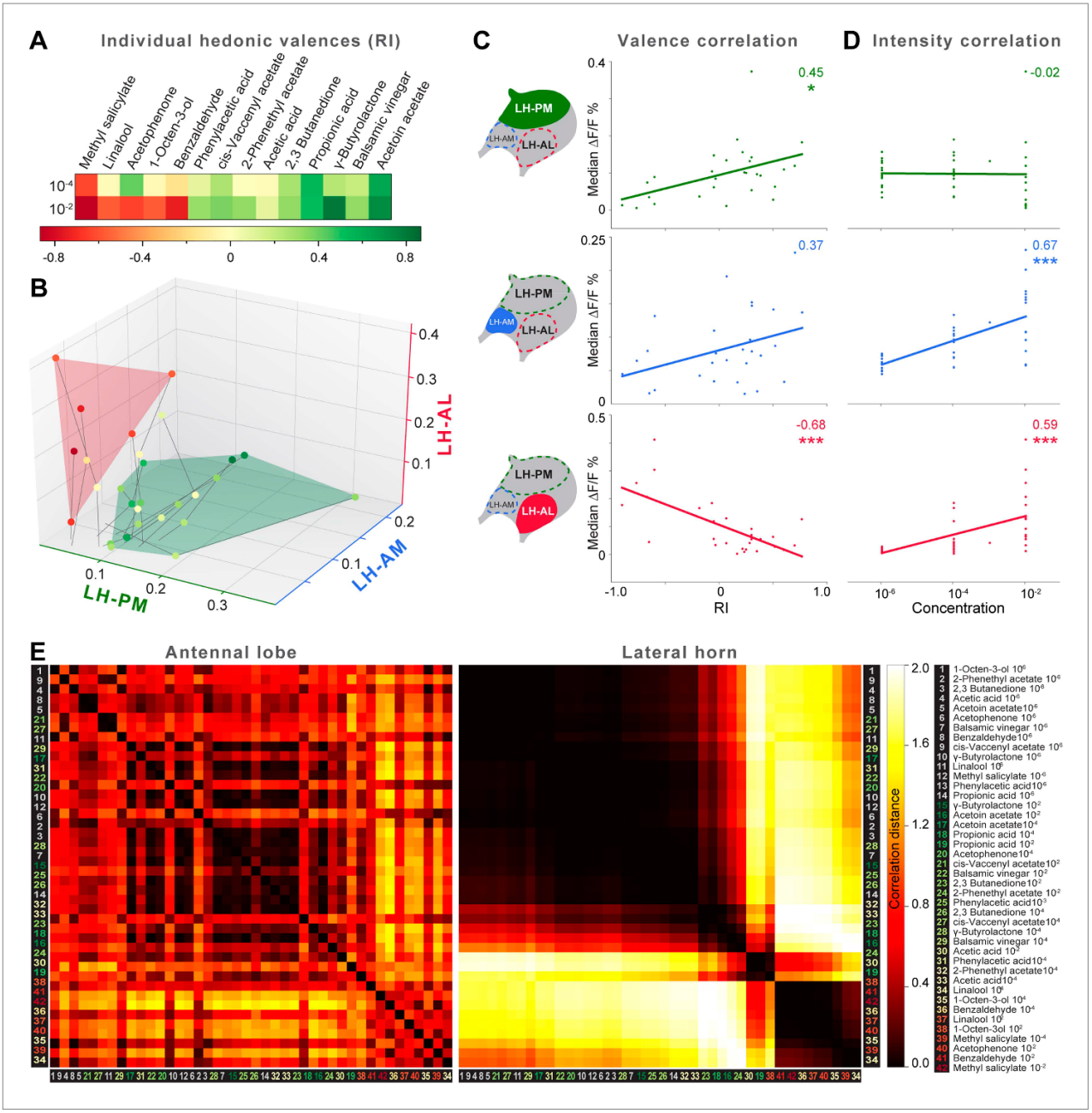

Figure 6. Integration of hedonic valence and odor concentration into ORDs. (**A**) Response indices of wild type flies for all odors at median and high concentrations. Odors are sorted from highly aversive (−1, red) to highly attractive (+1, green). (**B**) 3D-scatter plot of median Ca^{2+} responses of all odors based on the three ORDs. Odor-dots are labeled due to their RI shown in (**A**). Same odors at different concentrations are connected with a line: the dot at the end depicts 10^{-2}, the centered dot 10^{-4}, and the end of the line 10^{-6}. Attractive and aversive odor representations form separate clusters. (**C** and **D**) Left, schematic LH outlines with colored ORDs corresponding to data on the right. Correlation score r (upper right corner) between median activity and measured RI in T-maze experiments or odor concentration, respectively, with significance denoted below. Student's *t* test, *p < 0.05, ***p < 0.001. (**E**) Complete correlation matrices for Ca^{2+} response patterns of OSNs in the AL (left) and iPNs in the LH (right). The odors are arranged according to single linkage clustering of the LH activity patterns. Heatmap color-code refers to the correlation distance scale bar on the right. Correlation distance is

Figure 6. Continued on next page

Figure 6. Continued

defined as 1 − r, where r is the Pearson correlation coefficient between the response patterns of two odorants. Odor letters are color-coded according to hedonic valence; 10^{-6} RI values are labeled in grey (complete list right hand).

DOI: 10.7554/eLife.04147.015

The following figure supplements are available for figure 6:

Figure supplement 1. Odor valences determined with three different behavioral assays.

DOI: 10.7554/eLife.04147.016

Figure supplement 2. Calcium responses of OSNs.

DOI: 10.7554/eLife.04147.017

Figure supplement 3. Correlation matrices for odor-evoked responses in the AL and LH.

DOI: 10.7554/eLife.04147.018

Discussion

We augment our present understanding of the *Drosophila* olfactory circuitry by elucidating the coding properties of a parallel and behaviorally relevant higher-order processing pathway to the LH. Morphological, functional and behavioral approaches provide strong evidence for a functional subdivision of iPNs into neurons coding either odor attraction or odor intensity. Our behavioral experiments reveal that inhibitory properties of iPNs are necessary for innate odor-guided attraction. In addition, we characterize a third neural pathway coding odor repellence.

Do MZ699+ iPNs fulfill anatomical requirements to constitute a distinct processing channel in addition to ePNs? A remarkable anatomical feature of MZ699+ iPNs is their glomerular innervation pattern in the AL. Whereas GH146+ ePNs are uniglomerular and retain the topographic code in their axonal arrangement (***Marin et al., 2002***; ***Wong et al., 2002***; ***Jefferis et al., 2007***), most MZ699+ iPNs possess oligoglomerular innervations suggesting that these neurons might not convey precise odor-identity information. In addition, MZ699+ iPNs in the AL diverge only into specific glomerular subsets, and so might be pre-determined to selectively extract common features of distinct odors. We have previously shown that the AL map at the PN level exhibits a spatial segregation of valence representation (***Knaden et al., 2012***). Certain glomeruli, which have been classified as aversion coding at the GH146+ ePN level, are omitted by MZ699+ iPNs, whereas most glomeruli classified as attraction coding are particularly densely innervated. These results suggest that within the MZ699+ iPN population, mainly positive odor traits are extracted, whereas the odor information of negative valence is neglected. This conclusion is consistent with the recent finding that one type of LH neurons is receiving input from PNs that mainly innervate glomeruli coding fruity-smelling acetates (***Fisek and Wilson, 2014***) which represent attractive odor cues (***Knaden et al., 2012***). We furthermore demonstrate that the MZ699+ iPN population is split into two major morphological classes possessing a clear spatial segregation in the AL which is strictly maintained within the LH. It has to be kept in mind that we do not cover all iPNs by using MZ699-GAL4. Further experiments characterizing the ~6 missing MZ699–iPNs, which are labeled by GH146-GAL4 (***Wilson and Laurent, 2005***; ***Lai et al., 2008***), will elucidate if our assumptions apply for the whole iPN population.

So far only a handful neuroanatomical studies targeting GH146+ ePNs have dealt with the question of how olfactory information is integrated and read out by higher brain structures, in particular the LH (***Marin et al., 2002***; ***Wong et al., 2002***; ***Tanaka et al., 2004***; ***Jefferis et al., 2007***). A recent study that traced the projection pattern of PNs coding ammonia and amines as attractive stimuli and carbon dioxide and acids as repulsive signals suggests that sensory stimuli of opposing valence are represented in spatially distinct areas within the LH (***Min et al., 2013***). In addition the study by ***Liang et al. (2013)*** showed that MZ699+ iPNs selectively suppress the activity of vlPr neurons to food odors, while pheromone responses were not affected verifying the assumption that different odor features are processed separately. However, functional evidence for a feature-based, spatially segregated activity map in the LH was so far missing.

To unravel the coding properties of MZ699+ iPNs within the LH, we conducted Ca^{2+} imaging experiments of MZ699+ iPNs in the LH to odorants having different hedonic valences and intensities, and could classify the LH into three functional ORDs. Our neuronal tracing and transection experiments validated the LH segmentation into two medial domains that derive from MZ699+ iPNs, and the LH-AL domain formed by vlPr neurons. In line with our observations are morphological studies on ePNs and third-order LH neurons revealing a similarly tight constriction into three zones within the

LH (**Tanaka et al., 2004**), while single-cell labeling combined with image registration resulted in five ePN target zones (**Jefferis et al., 2007**). However, the ePN terminal zones do not necessarily correspond to the target domains of iPNs, since it has recently been shown that MZ699+ iPNs do not inhibit odor responses of GH146+ ePNs (**Liang et al., 2013**) and that the presynaptic sites of iPNs are spatially separated from those of ePNs (**Wang et al., 2014**). Hence both PN populations represent parallel processing pathways that most likely accomplish distinct processing tasks analogous to the honeybee olfactory system which possesses dual olfactory pathways to the higher brain that accomplish parallel processing of similar odors (**Brill et al., 2013**).

Silencing MB function revealed that the LH alone is sufficient for basic olfactory behavior (**de Belle and Heisenberg, 1994**; **Connolly et al., 1996**; **Heimbeck et al., 2001**). Our behavioral results demonstrate that selectively silencing MZ699+ iPNs severely reduced the flies' odor attraction behavior. Hence our results suggest that MZ699+ iPNs are capable of extracting specific features from the combinatorial code emerging in the AL. A behavioral study revealed that silencing MBc neurons impairs odor attraction but not repulsion (**Wang et al., 2003b**). The authors drew the conclusion that the LH is involved in mediating innate repulsion rather than attraction. These results are not necessarily contradictory to ours since some ePNs might activate the LH-AL domain exclusively (i.e., vlPr neurons). On the other hand, **Wang et al. (2003b)** did not include highly concentrated attractive odors. Therefore it is possible that in their experiments, the odor detection threshold was simply reduced, so that only highly concentrated odors, which induced odor aversion, could be distinguished. Our behavioral results, in contrast, revealed the constant influence of the MZ699+ iPNs in mediating attraction for odorants over a range of concentrations.

Our data suggests that odors with opposing hedonic valences are encoded by an interplay of distinct processing pathways. The study by **Liang et al. (2013)** showed that GABA release from MZ699+ iPNs directly inhibits responses of vlPr neurons to food odors as mentioned above. This finding fits well to our observations that iPNs are activated mainly by attractive odors while vlPr neurons are not, likely due to the inhibitory input from iPNs. VlPr neurons are, on the other hand, almost solely activated by repellent odors, which do hardly activate iPNs and therefore do not induce a strong inhibition to vlPr neurons. Repellent odors most likely activate vlPr neurons via ACh release of ePNs which is supported by immunostainings with pre- and postsynaptic markers indicating that vlPr neurons receive input in the LH, while the vlPr represents their major output region (**Parnas et al., 2013**). The vlPr is supposedly also a target of visual neurons from the optic lobe (**Tanaka et al., 2004**) implying that a certain integration of different sensory modalities takes place at this central processing relay. Given that iPNs are inhibitory neurons, the underlying mechanism of odor attraction behavior might therefore be an inhibition of aversive neuronal circuits from the LH to the vlPr that are mainly composed of vlPr neurons. However, this assumption needs to be verified with further experiments elucidating if vlPr neurons are sufficient and necessary to mediate odor aversion.

What is known about odor coding in the LH in other insect species? Notably, in locusts it has been shown that LH neurons receiving convergent PN input appeared to encode stimulus intensity in their net firing rates and in the phases of their spikes (**Gupta and Stopfer, 2012**). Hence these results support the idea that within the LH, general stimulus features such as odor intensity are extracted, which is well in line with our observation of the anterior LH domains whose activity is also significantly correlated to odor intensity. Also in line with our results is a study from honeybees which shows that the representation of different pheromone types is spatially segregated in the LH (**Roussel et al., 2014**), indicating that odors eliciting specific behaviors are coded according to their biological values.

In conclusion, our study provides an important step in unraveling higher olfactory processing mechanisms that are crucial for mediating innate behaviors in *Drosophila*. We provide functional evidence for a feature-based spatial arrangement of the LH decoding opposing hedonic valences and odor intensity. The role of the LH as a center for integrating biological values towards innate decisions by computing conveyed information of two processing pathways is thus expanded.

Materials and methods

Drosophila stocks

All fly stocks were maintained on conventional cornmeal-agar-molasses medium under L:D 12:12, RH = 70% and 25°C. For wild-type controls *D. melanogaster* of the Canton-S strain was used. Transgenic lines were obtained from Bloomington Stock Center (http://flystocks.bio.indiana.edu/) and Vienna

RNAi stock center (http://www.vdrc.at). Other fly stocks were kindly provided by Kei Ito (MZ699-GAL4) and Maria Luisa Vasconcelos (UAS-C3PA).

Immunohistochemistry

Whole-mount (wm) and vibratome (vt) immunofluorescence staining was carried out as described (***Laissue et al., 1999***; ***Vosshall et al., 2000***). Initially brains were dissected in Ringer's solution (130 mM NaCl, 5 mM KCl, 2 mM $MgCl_2$, 2 mM $CaCl_2$, 36 mM saccharose, 5 mM HEPES, [pH 7.3]) (***Estes et al., 1996***) and fixed in 4% PFA in PBS-T (PBS, 0.2–1% Triton-X). After washing with PBS-T (wm) or PBS (vt) brains were blocked with PBS-T, 2% bovine serum albumin (BSA) or PBS-T, 5% normal goat serum (NGS). Vt-sections were blocked using 5% NGS and 5% normal donkey serum (NDS). Primary antibodies were diluted in blocking solution or PBS-T and incubated at 4°C for 2–3 days (vt). Secondary antibody incubation lasted 1–2 days. Brains were mounted in VectaShield (Vector Laboratories). The following primary antibodies were used: rabbit α-GABA (1:500) (Sigma), mouse α-GFP (1:500) or chicken α-GFP (1:1000) or rabbit α-GFP (1:500) (all Invitrogen), mouse monoclonal α-ChAT (1:500) (DSHB), mouse α-Nc82 (1:30) (DSHB) or rabbit α-Nc82 and guinea pig α-Nc82 (1:500), kindly provided by Stefan Sigrist, rabbit α-RFP (1:500) and mouse α-HA (1:1000) (both Abcam). The following secondary antibodies were used: Alexa Fluor 488, goat anti-mouse IgG (1:500); Alexa Fluor 488, goat anti-rabbit (1:500); Alexa Fluor 546, goat anti-rabbit (1:500); Alexa Fluor 633, goat anti-mouse (1:200), Fluor 594 chicken anti mouse (1:200), Alexa Fluor 488 donkey anti-chicken 1:200 (all IgG Invitrogen).

Functional imaging

Fly preparation and functional imaging of the AL was conducted as previously described (***Stökl et al., 2010***; ***Strutz et al., 2012***). LH imaging was conducted similarly, except for the higher resolution achieved with a 60× water immersion objective (LUMPlanFI 60×/0.90 W Zeiss). The optical plane was ~30 μm below the most dorsal entrance point of the iPN tract into the LH. Binning on the CCD-camera chip resulted in a resolution of 1 pixel = 0.4 × 0.4 μm. For bilateral LH imaging during transection a 20× water immersion objective (NA 0.95, XLUM Plan FI, Olympus) was employed. All recordings lasted 10 s with a frame rate of 4 Hz. Odors included acids (propionic acid, acetic acid), lactones (γ-butyrolactone), terpenes (linalool), aromatics (acetophenone, methyl salicylate, benzaldehyde, phenylacetic acid), alcohols (1-octen-3-ol), esters (acetoin acetate, cis-vaccenyl acetate, 2-phenethyl acetate), ketones (2,3 butanedione) and balsamic vinegar diluted in mineral oil (all from Sigma Aldrich). Odors were applied during frame 8–14 (i.e., after 2 s, lasting for 2 s). Flies were imaged for up to 1 hr, with a minimum inter-stimulus interval of one minute. We selected conventional widefield Ca^{2+} imaging as the method of choice, since we were able to obtain single bouton resolution with this technique.

Imaging data analysis

Calcium imaging data of AL were analyzed with custom-written IDL software (ITT Visual Information Solutions) provided by Mathias Ditzen as previously described (***Stökl et al., 2010***; ***Strutz et al., 2012***). Regarding the Ca^{2+} imaging data in the LH, we repeated recordings of each odor at each concentration two to three times to ensure the reliability of the extracted domain information. To execute NNMF analysis (see below), at least 6–7 valid measurements, that is, animals with repeated identical recordings, were collected for each odor and employed for the analysis. Individual odor measurements were aligned using ImageJ (Fiji) to correct movement artifacts. Fluorescence changes (△F/F) for each odor were calculated in relation to background fluorescence using frames 0–6 (i.e., 2–0.5 s before odor application). A Gaussian low-pass filter (ó = 1px) was applied to compensate for remaining movement artifacts and pixel noise. To reduce the computational load, the frame rate was averaged by two consecutive frames, and recordings were spatially down-sampled by a factor of two. The resulting concatenated time-series of the recordings is denoted as measurement matrix Y with element $Y_{t,p}$ being the t^{th} observed value of pixel p.

NNMF—Non-Negative Matrix Factorization

In contrast to the AL, which consists of highly ordered glomerular subunits, the LH comprises a mainly homogenous neuropil which does not provide spatial or functional landmarks. Therefore, we used the automatic method NNMF to extract Ca^{2+} signals that exhibit common spatial or temporal features. NNMF, like other matrix factorization techniques (e.g., Principal Component Analysis (PCA) and Independent Component Analysis (ICA)), decompose the measurement matrix Y into k components, $Y=\sum_k x_k * a_k^T + R$. The time-course a_k of each component contains a common underlying time-courses

of all pixels and each pixel participation x_k declares how strongly each pixel is involved in this time-course. The residual matrix R contains the unexplained data. In order to perform NNMF, we implemented the HALS algorithm in Python including a spatial smoothness constraint (a_{sm} = 0.1) (***Cichocki and Phan, 2009***) and an additional spatial decorrelation constraint (a_{de} = 0.1) (***Chen and Cichocki, 2005***).

In PCA decomposition is performed such that either timecourses a_k or pixel participation x_k are uncorrelated, whereas ICA aims for timecourses (temporal ICA) or pixel participation (spatial ICA) to be independent. Although spatial ICA is able to segregate signals into functional similar neuropils (***Reidl et al., 2007***), we chose the NNMF approach, because it is known to achieve even a better parts-based representation compared to the more holistic results of PCA or ICA (***Lee and Seung, 1999***). In contrast to PCA and ICA, NNMF constrains both the extracted time-courses and pixel participations to be positive. Positive pixel participation enabled us to make a straightforward physiological interpretation, reading the participation values as the contribution strength of an underlying physiological domain. The restriction to positive time-courses reflects the fact that we did not observe any significant decrease of fluorescence in response to an odor in the original measurement data. For each animal we performed decomposition into k = 5 components. This was sufficient to explain most of the data's variance (88% + 8%, error is standard deviation across individuals). The remaining variance in the residual matrix R contained no additional domains but rather reflected remaining movement artifacts of the measurements (***Figure 2—figure supplement 2***). Of the five components extracted by NNMF, three stood out prominently (***Figure 2—figure supplement 3***): First, they were extracted in all animals at very clearly defined anatomical positions. Second, their responses to stimuli repetitions were highly reproducible in contrast to the other two components, that is, they exhibited a significant ($p < 2*10^{-8}$, t test) higher trial-to-trial correlation of 0.72 ± 0.20 in contrast to 0.52 ± 0.26 for the remaining components; third, the odorant spectra of their responses were characteristic across animals.

Though we cannot completely rule out that the remaining components of the factorization are ORDs of their own, there are several indications that they are not. On the one hand, they exhibit a lower trial-to-trial correlation than the three selected components. Second, those components did not consistently appear at similar anatomical position. Third, they were spatially overlapping with the selected three components. Instead of independent ORDs, these regions might convey fluorescence changes independent of odor stimulation or an overlapping region of two of the reliable ORDs. A validation of our NNMF-based results with spatial ICA yielded very similar, but slightly worse results. Whereas the three reliable ORDs from NNMF were also extracted in spatial ICA, the two remaining components exhibited much higher variability than when obtained with NNMF. Hence, we conclude that the LH area comprising MZ699+ neurons consists of three ORDs. We labeled those three components according to the anatomical position of their pixel participation within the LH.

Statistical analysis of imaging data

To determine the coding properties of extracted odor response domains (ORDs), we calculated the mean response of each animal within a time window of 1–4 s after stimulus onset. Hence, median responses over all animals defined the standard stimulated response r^o_{ORD} of an ORD to an odor o. Initially, regions were evaluated individually, and correlations were calculated between standard response spectra and the behavioral response index (RI), or odor concentration, respectively, using the 'linregress' function of the Python scipy.stat module. To analyze the combined ORD representations of odor patterns $p_o = \left(r^o_{PM}, r^o_{AM}, r^o_{AL}\right)$ we calculated for all odor pairs the pattern similarity as correlation distance $d_{o1,o2} = 1 - corr(p_{o1}, p_{o2})$. In order to visualize the correlation matrix in a comprehensible way, we then arranged odors according to the single linkage clustering of the Python scipy.cluster.hierarchy module. To compare the representation in the LH to those of the AL, we applied the same procedure to the dorsal glomerular odor activation pattern.

2-Photon photoactivation and neuronal reconstructions

For in vivo photoactivation experiments, 1–6 day old flies (Genotype: END1-2,UAS-C3PA;MZ699-GAL4) were dissected as in the imaging experiments except that tracts of the salivary glands were cut to prevent movement. Photoactivation was accomplished via continuous illumination with 760 nm for 15–25 min. After a 5-min break to permit full diffusion of the photoconverted molecules, 925 nm z-stacks of the whole brain were acquired and subsequently used for neuronal 3D-reconstruction. For all 3D reconstructions, the segmentation software AMIRA 5.3.3 (Mercury Computer Systems) was

used. Neurons of different individuals were embedded into the reference brain using a labelfield registration as previously described (**Rybak et al., 2010**). Briefly, segmented labels of brain neuropils (AL, MBc, LH) were registered onto a reference brain image using affine registration followed by elastic warping. In a second step, the calculated transformation matrix was applied to the respective neuron morphology that was then aligned to the reference brain image.

For morphological analysis of reconstructed iPNs, we first determined all terminal points of each iPN in the LH area. For each combination of terminals we calculated a similarity score (*s*) in analogy to (**Kohl et al., 2013**) as follows:

$$s(t_1, t_2) = \sqrt{e^{-\Delta(t_1,t_2)^2/2\sigma^2}},$$

where *t* is the terminal position, $\Delta(t1,t2)$ is the Euclidean distance and σ is a free parameter that determines how close in space terminal points must be to be considered similar; analogue to **Kohl et al. (2013)** we set this parameter to 3 µm. Finally we calculated the pairwise similarity score between two neurons as their average all-to-all terminal similarity scores, normalized to their self-scores as follows:

$$S(n_1, n_2) = \sum_{t_1,t_2} s(t_1, t_2) / \sqrt{\sum_{t_1} s(t_1, t_1) * \sum_{t_2} s(t_2, t_2)}$$

Effectively this quantifies the relative overlap of the target area of all pairs of iPNs. For clustering, the similarity scores were converted to distances (i.e., *1-S*) and a hierarchical clustering was performed using UPGMA method. Principal component analysis and one-way ANOSIM was performed using the statistical software PAST 3.x (Paleontological statistics software package for education and data analysis).

2-Photon-mediated transection

Transections of either the plF tract or the mACT were conducted in one brain hemisphere, each of the same fly. The target area was monitored with 925 nm and chosen to be close to the LH but distant enough not to affect neurites ramifying in the LH neuropil. For both tracts, lesioned areas had an average size of 34 µm and were illuminated with short pulses of 710 nm every 40 ms for 250 ms in 60 (plF)—80 (mACT) cycles in a single focal plane. After a fast z-stack with 925 nm to confirm complete lesion, a 5-min neuronal recovery interval followed before continuing the imaging procedure. Data were analyzed using NNMF.

Image acquisition

Photoactivation and transection procedures as well as image acquisition following immunohistochemistry were accomplished with a 2-photon confocal laser scanning microscope (2PCLSM, Zeiss LSM 710 meta NLO) equipped with a 40× (W Plan-Apochromat 40×/1.0 DIC M27) or 20× (W N-Achroplan 20×/0.5 M27). The 2PCLSM was placed on a smart table UT2 (Newport Corporation, Irvine, CA, USA) and equipped with an infrared Chameleon Ultra diode-pumped laser (Coherent, Santa Clara, CA, USA). Z-stacks were performed with argon 488 nm and helium-neon 543 nm laser or the Chameleon Laser 925 nm (BP500-550 for G-CaMP and LP555 for DsRed/tdTomato) and had a resolution of 1024 or 512 square pixels. The maximum step size for immuno-preparations or single neuron projections was 1 µm and for AL reconstructions 2 µm.

Behavioral assay

Flies carrying P[GAD1-RNAi];P[MZ699-GAL4] were crossed just before the experiment to prevent dosage compensation effects. T-maze experiments were performed as described (**Stensmyr et al., 2012**). WT, parental controls (P[GAD1-RNAi] or P[MZ699-GAL4]) and test flies carrying both insertions were tested separately under identical conditions. The response index (RI) was calculated as (O-C)/T, where O is the number of flies in the odor arm, C is the number of flies in the control arm, and T is the total number of flies used in the trial. Hence, the RI ranges from −1 (complete avoidance) to 1 (complete attraction). Each experiment was carried out on 30 flies and was repeated 12 times. Dunn's Multiple Comparison Test was used for global differences in the dataset. Whenever the Multiple Comparison Test was significant (i.e., $p < 0.05$), a posthoc test for selected pairs was performed, that is, between the GADi-flies and the other three control lines as we were not interested in differences among the different control lines. All RI were tested against 0 (no response) by using the Wilcoxon-rank-sum test.

Acknowledgements

We thank Silke Trautheim, Regina Stieber, Linda Gummlich and Sascha Bucks for excellent technical assistance and Emily Wheeler for editorial assistance.

Additional information

Competing interests

BSH: Vice president of the Max Planck Society, one of the three founding funders of *eLife*, and a member of *eLife's* Board of Directors. The other author declare that no competing interests exist.

Funding

Funder	Author
Bundesministerium für Bildung und Forschung (Federal Ministry of Education and Research)	Silke Sachse
Max-Planck-Gesellschaft (Max Planck Society)	Bill S Hansson

The funders had no role in study design, data collection and interpretation, or the decision to submit the work for publication.

Author contributions

AS, Conception and design, Acquisition of data, Analysis and interpretation of data, Drafting or revising the article; JS, Analysis and interpretation of data, Drafting or revising the article; AB, VG, JR, Acquisition of data, Analysis and interpretation of data; AF, Performed behavioral experiments; MK, Supervision of Abu Farhan, Analysis and interpretation of data; MS, Supervision of Jan Soelter, Analysis and interpretation of data; BSH, Provided intellectual and financial support, Conception and design; SS, Conception and design, Analysis and interpretation of data, Drafting or revising the article

Author ORCIDs

Amelie Baschwitz, http://orcid.org/0000-0003-0614-1667
Michael Schmuker, http://orcid.org/0000-0001-6753-4929

References

Bausenwein B, Dittrich AP, Fischbach KF. 1992. The optic lobe of *Drosophila melanogaster*. II. Sorting of retinotopic pathways in the medulla. *Cell and Tissue Research* **267**:17–28. doi: 10.1007/BF00318687.

Brill MF, Rosenbaum T, Reus I, Kleineidam CJ, Nawrot MP, Rössler W. 2013. Parallel processing via a dual olfactory pathway in the honeybee. *The Journal of Neuroscience* **33**:2443–2456. doi: 10.1523/jneurosci.4268-12.2013.

Caron SJ, Ruta V, Abbott LF, Axel R. 2013. Random convergence of olfactory inputs in the *Drosophila* mushroom body. *Nature* **497**:113–117. doi: 10.1038/nature12063.

Chakraborty TS, Goswami SP, Siddiqi O. 2009. Sensory correlates of Imaginal conditioning in *Drosophila melanogaster*. *Journal of Neurogenetics* **23**:210–219. doi: 10.1080/01677060802491559.

Chen Z, Cichocki A. 2005. Nonnegative matrix factorization with temporal smoothness and/or spatial decorrelation constraints. *Signal Processing*.

Cichocki A, Phan A. 2009. Fast local algorithms for large scale nonnegative matrix and tensor factorizations. *IEICE Transactions on Fundamentals of Electronics, Communications and Computer Sciences* **E92-A**:708–721. doi: 10.1587/transfun.E92.A.708.

Connolly JB, Roberts IJ, Armstrong JD, Kaiser K, Forte M, Tully T, O'Kane CJ. 1996. Associative learning disrupted by impaired Gs signaling in *Drosophila* mushroom bodies. *Science* **274**:2104–2107. doi: 10.1126/science.274.5295.2104.

Couto A, Alenius M, Dickson BJ. 2005. Molecular, anatomical, and functional organization of the *Drosophila* olfactory system. *Current Biology* **15**:1535–1547. doi: 10.1016/j.cub.2005.07.034.

Datta SR, Vasconcelos ML, Ruta V, Luo S, Wong A, Demir E, Flores J, Balonze K, Dickson BJ, Axel R. 2008. The *Drosophila* pheromone cVA activates a sexually dimorphic neural circuit. *Nature* **452**:473–477. doi: 10.1038/nature06808.

de Belle JS, Heisenberg M. 1994. Associative odor learning in *Drosophila* abolished by chemical ablation of mushroom bodies. *Science* **263**:692–695. doi: 10.1126/science.8303280.

Estes PS, Roos J, van der Bliek A, Kelly RB, Krishnan KS, Ramaswami M. 1996. Traffic of dynamin within individual *Drosophila* synaptic boutons relative to compartment-specific markers. *The Journal of Neuroscience* **16**:5443–5456.

Fiala A, Spall T, Diegelmann S, Eisermann B, Sachse S, Devaud JM, Buchner E, Galizia CG. 2002. Genetically expressed cameleon in *Drosophila melanogaster* is used to visualize olfactory information in projection neurons. *Current Biology* **12**:1877–1884. doi: 10.1016/S0960-9822(02)01239-3.

Fisek M, Wilson RI. 2014. Stereotyped connectivity and computations in higher-order olfactory neurons. *Nature Neuroscience* **17**:280–288. doi: 10.1038/nn.3613.

Fishilevich E, Vosshall LB. 2005. Genetic and functional subdivision of the *Drosophila* antennal lobe. *Current Biology* **15**:1548–1553. doi: 10.1016/j.cub.2005.07.066.

Grabe V, Strutz A, Baschwitz A, Hansson BS, Sachse S. 2014. Digital in vivo 3D atlas of the antennal lobe of *Drosophila melanogaster*. *The Journal of Comparative Neurology* doi: 10.1002/cne.23697.

Gupta N, Stopfer M. 2012. Functional analysis of a higher olfactory center, the lateral horn. *The Journal of Neuroscience* **32**:8138–8148. doi: 10.1523/jneurosci.1066-12.2012.

Heimbeck G, Bugnon V, Gendre N, Keller A, Stocker RF. 2001. A central neural circuit for experience-independent olfactory and courtship behavior in *Drosophila melanogaster*. *Proceedings of the National Academy of Sciences of USA* **98**:15336–15341. doi: 10.1073/pnas.011314898.

Heisenberg M. 2003. Mushroom body memoir: from maps to models. *Nature Reviews. Neuroscience* **4**:266–275. doi: 10.1038/nrn1074.

Hildebrand JG, Shepherd GM. 1997. Mechanisms of olfactory discrimination: Converging evidence for common principles across phyla. *Annual Review of Neuroscience* **20**:595–631. doi: 10.1146/annurev.neuro.20.1.595.

Ito K, Sass H, Urbach J, Hofbauer A, Schneuwly S. 1997. GAL4-responsive UAS-tau as a tool for studying the anatomy and development of the *Drosophila* central nervous system. *Cell and Tissue Research* **290**:1–10. doi: 10.1007/s004410050901.

Jefferis GS, Marin EC, Stocker RF, Luo L. 2001. Target neuron prespecification in the olfactory map of *Drosophila*. *Nature* **414**:204–208. doi: 10.1038/35102574.

Jefferis GS, Potter CJ, Chan AM, Marin EC, Rohlfing T, Maurer CR, Maurer CR Jnr, Luo L. 2007. Comprehensive maps of *Drosophila* higher olfactory centers: spatially segregated fruit and pheromone representation. *Cell* **128**:1187–1203. doi: 10.1016/j.cell.2007.01.040.

Keene AC, Stratmann M, Keller A, Perrat PN, Vosshall LB, Waddell S. 2004. Diverse odor-conditioned memories require uniquely timed dorsal paired medial neuron output. *Neuron* **44**:521–533. doi: 10.1016/j.neuron.2004.10.006.

Knaden M, Strutz A, Ahsan J, Sachse S, Hansson BS. 2012. Spatial representation of odorant valence in an insect brain. *Cell Reports* **1**:392–399. doi: 10.1016/j.celrep.2012.03.002.

Kohl J, Ostrovsky AD, Frechter S, Jefferis GS. 2013. A bidirectional circuit switch reroutes pheromone signals in male and female brains. *Cell* **155**:1610–1623. doi: 10.1016/j.cell.2013.11.025.

Lai SL, Awasaki T, Ito K, Lee T. 2008. Clonal analysis of *Drosophila* antennal lobe neurons: diverse neuronal architectures in the lateral neuroblast lineage. *Development* **135**:2883–2893. doi: 10.1242/dev.024380.

Laissue PP, Reiter C, Hiesinger PR, Halter S, Fischbach KF, Stocker RF. 1999. Three-dimensional reconstruction of the antennal lobe in *Drosophila melanogaster*. *The Journal of Comparative Neurology* **405**:543–552. doi: 10.1002/(SICI)1096-9861(19990322)405.

Larsson MC, Domingos AI, Jones WD, Chiappe ME, Amrein H, Vosshall LB. 2004. *Or83b* encodes a broadly expressed odorant receptor essential for *Drosophila* olfaction. *Neuron* **43**:703–714. doi: 10.1016/j.neuron.2004.08.019.

Lee DD, Seung HS. 1999. Learning the parts of objects by non-negative matrix factorization. *Nature* **401**:788–791. doi: 10.1038/44565.

Liang L, Li Y, Potter CJ, Yizhar O, Deisseroth K, Tsien RW, Luo L. 2013. GABAergic projection neurons route selective olfactory inputs to specific higher-order neurons. *Neuron* **79**:917–931. doi: 10.1016/j.neuron.2013.06.014.

Livingstone M, Hubel D. 1988. Segregation of form, color, movement, and depth: anatomy, physiology, and perception. *Science* **240**:740–749. doi: 10.1126/science.3283936.

Magee RJ, Kosaric N. 1987. The Microbial production of 2,3-butanediol. *Advances in Applied Microbiology* **32**:89–161. doi: 10.1016/S0065-2164(08)70079-0.

Manni E, Petrosini L. 2004. A century of cerebellar somatotopy: a debated representation. *Nature Reviews. Neuroscience* **5**:241–249. doi: 10.1038/nrn1347.

Marin EC, Jefferis GS, Komiyama T, Zhu H, Luo L. 2002. Representation of the glomerular olfactory map in the *Drosophila* brain. *Cell* **109**:243–255. doi: 10.1016/S0092-8674(02)00700-6.

Min S, Ai M, Shin SA, Suh GSB. 2013. Dedicated olfactory neurons mediating attraction behavior to ammonia and amines in *Drosophila*. *Proceedings of the National Academy of Sciences of USA* **110**:E1321–E1329. doi: 10.1073/pnas.1215680110.

Murthy M, Fiete I, Laurent G. 2008. Testing odor response stereotypy in the *Drosophila* mushroom body. *Neuron* **59**:1009–1023. doi: 10.1016/j.neuron.2008.07.040.

Nakai J, Ohkura M, Imoto K. 2001. A high signal-to-noise Ca(2+) probe composed of a single green fluorescent protein. *Nature Biotechnology* **19**:137–141. doi: 10.1038/84397.

Nassi JJ, Callaway EM. 2009. Parallel processing strategies of the primate visual system. *Nature Reviews. Neuroscience* **10**:360–372. doi: 10.1038/nrn2619.

Okada R, Awasaki T, Ito K. 2009. Gamma-aminobutyric acid (GABA)-mediated neural connections in the *Drosophila* antennal lobe. *The Journal of Comparative Neurology* **514**:74–91. doi: 10.1002/cne.21971.

Parnas M, Lin AC, Huetteroth W, Miesenböck G. 2013. Odor discrimination in *Drosophila*: from neural population codes to behavior. *Neuron* **79**:932–944. doi: 10.1016/j.neuron.2013.08.006.

Pasternak T, Greenlee MW. 2005. Working memory in primate sensory systems. *Nature Reviews. Neuroscience* **6**:97–107. doi: 10.1038/nrn1603.
Patterson GH, Lippincott-Schwartz J. 2002. A photoactivatable GFP for selective photolabeling of proteins and cells. *Science* **297**:1873–1877. doi: 10.1126/science.1074952.
Reidl J, Starke J, Omer DB, Grinvald A, Spors H. 2007. Independent component analysis of high-resolution imaging data identifies distinct functional domains. *Neuroimage* **34**:94–108. doi: 10.1016/j.neuroimage.2006.08.031.
Roussel E, Carcaud J, Combe M, Giurfa M, Sandoz JC. 2014. Olfactory coding in the honeybee lateral horn. *Current Biology* **24**:561–567. doi: 10.1016/j.cub.2014.01.063.
Ruta V, Datta SR, Vasconcelos ML, Freeland J, Looger LL, Axel R. 2010. A dimorphic pheromone circuit in *Drosophila* from sensory input to descending output. *Nature* **468**:686–690. doi: 10.1038/nature09554.
Rybak J, Kuß A, Hans L, Zachow S, Hege HC, Lienhard M, Singer J, Neubert K, Menzel R. 2010. The digital bee brain: integrating and managing neurons in a common 3D reference system. *Frontiers in Systems Neuroscience* **4**:30. doi: 10.3389/fnsys.2010.00030.
Sanes JR, Zipursky SL. 2010. Design principles of insect and vertebrate visual systems. *Neuron* **66**:15–36. doi: 10.1016/j.neuron.2010.01.018.
Semmelhack JL, Wang JW. 2009. Select *Drosophila* glomeruli mediate innate olfactory attraction and aversion. *Nature* **459**:218–223. doi: 10.1038/nature07983.
Shang Y, Claridge-Chang A, Sjulson L, Pypaert M, Miesenböck G. 2007. Excitatory local circuits and their implications for olfactory processing in the fly antennal lobe. *Cell* **128**:601–612. doi: 10.1016/j.cell.2006.12.034.
Silbering AF, Okada R, Ito K, Galizia CG. 2008. Olfactory information processing in the *Drosophila* antennal lobe: anything goes? *The Journal of Neuroscience* **28**:13075–13087. doi: 10.1523/jneurosci.2973-08.2008.
Steck K, Veit D, Grandy R, Badia SBi, Mathews Z, Verschure P, Hansson BS, Knaden M. 2012. A high-throughput behavioral paradigm for *Drosophila* olfaction - the Flywalk. *Scientific Reports* **2**:361. doi: 10.1038/srep00361.
Stensmyr MC, Dweck HK, Farhan A, Ibba I, Strutz A, Mukunda L, Linz J, Grabe V, Steck K, Lavista-Llanos S, Wicher D, Sachse S, Knaden M, Becher PG, Seki Y, Hansson BS. 2012. A conserved dedicated olfactory circuit for detecting harmful microbes in *Drosophila*. *Cell* **151**:1345–1357. doi: 10.1016/j.cell.2012.09.046.
Stocker RF, Heimbeck G, Gendre N, de Belle JS. 1997. Neuroblast ablation in *Drosophila* P[GAL4] lines reveals origins of olfactory interneurons. *Journal of Neurobiology* **32**:443–456. doi: 10.1002/(SICI)1097-4695(199705)32.
Stocker RF, Lienhard MC, Borst A, Fischbach KF. 1990. Neuronal architecture of the antennal lobe in *Drosophila melanogaster*. *Cell and Tissue Research* **262**:9–34. doi: 10.1007/BF00327741.
Stökl J, Strutz A, Dafni A, Svatos A, Doubsky J, Knaden M, Sachse S, Hansson BS, Stensmyr MC. 2010. A deceptive pollination system targeting Drosophilids through olfactory mimicry of yeast. *Current Biology* **20**:1846–1852. doi: 10.1016/j.cub.2010.09.033.
Strutz A, Voeller T, Riemensperger T, Fiala A, Sachse S. 2012. Calcium imaging of neural activity in the olfactory system of *Drosophila*. In: Martin JR, editor. *Genetically encoded functional indicators*. New York, USA: Springer Science+Business Media, LLC. p. 43–70. doi: 10.1007/978-1-62703-014-4_3.
Tanaka NK, Awasaki T, Shimada T, Ito K. 2004. Integration of chemosensory pathways in the *Drosophila* second-order olfactory centers. *Current Biology* **14**:449–457. doi: 10.1016/j.cub.2004.03.006.
Tian L, Hires SA, Mao T, Huber D, Chiappe ME, Chalasani SH, Petreanu L, Akerboom J, McKinney SA, Schreiter ER, Bargmann CI, Jayaraman V, Svoboda K, Looger LL. 2009. Imaging neural activity in worms, flies and mice with improved GCaMP calcium indicators. *Nature Methods* **6**:875–881. doi: 10.1038/nmeth.1398.
Tully T, Quinn WG. 1985. Classical conditioning and retention in normal and mutant *Drosophila melanogaster*. *Journal of Comparative Physiology A, Sensory, Neural, and Behavioral Physiology* **157**:263–277. doi: 10.1007/BF01350033.
Vosshall LB, Stocker RF. 2007. Molecular architecture of smell and taste in *Drosophila*. *Annual Review of Neuroscience* **30**:505–533. doi: 10.1146/annurev.neuro.30.051606.094306.
Vosshall LB, Wong AM, Axel R. 2000. An olfactory sensory map in the fly brain. *Cell* **102**:147–159. doi: 10.1016/S0092-8674(00)00021-0.
Wang JW, Wong AM, Flores J, Vosshall LB, Axel R. 2003a. Two-photon calcium imaging reveals an odor-evoked map of activity in the fly brain. *Cell* **112**:271–282. doi: 10.1016/S0092-8674(03)00004-7.
Wang K, Gong J, Wang Q, Li H, Cheng Q, Liu Y, Zeng S, Wang Z. 2014. Parallel pathways convey olfactory information with opposite polarities in *Drosophila*. *Proceedings of the National Academy of Sciences of USA* **111**:3164–3169. doi: 10.1073/pnas.1317911111.
Wang Y, Chiang AS, Xia S, Kitamoto T, Tully T, Zhong Y. 2003b. Blockade of neurotransmission in *Drosophila* mushroom bodies impairs odor attraction, but not repulsion. *Current Biology* **13**:1900–1904. doi: 10.1016/j.cub.2003.10.003.
Wilson RI, Laurent G. 2005. Role of GABAergic inhibition in shaping odor-evoked spatiotemporal patterns in the *Drosophila* antennal lobe. *The Journal of Neuroscience* **25**:9069–9079. doi: 10.1523/JNEUROSCI.2070-05.2005.
Wilson RI, Mainen ZF. 2006. Early events in olfactory processing. *Annual Review of Neuroscience* **29**:163–201. doi: 10.1146/annurev.neuro.29.051605.112950.
Wilson RI, Turner GC, Laurent G. 2004. Transformation of olfactory representations in the *Drosophila* antennal lobe. *Science* **303**:366–370. doi: 10.1126/science.1090782.
Wong AM, Wang JW, Axel R. 2002. Spatial representation of the glomerular map in the *Drosophila* protocerebrum. *Cell* **109**:229–241. doi: 10.1016/S0092-8674(02)00707-9.

Figure Supplements

Supplementary Figure 1: Charactreization of excitatory and inhibitory projection neurons.

Overlap of ePNs (QUAS-tdTomato) and iPNs (UAS-GCaMP3.0) in the LH area. The circle indicates the posterior lateral region, which is sparsely innervated by iPNs and dominated by ePN axonal terminal fields. Scale bar, 20 µm.

Supplementary Figure 2: Glomerular innervations of ePNs an iPNs

(**A**) Representative *in vivo* images of glomerular innervations. MZ699 and GH146 lines have been reconstructed with END1-2 background (two upper planes) and dual labeling via the Q-system and the GAL4-UAS expression system (lowest plane). Scale bar, 20 µm. (**B**) Detailed glomerular AL innervation. Green filled cells indicate innervation by MZ699-GAL4, magenta GH146-GAL4 innervation, respectively and grey, no innervation by the indicated line. Bottom rows, total number of innervated glomeruli with percentage share indicated below. Merge column: white filled with “x” indicates glomeruli innervated by both lines, grey only one line. Blue filled rows are glomeruli labeled by none of the enhancer trap lines.

Supplementary Figure 3: Odor-evoked activity patterns in the LH are reproducible and stereotypic

Odor-evoked Ca^{2+} responses (ΔF/F %) in the LH for the three odors acetoin acetate, balsamic vinegar and benzaldehyde in four animals are shown as false-color coded images. Two measurements in each animal are given to reveal that the activity patterns are highly reproducible within one animal. Comparison between the patterns among individuals shows that the activity regions are stereotypic. Numbers in the lower right corner indicate individual maxima. The ΔF/F scale bar is shown at the bottom.

Supplementary Figure 4: Odor-evoked activity patterns in the LH can be reconstructed with five components

Above, Odor-evoked Ca^{2+} responses (ΔF/F %) in the LH for the three odors acetic acid, balsamic vinegar and 1-octen-3-ol in three animals are shown as false-color

coded images. The ΔF/F scale bar is shown at the bottom. *Middle*, activity patterns were reconstructed using NNMF with five components. *Below*, residue of the pattern reconstructions with five components (as shown in the middle panel) revealing that no stimulus related activity remained.

Supplementary Figure 5: Odor-evoked activity patterns in the LH cluster into three components

Hierarchical clustering (UMPGA) of the odor response spectra of the NNMF components with a reliable stimulus response (trial-to-trial correlation >0.7, i.e. 28 out of 35 components in 7 animals). The response spectra segregate into three distinct clusters according to their stimulus response spectra. The corresponding response areas (left pictures) are located in similar regions of the LH.

Supplementary Figure 6: iPNs can be morphologically segregated according to their target and input region

(**A**) Principal component analysis based on the distances of the similarity scores of all terminal points of each individual iPN in the LH (for details see Material and Methods). LH-AM iPNs (blue) and LH-PM iPNs (green) form significantly distinct clusters (***p<0.001, One-Way ANOSIM, Bray-Curtis). (**B**) Principal component analysis based on the glomerular innervations of each individual iPN in the AL. Again, LH-AM iPNs (blue) and LH-PM iPNs (green) form significantly distinct clusters (***p<0.001, One-Way ANOSIM, Bray-Curtis).

Supplementary Figure 7: Glomerular innervations of individual iPNs

Binary innervation patterns of 25 individually labeled MZ699+ iPNs using PA-GFP. Columns represent innervation patterns of individual neurons which have been grouped according to their innervation properties; rows represent 51 glomeruli in the AL along with the innervation in the specific odor response domains in the LH (LH-PM, LH-AM) and/or the mushroom body calyx (MBc). Glomeruli have been sorted according to their iPN innervation. Grey, innervated; white, not innervated.

Supplementary Figure 8: Odor valences determined with three different behavioral assays

Odor-evoked behavioral responses of wild type flies for the 14 odors used in this study determined by T-maze assay, trap assay and the FlyWalk. The color denotes an attractive (green), aversive (red) or a neutral (light yellow) behavioral response. N/T, not tested. The majority of odors yielded similar results independent of the

behavioral assay used. In a few cases an attractive odor evoked a neutral response (i.e. no response), but never induced an aversive response in another assay.

Supplementary Figure 9: Calcium responses of OSNs

(**A**) Representative glomerular Ca^{2+}-responses of OSNs in the AL for a subset of odorants at three concentrations. Scale bar to the right. Control (mineral oil) recordings are shown additionally as full false-color coded images. (**B**) Glomerular AL atlas used for glomerular identification. (**C**) Median Ca^{2+}-activity traces of all glomeruli for all odorants at the three indicated concentrations. Scale bar and control measurement in the center. Odor application is indicated by the grey bar below the heatmaps (n=6-7).

Supplementary Figure 10: Correlation matrices for odor-evoked responses in the AL and LH

Complete correlation matrices for calcium activity patterns of OSNs in the AL (left) and iPNs in the LH (right). The odors are arranged according to single linkage clustering of the AL activity patterns. Heatmap color-code refers to the correlation distance scale bar below each matrix. Odor letters are color-coded according to hedonic valence; 10^{-6} RI values are labeled in grey (complete list right hand).

Strutz et al.
Figure 1 - Figure Supplement 1

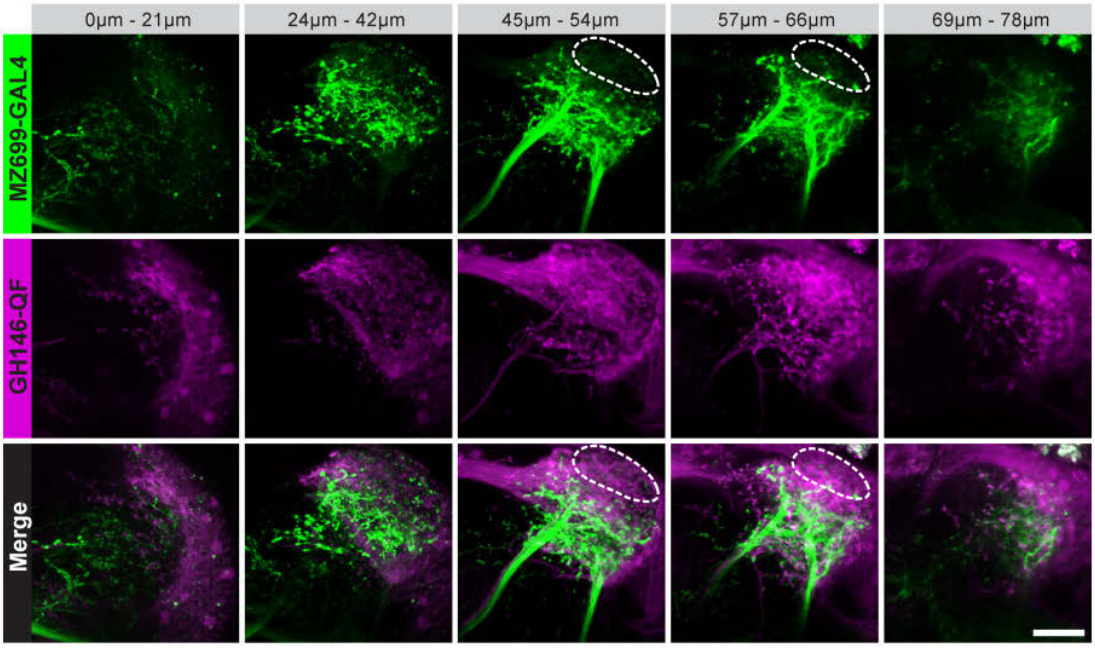

Strutz et al.
Figure 1 - Figure Supplement 2

A *In vivo* double labelings

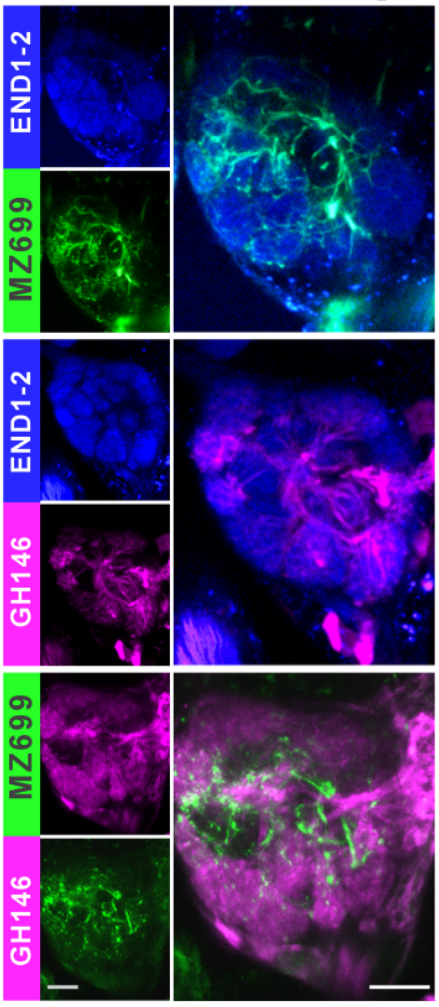

B

Glomerulus	MZ699	GH146	Merge
D			X
DA1			X
DA2			X
DA3			
DA4l			X
DA4m			
DC1			X
DC2			X
DC3			X
DC4			
DL1			
DL2d			
DL2v			
DL3			
DL4			X
DL5			
DM1			
DM2			X
DM3			X
DM4			X
DM5			X
DM6			X
DP1l			
DP1m			X
V			
VA1d			X
VA1v			X
VA2			X
VA3			X
VA4			
VA5			X
VA6			X
VA7l			X
VA7m			X
VC1			X
VC2			
VC3			
VC4			
VC5			
VL1			
VL2p			
VL2a			X
VM1			
VM2			X
VM3			X
VM4			
VM5d			
VM5v			
VM7d			X
VM7v			X
VP1			
VP4			
52	**40**	**37**	**28**
	76.92 %	**71.15 %**	**53.85 %**

Strutz et al.
Figure 2 - Figure Supplement 1

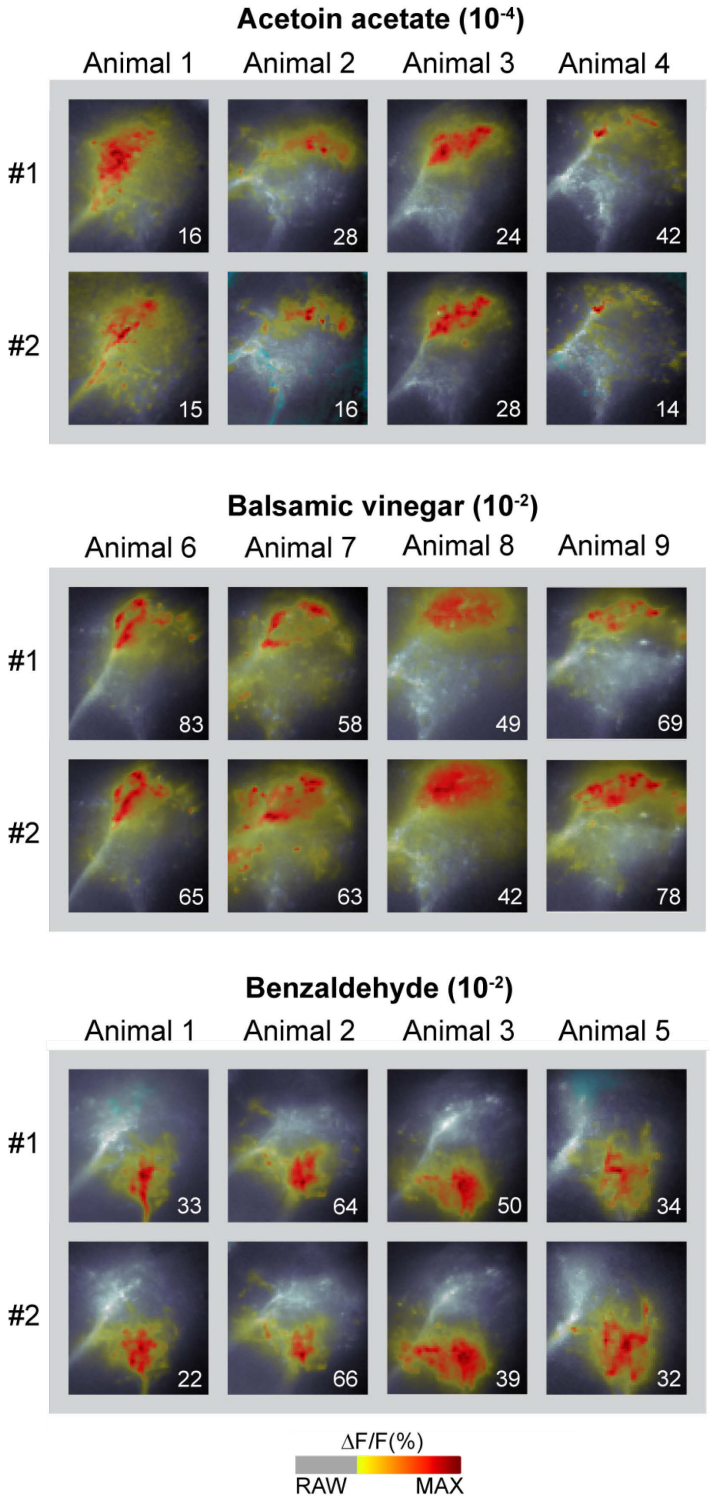

Strutz et al.
Figure 2 - Figure Supplement 2

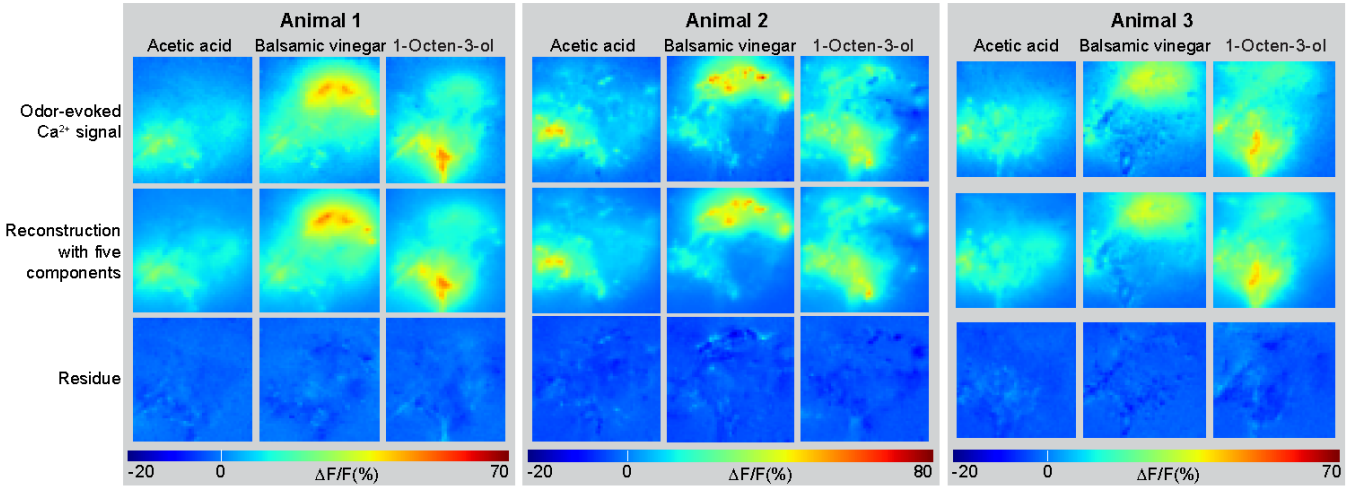

Strutz et al.
Figure 2 - Figure Supplement 3

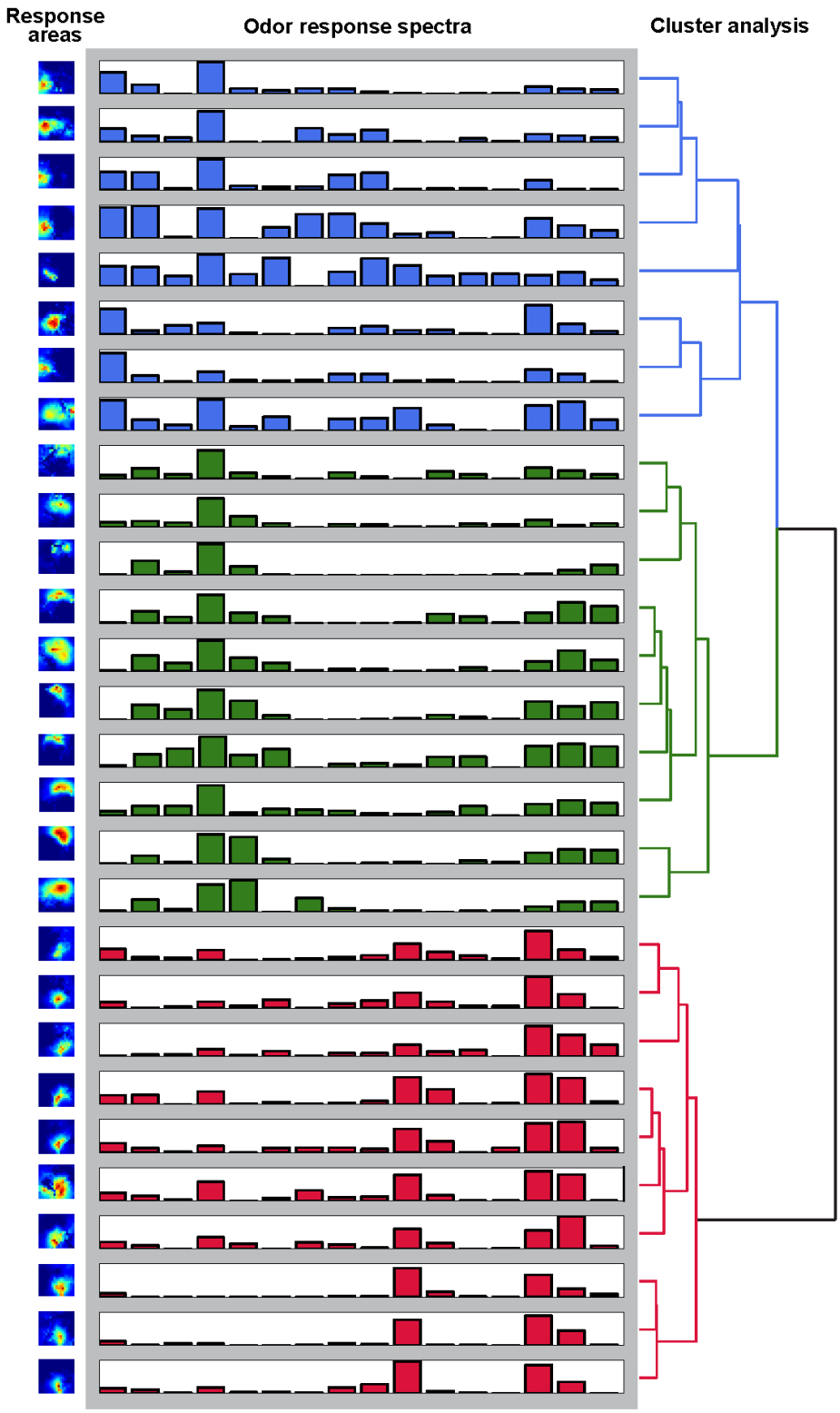

Strutz et al.
Figure 3 - Figure Supplement 1

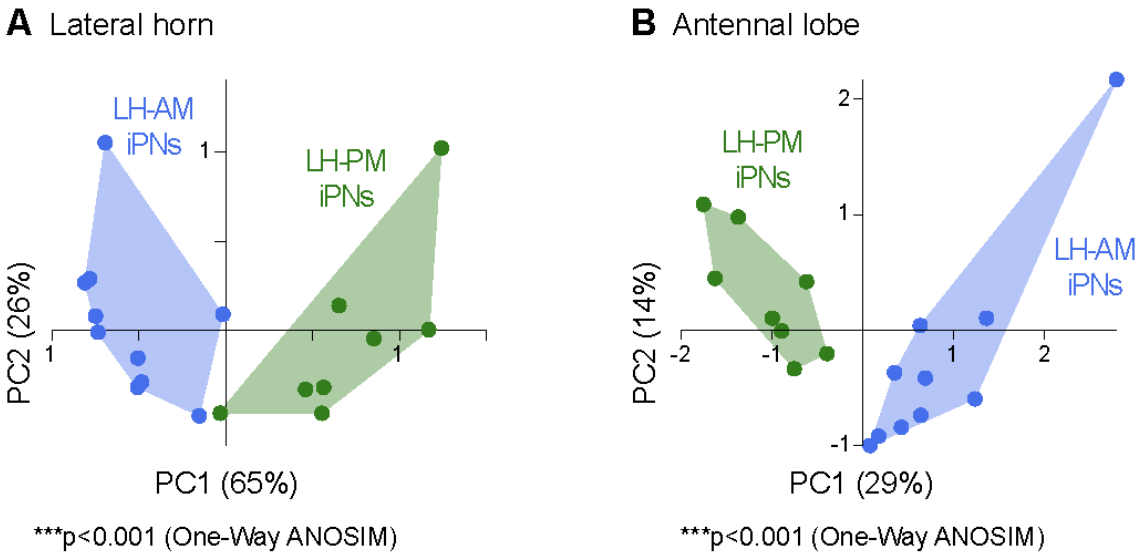

Strutz et al.
Figure 3 - Figure Supplement 2

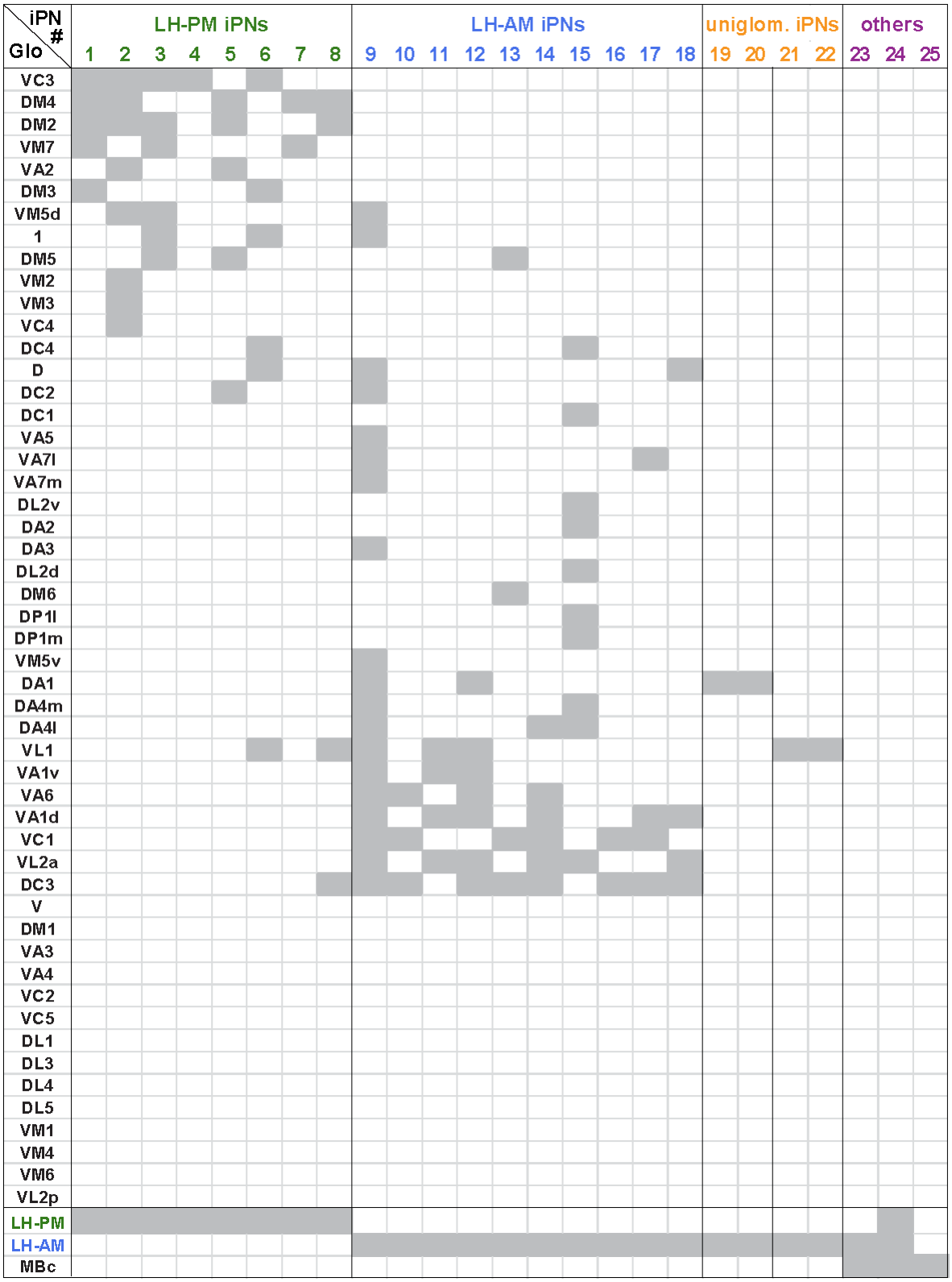

Strutz et al.
Figure 6 - Figure Supplement 1

Odor	T-maze	Trap assay	Fly Walk
Methyl salicylate			
Linalool			
Acetophenone			
1-Octen-3-ol			
Benzaldyhde			
Phenylacetic acid		N/T	N/T
cis-Vaccenyl acetate		N/T	
2-Phenylacetic acid			N/T
Acetic acid			N/T
2,3 Butanedione			
Propionic acid			N/T
γ-Butyrolactone			N/T
Balsamic vinegar			
Acetoin acetate		N/T	N/T

attractive aversive neutral N/T not tested

Strutz et al.
Figure 6 - Figure Supplement 2

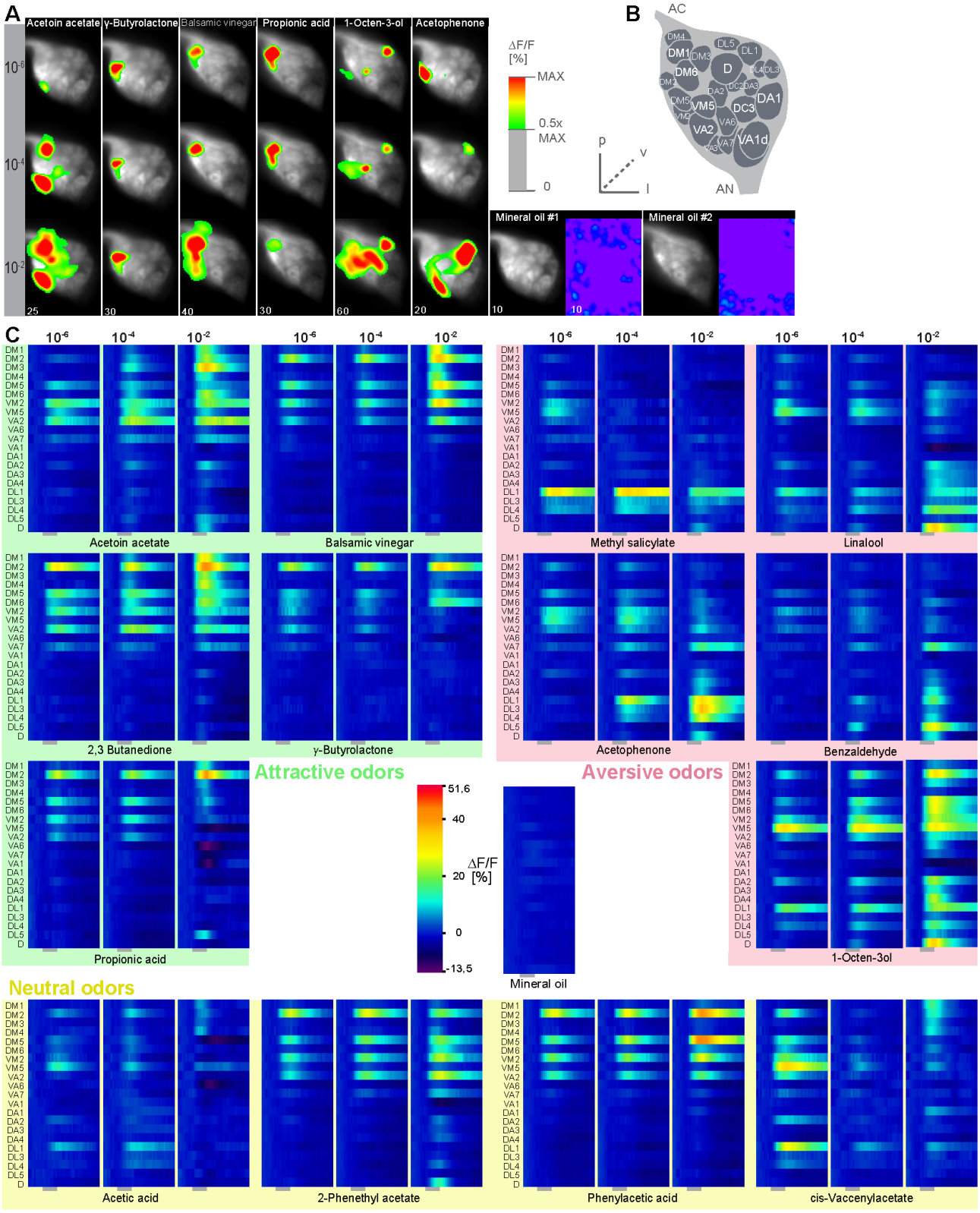

Strutz et al.
Figure 6 - Figure Supplement 3

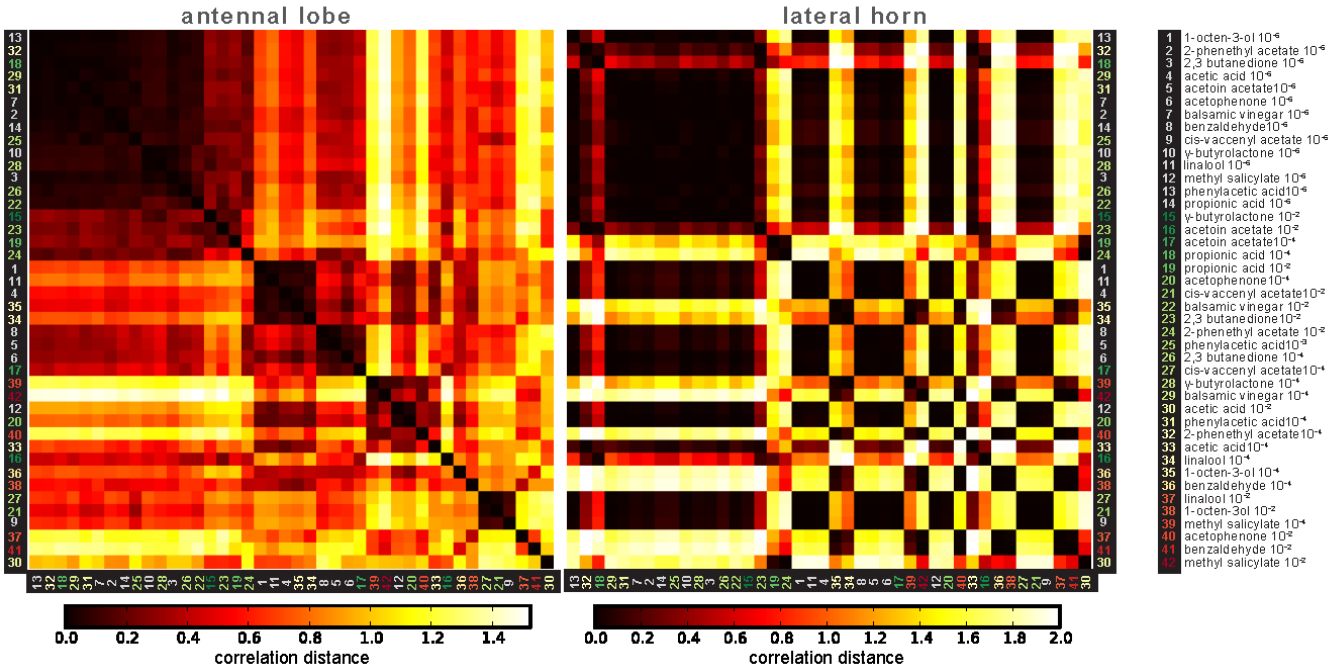

Manuscript IV

Love makes smell blind: mating suppresses pheromone attraction in Drosophila females via Or65a olfactory neurons

Sebastien Lébreton, Veit Grabe, Aman B. Omondi, Rickard Ignell, Paul G. Becher, Bill S. Hansson, Silke Sachse and Peter Witzgall

Published online in Scientific Reports, 19 November 2014

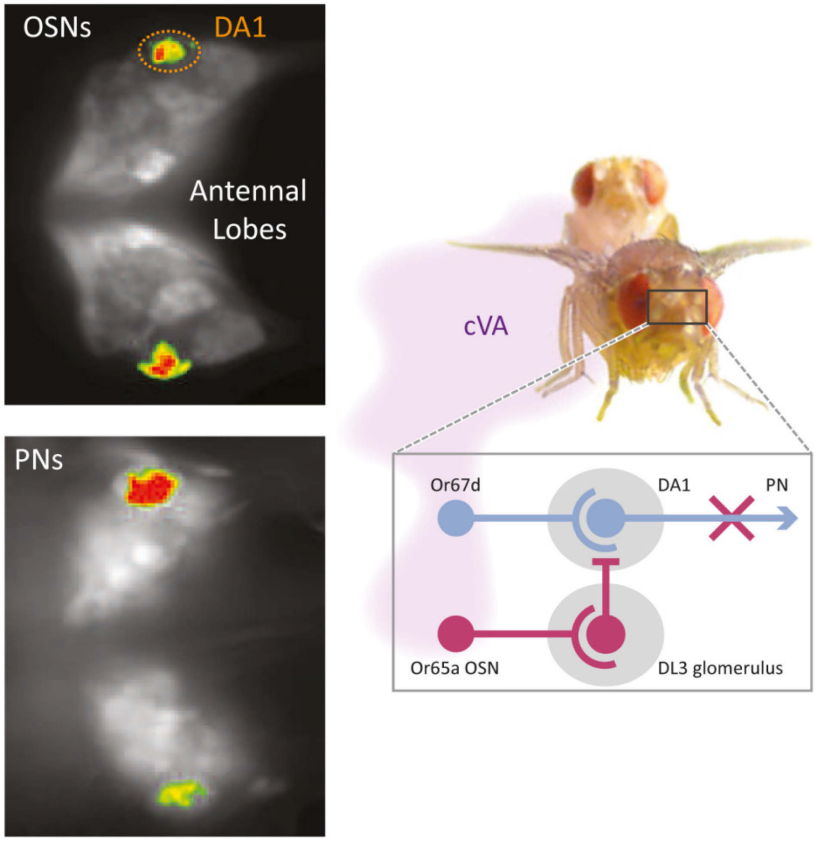

SCIENTIFIC REPORTS

OPEN

SUBJECT AREAS:
OLFACTORY RECEPTORS
BEHAVIOURAL ECOLOGY

Received
8 September 2014

Accepted
4 November 2014

Published
19 November 2014

Correspondence and requests for materials should be addressed to S.L. (sebastien.lebreton@slu.se)

* Bioversity International, Quartier INSS, Avenue d'Italie no 16, Bujumbura, Burundi.

Love makes smell blind: mating suppresses pheromone attraction in *Drosophila* females via Or65a olfactory neurons

Sébastien Lebreton[1,2], Veit Grabe[2], Aman B. Omondi[1]*, Rickard Ignell[1], Paul G. Becher[1], Bill S. Hansson[2], Silke Sachse[2] & Peter Witzgall[1]

[1]Swedish University of Agricultural Sciences, Department of Plant Protection Biology, Chemical Ecology Unit, 230 53 Alnarp, Sweden, [2]Department of Evolutionary Neuroethology, Max Planck Institute for Chemical Ecology, 07745 Jena, Germany.

In *Drosophila*, the male sex pheromone *cis*-vaccenyl acetate (cVA) elicits aggregation and courtship, through the odorant receptor Or67d. Long-lasting exposure to cVA suppresses male courtship, via a second channel, Or65a. In females, the role of Or65a has not been studied. We show that, shortly after mating, *Drosophila* females are no longer attracted to cVA and that activation of olfactory sensory neurons (OSNs) expressing Or65a generates this behavioral switch: when silencing Or65a, mated females remain responsive to cVA. Neurons expressing Or67d converge into the DA1 glomerulus in the antennal lobe, where they synapse onto projection neurons (PNs), that connect to higher neural circuits generating the attraction response to cVA. Functional imaging of these PNs shows that the DA1 glomerulus is inhibited by simultaneous activation of Or65a OSNs, which leads to a suppression of the attraction response to cVA. The behavioral role of postmating cVA exposure is substantiated by the observation that matings with starved males, which produce less cVA, do not alter the female response. Moreover, exposure to synthetic cVA abolishes attraction and decreases sexual receptivity in unmated females. Taken together, Or65a mediates an aversive effect of cVA and may accordingly regulate remating, through concurrent behavioral modulation in males and females.

Polyandry, females mating multiply with different males, leads to a gender conflict over optimum mating rates and remating intervals. Polyandry is widespread in *Drosophila* and other insects. Females mate more than once, since a single mating does not yield sufficient sperm to match their egg production capacity, whereas high mating rates decrease female fitness and lifetime. This gives rise to a sexual conflict, which mediates pre- and postcopulatory selection on female traits that influence optimum mating rates and remating intervals[1–4].

After mating, insect females undergo vital behavioral changes, regarding receptivity to further mating, feeding and egg laying[5–7]. In the fruit fly *D. melanogaster*, a single component of the seminal fluid, dubbed sex peptide (SP), has been shown to trigger the post-mating switch in female reproductive behavior[8–13]. After mating for the first time, SP increases female egg production, while multiple receipt of SP during consecutive matings reduces female lifetime and fecundity. On the other hand, SP transfer increases male fitness, since it delays remating in females and thus reduces male sperm competition[2,8,14–16].

Drosophila females become unreceptive immediately after mating. Two, partly overlapping components contribute to postmating physiological and behavioral changes, including the inhibition of remating: a short-lasting copulation effect and a long-lasting sperm effect, which is generated by seminal proteins including SP. The prolonged effect of insemination on female receptivity and egg production lasts several days, but becomes evident only several hours after mating. In contrast, the copulation effect persists only for about one day[14,17–19]. What triggers this immediate suppression of receptivity after mating is not known, but the male-produced sex pheromone *cis*-vaccenyl acetate (cVA) is a candidate stimulus, since it is transferred to the female via the ejaculate together with sperm[20].

cVA is a key compound regulating *Drosophila* social and sexual behaviors. It acts as an aggregation pheromone to attract males and females to feeding and mating sites[21], and elicits sex-specific courtship behaviors at close range[22–24]. On the fly antenna, cVA is detected by two odorant receptors, Or65a and Or67d, which are expressed in

different olfactory sensory neurons (OSNs)[22,25,26]. First- and second order olfactory neurons show identical pheromone responses in both sexes. Differences in male and female courtship behavior arise from dimorphic third-order circuits in the central brain[27], where neurons determined by the fruitless (*fru*) gene differentially couple sensory input to motor output in males and females[27–30], and where *doublesex* (*dsx*) neurons, which are responsive to cVA, regulate receptivity of unmated females to male courtship[31].

In males, cVA regulates courtship and aggression in a temporally differential manner: acutely, perception via Or67d elicits aggression and prevents courtship with other males[22,23]; chronically, perception via Or65a leads to a generalized suppression of aggression and courtship[20,32]. Or65a is not part of the *fru* circuit[28], yet it achieves a sex-specific effect on male courtship and aggression through lateral interaction with the Or67d channel[32]. This raises the question which behavioral consequences cVA mediates in females through Or65a. Since cVA increases female receptivity prior to, but not after mating, we investigated whether mating modulates the female response to cVA at the behavioral and neurophysiological level.

Results

Males inhibit female attraction to cVA after mating. cVA attraction was tested in a Y-tube olfactometer, where cVA was released in one arm at a constant rate. Test females were virgin, mated with fed males, or mated with males that had been starved during 3 d. Virgin females were attracted to cVA, but copulation with fed males abolished female attraction. In contrast, females that had been mated with starved males continued to be attracted to cVA (Figure 1).

Sex peptide does not modulate cVA attraction. Diverse mating-induced behavioral changes in *Drosophila* females, including reduced receptivity and increased oviposition, involve seminal fluid proteins[8,19,33]. Starvation has been shown to affect sperm-mediated traits[34] and may hence decrease copulation duration and sperm transfer, or even deteriorate sperm quality. However, we found no difference in copulation duration and reproductive success of starved and fed males (Figure 2A).

We then tested the hypothesis that sex peptide (SP) is involved in the termination of post-mating attraction to cVA. SP knockout

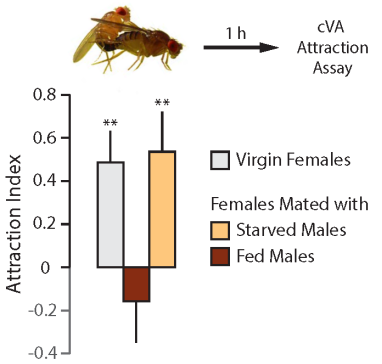

Figure 1 | Effect of mating on cVA attraction. Attraction of *D. melanogaster* females to cVA released at 15 ng/min in one arm of a y-tube olfactometer. Females were tested before mating, and 1 h after mating with fed males and starved males (n = 40, 27 and 20 respectively). The attraction index shows the time spent in the cVA arm of the olfactometer minus the time spent in the control arm divided by the total amount of time spent in both arms. Positive values indicate attraction to cVA whereas negative values show repellency. Asterisks indicate significant attraction (mean ± SEM, Wilcoxon test, ** $p < 0.01$). Photo by S. Lebreton.

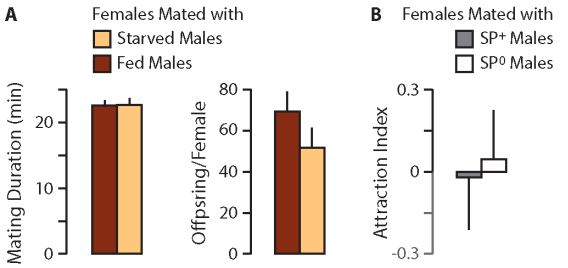

Figure 2 | Mating performance of fed and starved males and effect of SP on cVA attraction. (A) Copulation duration and offspring production of fed (n = 19) and starved males (n = 18). No difference was observed between fed and starved males (Mann-Whitney test). (B) Effect of SP on cVA attraction in mated females. Females were mated to virgin males lacking SP (SP^0) or control males producing SP (SP^+)(n = 27 for each). No effect of SP was observed. In both case females were not significantly attracted to cVA. Data are mean ± SEM.

males[2,8] were used to this purpose. However, SP did not account for changes in postmating cVA attraction in females, since cVA attraction was down-regulated in females mated with SP-deficient males as well as in females mated with control males producing SP (Figure 2B).

cVA exposure during mating abolishes postmating cVA attraction. We next asked whether cVA itself is the signal that shuts down postmating female attraction to cVA. During mating, males transfer cVA to females[21,35–37] and prolonged stimulation with cVA may ensue in behavioral modulation.

If olfactory exposure to cVA during mating causes the reduced female response, it would follow that starved males do not produce sufficient amounts of cVA to produce a female behavioral modulation. We employed chemical analysis to quantify cVA transfer during mating, showing (Figure 3A) that fed males transferred almost threefold more cVA to females during copulation than starved males. More cVA was extracted from females during 24 h than during 5 min (Figure 3A), which confirms that cVA is not only transferred onto the female cuticle, but also via the ejaculate into the genital tract[20,38].

cVA on the female cuticle is known to be detected by other males and to suppress further courtship[20,24,39]. Obviously, cVA is detected also by the female fly itself, since females carry odorant receptors (Ors) selectively tuned to cVA[26], while the behavioral consequences have not been investigated. Since fed males transfer more cVA during mating than starved males, it is conceivable that females are exposed to a higher amount of cVA during copulation with fed males.

We therefore tested the effect of exposure to synthetic cVA on subsequent attraction of virgin females to cVA. Pre-exposure to a filter paper loaded with 300 ng cVA, corresponding to the amount of cVA transferred by starved males, did not have an effect on unmated females; whereas exposure to 600 ng, corresponding to the amount of cVA transferred by fed males, abolished attraction of unmated females to cVA (Figures 3A, B). The attraction response of virgin females, following olfactory exposure to a low and high dose of synthetic cVA, matched the behavior observed in females mated with starved and fed males, respectively (Figure 1).

In unmated females, cVA promotes sexual receptivity[22]. The abolished attraction response led thus to the question whether cVA pre-exposure also has an effect on female mating behavior. Exposure of unmated females to 600 ng and 1.200 ng synthetic cVA significantly reduced their receptivity to male courtship (Figure 3C), showing that exposure of females to cVA leads to a reduction of mating.

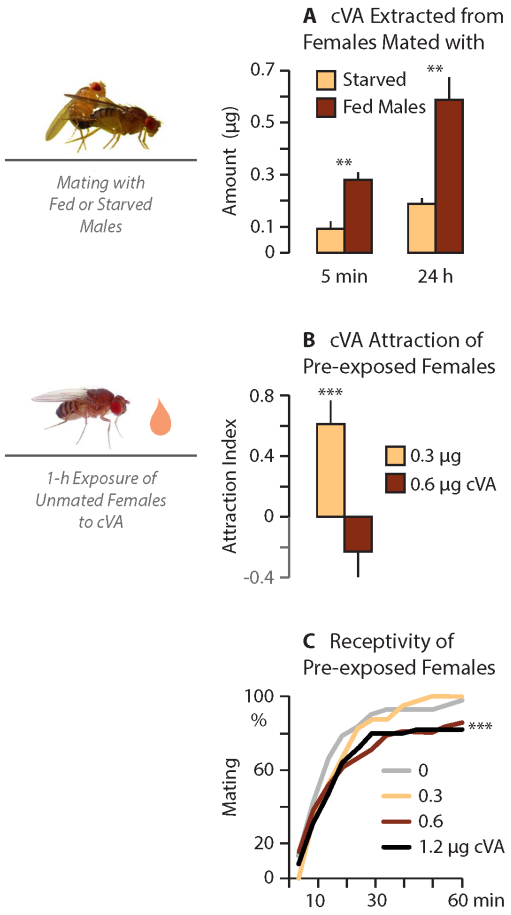

Figure 3 | Effect of cVA exposure, during mating or to synthetic cVA, on subsequent cVA attraction and female receptivity. (A) Amount of cVA extracted from females after mating with fed (n = 8) and starved males (n = 6). Single females were dropped in hexane, immediately after mating, and extracted during 5 min or 24 h. Amounts found on females mated with fed and starved males were analyzed with a Mann-Whitney test (** $p < 0.01$). (B) Virgin females were exposed to 0.3 or 0.6 µg of synthetic cVA during 1 h and then tested for cVA attraction. Asterisks above bars indicate significant attraction (Wilcoxon test, *** $p < 0.001$; data are mean ± SEM). (C) Receptivity of unmated females. Females were exposed to 0 (hexane), 0.3, 0.6 or 1.2 µg of cVA (n = 44, 40, 43 and 41, respectively) during 1 h, before they came in contact with a random virgin fed male during 1 h. Data were analyzed using a Mixed-effect model followed by a multiple comparison test (for details see *SI Material and Methods*, *** $p < 0.001$). Photos by S. Lebreton.

Mating reduces DA1 activity through activation of Or65a and suppresses cVA attraction. Olfactory input from Or67d-expressing olfactory sensory neurons (OSNs) is relayed, via the DA1 glomerulus in the AL, to a sexually dimorphic circuit in the lateral horn of the protocerebrum, which accounts for sex-specific behaviors to cVA[27,40]. In *Drosophila* males, acute stimulation of Or67d OSNs by cVA enhances aggression, whereas prolonged stimulation of neurons expressing Or65a, a receptor known to respond to large amount of cVA, down-regulates aggression and suppresses male courtship[20,23,32]. Recently, it has been shown that perception of cVA via Or65a OSNs activates a network of local interneurons (LNs) in the AL, which is thought to regulate the male behavioral response to cVA stimulus input via Or67d[32]. We therefore investigated the role of the Or65a and Or67d olfactory channels with respect to the cVA-induced response modulation in *Drosophila* females.

We first examined whether mating changes the sensitivity of Or67d OSNs in T1 sensilla on the female antenna, using single sensillum recordings. However, the response of Or67d OSNs to cVA did not change after mating (Figure 4A, B). Consequently, inhibition of cVA attraction cannot be attributed to a peripheral modulation at the OSN level.

Next, using transgenic flies expressing the calcium sensor GCaMP specifically in OSNs (*Orco-Gal4* driver) or PNs (*GH146-Gal4* driver), we recorded the activity of the DA1 glomerulus in response to cVA. At the presynaptic level (OSNs), the response to cVA was not affected (Figure 4C), whereas at the postsynaptic level (PNs), the response to cVA decreased significantly after mating (Figure 4D). This down-regulation of the DA1 output signal is consistent with the observed change in cVA attraction after mating (Figure 1). Moreover, processing of the cVA signal in the AL lends support to the idea that lateral interaction between Or67d and Or65a olfactory channels modulates the response to cVA not only in males[32], but also in females.

In order to confirm that cVA exposure during mating suppresses further cVA attraction and that Or65a is involved, we targeted the expression of tetanus toxin light chain (TeTxLC tnt) to Or65a neurons, using two independent lines. TeTxLC blocks synaptic transmission by preventing neurotransmitter release and therefore suppresses any response from neurons in which it is expressed[41]. After mating, females expressing TeTxLC in Or65a OSNs remained to be attracted to cVA. This was not the case when an inactive form of TeTxLC (TeTxLC (−)) was expressed (Figure 4E), showing that input from Or65a OSNs is required to suppress cVA attraction after mating. Moreover, our results confirm that Or65a neurons are not needed for cVA attraction *per se*.

Discussion

Our study brings new insights into how postmating behavior in *Drosophila* females is regulated by the male-produced sex pheromone cVA. We show, for the first time, that chronic exposure to cVA abolishes attraction of females to cVA and that it reduces receptivity to male courtship (Figures 1, 3).

The response to cVA is mediated via the same odorant receptors in both sexes: acute input via Or67d triggers direct responses, male-male aggression and attraction of females to males, respectively[22,23]; prolonged exposure via Or65a generates a response inhibition in males[20,32], as well as in females (Figures 3, 4). A behavioral role of the Or65a channel in *Drosophila* females has not yet been described.

We show that exposure of females to cVA during mating activates Or65a OSNs, and reduces the activity of the DA1 glomerulus receiving simultaneous input from Or67d OSNs (Figure 4C, D), which leads to a suppression of the female behavioral response to cVA following mating. Flies in which Or65a is silenced continue to be attracted to cVA even after mating (Figure 4E)

Or65a, which is not part of the fruitless circuit[28], elicits nonetheless a gender-specific behavioral response. Or67d and Or65a OSNs converge in the adjacent DA1 and DL3 glomeruli, respectively[42] and it has been suggested that the fine-tuning of male-to-male aggression response involves LNs that interconnect these two glomeruli[32]. We therefore propose that Or65a modulates the sex-specific Or67d olfactory channel[27] through local circuits also in female flies (Figure 4F).

PN activity in DA1 is decreased in mated females, as shown by calcium imaging (Figure 4C, D). Most LNs in the AL are GABAergic and therefore inhibitory[43] and GABAergic LNs are responsible for olfactory habituation[44]. It has been established that the activity of DA1 is modulated by activation of $GABA_B$ receptors, which are

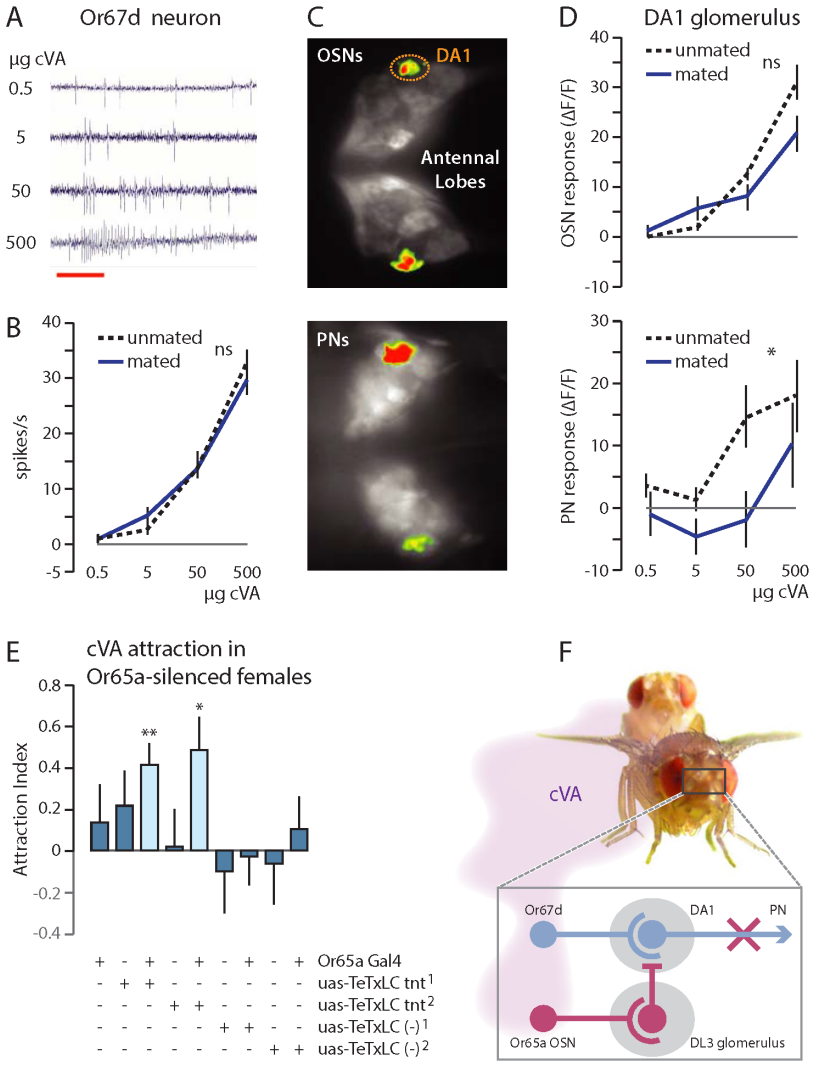

Figure 4 | **Mating decreases DA1 activity and requires Or65a OSNs to suppress cVA attraction.** (A and B) Or67d OSN response to different amounts of cVA. (A) Spike trains in response to cVA (red bar shows stimulus duration) recorded from unmated females and (B) comparison between virgin and mated females (n = 10 for each). (C and D) Calcium imaging during cVA application in the DA1 glomerulus at the presynaptic (OSNs) and postsynaptic (PNs) level. (C) Representative false color-coded images showing the antennal lobe after stimulation with cVA in OSNs and PNs in unmated females. (D) Comparison of DA1 calcium activity in virgin (ORNs, n = 6; PNs, n = 9) and mated (ORNs, n = 7; PNs, n = 5) females elicited by cVA. Asterisks show significant differences between virgin and mated females (GLMM). (E) Effect of blocking Or65a OSN response on cVA attraction of mated females (n = 20 to 28). Tetanus toxin light chain (TeTxLC) was expressed in Or65a OSNs, using two independent lines (TeTxLC tnt^1 and TeTxLC tnt^2). As a negative control an inactive form of TeTxLC was expressed (TeTxLC (−)^1 and TeTcLC (−)^2). Asterisks above bars indicate significant attraction (Wilcoxon test, * $p < 0.05$, ** $p < 0.01$). Data are mean ± SEM. (F) Proposed mechanism underlying the suppression of cVA attraction in females after mating. During mating, females are exposed to high amounts of cVA, which activates Or65a neurons. Or65a OSNs decrease the activity of DA1 glomerulus, probably via LNs. Decreased DA1 activity results in an inhibition of cVA attraction. Photo by S. Lebreton.

expressed in OSNs projecting to DA1, and the particularly high level of presynaptic inhibition in OSNs projecting to DA1[45] underlines the importance of gain control in pheromone detection and behavior.

The *Drosophila* SP has a long-term effect on female receptivity[8,14,19], but a suppression of female receptivity during the first few hours following copulation cannot be attributed to SP[17,18]. Males transfer large amount of cVA to the females during mating, which consequently repels other males[35,36,38]. Here we show that the transfer of cVA elicits, in addition, the female short-term postmating response (Figure 3), well before SP induces long-term effects.

Polyandry in *Drosophila* drives pre- and postcopulatory sexual selection of female and male reproductive behaviour. Although is adaptive for females to mate more than once, multiple matings comprise a fitness cost[14,16,46–49]. However, females traits, including the sensory perception of male fecundity, are understudied in comparison with male traits, such as seminal fluid proteins[49–51].

One element of *Drosophila* polyandry is that multiple matings diminish male fertility, probably due to sperm depletion[43,52], which is congruent with the finding that females, after mating with recently mated males, show less pronounced postmating behavioral changes[53,54]. Shortly after mating with fed males, female receptivity decreases[8] and abolished attraction to cVA prevents exposure to courting males at aggregation sites, from where cVA is being released in substantial amounts (Figures 1, 3)[21]. In contrast, matings with starved males, or exposure to smaller amounts of cVA, do not abolish attraction to cVA (Figures 1, 3).

Since high amounts of cVA are being transferred during first matings, it is conceivable that males transfer less cVA during subsequent matings, reflecting their reduced fecundity. The amount of cVA transferred may thus allow females to detect male mating status and to adjust sexual receptivity and remating rate accordingly.

Sexual selection is partitioned into male-male competition and female mate choice[55]. The Or65a olfactory channel, mediating the long-term effect of cVA exposure, is subject to sexual selection in *Drosophila* males and females. Or65a functions in both sexes to reinforce the effect of cVA on male competitors, through suppression of courtship in males[20], and through reduced cVA attraction and receptivity in females (Figures 3, 4). In addition, cVA input through Or65a regulates remating in females as a function of the amount of cVA transferred by males, reflecting male quality (Figures 1, 3). The Or65a channel modulates accordingly polyandry in *Drosophila*.

Methods

Additional methods are provided in *SI Material and Methods*.

Fly stocks, crossings and rearing conditions. The Dalby strain of the fruit fly *Drosophila melanogaster* was used as a wild-type strain[56]. Optical imaging was performed using a transgenic fly line labeled in OSNs *Orco-GAL4; END1-2,UAS-GC3.0; TM2/TM6B* or labeled in PNs *yw; GH146-GAL4, UAS-GCaMP-3.0/CyO; TM2/TM6B*. The role of sex-peptide (SP) was assessed by using males lacking SP (SP^0) and control males producing SP (SP^+)[2]. SP^0 males were obtained by crossing SP^0/*TM3,Sb,ry* males to *Δ130/TM3,Sb,ry* females. Control males were produced by crossing SP^0,SP^+/*TM3,Sb,ry* males to *Δ130/TM3,Sb,ry* females, resulting in SP^0,SP^+/*Δ130* (SP^+) males. SP^0/*TM3,Sb,ry*, SP^0,SP^+/*TM3,Sb,ry* and *Δ130/TM3,Sb,ry* lines were obtained from Claudia Fricke (University of East Anglia). To silence Or65a OSNs, we expressed a light chain of the tetanus toxin (TeTxLC) in these neurons using the UAS-GAL4 system. For that purpose, two *UAS-TeTxLC tnt* strains (Bloomington stock 28838 and 28997, respectively referred as 1 and 2 in this article) were crossed with a *Or65a-GAL4* line (Bloomington stock 9994). Control experiments were done by expressing an inactive form of TeTxLC (*UAS-TeTxLC (−)*) using two independent strains (Bloomington stock 28840 and 28841, respectively referred as 1 and 2).

Flies were reared on a standard sugar-yeast-cornmeal medium diet at room temperature (19–22°C) and under a 10 : 14 h L : D photoperiod. For optical imaging experiments, flies were reared at 25°C. Newly emerged flies were anesthetized under CO_2 and sexed under a microscope. Flies of the same sex were then kept together in 30 ml plastic tubes with fresh diet (fed flies) or with a humidified piece of cotton wool (starved males). All flies tested were 3 d old.

cVA attraction. Attraction to cVA was tested in a Y-tube olfactometer[57]. The olfactometer was composed of two branches (30 cm long glass tubes). Each branch was vertically connected to a 25-mL glass vial at its extremity. Both vials were filled with 8 ml of vinegar, producing a food odor background. cVA (1.5 ng/μL in hexane) was tested against hexane (control). These two solutions were released in each branch of the olfactometer from a glass capillary connected to a piezoelectric sprayer[58] at a rate of 10 μL/min. An air-stream of 0.25 m/s was produced in each branch of the olfactometer.

Single females were introduced at the entrance of the Y-tube. The time spent in each branch was recorded. The tests lasted 5 min. An Attraction Index (AI) was calculated as follows: AI = (Time spent in the stimulus branch − Time spent in the control branch)/(Time spent in the stimulus branch + Time spent in the control branch). Inactive flies remaining at the entrance of the olfactometer were not taken into account.

Single sensillum recordings (SSR). Extracellular recordings from OSNs were done using wild-type females, which were virgin or mated with fed wild-type males. A female fly was wedged into the narrow end of a 200-μL micropipette yellow tip with gentle pressure, leaving about half of the compound eye and antennae exposed. The right antenna was gently exposed and gently held between a double adhesive tape and a glass capillary, pressing on the second antennomere. This set up was mounted under a microscope (Nikon Eclipse E600FN) at ×750 magnification, in a stream of moist air. The insect was grounded through the eye using an electrode sharpened to about 1 μm. A second electrode was used to establish contact with the base of a T1 sensillum on the antenna. These sensilla could easily be identified by their characteristic spontaneous activity and single spike amplitude (OSN). The signals were pre-amplified 10× and fed into a computer via an IDAC 4 and recorded by Autospike software (Syntech, Hilversum, The Netherlands). Signals were recorded for 12 s, beginning 2 s prior to stimulation. Details about stimuli and odor delivery are provided in *SI Material and Methods*.

Optical imaging. Flies were dissected as previously described[59]. Briefly, flies were anesthetized on ice and mounted into a plastic stage whereby the head was fixed with Protemp II (3M ESPE). To prevent the antennae from getting in contact with saline, we bent the anterior part with a fine gold wire and placed a plate with a window on top that was sealed with two-component-silicone (KwikSil). Under saline (130 mM NaCl, 5 mM KCl, 2 mM $MgCl_2$, 2 mM $CaCl_2$, 36 mM saccharose, 5 mM HEPES, 1 M NaOH, pH 7.3) the vertex was opened between the eyes, the ocelli and the basis of the antennae. After removing the cuticle, fatty tissue and tracheal sacs, the antennal lobes was visible.

Imaging datasets were acquired using a CCD-camera (Pro-Imaging, Sensi-Cam) attached to an upright fluorescent microscope (OLYMPUS BX51WI), which was controlled via TILL visION (TILL Photonics). Excitation of the GCaMP-3.0 was provided via a Polychrome V (TILL Photonics). The stimulus was applied using a stimulus controller (Syntech Stimulus Controller CS-55; Kirchzarten, Germany) generating a continuous air flow of 1.0 L/min added with a stimulus flow of 0.5 L/min which was shifted between a blank and a stimulus pipette to prevent mechanical stimulation. cVA diluted in paraffin oil was applied on a circular filter paper (0.5, 5, 50 or 50 μg) and placed in Pasteur pipettes. These were then attached to the tubing of the CS-55. The imaging protocol lasted for 40 frames at 4 Hz with a stimulus duration of 2 s.

Further analysis was carried out with custom-written programs in IDL 6.4 (ITT Visual Information Solutions). Beginning with a background (percentage of change from background), bleach and movement correction to minimize artifacts and continuing with identification of the observed glomeruli, a precise response kinetic (ΔF/F) for each glomerulus was calculated.

Chemical analysis. We analyzed the amount of cVA transferred to females during mating with fed and starved males. Just after mating, individual females were dropped into a 1.5-mL glass vial containing 100 μL hexane, to which 200 ng of heptadecenyl acetate was added as an internal standard, during 5 min, for a brief extraction of compounds present on the cuticle, or during 24 h. These extracts were then analyzed on a gas chromatograph coupled with a mass spectrometer (GC-MS). For details on chemical analysis, see *SI Material and Methods*.

Statistics. For details, see *SI Material and Methods*.

1. Arnqvist, G. & Nilsson, T. The evolution of polyandry: multiple mating and female fitness in insects. *Anim. Behav.* **60**, 145–164 (2000).
2. Fricke, C., Wigby, S., Hobbs, R. & Chapman, T. The benefits of male ejaculate sex peptide transfer in *Drosophila melanogaster*. *J. Evol. Biol.* **22**, 275–286 (2009).
3. Long, T. A. F., Pischedda, A., Nichols, R. V. & Rice, W. R. The timing of mating influences reproductive success in *Drosophila melanogaster*: implications for sexual conflict. *J. Evol. Biol.* **23**, 1024–1032 (2010).
4. Kvarnemo, C. & Simmons, L. W. Polyandry as a mediator of sexual selection before and after mating. *Phil. Trans. R. Soc. B* **368**, 20120042 (2013).
5. Ringo, J. Sexual receptivity in insects. *Annu. Rev. Entomol.* **41**, 473–494 (1996).
6. Vargas, M. A., Luo, N. G., Yamaguchi, A. & Kapahi, P. A role for S6 kinase and serotonin in postmating dietary switch and balance of nutrients in *D. melanogaster*. *Curr. Biol.* **20**, 1006–1011 (2010).
7. Saveer, A. M. *et al.* Floral to green: mating switches moth olfactory coding and preference. *Proc. R. Soc. B* **279**, 2314–2322 (2012).
8. Liu, H. F. & Kubli, E. Sex-peptide is the molecular basis of the sperm effect in *Drosophila melanogaster*. *Proc. Natl. Acad. Sc. USA* **100**, 9929–9933 (2003).
9. Yapici, N., Kim, Y.-J., Ribeiro, C. & Dickson, B. J. A receptor that mediates the post-mating switch in *Drosophila* reproductive behaviour. *Nature* **451**, 33–38 (2008).
10. Hasemeyer, M., Yapici, N., Heberlein, U. & Dickson, B. J. Sensory neurons in the *Drosophila* genital tract regulate female reproductive behavior. *Neuron* **61**, 511–518 (2009).
11. Yang, C. H. *et al.* Control of the postmating behavioral switch in *Drosophila* females by internal sensory neurons. *Neuron* **61**, 519–526 (2009).
12. Rezaval, C. *et al.* Neural circuitry underlying *Drosophila* female postmating behavioral responses. *Curr. Biol.* **22**, 1155–1165 (2012).
13. Haussmann, I. U., Hemani, Y., Wijesekera, T., Dauwalder, B. & Soller, M. Multiple pathways mediate the sex peptide-regulated switch in female *Drosophila* reproductive behaviours. *Proc. R. Soc. B* **280**, 20131938 (2013).
14. Chapman, T. *et al.* The sex peptide of *Drosophila melanogaster*: female post-mating responses analyzed by using RNA interference. *Proc. Natl. Acad. Sci. USA* **100**, 9923–9928 (2003).
15. Wigby, S. & Chapman, T. Sex peptide causes mating costs in female *Drosophila* melanogaster. *Curr. Biol.* **15**, 316–321 (2005).

16. Kuijper, B., Stewart, A. D. & Rice, W. R. The cost of mating rises nonlinearly with copulation frequency in a laboratory population of *Drosophila melanogaster*. *J. Evol. Biol.* **19**, 1795–1802 (2006).
17. Manning, A. Control of sexual receptivity in female *Drosophila*. *Anim. Behav.* **15**, 239–250 (1967).
18. Scott, D. The timing of the sperm effect on female *Drosophila melanogaster* receptivity. *Anim. Behav.* **35**, 142–149 (1987).
19. Ram, K. R. & Wolfner, M. F. A network of interactions among seminal proteins underlies the long-term postmating response in *Drosophila*. *Proc. Ntl. Acad. Sc. USA* **106**, 15384–15389 (2009).
20. Ejima, A. *et al.* Generalization of courtship learning in *Drosophila* is mediated by cis-vaccenyl acetate. *Curr. Biol.* **17**, 599–605 (2007).
21. Bartelt, R. J., Schaner, A. M. & Jackson, L. L. cis-Vaccenyl acetate as an aggregation pheromone in *Drosophila melanogaster*. *J. Chem. Ecol.* **11**, 1747–1756 (1985).
22. Kurtovic, A., Widmer, A. & Dickson, B. J. A single class of olfactory neurons mediates behavioural responses to a *Drosophila* sex pheromone. *Nature* **446**, 542–546 (2007).
23. Wang, L. & Anderson, D. J. Identification of an aggression-promoting pheromone and its receptor neurons in *Drosophila*. *Nature* **463**, 227–231 (2010).
24. Keleman, K. *et al.* Dopamine neurons modulate pheromone responses in *Drosophila* courtship learning. *Nature* **489**, 145–U210 (2012).
25. Ha, T. S. & Smith, D. P. A pheromone receptor mediates 11-cis-vaccenyl acetate-induced responses in *Drosophila*. *J. Neurosc.* **26**, 8727–8733 (2006).
26. Van der Goes van Naters, W. & Carlson, J. R. Receptors and neurons for fly odors in *Drosophila*. *Curr. Biol.* **17**, 606–612 (2007).
27. Kohl, J., Ostrovsky, A. D., Frechter, S. & Jefferis, G. S. X. E. A bidirectional circuit switch reroutes pheromone signals in male and female brains. *Cell* **155**, 1610–1623 (2013).
28. Stockinger, P., Kvitsiani, D., Rotkopf, S., Tirian, L. & Dickson, B. J. Neural circuitry that governs *Drosophila* male courtship behavior. *Cell* **121**, 795–807 (2005).
29. Ruta, V. *et al.* A dimorphic pheromone circuit in *Drosophila* from sensory input to descending output. *Nature* **468**, 686–U106 (2010).
30. Dauwalder, B. The roles of fruitless and doublesex in the control of male courtship. *Int. Rev. Neurobiol.* **99**, 87–105 (2011).
31. Zhou, C., Pan, Y. F., Robinett, C. C., Meissner, G. W. & Baker, B. S. Central brain neurons expressing doublesex regulate female receptivity in *Drosophila*. *Neuron* **83**, 149–163 (2014).
32. Liu, W. W. *et al.* Social regulation of aggression by pheromonal activation of Or65a olfactory neurons in *Drosophila*. *Nat. Neurosc.* **14**, 896–U119 (2011).
33. Wigby, S. *et al.* Seminal fluid protein allocation and male reproductive success. *Curr. Biol.* **19**, 751–757 (2009).
34. Fricke, C., Bretman, A. & Chapman, T. Adult male nutrition and reproductive success in *Drosophila melanogaster*. *Evolution* **62**, 3170–3177 (2008).
35. Yew, J. Y., Cody, R. B. & Kravitz, E. A. Cuticular hydrocarbon analysis of an awake behaving fly using direct analysis in real-time time-of-flight mass spectrometry. *Proc. Natl. Acad. Sci. USA* **105**, 7135–7140 (2008).
36. Yew, J. Y. *et al.* A new male sex pheromone and novel cuticular cues for chemical communication in *Drosophila*. *Curr. Biol.* **19**, 1245–1254 (2009).
37. Everaerts, C., Farine, J.-P., Cobb, M. & Ferveur, J.-F. *Drosophila* cuticular hydrocarbons revisited: mating status alters cuticular profiles. *PloS One* **5**, e9607 (2010).
38. Butterworth, F. M. Lipids of *Drosophila*: a newly detected lipid in the male. *Science* **163**, 1356–1357 (1969).
39. Zawistowski, S. & Richmond, R. C. Inhibition of courtship and mating of *Drosophila melanogaster* by the male-produced lipid, cis-vaccenyl acetate. *J. Insect Physiol.* **32**, 189–192 (1986).
40. Cachero, S., Ostrovsky, A. D., Yu, J. Y., Dickson, B. J. & Jefferis, G. S. X. E. Sexual dimorphism in the fly brain. *Curr. Biol.* **20**, 1589–1601 (2010).
41. Sweeney, S. T., Broadie, K., Keane, J., Niemann, H. & O'Kane, C. J. Targeted expression of tetanus toxin light chain in *Drosophila* specifically eliminates synaptic transmission and causes behavioral defects. *Neuron* **14**, 341–351 (1995).
42. Couto, A., Alenius, M. & Dickson, B. J. Molecular, anatomical, and functional organization of the *Drosophila* olfactory system. *Curr. Biol.* **15**, 1535–1547 (2005).
43. Olsen, S. R. & Wilson, R. I. Lateral presynaptic inhibition mediates gain control in an olfactory circuit. *Nature* **452**, 956–960 (2008).
44. Das, S. *et al.* Plasticity of local GABAergic interneurons drives olfactory habituation. *Proc. Natl. Acad. Sci. USA* **108**, E646–E654 (2011).
45. Root, C. M. *et al.* A presynaptic gain control mechanism fine-tunes olfactory behavior. *Neuron* **59**, 311–321 (2008).
46. Chapman, T., Liddle, L. F., Kalb, J. M., Wolfner, M. F. & Partridge, L. Cost of mating in *Drosophila melanogaster* females is mediated by male accessory gland products. *Nature* **373**, 241–244 (1995).
47. Pitnick, S. & García-González, F. Harm to females increases with male body size in *Drosophila melanogaster*. *Proc. R. Soc. B* **269**, 1821–1828 (2002).
48. Wigby, S., Chapman, T., Building, D. & Street, G. Sex peptide causes mating costs in female *Drosophila melanogaster*. *Curr. Biol.* **15**, 316–321 (2005).
49. Wolfner, M. F. Battle and ballet: molecular interactions between the sexes in *Drosophila*. *J. Hered.* **100**, 399–410 (2009).
50. Pischedda, A. & Rice, W. R. Partitioning sexual selection into its mating success and fertilization success components. *Proc. Natl. Acad. Sci. USA* **109**, 2049–2053 (2012).
51. Kvarnemo, C. & Simmons, L. W. Polyandry as a mediator of sexual selection before and after mating. *Phil. Trans. R. Soc. B* **368**, 20120042 (2013).
52. Markow, T. A., Quaid, M. & Kerr, S. Male mating experience and competitive courtship success in *Drosophila melanogaster*. *Nature* **276**, 821–822 (1978).
53. Van Vianen, A. & Bijlsma, R. The adult component of selection in *Drosophila melanogaster* - some aspects of early-remating activity of females. *Heredity* **71**, 269–276 (1993).
54. Avila, F. W., Sirot, L. K., LaFlamme, B. A., Rubinstein, C. D. & Wolfner, M. F. Insect seminal fluid proteins: identification and function. *Annu. Rev. Entomol.* **56**, 21–40 (2011).
55. Hunt, J., Breuker, C. J., Sadowski, J. A. & Moore, A. J. Male-male competition, female mate choice and their interaction: determining total sexual selection. *J. Evol. Biol.* **22**, 13–26 (2009).
56. Ruebenbauer, A., Schlyter, F., Hansson, B. S., Löfstedt, C. & Larsson, M. C. Genetic variability and robustness of host odor preference in *Drosophila melanogaster*. *Curr. Biol.* **18**, 1438–1443 (2008).
57. Lebreton, S., Becher, P. G., Hansson, B. S. & Witzgall, P. Attraction of *Drosophila melanogaster* males to food-related and fly odours. *J. Insect Physiol.* **58**, 125–129 (2012).
58. Becher, P. G., Bengtsson, M., Hansson, B. S. & Witzgall, P. Flying the fly: long-range flight behavior of *Drosophila melanogaster* to attractive odors. *J. Chem. Ecol.* **36**, 599–607 (2010).
59. Strutz, A., Völler, T., Riemensperger, T., Fiala, A. & Sachse, S. Calcium imaging of neural activity in the olfactory system of *Drosophila*. *Neuromethods/Genetically Encoded Functional Indicators*, pp 43–70, ed. Martin, J.-R. (Humana Press, Totowa, NJ, 2012).

Acknowledgments

This work was funded by the Linnaeus grant "Insect Chemical Ecology, Ethology, and Evolution" IC-E3 (Formas, SLU). We thank Claudia Fricke (University of East Anglia) for supplying fly lines.

Author contributions

S.L. and P.W. wrote the main manuscript text and prepared the figures. V.G., S.S. and B.S.H. designed and conducted functional imaging tests, A.B.O. and R.I. did single cell recordings, P.G.B. contributed to behavioural studies. All authors reviewed the manuscript.

Additional information

Supplementary information accompanies this paper at http://www.nature.com/scientificreports

Competing financial interests: The authors declare no competing financial interests.

How to cite this article: Lebreton, S. *et al.* Love makes smell blind: mating suppresses pheromone attraction in *Drosophila* females via Or65a olfactory neurons. *Sci. Rep.* **4**, 7119; DOI:10.1038/srep07119 (2014).

Supplementary Methods

Mating and sexual receptivity

Randomly chosen fed females were mated with a random wild-type male (fed or starved) in round Plexiglass containers (45 x 30 mm). During mating, flies were exposed to a filter paper (1 x 2 cm) containing 10 µL of pure white wine vinegar. Mating was verified by direct observation and mating duration was recorded. Mated females for cVA attraction experiments were used 1 h after mating.

To test fly sexual behavior after mating (or cVA exposure), females were placed in a second Plexiglass container, with a random fed wild-type male. Flies were exposed to white wine vinegar as previously described. Males were considered as courting when they engaged in a courtship sequence and displayed wing vibration. Females were considered as sexually receptive when accepting to mate with a courting male.

Offspring production

Wild type females mated with starved and fed males were placed individually in a rearing tube with fresh food during five days. After 5 d females were removed. Emerging offspring were counted and their sex was noted.

cVA exposure

Two virgin fed females were introduced in the same dishes used for mating. Females were exposed to a filter paper containing 10 µL of white wine vinegar and 0, 0.3 µg, 0.6 µg or 1.2 µg of cVA (11-*cis*-vaccenyl acetate; (*Z*)-11-octadecenyl acetate). Exposure lasted 1 h. Females were then tested for their sexual receptivity. Females exposed to 0.3 µg and 0.6 µg of cVA were also test for cVA attraction.

Single sensillum recordings (SSR)

Four different amounts of cVA diluted in paraffin oil (0.5, 5, 50 and 50 µg) were used. Stimulants were applied onto a square filter paper (0.5 x 1 cm) in pasteur pipettes and immediately sealed with a 1-mL micropipette tip. Paraffin oil was used as a control. Pipettes so prepared were used twice, with 1 h between puffs of a single pipette. A continuous flow of charcoal-filtered humidified air was passed over the preparation through a glass tube held about 1 cm from the antenna at 1.5 L per minute. Stimulation was done by injecting a stream of stimulant-laden air in pipettes into the airstream (at 1.5 mL flow rate) of charcoal-filtered moistured air. For stimulation, a 0.5 L/min air stream was diverted through the pipette onto the preparation during 0.5 s,

thus maintaining the total air flow over the antenna. Response was counted from the onset of the highest concentration (about 300 ms after onset of stimulation) and compared to the baseline activity (500 ms before stimulation). Stimulations were 1 min apart. For reliably delivering odor puffs without cross-contamination, we used the headspace from 5-mL disposable syringes. Once mounted, every insect was used for only a single set of recording, presented in increasing concentration.

Chemical analysis

Extracts were analyzed on a gas chromatograph coupled with a mass spectrometer (GC-MS; 6890 GC and 5975 MS, Agilent technologies Inc., Santa Clara, CA, USA). For each extract, 2 µL were injected into a HP-5MS silica capillary column (30 m x 0.25 mm x 0.25 µm film thickness; Agilent technologies Inc.) that was temperature-programmed from 30°C to 225°C at 8°C/min. cVA was quantified by peak integration and comparison with the internal standard. Identification of cVA was done on the basis of the mass spectra and retention time, in comparison with synthetic standard.

Statistics

PIs were compared using a nonparametric Kruskal-Wallis test followed by a multiple pairwise Mann-Whitney test with fdr correction. To test whether attraction was significant, PIs were compared with a theoretical value of zero (no attraction) using a nonparametric Wilcoxon test. Pheromones transferred by starved and fed males were compared with a nonparametric Mann-Whitney test. Female receptivity, SSR and optical imaging data were analyzed using a mixed linear model (GLMM) for repeated measurements. All statistical analysis was done using R (R 2.1.1, R Development Core Team, Free Software Foundation Boston, MA, USA).

General Discussion

The overall topic of this thesis was to clarify and emphasize the correlation of structure and function in complex neuropils such as the antennal lobe (AL) of *Drosophila melanogaster* (Hansson and Anton, 2000). By executing this task, I participated in four projects divided in two parts, one on the morphological basis of the *Drosophila* olfactory system and its physiological implications (Manuscript I and II) and one on the behavioral output and its anatomical and functional origins (Manuscript III and IV).

The first project primarily dealt with the urgent requirement of thorough *in vivo* anatomy to support the growing number of *in vivo* applications (Brand and Perrimon, 1993; Feinberg et al., 2008; Patterson and Lippincott-Schwartz, 2002) investigating increasingly detailed physiological properties (Liu and Wilson, 2013; Mosca and Luo, 2014; Tanaka et al., 2012; Zhu et al., 2013). As a major effort our novel generated transgenic fly line, END1-2, permitted a direct comparison of *in vivo* and *in vitro* morphology, especially the volume, to clarify the actual need for an *in vivo* atlas of the AL. Utilizing the presynaptic DsRed labelling of the line for confocal scans of the AL in the living fly we could bypass the commonly used nc82 *in vitro* neuropil antibody staining (Laissue et al., 1999; Rein et al., 2002). The volumetric measures displayed a strongly variable impact of fixation on the neuropil and glomerular volume compared with immunostaining. Some glomeruli were not affected at all while others lost up to 60% of their initial size. Concerned about the resulting putative distortions of the AL in total, we used the possibilities of 3D reconstruction (Laissue et al., 1999; Stocker et al., 1990) to calculate the positional changes as Euclidean distances of glomerular coordinates in relation to each other *in vivo* and *in vitro*. These additional factors of fixation depicted a highly various effect on the glomerulus distances as well as angles which could be explained mainly through the dissection of the brain out of the head capsule. Severing the antennal nerve and mounting the brain leads to an overall depression of the flexible AL structure together with an interglomerular dislocation. These findings clarified why the application of available *in vitro* atlases (Couto et al., 2005; Endo et al., 2007; Laissue et al., 1999; Silbering et al., 2011; Stocker et al., 1990; Tanaka et al., 2012) for *in vivo* techniques represents in most cases an actual challenge. Struggling with these technical drawbacks we decided to

generate the first *in vivo* atlas of the AL based on the END1-2 line combined with a large set of specific chemosensory receptor (CR)-GAL4 lines for secure identification (Couto et al., 2005; Fishilevich and Vosshall, 2005). This considerably improved and eased the task of glomerulus identification in the following projects (Manuscript II, III and IV) as we predicted by applying it on two GAL 4-lines frequently used in imaging experiments, Orco- (Larsson et al., 2004) and GH146-GAL4 ((Stocker et al., 1997), Manuscript III and IV) labelling a large proportion of OSNs and PNs, respectively. Our results emphasize a general crucial need for least artificial anatomical studies of flexible neuropils in parallel to their physiological investigation. In form of the END1-2 fly line and our *in vivo* AL atlas we provide novel tools for this purpose in *Drosophila melanogaster*.

As a follow-up project we utilized our new tool – the *in vivo* atlas of the *Drosophila* AL (Manuscript I) – for a comprehensive screen of the structural properties of the spherical subunits of the AL, the glomeruli. Their long history of research in *Drosophila* already began in the mid-19th century (Leydig, 1857) as they were mistaken as cell bodies approximately 27 years after the initial description of *Drosophila melanogaster* (Meigen, 1830). The following 100 years lead to the discovery of projection neurons (PNs, (Kenyon, 1896)), the discussion of the deutocerebrum being involved in sensory tasks at all (Bretschneider, 1914; Hanström, 1928) and the sensilla being depicted on the antennal funiculus (Miller, 1950). The second half of the 20th century with its tremendous methodological progress was bound to increasing depth of morphological analyses (del Valle Rodriguez et al., 2012) to describe rising complexity of the system which we wanted to press ahead with (Manuscript II). Therefore we carried out a large screen of the anatomical composition of glomeruli in the living fly, building a foundation to examine the relation of form and function. First we took advantage of the available specific CRX-GAL4 fly lines (Fishilevich and Vosshall, 2005; Kurtovic et al., 2007; Silbering et al., 2011) to map the exact olfactory sensory neuron (OSN) somata distributions on the funiculus for five sensilla classes and their 22 incorporated types, which was only done for the sensillum classes so far (De Bruyne et al., 1999; Shanbhag et al., 1999). This additionally allowed a precise quantification for each of the sensillum types and as all OSNs expressing the same CR converge onto the same glomerulus in the AL (Gao et al., 2000) we acquired also the accurate OSN input numbers for each glomerulus. This sort of quantification was so far only done for a minute group of

receptors (Dobritsa et al., 2003; Gao et al., 2000). Comparing the numbers to the previously published ones displayed some divergence but as our total amounts for sensillum types and classes were matching with the comparably detailed classical morphological works (Shanbhag et al., 1999; Stocker et al., 1990), we sustained the analysis. Next, we continued working on the volumetric foundation shown in Manuscript I by analyzing the *in vivo* dimensions for all remaining glomeruli. These two primary datasets – OSNs and volume – allowed us to prove the previously published indirect assumption on the major impact of OSN quantity on the glomerular volume (Acebes and Ferrús, 2001). Having characterized one major component of glomerular composition – the OSNs – we now focused on the PNs to get a basic understanding of the morphological principles of glomerulus-specific input and output (Jefferis et al., 2007; Masse et al., 2009). Via photoactivation (Patterson and Lippincott-Schwartz, 2002) of GH146-positive uniglomerular PNs in single glomeruli, assisted by our *in vivo* atlas and GH146 characterization (Manuscript I), we again screened a large proportion of glomeruli. The initial description of one to three PNs per glomerulus hold true in most cases (Wong et al., 2002), while we also observed counts of up to 10 PNs. Interestingly most of those glomeruli were known to participate in crucial behavioral pathways such as mating (DA1 – (Kurtovic et al., 2007)), oviposition site evaluation (DC3 – (Dweck et al., 2013; Ronderos et al., 2014)) or aversion to noxious bacteria and CO_2 (DA2 – (Stensmyr et al., 2012), V – (Suh et al., 2004)). Additionally we could describe a group of glomeruli as putatively significant, based on this potential link between a high PN number and functional specificity of the glomerulus' output. The glomerulus DL3, as one of these candidates, was later described as part of an important behavioral switch in female receptivity (Manuscript IV). To complete the neuronal set of the glomerular architecture we included the results of an external publication (Chou et al., 2010) on the glomerulus-specific local interneurons (LN) innervation frequency as a measure for the putative strength of lateral interactions between glomeruli. The general assumption on LNs distributing and modulating information within (Root et al., 2008) and between glomeruli (Seki et al., 2010) provoked postulation of glomeruli which are less innervated by LNs to be more selective as they are part of a hard-wired information path with no strong lateral in- or output in the AL (Root et al., 2008; Stowers, 2004). In accordance with the high PN numbers in glomeruli, underlining their importance, we observed also low numbers of LN innervations in these

glomeruli supporting our assumption even more. The DL3 glomerulus, displaying the lowest LN innervation frequency (Manuscript II), again serves as a valuable prediction of specific functionality based on special structure. To include an actual measure for receptor/glomerulus selectivity we calculated the lifetime sparseness (Bhandawat et al., 2007; Perez-Orive et al., 2002; Vinje, 2000) from the available thorough response profile databases (Galizia et al., 2010; Hallem and Carlson, 2006). In the case of missing or weak represented glomeruli we generated our own profiles via single sensillum recording screens. The lifetime sparseness as a value for the likeliness of a receptor to respond to any given odor based on the characterized responses to any odor so far shows significant correlations with the number of PNs per glomerulus as well as with the LN innervation frequency. This again supports our hypothesis that higher PN counts go along with higher lifetime sparseness, meaning higher selectivity, and lower LN numbers pre glomerulus. Lastly we could show the distinct effect of OSNs, PNs and LNs on the glomerulus volume. Interestingly only the OSNs and LNs have a significant impact. As it was shown that also seemingly uniform neuronal populations can display quite unique properties like dissimilar synaptic density in OSNs coming from the same sensillum (Mosca and Luo, 2014) or segregated intraglomerular distribution of LNs developing from the same mother cell (Chou et al., 2010), we expect future increase in the detail of structural discriminators. Especially the advances in superresolution microscopy will improve this field significantly in the future (Hell, 2009). Our contributions to published physiological datasets (Galizia et al., 2010; Hallem and Carlson, 2006) and the provided comprehensive morphological database of major glomerulus defining parameters encourage further physiological and anatomical work as well as combinations of the two.

The functional part of this thesis dealt with two examples for the interplay of structure and physiology. One illuminates the connection of the AL with the lateral horn (LH) via inhibitory PNs (Manuscript III) and the other focusses on the behavioral characterization of Or65a (Manuscript IV), a receptor predicted to have a crucial function by our anatomical screen (Manuscript II).

Target patterns of PNs leaving the AL to the mushroom body or the LH are often discussed to reveal functional implications (Caron et al., 2013; Jefferis et al., 2007; Liang et al., 2013; Parnas et al., 2013) but the exact modeling of these interactions still remains open. In the third project we concentrated on the multiglomerular

inhibitory PNs (iPNs) labelled by the enhancer trap-line MZ699-GAL4 (Ito et al., 1997) and their role in the coding of odor quality and intensity in the LH of *Drosophila melanogaster*. The LH represents one of the primary output centers of the AL gathering a combinatorial code of glomerular responses (Jefferis et al., 2007). Initially, a detailed identification of the iPN innervated glomeruli, assisted by our *in vivo* atlas (Manuscript I), depicted a clear omitting of glomeruli coding for repellent odors and dense innervation of attractiveness coding glomeruli (Knaden et al., 2012). This supports the segregation of attractive and aversive odor representations in the LH (Min et al., 2013). Further we could segregate the iPN population via photoactivation of single neurons in two classes which receive input from a distinct set of glomeruli in the AL and innervate separate regions in the LH. Interestingly these regions depict nicely isolated response patterns during optical imaging, why we named them odor response domains (ORDs). These domains seem to code for odor intensity as they display a shift of the iPN odor responses from one ORD to the other along an odor gradient. Additionally the iPNs differentiate from the excitatory PNs (ePNs) in the LH regarding function (Liang et al., 2013) and morphology (Jefferis et al., 2007; Wang et al., 2014), depicting separate processing channels similar as in bees (Brill et al., 2013). EPNs and iPNs do not form shared synapses but interact with the same class of 3rd order neurons, descending to the ventrolateral protocerebrum (vlPr neurons). These neurons were previously shown to receive major input from ePNs (Parnas et al., 2013). Imaging experiments clarified that vlPr neurons are also gathering input from the aversion coding region of the LH where they can be inhibited by iPNs (Liang et al., 2013). When silencing the iPNs in behavioral T-maze assays (Quinn et al., 1974) we observed a reduced attraction to odors. Due to the glomerular separation in the AL, attractive hedonic valence is mainly coded by MZ699 positive iPNs while GH146 positive ePNs code for repulsion and attraction. The conclusive circuit model depicts the encoding of odors with opposing hedonic valence by interplay of distinct processing pathways in the LH. Attractive odors mainly activate iPNs but not the vlPr neurons as those are inhibited by the iPNs. In turn the vlPr neurons are largely activated by ePNs transmitting responses to repulsive odors but only until an inhibitory signal indicates an attractive cue. Henceforth the ventrolateral protocerebrum primarily receives information on the presence of aversive cues putatively integrating those with optical information (Tanaka et al., 2004). As soon as an attractive odor leads to excitation of the iPNs,

they inhibit the aversive representation in the LH permitting innate attractive behavior by shutting down the vlPr neurons. The depicted segregation of innervation and response patterns of two distinct groups of PNs in the AL and the LH in parallel and their partly convergence on the same vlPr neuron population leads to a crucial behavioral switch between aversion and attraction. This again underlines the initial question for a relation of form and function on a whole different level than plain glomerulus-specific morphology. Description of a novel behavioral switch in the LH supports its innate functionality and the direct correlation of morphological discernable pathways with respective ethological effects.

Manuscript IV portraits another example for the relation of structure and function based on specific glomerular morphology predicting a particular physiological function and vice versa. Mating in female flies is triggered via the perception of the male pheromone cVA (Kurtovic et al., 2007) which also provokes male-male aggression (Liu et al., 2011). The initial observation of female flies repeatedly mating more frequently after mating with starved males than with fed ones suggests a behavioral switch which depends on the nutritional status of the male fly and the putatively linked amount of cVA production. Primary mating itself did not vary between the male groups although the starved ones produced less offspring, but the amount of cVA transferred during mating reduced significantly. Therefore males' initial attractiveness is independent from their cVA level but their fitness is potentially reduced as the transferred cVA usually prevents other males from approaching females (Ejima et al., 2007; Keleman et al., 2012; Zawistowski and Richmond, 1985). The diminishing of cVA could explain the higher mating rate after mating with starved males, as other males are not repulsed. Alternatively the constant presence of cVA on and within the female body (Ejima et al., 2007) after mating serves as a modulatory cue to reduce their motivation to copulate again or the mating evokes expression level changes of the responsible receptor (Zhou et al., 2009). Pre-exposing virgin females to cVA can mimic the described effect which emphasizes the importance of the odor itself. CVA is described as the best known ligand for Or67d (van der Goes van Naters and Carlson, 2007) whose OSNs converge in the DA1 glomerulus (Couto et al., 2005). To see if the cVA exposure during mating makes a difference in perception we imaged the odor responses in virgins and in females mated to fed males. Or67d OSNs did not show any effect of the mating. The regarding PNs, labelled with GH146-GAL4, displayed a significant drop in response

strength. Since the effect in DA1 was not evoked by its own OSNs where could it originate from? Recent studies showed that cVA triggers a lateral interglomerular circuit via LNs originating from the DL3 (Liu et al., 2011), whose OSNs express Or65a and respond to high amounts and long exposure of cVA. A behavioral impact for this circuit was never shown but silencing the Or65a pathway with tetanus toxin (Sweeney et al., 1995) also blocked the loss of attraction. The potential inhibitory lateral input via LNs from the DL3 to the DA1 as a form of postsynaptic, rather than presynaptic gain control (Root et al., 2008) would also explain the weaker cVA imaging responses in PNs descending from the DA1. Reduced activity of PNs transmitting crucial cVA responses to the mushroom body calyx (Caron et al., 2013) and the LH (Jefferis et al., 2007) could then lead to abolished courtship. This behavioral shift and its potential morphological basis would demand another level of complexity in LN classification. Based on our structural screen and the LN frequency data (Chou et al., 2010) we suggested that glomeruli with a highly specific information pathway have less LNs since they do not require lateral processing. The DL3 glomerulus was predicted by us as a putatively important glomerulus due to its high PN and the lowest LN count (Manuscript I). Initially puzzled by its minute size and dimorphism we now postulate another hypothesis on the DL3 glomerulus serving as a modulatory glomerulus being slightly selective to cVA. The modulation is somewhat similar to glomerulus VA2 in the CO_2 pathway (Turner and Ray, 2009). Strong or long lasting exposure to cVA due to mating with a fed male permits a modulation of attraction via a small but putatively specific LN population inhibiting DA1 PNs as well as their output in higher brain centers and therefore reduces receptivity. This physiological and ethological demonstration of a behavioral importance predicted on the basis of a unique combination of structural features illuminates the helpful interdependence of these disciplines.

In this thesis I made an effort to illuminate the link between a strict and discrete examination of structural attributes of a neuropil *in vivo* on one side, and the complex investigation of modulated behavioral output of the system on the other side. By generating an extensive morphological and partly functional dataset of the subunits of the *Drosophila melanogaster* AL and simultaneously depicting two distinct behavioral pathways, both incorporating an ethological switch, we provided the basis for their thorough comparison. The fact that the anatomical database alone permitted predictions on rarely investigated glomeruli, which could be physiologically proved,

supports the tight interdependence of structure and physiology – of form and function.

Still observing exceptions from our rules I look forward to the enhanced capabilities of newly emerging or tremendously improving techniques to allow more and more detailed research. Already now, ultrastructures of already concise neuropil subunits are depicted and we will be staggered by what awaits us in the coming decades.

Summary

For most of the time neuroscientific research in invertebrates as in vertebrates was exclusively descriptive. Lacking the possibilities to alter wiring circuits in a neuropile at a satisfying level of detail restricted most studies to concentrate on morphological properties and external recordings. Meanwhile, the ever increasing variability of genetic tools helped to cross this border, especially in mice, *Caenorhabditis elegans*, zebra fish and *Drosophila melanogaster*. The vinegar fly functions as a model organism in many neuroscientific fields but especially olfaction is investigated in insects. Perception and orientation of flies in their vast, changing and complex chemical environment to fulfil variable behavioral tasks like search and evaluation of food and oviposition sites, predator avoidance and courtship demands an evenly complex sensory system. These various ethological functions and the structural foundation are well described but often exclusively for either of the two.

The main goal of this thesis was to approach the question for a correlation between structural and functional properties in a complex sensory neuropile from both sides. Therefore we focused on the olfactory system of the vinegar fly and its single units, the antenna, antennal lobe (AL) and lateral horn (LH). Primary generation of an *in vivo* atlas of the AL and its sub units, the glomeruli, provided a comprehensive basis for the sequential studies (Manuscript I). The essential need for this atlas was depicted by a detailed investigation of the artificial impact of fixation on the glomerular volume and relative location. These distortions made it often tedious to apply *in vitro* atlases of the AL in the increasing number of *in vivo* applications in *Drosophila*. This foundation permitted the in depth analysis of specific glomerular parameters (Manuscript II). Uniquely precise quantifications of glomerulus specific olfactory sensory neurons (OSNs), volume and projection neurons (PNs) together with functional characterizations of response profiles via single sensillum recordings and published local interneuron innervation frequencies serve as a thorough database for glomerulus classification. In combination with known specific functionalities we could identify certain combinations of parameters as descriptors for specific functionalities in scarcely described glomeruli. To test our predictions we examined one glomerulus with a remarkable structural composition, the DL3 (Manuscript IV), which is in parallel barely characterized. Observations on it being involved in a behavioral switch affecting the pheromone attraction in female flies

supported our assumptions on a relation of form and function. Further we utilized the *in vivo* atlas during the description of the innervation pattern of multiglomerular inhibitory PNs (iPNs), connecting the AL and the LH, and their coding for odor quality and intensity (Manuscript III). These iPNs are selectively gathering input from AL glomeruli which code for attractive hedonic valence and represent it in the LH, a center for innate behavior in the protocerebrum of the fly. There the iPNs synapse on to third order output neurons of the LH and inhibit their innate representation of aversive cues which is mainly transmitted by excitatory PNs (ePNs) descending from the respective glomeruli coding for aversion in the AL. Hence, two distinct populations of PNs build a behavioral switch in flies depicting an originally aversive circuit from the AL to the LH via ePNs which can be modulated through the presence of attractive cues activating iPNs. Silencing of the iPNs abolishes this switch and reduces the overall attraction. This crucial circuit of innate behavior which is almost completely represented via two morphologically and physiologically distinct populations of PNs underlines our hypothesis on a prominent link between form and function. Upcoming ultrastructural analyses of the glomerular parameters with the aid of superresolution microscopy in combination with increasingly sophisticated genetic tools in *Drosophila* will enhance this morphological descriptive database of attributes even further.

The findings of this thesis are important because they emphasize an enlightening correlation between the structure and function of such complex neuropils as the antenna, AL, its glomeruli and the LH. Therefore, profound knowledge of morphological properties and exemplified functional studies allow the prediction of putative importance for ethologically unknown structures.

Zusammenfassung

Lange Zeit war die Neurowissenschaft in Invertebraten und Vertebraten gleichermaßen ausschließlich beschreibend. In Ermangelung der Möglichkeit zur Manipulation der neuronalen Vernetzung eines Neuropils beschränkten sich die meisten Studien auf anatomische Eigenschaften und externe Ableitungen. Inzwischen hat die immer weiter steigende Vielzahl an Werkzeugen zur genetischen Manipulation diese Grenze insbesondere in der Maus, *Caenorhabditis elegans*, dem Zebrafisch und *Drosophila melanogaster* durchbrochen. Die Essigfliege fungiert in vielen neurowissenschaftlichen Feldern als Modellorganismus wobei insbesondere die Olfaktion stark in Insekten untersucht wird. Wahrnehmung und Orientierung der Fliege in ihrer weiten, wechselhaften und komplexen chemischen Umgebung verlangt ein ähnlich komplexes sensorisches System zur Ausführung verschiedener Verhalten wie der Suche und Bewertung von Nahrung sowie Eiablageplätzen, dem Ausweichen von Prädatoren oder der Paarung. Diese vielfältigen ethologischen Funktionen und ihre strukturellen Grundlagen sind gut untersucht aber häufig nur unter jeweils einem der beiden Blickwinkel.

Das Hauptziel der vorliegenden Dissertation ist die Annäherung an die Frage nach einem Zusammenhang zwischen strukturellen und funktionellen Eigenschaften eines komplexen sensorischen Neuropils von beiden Seiten. Um diese Frage hinreichend zu beantworten rückten wir das olfaktorische System der Essigfliege mit seinen Untereinheiten, der Antenne, dem Antennallobus (AL) und dem lateralen Horn (LH) in den Mittelpunkt. Die anfängliche Erstellung eines *in vivo* Atlanten des AL sowie seiner eigenen Untereinheiten, den Glomeruli, erzeugte eine umfassende Basis für die folgenden Studien (Manuskript I). Die essentielle Notwendigkeit eines solchen Atlanten wurde deutlich bei genauerer Untersuchung der artifiziellen Einflüsse auf Volumen und relative Position der Glomeruli während der ansonsten notwendigen *in vitro* Fixierung. Diese Verformungen erschwerten häufig die adäquate Anwendung von *in vitro* Atlanten des AL in der steigenden Anzahl von *in vivo* Anwendungen in *Drosophila*. Das neue anatomische Fundament ermöglichte eine tiefgehende Analyse der Glomerulus-spezifischen Parameter (Manuskript II). Die einzigartig präzise Quantifizierung der Glomerulus-spezifischen olfaktorisch-sensorischen Neurone (OSNs), des Volumens und der Projektionsneurone (PN) zusammen mit der funktionellen Charakterisierung von Antwortprofilen mittels Einzelsensillenableitung

sowie der publizierten Daten zu Innervationsfrequenzen von lokalen Interneuronen dient als gründliche Datenbank zur Klassifizierung der Glomeruli. Durch Verknüpfung der Datenbank mit beschriebenen spezifischen Funktionen einzelner Glomeruli konnten wir spezielle anatomische Mekmalskombinationen ermitteln welche eine ebenfalls spezifische Funktion in bisher kaum beschriebenen Glomeruli vorhersagen. Um diese Vorhersagen zu testen wählten wir einen einzelnen Glomerulus mit bemerkenswerter neuronaler Zusammensetzung, den DL3 (Manuskript IV), wessen Funktion zugleich nahezu unbeschrieben ist. Die Beobachtungen deuteten auf seine Beteiligung an einem modulierten Verhaltensmuster in weiblichen Fliegen hin welches zu einer verringerten Attraktion zu dem einzigen bekannten Pheromon führt. Dieser Zusammenhang erhärtete unsere Annahme von einer Kausalität zwischen Form und Funktion. Weiterhin nutzten wir den *in vivo* Atlanten des AL während der Beschreibung eines komplexen Innervationsmusters multiglomerulärer inhibitorischer PNs (iPNs) welche den AL und das LH verbinden und zur Kodierung von Duftqualität sowie –intensität beitragen (Manuskript III). Durch ihre selektive Innervation des AL vereinen diese iPNs fast ausschließlich Input von Glomeruli auf sich welche für attraktive Umgebungsdüfte kodieren. Diese Information leiten sie an das LH, ein Neuropil des Protozerebrums welches für angeborenes Verhalten zuständig ist, weiter. Dort angekommen bilden die iPNs Synapsen mit den Ausgangsneuronen des LH und inhibieren deren grundlegende Kodierung von aversiven Duftreizen, welche sie wiederum von exzitatorischen PNs (ePNs) des AL erhalten. Diese zwei unterschiedlichen Populationen von PNs erzeugen einen verhaltensbiologischen Schalter in Fliegen welcher einen, ursprünglich Aversion kodierenden, Schaltkreis zwischen AL und LH mittels iPNs abschalten kann die wiederum durch attraktive Düfte aktiviert werden. Reduziert man den Einfluss der iPNs mittels gezielter Mutationen wird die generelle Attraktion der Fliegen ebenfalls reduziert. Dieser wichtige Verhaltensschaltkreis, welcher nahezu ausschließlich durch die zwei morphologisch sowie physiologisch unterschiedlichen Populationen von PNs dargestellt wird, unterstreicht unsere Hypothese von einem deutlichen Zusammenhang zwischen Form und Funktion. Unter Zuhilfenahme von Hochauflösender Mikroskopie in Kombination mit den zunehmend weiterentwickelten genetischen Werkzeugen in *Drosophila* werden ultrastrukturelle Untersuchungen die glomerulären Parameter sicherlich noch weiterentwickeln. Die Aussagekraft der daraus erwachsenden Vorhersagen wird dadurch immer weiter zunehmen.

Die Erkenntnisse dieser Dissertation sind dahingehend wichtig da sie den wichtigen Zusammenhang von Struktur und Funktion neu beleuchten. Daher stellen wir fest dass profundes Wissen über anatomische Eigenschaften sowie exemplarische funktionelle Studien die Vorhersage von vermeintlich wichtigen und bis dato ethologisch unbeschriebenen Strukturen ermöglicht.

References

Abuin, L., Bargeton, B., Ulbrich, M.H., Isacoff, E.Y., Kellenberger, S., and Benton, R. (2011). Functional architecture of olfactory ionotropic glutamate receptors. Neuron 69, 44-60.

Acebes, A., and Ferrús, A. (2001). Increasing the Number of Synapses Modifies Olfactory Perception in Drosophila. The Journal of neuroscience : the official journal of the Society for Neuroscience 21, 6264-6273.

Adam, V., Berardozzi, R., Byrdin, M., and Bourgeois, D. (2014). Phototransformable fluorescent proteins: Future challenges. Current opinion in chemical biology 20, 92-102.

Ai, M., Min, S., Grosjean, Y., Leblanc, C., Bell, R., Benton, R., and Suh, G.S. (2010). Acid sensing by the Drosophila olfactory system. Nature 468, 691-695.

Akerboom, J., Rivera, J.D., Guilbe, M.M., Malave, E.C., Hernandez, H.H., Tian, L., Hires, S.A., Marvin, J.S., Looger, L.L., and Schreiter, E.R. (2009). Crystal structures of the GCaMP calcium sensor reveal the mechanism of fluorescence signal change and aid rational design. J Biol Chem 284, 6455-6464.

Benton, R., Vannice, K.S., Gomez-Diaz, C., and Vosshall, L.B. (2009). Variant ionotropic glutamate receptors as chemosensory receptors in Drosophila. Cell 136, 149-162.

Bhandawat, V., Olsen, S.R., Gouwens, N.W., Schlief, M.L., and Wilson, R.I. (2007). Sensory processing in the Drosophila antennal lobe increases reliability and separability of ensemble odor representations. Nature neuroscience 10, 1474-1482.

Boeckh, J., and Tolbert, L.P. (1993). Synaptic Organization and Development of the Antennal Lobe in Insects. Microsc Res Tech 24, 260-280.

Brand, A., and Perrimon, N. (1993). Targeted gene expression as a means of altering cell fates and generating dominant phenotypes. Development 118.

Bretschneider, F. (1914). Über die Gehirne der Küchenschabe und des Mehlkäfers. Jena Z Naturw 52, 296-362.

Brill, M.F., Rosenbaum, T., Reus, I., Kleineidam, C.J., Nawrot, M.P., and Rossler, W. (2013). Parallel processing via a dual olfactory pathway in the honeybee. The Journal of neuroscience : the official journal of the Society for Neuroscience 33, 2443-2456.

Busch, S., Selcho, M., Ito, K., and Tanimoto, H. (2009). A map of octopaminergic neurons in the Drosophila brain. The Journal of comparative neurology 513, 643-667.

Busto, G.U., Cervantes-Sandoval, I., and Davis, R.L. (2010). Olfactory learning in Drosophila. Physiology 25, 338-346.

Carlsson, M.A., Diesner, M., Schachtner, J., and Nassel, D.R. (2010). Multiple neuropeptides in the Drosophila antennal lobe suggest complex modulatory circuits. The Journal of comparative neurology 518, 3359-3380.

Caron, S.J., Ruta, V., Abbott, L.F., and Axel, R. (2013). Random convergence of olfactory inputs in the Drosophila mushroom body. Nature 497, 113-117.

Chiang, A.S., Lin, C.Y., Chuang, C.C., Chang, H.M., Hsieh, C.H., Yeh, C.W., Shih, C.T., Wu, J.J., Wang, G.T., Chen, Y.C.*, et al.* (2011). Three-dimensional reconstruction of brain-wide wiring networks in Drosophila at single-cell resolution. Current biology : CB 21, 1-11.

Chou, Y.H., Spletter, M.L., Yaksi, E., Leong, J.C., Wilson, R.I., and Luo, L. (2010). Diversity and wiring variability of olfactory local interneurons in the Drosophila antennal lobe. Nature neuroscience 13, 439-449.

Clyne, P.J. (2000). Candidate Taste Receptors in Drosophila. Science 287, 1830-1834.

Clyne, P.J., Grant, A., O'Connell, R., and Carlson, J.R. (1997). Odorant response of individual sensilla on the Drosophila antenna. Invertebr Neurosci 3, 127-135.

Couto, A., Alenius, M., and Dickson, B.J. (2005). Molecular, anatomical, and functional organization of the Drosophila olfactory system. Current biology : CB 15, 1535-1547.

De Bruyne, M., Clyne, P.J., and Carlson, J.R. (1999). Odor Coding in a Model Olfactory Organ: The Drosophila Maxillary Palp. The Journal of neuroscience : the official journal of the Society for Neuroscience 19, 4520-4532.

De Bruyne, M., Foster, K., and Carlson, J.R. (2001). Odor Coding in the Drosophila Antenna. Neuron 30, 537-552.

Dekker, T., Ibba, I., Siju, K.P., Stensmyr, M.C., and Hansson, B.S. (2006). Olfactory shifts parallel superspecialism for toxic fruit in Drosophila melanogaster sibling, D. sechellia. Current biology : CB 16, 101-109.

del Valle Rodriguez, A., Didiano, D., and Desplan, C. (2012). Power tools for gene expression and clonal analysis in Drosophila. Nature methods 9, 47-55.

Devaud, J.-M., Acebes, A., and Ferrús, A. (2001). Odor Exposure Cuases Central Adaptation and Morphological Changes in Selected Olfactory

Glomeruli in Drosophila. The Journal of neuroscience : the official journal of the Society for Neuroscience 21, 6274-6282.

Devaud, J.-M., Acebes, A., Ramaswami, M., and Ferrús, A. (2003). Structural and Functional Changes in the Olfactory Pathway of Adult Drosophila Take Place at a Critical Age. J Neurobiol, 13-23.

Dobritsa, A., Van der Goes van Naters, W., Warr, C.G., Steinbrecht, R.A., and Carlson, J.R. (2003). Integrating the molecular and Cellular Basis of Odor Coding in the Drosophila Antenna. Neuron 37, 827-841.

Dweck, H.K. (2014). Novel pheromones mediate copulation and aggregation in Drosophila.

Dweck, H.K., Ebrahim, S.A., Kromann, S., Bown, D., Hillbur, Y., Sachse, S., Hansson, B.S., and Stensmyr, M.C. (2013). Olfactory preference for egg laying on citrus substrates in Drosophila. Current biology : CB 23, 2472-2480.

Eisthen, H.L. (2002). Why Are Olfactory Systems of Different Animals So Similar? Brain Behav Evolut 59, 273-293.

Ejima, A., Smith, B.P., Lucas, C., van der Goes van Naters, W., Miller, C.J., Carlson, J.R., Levine, J.D., and Griffith, L.C. (2007). Generalization of courtship learning in Drosophila is mediated by cis-vaccenyl acetate. Current biology : CB 17, 599-605.

Endo, K., Aoki, T., Yoda, Y., Kimura, K., and Hama, C. (2007). Notch signal organizes the Drosophila olfactory circuitry by diversifying the sensory neuronal lineages. Nature neuroscience 10, 153-160.

Fan, J., Francis, F., Liu, Y., Chen, J.L., and Cheng, D.F. (2011). An overview of odorant-binding protein functions in insect peripheral olfactory reception. Genetics and molecular research : GMR 10, 3056-3069.

Feinberg, E.H., Vanhoven, M.K., Bendesky, A., Wang, G., Fetter, R.D., Shen, K., and Bargmann, C.I. (2008). GFP Reconstitution Across Synaptic Partners (GRASP) defines cell contacts and synapses in living nervous systems. Neuron 57, 353-363.

Fishilevich, E., and Vosshall, L.B. (2005). Genetic and functional subdivision of the Drosophila antennal lobe. Current biology : CB 15, 1548-1553.

Galizia, C.G., Munch, D., Strauch, M., Nissler, A., and Ma, S. (2010). Integrating heterogeneous odor response data into a common response model: A DoOR to the complete olfactome. Chemical senses 35, 551-563.

Galizia, C.G., Sachse, S., Rappert, A., and Menzel, R. (1999). The glomerular code for odor representation is species specific in the honeybee Apis mellifera. Nature neuroscience 2, 473-478.

Gallio, M., Ofstad, T.A., Macpherson, L.J., Wang, J.W., and Zuker, C.S. (2011). The coding of temperature in the Drosophila brain. Cell 144, 614-624.

Gao, Q., Yuan, B., and Chess, A. (2000). Convergent projections of Drosophila olfactory neurons to specific glomeruli in the antennal lobe. Nature neuroscience 3, 780-785.

Grabe, V., Strutz, A., Baschwitz, A., Hansson, B.S., and Sachse, S. (2014). Digital in vivo 3D atlas of the antennal lobe of Drosophila melanogaster. The Journal of comparative neurology.

Gruntman, E., and Turner, G.C. (2013). Integration of the olfactory code across dendritic claws of single mushroom body neurons. Nature neuroscience 16, 1821-1829.

Ha, T.S., and Smith, D.P. (2006). A pheromone receptor mediates 11-cis-vaccenyl acetate-induced responses in Drosophila. The Journal of neuroscience : the official journal of the Society for Neuroscience 26, 8727-8733.

Hallem, E.A., and Carlson, J.R. (2004). The odor coding system of Drosophila. Trends in genetics : TIG 20, 453-459.

Hallem, E.A., and Carlson, J.R. (2006). Coding of odors by a receptor repertoire. Cell 125, 143-160.

Hansson, B.S., and Anton, S. (2000). Function and Morphology of the Antennal Lobe: New Developments. Annual review of entomology 45, 203-231.

Hansson, B.S., Knaden, M., Sachse, S., Stensmyr, M.C., and Wicher, D. (2010). Towards plant-odor-related olfactory neuroethology in Drosophila. Chemoecology 20, 51-61.

Hansson, B.S., Ljungberg, H., Hallberg, E., and Löfstedt, C. (1992). Functional Specialization of Olfactory Glomeruli in a Moth. Science 256, 1313-1315.

Hanström, B. (1928). Vergleichende Anatomie der Nervensysteme des wirbellosen Tiere unter Berücksichtigung seiner Funktion (Berlin: Springer).

Heimbeck, G., Bugnon, V., Gendre, N., Keller, A., and Stocker, R.F. (2001). A central neural circuit for experience-independent olfactory and courtship behavior in Drosophila melanogaster. Proc Natl Acad Sci U S A 98, 15336-15341.

Heisenberg, M. (2003). Mushroom body memoir: from maps to models. Nature reviews Neuroscience 4, 266-275.

Hell, S.W. (2009). Microscopy and its focal switch. Nature methods 6, 24-32.

Hires, S.A., Tian, L., and Looger, L.L. (2008). Reporting neural activity with genetically encoded calcium indicators. Brain cell biology 36, 69-86.

Hummel, T., and Zipursky, S.L. (2004). Afferent Induction of Olfactory Glomeruli Requires N-Cadherin. Neuron 42, 77-88.

Ignell, R., Dekker, T., Ghaninia, M., and Hansson, B.S. (2005). Neuronal architecture of the mosquito deutocerebrum. The Journal of comparative neurology 493, 207-240.

Ito, H., Fujitani, K., Usui, K., Shimizu-Nishikawa, K., Tanaka, S., and Yamamoto, D. (1996). Sexual orientation in Drosophila ia altered by the satori mutation in the sex-determination gene fruitless that encodes a zinc finger protein with aBTB domain. Proc Natl Acad Sci U S A 93, 9687-9692.

Ito, H., Sato, K., Koganezawa, M., Ote, M., Matsumoto, K., Hama, C., and Yamamoto, D. (2012). Fruitless recruits two antagonistic chromatin factors to establish single-neuron sexual dimorphism. Cell 149, 1327-1338.

Ito, K., Sass, H., Urban, J., Hofbauer, A., and Schneuwly, S. (1997). GAL4-responsive UAS-tau as a tool for studying the anatomy and development of the Drosophila central nervous system. Cell and tissue research 290, 1-10.

Ito, K., Shinomiya, K., Ito, M., Armstrong, J.D., Boyan, G., Hartenstein, V., Harzsch, S., Heisenberg, M., Homberg, U., Jenett, A*., et al.* (2014). A systematic nomenclature for the insect brain. Neuron 81, 755-765.

Jefferis, G.S., Marin, E.C., Stocker, R., and Luo, L. (2001). Target neuron prespecification in the olfactory map of Drosophila. Nature 414, 204-208.

Jefferis, G.S., Potter, C.J., Chan, A.M., Marin, E.C., Rohlfing, T., Maurer, C.R., Jr., and Luo, L. (2007). Comprehensive maps of Drosophila higher olfactory centers: spatially segregated fruit and pheromone representation. Cell 128, 1187-1203.

Kain, P., Boyle, S.M., Tharadra, S.K., Guda, T., Pham, C., Dahanukar, A., and Ray, A. (2013). Odour receptors and neurons for DEET and new insect repellents. Nature 502, 507-512.

Kazama, H., and Wilson, R.I. (2009). Origins of correlated activity in an olfactory circuit. Nature neuroscience 12, 1136-1144.

Keleman, K., Vrontou, E., Kruttner, S., Yu, J.Y., Kurtovic-Kozaric, A., and Dickson, B.J. (2012). Dopamine neurons modulate pheromone responses in Drosophila courtship learning. Nature 489, 145-149.

Kenyon, F.C. (1896). The brain of the bee. The Journal of comparative neurology 6, 133-210.

Knaden, M., Strutz, A., Ahsan, J., Sachse, S., and Hansson, B.S. (2012). Spatial representation of odorant valence in an insect brain. Cell reports 1, 392-399.

Kondoh, Y., Kaneshiro, K.Y., Kimura, K., and Yamamoto, D. (2003). Evolution of sexual dimorphism in the olfactory brain of Hawaiian Drosophila. Proceedings Biological sciences / The Royal Society 270, 1005-1013.

Kreher, S.A., Mathew, D., Kim, J., and Carlson, J.R. (2008). Translation of sensory input into behavioral output via an olfactory system. Neuron 59, 110-124.

Kurtovic, A., Widmer, A., and Dickson, B.J. (2007). A single class of olfactory neurons mediates behavioural responses to a Drosophila sex pheromone. Nature 446, 542-546.

Lai, J.S., Lo, S.J., Dickson, B.J., and Chiang, A.S. (2012). Auditory circuit in the Drosophila brain. Proc Natl Acad Sci U S A 109, 2607-2612.

Lai, S.L., Awasaki, T., Ito, K., and Lee, T. (2008). Clonal analysis of Drosophila antennal lobe neurons: diverse neuronal architectures in the lateral neuroblast lineage. Development 135, 2883-2893.

Laissue, P.P., Reiter, C., Hiesinger, P.R., Halter, S., Fischbach, K.F., and Stocker, R.F. (1999). Three-dimensional reconstruction of the antennal lobe in Drosophila melanogaster. Journal of Comparative Neurology 405, 543-552.

Larsson, M.C., Domingos, A.I., Jones, W.D., Chiappe, M.E., Amrein, H., and Vosshall, L.B. (2004). Or83b encodes a broadly expressed odorant receptor essential for Drosophila olfaction. Neuron 43, 703-714.

Lebreton, S., Grabe, V., Omondi, A.B., Ignell, R., Becher, P.G., Hansson, B.S., Sachse, S., and Witzgall, P. (2014). Love makes smell blind: mating suppresses pheromone attraction in Drosophila females via Or65a olfactory neurons. Scientific reports 4, 7119.

Lee, G., Foss, M., Goodwin, S.F., Carlo, T., Taylor, B.J., and Hall, J.C. (2000). Spatial, Temporal and Sexually Dimorphic Expression Patterns of the fruitless Gene in the Drosophila Central Nervous System. J Neurobiol, 404-426.

Lee, J.C., Bruck, D.J., Dreves, A.J., Ioriatti, C., Vogt, H., and Baufeld, P. (2011). In Focus: Spotted wing drosophila, Drosophila suzukii, across perspectives. Pest management science 67, 1349-1351.

Leydig, F. (1857). Lehrbuch der Histologie des Menschenund der Thiere - Meidinger Sohn, Frankfurt am Main.pdf> (Frankfurt am Main: Meidinger Sohn).

Liang, L., Li, Y., Potter, C.J., Yizhar, O., Deisseroth, K., Tsien, R.W., and Luo, L. (2013). GABAergic projection neurons route selective olfactory inputs to specific higher-order neurons. Neuron 79, 917-931.

Liang, L., and Luo, L. (2010). The olfactory circuit of the fruit fly Drosophila melanogaster. Science China Life sciences 53, 472-484.

Lin, H.H., Chu, L.A., Fu, T.F., Dickson, B.J., and Chiang, A.S. (2013). Parallel neural pathways mediate CO2 avoidance responses in Drosophila. Science 340, 1338-1341.

Linz, J., Baschwitz, A., Strutz, A., Dweck, H.K., Sachse, S., Hansson, B.S., and Stensmyr, M.C. (2013). Host plant-driven sensory specialization in Drosophila erecta. Proceedings Biological sciences / The Royal Society 280, 20130626.

Liu, W., Liang, X., Gong, J., Yang, Z., Zhang, Y.H., Zhang, J.X., and Rao, Y. (2011). Social regulation of aggression by pheromonal activation of Or65a olfactory neurons in Drosophila. Nature neuroscience 14, 896-902.

Liu, W., and Wilson, R.I. (2013). Glutamate is an inhibitory neurotransmitter in the Drosophila olfactory system. Proc Natl Acad Sci U S A 110, 10294-10299.

Luo, L. (2007). Fly MARCM and mouse MADM: genetic methods of labeling and manipulating single neurons. Brain research reviews 55, 220-227.

Marin, E.C., Jefferis, G.S., Komiyama, T., Zhu, H., and Luo, L. (2002). Representation of the Glomerular Olfactory Map in the Drosophila Brain. Cell 109, 243-255.

Marin, E.C., Watts, R.J., Tanaka, N.K., Ito, K., and Luo, L. (2005). Developmentally programmed remodeling of the Drosophila olfactory circuit. Development 132, 725-737.

Masse, N.Y., Turner, G.C., and Jefferis, G.S. (2009). Olfactory information processing in Drosophila. Current biology : CB 19, R700-713.

McMeniman, C.J., Corfas, R.A., Matthews, B.J., Ritchie, S.A., and Vosshall, L.B. (2014). Multimodal integration of carbon dioxide and other sensory cues drives mosquito attraction to humans. Cell 156, 1060-1071.

Meigen, J.W. (1830). Systematische Beschreibung der bekannten europäischen zweiflügeligen Insekten, Vol 6 (Hamm: Schulzische Buchahandlung).

Miller, A. (1950). The internal anatomy of the imago of Drosophila melanogaster. In Biology of Drosophila, Demerec, ed. (New York), pp. 420-534.

Min, S., Ai, M., Shin, S.A., and Suh, G.S. (2013). Dedicated olfactory neurons mediating attraction behavior to ammonia and amines in Drosophila. Proc Natl Acad Sci U S A 110, E1321-1329.

Mosca, T.J., and Luo, L. (2014). Synaptic organization of the Drosophila antennal lobe and its regulation by the Teneurins. eLife.

Murthy, M., Fiete, I., and Laurent, G. (2008). Testing odor response stereotypy in the Drosophila mushroom body. Neuron 59, 1009-1023.

Neville, M.C., Nojima, T., Ashley, E., Parker, D.J., Walker, J., Southall, T., Van de Sande, B., Marques, A.C., Fischer, B., Brand, A.H.*, et al.* (2014). Male-specific fruitless isoforms target neurodevelopmental genes to specify a sexually dimorphic nervous system. Current biology : CB 24, 229-241.

Ng, M., Roorda, R.D., Lima, S.Q., Zemelman, B.V., Morcillo, P., and Miesenbock, G. (2002). Transmission of Olfactory Information between Three Populations of Neurons in the Antennal Lobe of the Fly. Neuron 36, 463-474.

Okada, R., Awasaki, T., and Ito, K. (2009). Gamma-aminobutyric acid (GABA)-mediated neural connections in the Drosophila antennal lobe. The Journal of comparative neurology 514, 74-91.

Olsen, S.R., Bhandawat, V., and Wilson, R.I. (2007). Excitaory Interactions Between Olfactory Processing Channels in the Drosophila Antennal Lobe. Neuron 54, 89-103.

Parnas, M., Lin, A.C., Huetteroth, W., and Miesenbock, G. (2013). Odor discrimination in Drosophila: from neural population codes to behavior. Neuron 79, 932-944.

Patterson, G.H., and Lippincott-Schwartz, J. (2002). A photoactivatable GFP for selective photolabeling of proteins and cells. Science 297, 1873-1877.

Pelz, D., Roeske, T., Syed, Z., de Bruyne, M., and Galizia, C.G. (2006). The molecular receptive range of an olfactory receptor in vivo (Drosophila melanogaster Or22a). J Neurobiol 66, 1544-1563.

Perez-Orive, J., Mazor, O., Turner, G.C., Cassenaer, S., Wilson, R.I., and Laurent, G. (2002). Oscillations and sparsening of odor representations in the mushroom body. Science 297, 359-365.

Polanska, M.A., Tuchina, O., Agricola, H., Hansson, B.S., and Harzsch, S. (2012). Neuropeptide complexity in the crustacean central olfactory pathway: immunolocalization of A-type allatostatins and RFamide-like peptides in the brain of a terrestrial hermit crab. Molecular brain 5, 29.

Quinn, W.G., Harris, W.A., and Benzer, S. (1974). Conditioned Behavior in Drosophila melanogaster. Proc Natl Acad Sci U S A 71, 708-712.

Ramaekers, A., Magnenat, E., Marin, E.C., Gendre, N., Jefferis, G.S., Luo, L., and Stocker, R.F. (2005). Glomerular maps without cellular redundancy at successive levels of the Drosophila larval olfactory circuit. Current biology : CB 15, 982-992.

Rein, K., Zöckler, M., Mader, M.T., Grübel, C., and Heisenberg, M. (2002). The Drosophila Standard Brain. Current Biology 12, 227-231.

Ronderos, D.S., Lin, C.C., Potter, C.J., and Smith, D.P. (2014). Farnesol-detecting olfactory neurons in Drosophila. The Journal of neuroscience : the official journal of the Society for Neuroscience 34, 3959-3968.

Root, C.M., Masuyama, K., Green, D.S., Enell, L.E., Nassel, D.R., Lee, C.H., and Wang, J.W. (2008). A presynaptic gain control mechanism fine-tunes olfactory behavior. Neuron 59, 311-321.

Root, D.H., Mejias-Aponte, C.A., Zhang, S., Wang, H.L., Hoffman, A.F., Lupica, C.R., and Morales, M. (2014). Single rodent mesohabenular axons release glutamate and GABA. Nature neuroscience 17, 1543-1551.

Ruta, V., Datta, S.R., Vasconcelos, M.L., Freeland, J., Looger, L.L., and Axel, R. (2010). A dimorphic pheromone circuit in Drosophila from sensory input to descending output. Nature 468, 686-690.

Salvaterra, P.M., and Kitamoto, T. (2001). Drosophila cholinergic neurons and processes visualized with Gal4/UAS-GFP. Gene Expr Patterns 1, 73-82.

Schneiderman, A.M., Hildebrand, J.G., Brennan, M.M., and Tumlinson, J.H. (1986). Trans-sexually grafted antennae alter pheromone-directed behaviour in a moth. Nature 323, 801-803.

Seki, Y., Rybak, J., Wicher, D., Sachse, S., and Hansson, B.S. (2010). Physiological and morphological characterization of local interneurons in the Drosophila antennal lobe. Journal of neurophysiology 104, 1007-1019.

Semmelhack, J.L., and Wang, J.W. (2009). Select Drosophila glomeruli mediate innate olfactory attraction and aversion. Nature 459, 218-223.

Shanbhag, S.R., Müller, B., and Steinbrecht, R.A. (1999). Atlas of olfactory organs of Drosophila melanogaster 1. Types, external organization, innervation and distribution of olfactory sensilla. Int J Insect Morphol & Embryol 28, 377-397.

Shanbhag, S.R., Singh, K., and Singh, R.N. (1995). Fine structure and primary sensory projection of sensilla located in the sacculus of the antenna of Drosophila melanogaster. Cell and tissue research 282, 237-249.

Shang, Y., Claridge-Chang, A., Sjulson, L., Pypaert, M., and Miesenbock, G. (2007). Excitatory local circuits and their implications for olfactory processing in the fly antennal lobe. Cell 128, 601-612.

Silbering, A.F., Rytz, R., Grosjean, Y., Abuin, L., Ramdya, P., Jefferis, G.S., and Benton, R. (2011). Complementary function and integrated wiring of the evolutionarily distinct Drosophila olfactory subsystems. The Journal of neuroscience : the official journal of the Society for Neuroscience 31, 13357-13375.

Singh, R.N., and Nayak, S.V. (1985). Fine Structure and Primary Sensory Projections of Sensilla on the Maxillary Palp of Drosophila melanogaster Meigen (Diptera : Drosophilidae). Int J Insect Morphol & Embryol 14, 291-306.

Stachniak, T.J., Ghosh, A., and Sternson, S.M. (2014). Chemogenetic synaptic silencing of neural circuits localizes a hypothalamus-->midbrain pathway for feeding behavior. Neuron 82, 797-808.

Stensmyr, M.C., Dweck, H.K., Farhan, A., Ibba, I., Strutz, A., Mukunda, L., Linz, J., Grabe, V., Steck, K., Lavista-Llanos, S.*, et al.* (2012). A conserved dedicated olfactory circuit for detecting harmful microbes in Drosophila. Cell 151, 1345-1357.

Stocker, R., and Lawrence, P.A. (1981). Sensory Projections from Normal and Homoeotically Transformed Antennae in Drosophila. Developmental biology 82, 224-237.

Stocker, R., Lienhard, M.C., Borst, A., and Fischbach, K.-F. (1990). Neuronal architecture of the antennal lobe in Drosophila melanogaster. Cell and tissue research 262, 9-34.

Stocker, R., Singh, R.N., Schorderet, M., and Siddiqi, O. (1983). Projection patterns of different types of antennal sensilla in the antennal glomeruli of Drosophila melanogaster. Cell and tissue research 232, 237-248.

Stocker, R.F. (1994). The organization of the chemosensory system in Drosophila melanogaster: a review. Cell and tissue research 275, 3-26.

Stocker, R.F. (2001). Drosophila as a focus in olfactory research: mapping of olfactory sensilla by fine structure, odor specificity, odorant receptor expression, and central connectivity. Microsc Res Tech 55, 284-296.

Stocker, R.F., Heimbeck, G., Gendre, N., and de Belle, J.S. (1997). Neuroblast Ablation in Drosophila P [GAL4] Lines Reveals Origins of Olfactory Interneurons. J Neurobiol 32, 443-457.

Stockinger, P., Kvitsiani, D., Rotkopf, S., Tirian, L., and Dickson, B.J. (2005). Neural circuitry that governs Drosophila male courtship behavior. Cell 121, 795-807.

Stowers, L. (2004). Neuronal Development: Specifying a Hard-Wired Circuit. Current Biology 14, R62-R64.

Strausfeld, N. (1976). Atlas of an Insect Brain (Springer Verlag).

Strutz, A., Soelter, J., Baschwitz, A., Farhan, A., Grabe, V., Rybak, J., Knaden, M., Schmuker, M., Hansson, B.S., and Sachse, S. (2014). Decoding Odor Quality and Intensity in the Drosophila brain. eLIFE.

Strutz, A., Völler, T., Riemensperger, T., Fiala, A., and Sachse, S. (2012). Calcium Imaging of Neural Activity in the Olfactory System of Drosophila. In Genetically Encoded Functional Indicators, J.-R. Martin, ed. (Springer Science+Business Media), pp. 43-70.

Suh, G.S., Wong, A.M., Hergarden, A.C., Wang, J.W., Simon, A.F., Benzer, S., Axel, R., and Anderson, D.J. (2004). A single population of olfactory sensory neurons mediates an innate avoidance behaviour in Drosophila. Nature 431, 854-859.

Sweeney, S.T., Broadie, K., Keane, J., Niemann, H., and O'Kane, C.J. (1995). Target Expression of Tetanus Toxin Light Chain in Drosophila Specifically Eliminates Synaptic Transmission and Causes Behavioral Defects. Neuron 14, 341-351.

Tanaka, N.K., Awasaki, T., Shimada, T., and Ito, K. (2004). Integration of chemosensory pathways in the Drosophila second-order olfactory centers. Current biology : CB 14, 449-457.

Tanaka, N.K., Endo, K., and Ito, K. (2012). Organization of antennal lobe-associated neurons in adult Drosophila melanogaster brain. The Journal of comparative neurology 520, 4067-4130.

Tian, L., Hires, S.A., Mao, T., Huber, D., Chiappe, M.E., Chalasani, S.H., Petreanu, L., Akerboom, J., McKinney, S.A., Schreiter, E.R.*, et al.* (2009). Imaging neural activity in worms, flies and mice with improved GCaMP calcium indicators. Nature methods 6, 875-881.

Turner, S.L., and Ray, A. (2009). Modification of CO2 avoidance behaviour in Drosophila by inhibitory odorants. Nature 461, 277-281.

van der Goes van Naters, W., and Carlson, J.R. (2007). Receptors and neurons for fly odors in Drosophila. Current biology : CB 17, 606-612.

Vinje, W.E. (2000). Sparse Coding and Decorrelation in Primary Visual Cortex During Natural Vision. Science 287, 1273-1276.

Vosshall, L.B., Amrein, H., Morozov, P.S., Rzhetsky, A., and Axel, R. (1999). A Spatial Map of Olfactory Receptor Expression in the Drosophila Antenna. Cell 96, 725-736.

Vosshall, L.B., and Stocker, R.F. (2007). Molecular architecture of smell and taste in Drosophila. Annu Rev Neurosci 30, 505-533.

Vosshall, L.B., Wong, A.M., and Axel, R. (2000). An Olfactory Sensory Map in the Fly Brain. Cell 102, 147-159.

Wang, J.W., Wong, A.M., Flores, J., Vosshall, L.B., and Axel, R. (2003a). Two-Photon Calcium Imaging Reveals an Odor-Evoked Map of Activity in the Fly Brain. Cell 112, 271-282.

Wang, T.M., Holzhausen, L.C., and Kramer, R.H. (2014). Imaging an optogenetic pH sensor reveals that protons mediate lateral inhibition in the retina. Nature neuroscience 17, 262-268.

Wang, Y., Chiang, A.-S., Xia, S., Kitamoto, T., Tully, T., and Zhong, Y. (2003b). Blockade of Neurotransmission in Drosophila Mushroom Bodies Impairs Odor Attraction, but Not Repulsion. Current Biology 13, 1900-1904.

Willig, K.I., and Barrantes, F.J. (2014). Recent applications of superresolution microscopy in neurobiology. Current opinion in chemical biology 20, 16-21.

Wilson, R.I. (2013). Early olfactory processing in Drosophila: mechanisms and principles. Annu Rev Neurosci 36, 217-241.

Wilson, R.I., and Laurent, G. (2005). Role of GABAergic inhibition in shaping odor-evoked spatiotemporal patterns in the Drosophila antennal lobe. The Journal of neuroscience : the official journal of the Society for Neuroscience 25, 9069-9079.

Wilson, R.I., Turner, G.C., and Laurent, G. (2004). Transformation of olfactory representations in the Drosophila antennal lobe. Science 303, 366-370.

Wong, A.M., Wang, J.W., and Axel, R. (2002). Spatial Representation of the Glomerular Map in the Drosophila Protocerebrum. Cell 109, 229-241.

Yaksi, E., and Wilson, R.I. (2010). Electrical coupling between olfactory glomeruli. Neuron 67, 1034-1047.

Yu, H.H., Kao, C.F., He, Y., Ding, P., Kao, J.C., and Lee, T. (2010). A complete developmental sequence of a Drosophila neuronal lineage as revealed by twin-spot MARCM. PLoS biology 8.

Zawistowski, S., and Richmond, R.C. (1985). Experience-Mediated Courtship Reduction and Competition for Mates by Male Drosophila melanogaster. Behav Genet 15, 561-569.

Zhou, S., Stone, E.A., Mackay, T.F., and Anholt, R.R. (2009). Plasticity of the chemoreceptor repertoire in Drosophila melanogaster. PLoS genetics 5, e1000681.

Zhu, P., Frank, T., and Friedrich, R.W. (2013). Equalization of odor representations by a network of electrically coupled inhibitory interneurons. Nature neuroscience 16, 1678-1686.

Declaration of independent Assignment

I Declare in accordance with the conferral of the degree of doctor from the school of Biology and Pharmacy of Friedrich Schiller University Jena that the submitted thesis was written only with the assistance and literature cited in the text.

People who assisted in the experiments, data analysis and writing of the manuscripts are listed as coauthors of the respective manuscripts. I was not assisted by a consultant for doctorate theses.

The thesis has not been previously submitted whether to the Friedrich Schiller University Jena or to any other university.

Jena, Veit Grabe